APPLICATION OF WAVE FIELD SYNTHESIS IN ROOM ACOUSTICS

PROEFSCHRIFT

ter verkrijging van de graad van doctor
aan de Technische Universiteit Delft,
op gezag van de Rector Magnificus,
prof.ir. K.F. Wakker,
in het openbaar te verdedigen
ten overstaan van een commissie,
aangewezen door het College van Dekanen
op woensdag 22 december 1993 te 16.00 uur door

PETER VOGEL

geboren te Den Haag

natuurkundig ingenieur

Gebotekst Zoetermeer / 1993

Dit proefschrift is goedgekeurd door de promotor:
prof.dr.ir. A.J. Berkhout

Toegevoegd promotor:
dr.ir. D. de Vries

CIP-DATA KONINKLIJKE BIBLIOTHEEK, DEN HAAG

Vogel, Peter

Application of wave field synthesis in room acoustics / Peter Vogel
[S.l. : s.n.] (Zoetermeer : Gebotekst)
Thesis Technische Universiteit Delft. - With ref. - With summary in Dutch.
ISBN 90-9006659-4
Subject headings: room acoustics / wave field synthesis.

OMSLAGONTWERP
NoorderBreedte ontwerpbureau Delft

SUPPORT
The research for this thesis has been financially supported by the Dutch Technology Foundation S.T.W. (project DTN 70.1276).

Printed in The Netherlands by: N.K.B. Offset bv, Bleiswijk

Aan mijn ouders

PREFACE

In this thesis a report is given of my research work at the Laboratory of Seismics and Acoustics of the Applied Physics department at Delft University of Technology between August 1988 and December 1993. This research was financially supported by the Dutch Technology Foundation (STW project DTN70.1276).
Many people have, directly or indirectly, contributed to the realisation of this thesis. Some of them I want to mention explicitly here.
First I want to thank my mentor and co-promotor dr.ir. Diemer de Vries for his enthousiasm in supporting my work and the time he spent in improving the manuscript for this thesis. Next I want to thank my promotor prof.dr.ir. A.J. Berkhout for his stimulating ideas and the safeguarding of the scientific depth of the project.
Some others that should be mentioned are dr.ir. Kees Wapenaar for his advice on the theoretical chapters, prof.dr. A.J.M. Houtsma for the accurate checking of the manuscript, my room mates Evert, Antwan and Edwin for their moral support, Henry and Leen for their assistance in designing the analog equipment, all lunch-time runners (esp. Harry) for keeping up the speed during the training sessions, the medical and nursery staff of the Academic Hospital Leiden and the Red Cross Hospital Den Haag for keeping me alive and all members of the Laboratory of Seismics and Acoustics for creating an inspiring environment for the daily work.

Peter Vogel, december 1993

TABLE OF CONTENTS

1. A SURVEY OF ROOM ACOUSTICS

1.1 Introduction

If an omnidirectional acoustic source is placed in an unbounded, homogeneous medium it will radiate spherical sound waves. Neglecting damping effects due to inelastic losses in the medium, the spherical wave fronts travel away from the source with a speed determined by two basic properties of the medium, viz. density and compressibility. The amplitude of the waves decreases with increasing distance from the source, because the sound energy carried by the waves is spread out over a larger surface for increasing distance (geometrical spreading).
In practice, the free field conditions described above do not exist because of the presence of sound reflecting obstacles. The best approximation to a free field is found in an anechoic chamber in which, above a certain frequency, practically all sound energy reaching the room boundaries is dissipated in the sound absorbing material covering the walls, instead of being reflected back into the room volume (see figure 1.1.1).
When listening to a sound source, e.g., a voice, in such an anechoic chamber, it is striking that the location of the source can be determined more accurately than in a normal room, while the loudness is much less. These effects are caused by the (almost) complete absence of reflected sound.
The opposite of the free field conditions described above would be obtained in a room enclosed by infinitely hard walls, which reflect all incident sound energy back into the room. Neglecting damping effects again, a stationary sound source in this kind of environment would theoretically lead to infinite intensity because the source continually

radiates energy into the room volume, while no energy leaves the enclosure. A physical description of the acoustic phenomena under these circumstances will be extremely difficult, as the region in which non-linear effects are important will be entered soon after switching on the sound source. Due to the changing acoustic impedance of the medium under the extreme conditions sketched, the energy radiated by any physical source would decrease to zero in a short time.

As with the free field case, a room without energy loss cannot be constructed in practice. Only a room made completely out of a very hard, non porous material like concrete, can give an approximation to it. An example of this kind of enclosure is the reverberation room, found in most professional acoustics laboratories (see figure 1.1.2).

When listening to a sound source in a reverberation room it appears that it sounds much louder than in the anechoic environment, while the source location is less well defined. These effects are caused by the very large number of sound reflections arriving at the listener from all possible directions, which all add up to a diffuse sound field.

In an acoustics laboratory, the anechoic chamber is used to measure the properties (e.g., frequency response and directivity pattern) of transducers like microphones and loudspeakers. For these measurements, free field conditions are required. The reverberation room is used for sound power and absorption measurements, for which highly reverberant conditions (diffuse field) are necessary.

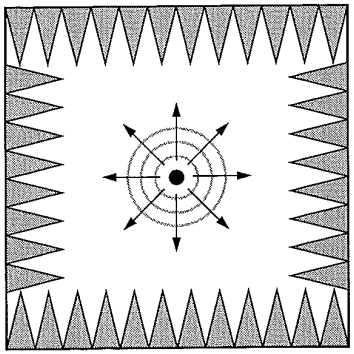

Figure 1.1.1: *Almost perfect free field conditions can be found in an anechoic chamber, in which the walls, floor and ceiling are covered with a sound absorbing material.*

The totally different perception of sound in the two extreme acoustical situations as described above indicates that the amount of reverberation is a very important property in the acoustical description of a room. This fact was already known around the beginning of this century to the pioneer of room acoustics W.C. Sabine, when he started to measure the amount of reverberation of several concert halls and theatres in the United States.

Although the amount of reverberation is an important acoustical property of a room, it is certainly not sufficient as a complete characterisation. In order to obtain a more accurate description, more refined parameters like early-to-late energy ratios and lateral-to-omnidirectional energy ratios have been introduced. None of these parameters has thus far been as successful as the reverberation time in giving an indication of the suitability of a given hall for a particular application. However, when used in conjunction with the reverberation time, these new parameters can give an important refinement to the characterisation of a hall.

In the next section a description of the hall in terms of a distribution of sound reflections (impulse response) will be given. In section 1.3 several global acoustical parameters will be discussed, together with their relation to the impulse response.

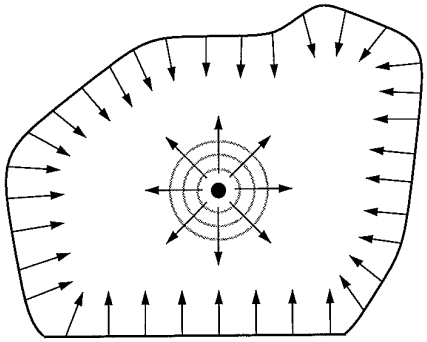

Figure 1.1.2: *A reverberation room usually is an irregularly shaped room, with walls and floor made of an acoustically reflecting material, such that only a small amount of the sound energy inside the room will leave the enclosure.*

1.2 The impulse response

Consider the simple, two-dimensional situation sketched in figure 1.2.1: a sound source S placed in a rectangular room generates a sound field that is recorded by a receiver R in the same room. The receiver acquires sound energy coming from the source directly as well as sound energy that has been reflected against the room boundaries one or more times.
The energy distribution of the reflected sound is determined by both the geometry of the room (arrival time and direction of incidence of each reflection) and the amount of energy absorption for each reflection (strength of each particular reflection). The different subjective sound quality for different halls is due to the different distribution of reflections arriving at the receiver with respect to relative arrival time, energy and orientation. Thus, a description of the acoustical properties of a hall in terms of the reflection distribution will yield a complete characterisation. This description is usually

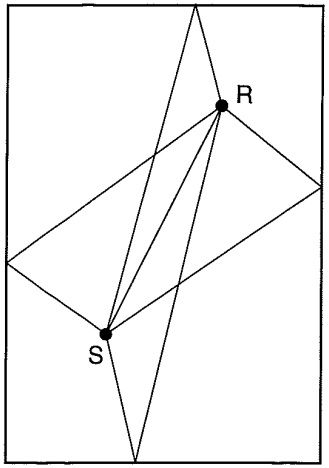

Figure 1.2.1: *Sound 'rays' from the source S reach the receiver R either directly or after one or more reflections against the room boundaries. For clarity, only the first order reflections have been drawn in the graph.*

referred to as the impulse response. Note that the reflection pattern will depend both on the position of the source and on the position of the receiver. Thus, mentioning the impulse response of a hall will usually mean the impulse response for a particular source-receiver combination. To characterise a hall fully, all relevant source-receiver combinations should be taken into account.
An impulse response h(t) of a room may be formulated as

$$h(t) = \sum_{i=0}^{\infty} a_i(t) * \delta(t-\tau_i) = \sum_{i=0}^{\infty} a_i(t-\tau_i) \ , \qquad (1.2.1)$$

where $\delta(t)$ is the Dirac delta function, τ_i the delay time and $a_i(t)$ defines the shape and amplitude of reflection i. Note that for a given hall the impulse response will depend on the source pulse and on the particular source and receiver position.
Equation (1.2.1) can be interpreted as follows: when the sound source emits a sound pulse, the receiver will detect the direct sound first (assuming that the direct wave path exists). Next, the reflections from the walls, the floor and the ceiling arrive. It can be shown (see e.g. Kuttruff,1979) that the average number of sound reflections $\overline{n(t)}$ arriving at the receiver increases according to a quadratic law with respect to time:

$$\overline{n(t)} = 4\pi \frac{c^3 t^2}{V} \ , \qquad (1.2.2)$$

where V denotes the room volume. The total number of reflections N(t) arriving at the receiver up to a certain time t is the running integral of the reflection density $\overline{n(t)}$:

$$N(t) = \int_0^t \overline{n(\tau)}\, d\tau = \frac{4\pi}{3} \frac{c^3 t^3}{V} \ . \qquad (1.2.3)$$

The amplitude of the individual reflections decreases with increasing time, due to both the geometrical spreading of the sound field and the absorption during reflection against a room boundary. For the very high frequencies the absorption in air should be included as well. The energy decrease of the reflections caused by the geometrical spreading is proportional to the squared distance from the source:

$$E_i(t) \propto \frac{1}{r^2} = \frac{1}{c^2 t^2} \ , \qquad (1.2.4)$$

where $E_i(t)$ denotes the energy of reflection i arriving at the receiver at time t. On a mac-

roscopic scale this energy decrease is exactly compensated for by the increase in reflection density, thus leaving only the exponential decay caused by the absorption at the walls:

$$\bar{E}(t) \propto (1-\bar{\alpha})^{ct/\bar{\ell}}. \qquad (1.2.5)$$

In equation (1.2.5) $\bar{E}(t)$ denotes the average energy at the receiver at time t, $\bar{\alpha}$ the average energy loss at each reflection of the sound wave at a room boundary and $\bar{\ell}$ is the mean free path in the room, i.e., the mean distance travelled between two consecutive reflections, which is given by

$$\bar{\ell} = \frac{4V}{S}, \qquad (1.2.6)$$

with V denoting the room volume and S the total surface (walls, floor and ceiling), as was shown by Kosten (1960).

In summary, an impulse response consists of an infinite number of impulses, the number of pulses per unit time increasing with time, while their amplitude is decreasing. As the energy absorption on sound reflection against the room boundaries is usually frequency dependent, the pulse shape will also change with time.

As an example, in figure 1.2.3a a realisation of the statistical model discussed above is shown. This yields an impulse sequence that has no relation with any particular room geometry. For a more accurate prediction of a hall impulse response a more sophisticated model is required. One such model is the image source algorithm, a model that will be discussed further in chapter 5. An impulse response calculated using this algorithm is shown in figure 1.2.3b. The simulated reflections show more spreading in amplitude and arrival time than in the statistical response of figure 1.2.3a. Note that both simulation models assume frequency independent absorption.

In practice, a measured room impulse response will always have finite bandwidth. When the absorption coefficients of the room boundaries are independent of frequency within the bandwidth of the measurement signal, the measured response is the convolution of the infinite bandwidth impulse response with the source signal.

In appendix A it is discussed that a band limited impulse response can be obtained from a measured sweep response by applying a deconvolution filter. When this technique is applied to the impulse responses of figure 1.2.3, using a sweep signal with a frequency range from 300 Hz to 3 kHz, the responses of figure 1.2.3 are obtained. Note that the sharp impulses of figure 1.2.3 are transformed into band limited zero-phase

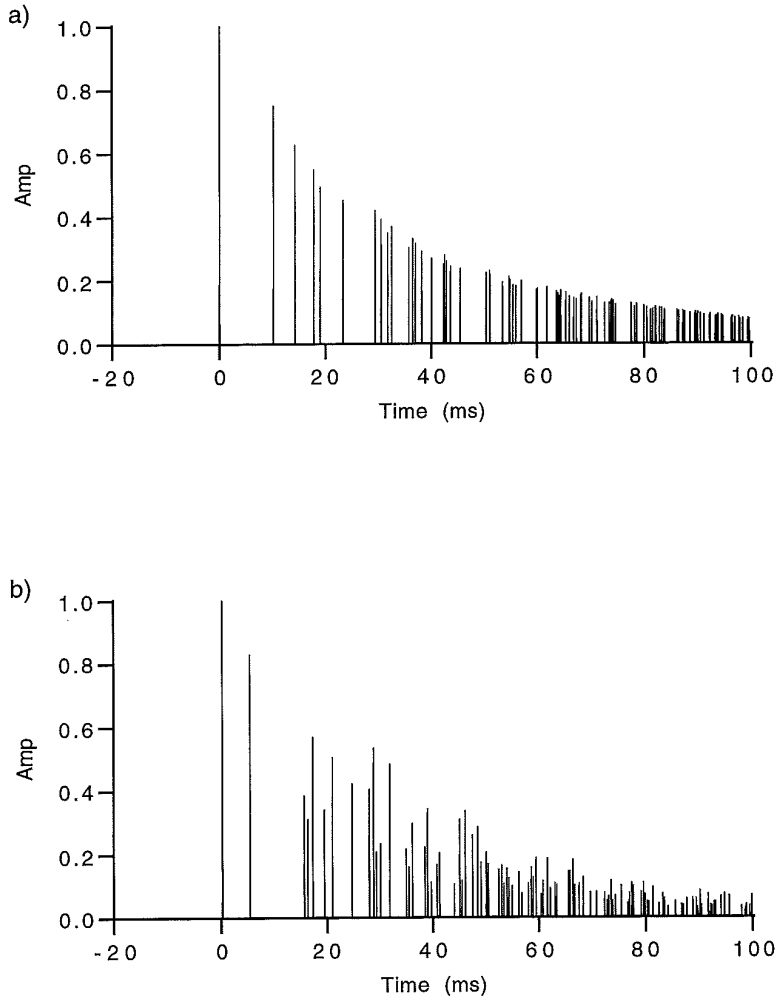

Figure 1.2.2: *Two simulated impulse responses for the same rectangular room*
a) realisation of the statistical model discussed in section 1.2
b) response calculated using the image source method

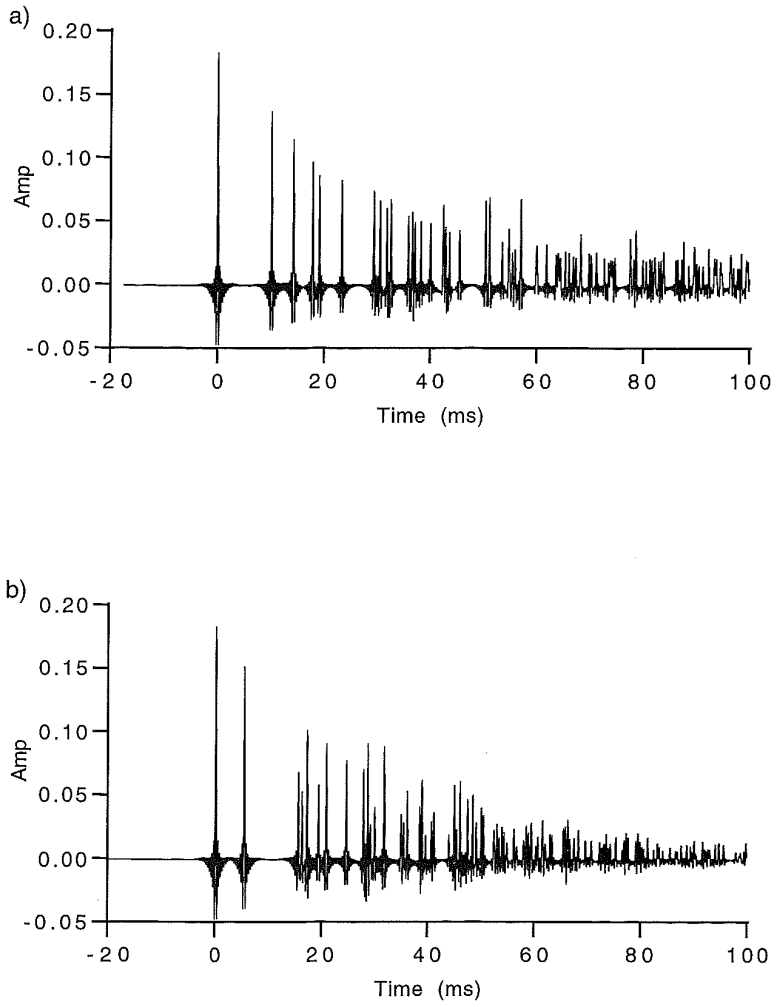

Figure 1.2.3: *Two simulated band limited impulse responses (300 - 3000 Hz)*
a) realisation of the statistical model discussed in section 1.2
b) response calculated using the image source method

impulses. In this example it was assumed that the absorption coefficients of the room boundary are independent of frequency in the range from 300 Hz to 3 kHz.
From a perception point of view, the impulse response can be divided into three time windows, each related to a specific perceptual aspect (see figure 1.2.4).

A: Primary sound

The primary sound is built up from the direct (non-reflected) part of the sound field, together with the very early reflections arriving at the receiver up to 20 ms after the direct sound. Due to the integration properties of the human hearing mechanism with an integration time of about 20 ms (Haas, 1951), the reflected energy arriving at the receiver at this time interval will be perceived as a reinforcement of the direct sound such that these very early reflections are often called the 'pseudo-direct' sound. The energy of the primary sound should be high compared to the reflected energy to obtain good speech intelligibility and music transparency.

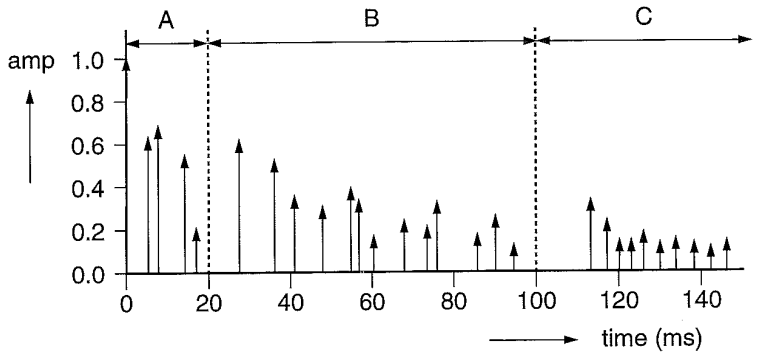

Figure 1.2.4: *The impulse response of a hall can be divided into three time windows: the primary sound (A), the early reflections (B) and the reverberation (C).*

B: Early reflections

The reflections arriving at the receiver between 20 and 100 ms after the direct sound are called early reflections. The early reflections are known to contribute to the 'presence' of sound (Beranek, 1963) and to have, together with the primary sound, a large influence on the perceived clarity or transparency of the sound field. Reflections with arrival times up to 50 ms contribute to speech intelligibility (Lochner et al., 1958). Early reflections reaching a listener from aside will increase the perceived spaciousness of the hall (Barron and Marshall, 1981), a situation preferred by most listeners to music.
For an orchestra on stage the early reflections are required for good ensemble playing. As the direct sound path is usually blocked by the musicians themselves, they are able to hear each other via reflected sound only. Some strong early reflections at the stage can improve the conditions for the musicians significantly.

C: Reverberation

Reflections arriving at the receiver more than 100 ms after the direct sound build up the reverberation in the hall. In this time range a description in terms of individual reflections is no longer useful, a statistical evaluation in terms of reflection density and energy density is more appropriate. The reverberation is related to subjective parameters like warmth, brilliance and liveliness. The amount of reverberation required depends strongly on the performance the hall is used for. The reverberation time of a hall (defined in section 1.3.1) might range from about 1.0 second for theatres up to 5.0 seconds (or even more) in large churches or cathedrals.

1.3 Acoustic parameters

An important theorem in system analysis says that each linear, time invariant system is fully characterised by its impulse response (see e.g. Oppenheim et al., 1982). For a room, as an example of a linear time invariant system, this means that once the impulse response is known for all possible source and receiver combinations, all its

acoustic properties are known. Although this statement is correct in principle, the number of possible source and receiver combinations is infinite. Apart from that, the impulse response is neither suitable for easy interpretation, nor for simple comparison of different rooms. This is caused by the very detailed information present in the impulse response.
As an example consider the impulse responses shown in figure 1.3.1. The graphs shown are impulse responses measured in a 600 seat theatre, at two receiver positions only 0.1 m apart. The different 'microscopic' structure for these two measurements is typical for hall impulse responses. Although this fine structure of the impulse responses at two neighbouring positions is quite different, the perception of the acoustical quality usually is not. As a consequence some more global quantities should be calculated from the impulse response. These 'macroscopic' parameters make comparisons between different rooms much easier.
Another indication that the detailed time information in the impulse response will not be important comes from the fact that the human hearing mechanism performs a short time integration over incoming signals. E.g., Moore et al. (1988) found a time window with an equivalent rectangular duration of 8 ms, while Kollmeier et al. (1990) found time constants in the range from 10 to 45 ms.
To account for the ear's integration process, some acousticians use a moving average filter with a width of 20 ms on the squared impulse response. This filtered impulse response shows less detail and can be useful in comparing different halls. As an example, this filtering process is applied to the impulse responses shown in figure 1.3.1. From figure 1.3.2 it can be seen that the difference between the two processed responses is less than for the original ones.
Numerous single number indicators, derived from impulse responses, for the characterisation of acoustical quality can be found in the literature. In the next subsections the most important of these so called global parameters will be discussed, together with their relation to the impulse response.

1.3.1 Reverberation Time

As already stated in section 1.1 the reverberation time of a hall is a very important acoustical parameter. It is defined as the time in which the sound pressure level drops by 60 dB after switching off a stationary sound source (Sabine, 1900). Generally the

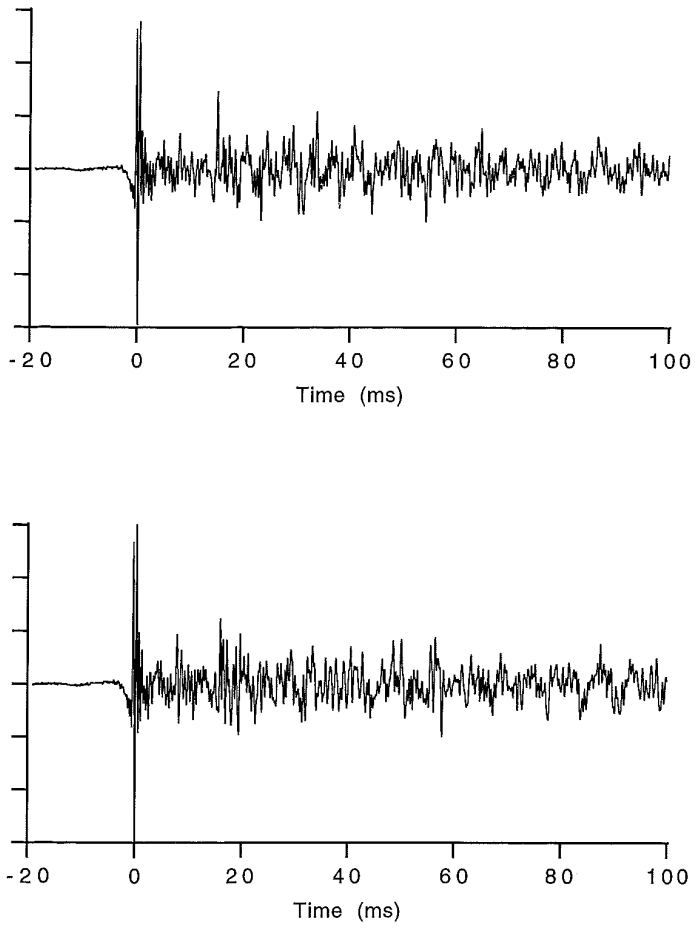

Figure 1.3.1: *Impulse responses measured in a hall at two receiver positions with an intermediate distance of 0.1 m. The 'microscopic' structure of the responses changes rapidly with positions, while the perception of the acoustical quality of the room does not.*

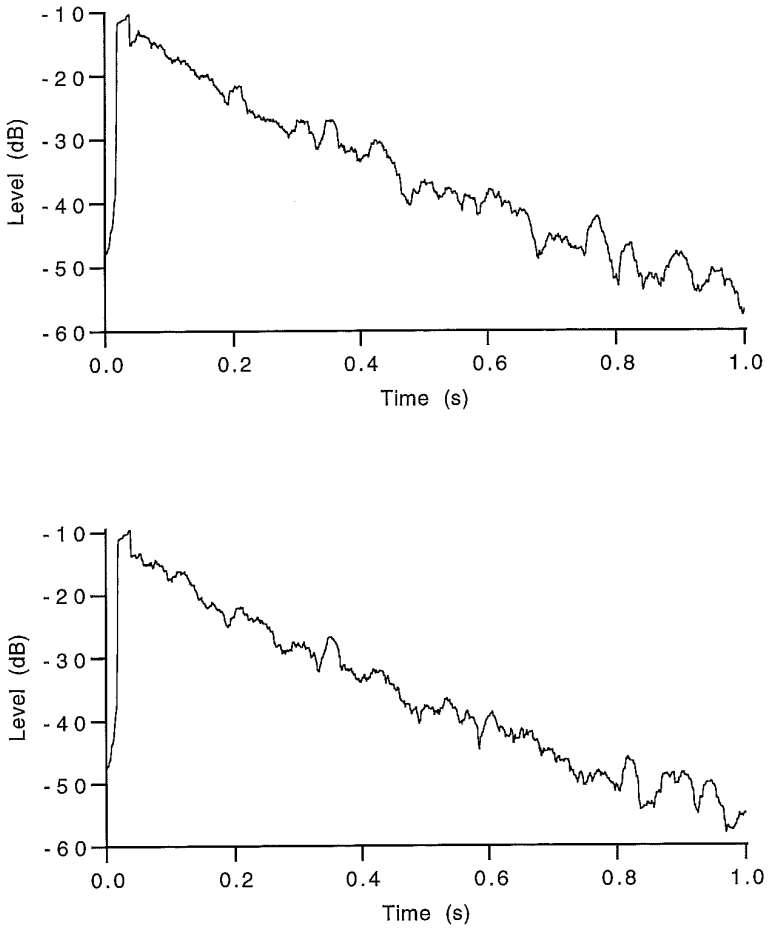

Figure 1.3.2: *Squared versions of the impulse responses of figure 1.3.1, filtered with a moving average filter with a width of 20 ms. The new responses show much more similarity than the original impulse responses.*

reverberation time varies with frequency and with the position of the source and the receiver. Therefore it is normally specified in frequency bands (e.g., octaves or third octaves) and averaged over several source-receiver position combinations.
The relation of the reverberation time to the impulse response is not directly clear from its definition, but it can be found by calculating the response of the room on a driving noise signal that is interrupted suddenly.
From system theory it is known that the response of a linear time invariant system due to an arbitrary input signal can be found by convolving the input signal with the impulse response of the system (see figure 1.3.3). Now assume that the acoustical transmission path under investigation can be characterised by an impulse response h(t), while the interrupted noise signal s(t) is given by:

$$s(t) = n(t)\,(1-u(t))\,. \tag{1.3.1}$$

The signals n(t) and u(t) introduced in equation (1.3.1) denote the random noise generator signal and the unit step function defined as

$$\begin{aligned} u(t) &= 0, t<0\,, \\ u(t) &= \frac{1}{2}, t=0\,, \\ u(t) &= 1, t>0\,, \end{aligned} \tag{1.3.2}$$

respectively.

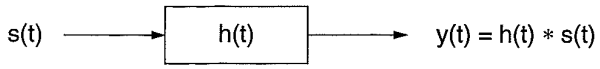

Figure 1.3.3: *The response of a linear time invariant system on an arbitrary input signal can be found by convolving the input signal with the impulse response of the system.*

The response p(t) on the interrupted noise signal s(t) is

$$p(t) = h(t) * s(t) = \int_{-\infty}^{\infty} h(\tau)\, s(t-\tau)\, d\tau, \tag{1.3.3}$$

in which the symbol * denotes convolution.
Using definition (1.3.2) of the unit step function u(t), s(t-τ) can be written as:

$$\begin{aligned} s(t-\tau) &= n(t-\tau), t<\tau, \\ s(t-\tau) &= \frac{1}{2} n(t-\tau), t=\tau, \\ s(t-\tau) &= 0, t>\tau. \end{aligned} \tag{1.3.4}$$

Substitution of this equation in the convolution integral (1.3.3) gives:

$$p(t) = \int_{t}^{\infty} h(\tau)\, n(t-\tau)\, d\tau. \tag{1.3.5}$$

Note that, for t > 0, p(t) represents the decaying sound field after source switch-off, in terms of sound pressure.
From equation (1.3.5) the effective sound pressure $p_{rms}(t)$ can be found, using the expectation operator:

$$p_{rms}^2(t) = E[p^2(t)]\,. \tag{1.3.6}$$

Assuming n(t) is a zero-mean, stationary white noise process, which means that

$$\begin{aligned} E[n(t)] &= 0, \\ E[n(t)\, n(t-\tau)] &= \sigma^2 \delta(\tau), \end{aligned} \tag{1.3.7}$$

in which σ is a constant (the standard deviation of the noise) and δ(t) is the Dirac delta

function, the squared effective sound pressure $p^2_{rms}(t)$ is found to be

$$p^2_{rms}(t) = E\left[\left(\int_t^\infty h(\tau)\, n(t-\tau)\, d\tau\right)^2\right]$$

$$= E\left[\int_t\int_t^{\infty\infty} h(\tau)\, n(t-\tau)\, h(\mu)\, n(t-\mu)\, d\tau d\mu\right] . \qquad (1.3.8)$$

Using the linearity of the expectation operator this can be rewritten as

$$p^2_{rms}(t) = \int_t\int_t^{\infty\infty} h(\tau)\, h(\mu)\, E[n(t-\tau)\, n(t-\mu)]\, d\tau d\mu . \qquad (1.3.9)$$

Using equation (1.3.7) this can be evaluated to

$$p^2_{rms}(t) = \sigma^2 \int_t\int_t^{\infty\infty} h(\tau)\, h(\mu)\, \delta(\tau-\mu)\, d\tau d\mu = \sigma^2 \int_t^\infty h^2(\tau)\, d\tau . \qquad (1.3.10)$$

From the effective sound pressure the sound pressure level $L_p(t)$ can be calculated:

$$L_p(t) = 10\log\left(\frac{p^2_{rms}(t)}{p^2_{ref}}\right) = 10\log\left(\sigma^2 \int_t^\infty h^2(\tau)\, d\tau\right), \qquad (1.3.11)$$

in which the reference sound pressure p_{ref} is taken to be 1, for convenience. Thus, the sound pressure level as a function of time can be calculated from the impulse response h(t) using equation (1.3.11). The result of this calculation (usually referred to as reverberation curve or decay curve) can be used to find the instant at which the sound pressure level reaches 60 dB below the starting level. This method of obtaining reverberation times was first discussed by Schroeder (1965).
Note that the integration interval in equation (1.3.11) reaches to infinity. In practice a measured hall's impulse response will always have finite length, so for each time only an approximation of the effective sound pressure can be obtained. In appendix A the minimum impulse response registration time for a given accuracy of the reverberation curve is discussed. The error in the effective sound pressure caused by the finite length of the impulse response recording appears to increase exponentially with time.

1.3.2 Early Decay Time

During a musical performance in a room, a decay in sound pressure level of 60 dB only occurs after a loud accent or final chord. The decay of a signal during running music, however, will be partly masked by the following signals. In this case only the first part of the decay process will be perceived. This means that especially the first part of the decay process is acoustically important. It is usually specified by a quantity called the early decay time (EDT), defined as the time in which the sound pressure level drops by 10 dB after switching off a stationary sound source, multiplied by a factor of 6 (Jordan, 1969).
When measuring decay curves with noise as a test signal, the sound pressure level with the source switched on is fluctuating in time. Therefore the exact moment the source was switched off is hard to find from the reverberation curve. Thus in practice the start of the interval over which the EDT is determined is usually chosen a few decibels below the average stationary level. Most acousticians determine the EDT as the average slope over the time interval in which the sound pressure level drops from 1 to 11 dB below the average stationary level. Some other authors prefer to use the interval from 1 to 15 dB below the stationary level, with a multiplication factor adapted to the changed dynamic range (Kuttruff, 1979). The multiplication factor in the definition of the EDT makes the numeric value of the early decay time directly comparable with the 60 dB reverberation time. As with the reverberation time, the early decay time should be specified in frequency bands and averaged over several source-receiver combinations.

1.3.3 Energy ratios

Another group of important acoustical parameters is formed by the energy ratios. All of these parameters express ratio of the energy in two different time windows of the impulse response.

Generally this group of parameters can be described by the formula

$$ER(t_0, t_1, t_2, t_3) = \frac{E(t_0, t_1)}{E(t_2, t_3)} = \frac{\int_{t_0}^{t_1} h^2(t)\,dt}{\int_{t_2}^{t_3} h^2(t)\,dt}. \qquad (1.3.12)$$

In the past, many different values for the time boundaries in this expression have been used. The acoustical parameters obtained this way all seem to correlate well with the subjective preference of some group of listeners, but different groups of researchers usually found different optimal values.
One energy ratio that has been accepted widely as an important parameter is the clarity index (Reichardt et al., 1975), which is usually denoted as C_{80}:

$$C_{80} = 10\log\left(\frac{\int_{0}^{80ms} h^2(t)\,dt}{\int_{80ms}^{\infty} h^2(t)\,dt}\right)\ [dB]. \qquad (1.3.13)$$

Because of the logarithm in equation (1.3.13) the clarity index is expressed in decibels. When the clarity index equals 0 dB, the total energy of all reflections up to 80 ms, including the direct sound is equal to the energy of all reflections arriving after 80 ms. A positive value of the clarity index means that the early reflection energy part is stronger than the late energy contributions. In this case the perceived sound will have a high subjective clarity, while a negative value of the clarity index indicates a less transparent sound.
For speech intelligibility, the early reflection part of the sound must be as high as possible. This suggests that the clarity index might be used as an indicator of speech intelligibility, but investigations have shown that only reflections up to 50 ms after the direct sound contribute to the intelligibility (see e.g. Lochner et al., 1958), while all reflections arriving later have a detrimental effect. Thus a better measure is found by

using $t_1 = t_2 = 50$ ms in equation (1.3.12). This quantity will be referred to as C_{50}:

$$C_{50} = 10\log\left(\frac{\int_{0}^{50ms} h^2(t)\,dt}{\int_{50ms}^{\infty} h^2(t)\,dt}\right)\ [dB]. \qquad (1.3.14)$$

Another measure for speech intelligibility is the Deutlichkeit D (Thiele, 1953) defined as

$$D = \frac{\int_{0}^{50ms} h^2(t)\,dt}{\int_{0}^{\infty} h^2(t)\,dt}. \qquad (1.3.15)$$

Comparison of equation (1.3.14) and (1.3.15) shows that both measures yield similar information.
Another measure for early sound energy is called "Schwerpunktszeit" t_s, or in English centre time, (Kürer, 1969) and is defined as

$$t_s = \frac{\int_{0}^{\infty} t h^2(t)\,dt}{\int_{0}^{\infty} h^2(t)\,dt}\ [s]. \qquad (1.3.16)$$

Note the extra factor t in the numerator of equation (1.3.16), making this measure deviate from the general definition (1.3.12). In chapter 5 it will be shown that the centre time is equal to the first order length of the impulse response. A low value of the centre time indicates a high level of the primary sound and the early reflections, thus yielding good speech intelligibility and a transparent sound.

1.3.4 Measures for spatial impression

In an enclosure, a listener has the impression of being more or less surrounded by the

sound. This impression is usually described by the term spaciousness. Subjective experiments have pointed out that the perceived spaciousness is well correlated with the amount of early lateral reflections present in the sound field. Thus, spaciousness can be quantified by measures as the lateral energy fraction (Barron et al., 1981), which is defined as the energy ratio of the lateral reflections arriving between 5 and 80 ms after the direct sound to the omni-directional reflections arriving between 0 and 80 ms including the direct sound:

$$LEF = \frac{\int_{5ms}^{80ms} (h^2)_{lat}(t)\,dt}{\int_{0}^{80ms} h^2_{omni}(t)\,dt}. \qquad (1.3.17)$$

In this definition the lateral energy term $(h^2)_{lat}$ means that the squared sound pressure of the reflections arriving at the receiver must be weighted with the cosine of the angle θ between the direction of the reflection and the line through the ears of a virtual listener at the place of the receiver (see figure 1.3.4). The lower limit in the integral of the lateral energy is 5 ms to exclude possible lateral components in the primary sound, as these components do not contribute to spatial impression.
In the literature several other measures of spatial impression in relation to lateral energy can be found, like the lateral efficiency LE (Jordan, 1981) defined as

$$LE = \frac{\int_{25ms}^{80ms} (h_{lat})^2(t)\,dt}{\int_{0}^{80ms} h^2_{omni}(t)\,dt}, \qquad (1.3.18)$$

in which the term $(h_{lat})^2$ means that the effective sound pressure (and not its square) of the reflections arriving at the receiver must be weighted with the cosine of the angle θ between the direction of the reflection and the line through the ears of a virtual listener at the place of the receiver (see figure 1.3.4). An advantage of this measure to the lateral energy fraction is that the lateral term can be measured with a figure eight microphone, while for the LEF a (more expensive) intensity probe should be used in order to weight the squared sound pressure with the cosine factor (Kleiner, 1989).
Another measure for spatial impression is the Raumeindrucksmaß R (Reichardt et

al.,1978) defined as:

$$R = 10\log\left(\frac{\int_{25ms}^{\infty}\left(h^2_{omni}(t)\,dt - \int_{25ms}^{80ms} h^2_R(t)\,dt\right)}{\int_{0}^{25ms}\left(h^2_{omni}(t)\,dt + \int_{25ms}^{80ms} h^2_R(t)\,dt\right)}\right)\ [dB]. \qquad (1.3.19)$$

The term $h_R(t)$ in equation (1.3.19) denotes the frontal mean-square sound pressure arriving at the listener, measured using a figure eight microphone directed forward.
A different type of measure that correlates well with the subjective spatial impression is the interaural cross correlation coefficient (Ando,1985). This measure, usually abbreviated as IACC, is difficult to calculate because it should be determined from a binaural signal. This means that the response of a (dummy) head must be included in the calculations. During measurements, however, a dummy head can be used for recording instead of a normal microphone, making the signals at both ears available in a simple way. As the IACC is determined from the cross correlation between the sig-

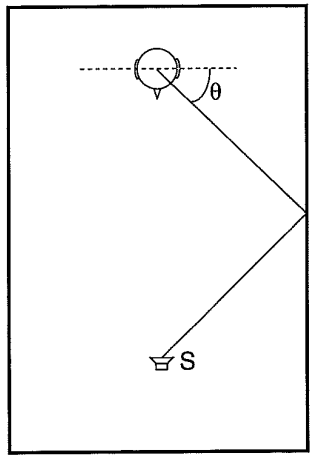

Figure 1.3.4: *The angle θ between the line through the ears of a (dummy) head and the direction of the incident sound is used to indicate the direction of a reflection.*

nals at both ears of the listener, it depends both on the hall response and on the auto correlation of the source signal. It appeared that the spaciousness predicted by the IACC is not valid for all types of source signal.
A recent study (Potter, 1992) has shown that a measure of spaciousness called the central modulation coefficient (CMC) can predict auditory spaciousness quite well for a large class of source signals. This measure is based on the central spectrum theory (Raatgever and Bilsen, 1986), that describes the binaural processing of acoustic signals by the human brain in terms of a central activity pattern, that is a function of frequency and internal interaural delay. The CMC can be calculated from the modulation depth of this central activity pattern for a given binaural stimulus or a dummy head recording.

1.3.5 Stage parameters

For an orchestra to be able to play together, the members should be able to hear each other well. Because the path of the direct sound from one side of the stage to the other is usually blocked by the musicians themselves, some early reflections are absolutely necessary on stage. The boundaries of the time window for the reflections to be useful is given by 17<t<35 ms (Marshall et al., 1978). Apart from these early reflections, some feedback of the hall response (reverberation) is usually preferred by the musicians.
A measure for the support of the musicians by the environment called ST1 is defined as the logarithmic ratio between the mean-square sound pressure of the reflections arriving between 20 and 100 ms after the direct sound, and the direct sound including the possible reflections within 10 ms:

$$ST1 = 10\log\left(\frac{\int_{20ms}^{100ms} h^2(t)\,dt}{\int_{0}^{10ms} h^2(t)\,dt}\right) \text{[dB]}. \qquad (1.3.20)$$

This measure gives an indication of the possibility for musicians to hear each other on stage.
A measure that correlates well with the overall impression of the acoustics on stage relates the mean-square sound pressure of the reflections arriving in the first 10 ms

after the direct sound to the mean-square sound pressure of the reflections arriving between 20 and 200 ms. This measure is called ST2 and is defined as:

$$ST2 = 10\log\left(\frac{\int_{20ms}^{200ms} h^2(t)\,dt}{\int_{0}^{10ms} h^2(t)\,dt}\right) \text{[dB]}. \qquad (1.3.21)$$

It is clear that this measure is highly correlated with ST1, but due to the longer integration range in the numerator, ST2 contains some more information of the hall response feedback to the stage. Both measures ST1 and ST2 were introduced by Gade (1990).

1.4 Acoustical requirements for several types of halls

Although it is impossible to formulate the exact acoustical requirements of a hall for a given performance, some global statements can be made that are generally accepted in the world of acoustics. In the next subsections such a global description will be given for several types of halls. The requirements will be formulated in terms of primary sound, early reflections and reverberation. A more thorough overview of the acoustic research in the last century is given by Beranek (1992).

1.4.1 Lecture halls

In the past the subject of speech intelligibility has been examined thoroughly. From this research it can be concluded that sound reflections up to about 50 ms after the direct sound lead to improved intelligibility, while all reflections arriving later are detrimental (Lochner et al., 1958). Thus for lecture halls the primary sound and the early reflections should contain much more energy than the reverberation in order to obtain a good speech intelligibility.
For the lecturer it is important to hear some hall response feedback, in order to determine whether his voice reaches the audience at a sufficient level or not. Usually this is accomplished when the hall has a reverberation time of 1.0 second, yielding a good

compromise between intelligibility for the audience and 'monitoring' for the speaker.

1.4.2 Theatres

In a theatre the speech intelligibility is of main importance. This means that the acoustic requirements for a theatre are more or less the same as for a lecture hall. Some strong early reflections from the side walls may be required to increase the spaciousness perceived. The acoustical requirements for theatres used for musical or operetta will be discussed together with the opera houses in section 1.4.7.

1.4.3 Halls for recitals

During a recital the intimacy is an acoustic parameter of great importance. A hall for recitals needs clear primary sound, some early reflections and a reverberation time of about 1.2 seconds. A large spaciousness is often disliked.

1.4.4 Halls for chamber music

For the performance of chamber music most listeners prefer a clear direct sound, supported by little reverberation. The clear sound can be obtained by adding a significant amount of early reflections to the direct sound, which is most easily obtained in a rather small room (chamber). When the absorption at the room boundaries is not too large, there will also be a reasonable amount of reverberation. The preferred reverberation time is between 1.2 and 1.6 seconds.
When chamber music is performed in small halls (as is often the case), the absorption at the room boundaries should be much larger than in the small chamber discussed above, in order to arrive at the required reverberation time. The hall shape should be chosen such that at each listening position a sufficient amount of primary sound and early reflections will be present.

1.4.5 Halls for symphonic and choral music

The optimal conditions for listening to a large symphony orchestra depend largely on the kind of music performed. E.g., for baroque music the reverberation time should not be too large (less than 1.5 seconds), while the early energy parts must be relatively high. For romantic music, on the contrary, much more reverberation can be allowed (reverberation times up to about 2.5 second) for the same amount of early energy. Especially for large choirs and for community singing a long reverberation time is preferred, both by the audience and by the performers. The optimum reverberation time of a hall also depends on its size, i.e., in a large hall the reverberation time must be larger than in a small hall to obtain the same preference.

1.4.6 Churches and cathedrals

Especially the old churches and cathedrals all over the world are famous for their long reverberation times of 5 seconds or even more. These buildings are acoustically well suited for the old, rather slow church music (choir, organ). Due to the large dimensions, the early sound reflection energies in these buildings are very small, while the reverberant energy is very large.
A consequence of the large reverberation time is that in churches usually the transparency is low and the speech intelligibility is very bad. A reflector behind and/or above the lectern will increase the primary sound and thus contribute to the speech intelligibility, but for very large churches the effect of these reflectors is usually not enough. Therefore, usually electro-acoustic direct sound enhancement systems are used.

1.4.7 Opera houses

For the intelligibility of the text sung by opera performers the same conditions as those for speech should be fulfilled. At the same time, the music played by the orchestra is best suited with the conditions discussed in section 1.4.5. It is clear that these conditions contradict each other, so that a compromise is needed. Usually, the reverberation

time in opera houses is about 1.6 seconds, with as much early reflections as possible to improve intelligibility.
In most opera houses, the orchestra is placed in the orchestra pit. As a consequence, the direct sound from the orchestra, both to the audience and to the actors on stage is (almost completely) absent. A large reflector above the orchestra pit can create some early reflections for the audience, but the orchestra sound will always be less clear than in the concert hall situation, with the orchestra on stage. Nowadays, electro-acoustic monitoring of the orchestra on the stage is often applied.

1.5 Multi-purpose halls and variable acoustics

In section 1.4.7 the discussion of the acoustical requirements of an opera house already indicated that combining the contradictory requirements for speech intelligibility and musical quality necessarily leads to a compromise. For multipurpose halls the situation is even worse, because these types of halls are used for all different kinds of performances ranging from lectures to symphonic concerts. Most multipurpose halls are designed for good speech transmission, which makes them suitable for lectures and drama, but a direct consequence is that their qualities for musical performances are usually rather poor.
To make a multipurpose hall really suitable for all kinds of performances, it must be possible to change the acoustical properties in a simple way. Full acoustic control can be obtained by having the ability to change the primary sound, the early reflections and the reverberation independently. In the next subsections the realisation of variable acoustics will be discussed, using either architectural or electro-acoustic solutions.

1.5.1 Variable acoustics by architectural means

As discussed in section 1.2 the impulse response for a particular source-receiver combination in a hall is determined by both the hall shape and the reflecting properties of the hall boundaries. Hence it is possible to change the hall response by changing either the reflecting properties of the boundaries or by changing the hall shape. Both methods will be briefly discussed here.

To control the primary sound with architectural means some (re-)movable reflectors must be attached near the sound source. In lecture rooms and churches often a reflector is found above the lectern to add some reflections that arrive at the listeners shortly after the direct sound (see figure 1.5.1).Some additional reflectors might be found at the side edges of the stage. By changing the absorption coefficient of the reflector surface or the direction of the reflector the primary sound can be altered.
To control the early reflection part of the sound field the reflecting properties of the side walls, the ceiling and the backstage wall should be variable. This can be accomplished most easily by providing (part of) the side walls with heavy curtains. Better results can be obtained by attaching pivoting panels to the side walls with two or more surfaces, each with different sound reflecting properties (see figure 1.5.2). The required amount of early reflections can be obtained by making an appropriate distribution of absorption coefficients along the walls.
A more rigorous method to change the early reflections in the hall is by making the walls and the ceiling movable, such that the room shape can be altered. In this way the total reflection pattern within the room will be changed. In combination with the pivoting wall panels described before the ranges of variability for the early reflections become very large. The IRCAM hall in Paris is the ultimate example of a hall with variable acoustics by architectural means.
The reverberation in a room is formed by the sound that has been reflected several times against the room boundaries. The amount of reverberation is determined by the average absorption coefficient of all surfaces and the average wave front travel time between two consecutive reflections against a room boundary. The average absorp-

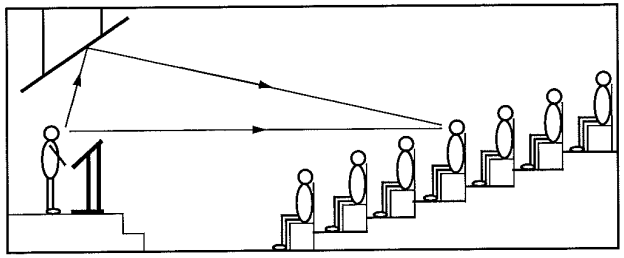

Figure 1.5.1: *A sound reflector above the lectern in a lecture hall to increase the primary sound.*

tion can be changed by changing the absorption coefficient of one or more surface elements. As for the early reflections discussed before, this can be accomplished either by providing part of the walls with heavy curtains or by using pivoting panels with different absorption coefficients at each side.
A larger change in the reverberation of the hall can be obtained by changing the volume. This can be accomplished by changing the position of the walls, the floor or the ceiling of the room, thus changing the reflection pattern and the average time between the reflections.
A special note should be made about the orchestra environment. In a concert hall the orchestra platform is usually surrounded by some reflecting walls which radiate some of the generated energy back to the musicians. Because of the almost complete absence of direct sound from one orchestra member to the other, these reflections are very important for the musicians to hear each other.
In a multi-purpose hall the orchestra is placed on a stage meant for drama performances. This means that the reflecting side walls near the orchestra are absent, while

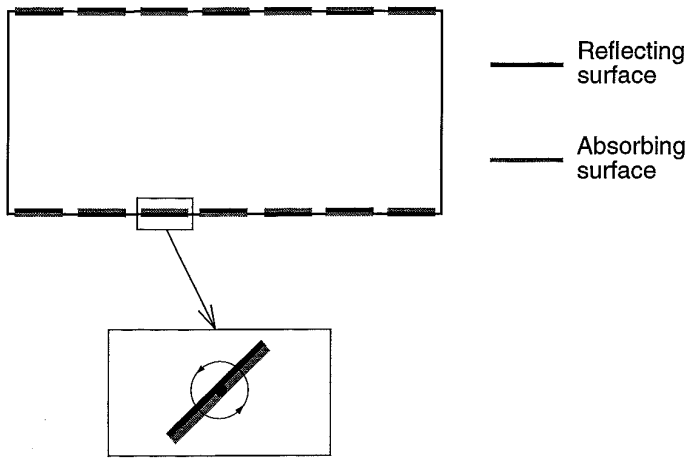

Figure 1.5.2: *A hall with pivoting panels at the side walls to change the early reflection properties of the hall.*

the stage tower above the orchestra, often filled with sound absorbing objects, makes reflections from the ceiling (if any) arrive too late. In order to create some useful sound reflections, the orchestra is sometimes surrounded at the top, the back and the sides by a removable orchestra shell. The reflections from this structure can drastically improve the acoustical situation for the musicians.
Some examples of variable acoustics by architectural means are given by Heringa et al. (1989).

1.5.2 Variable acoustics by electro-acoustic means

The architectural solutions to variable acoustics discussed in the previous section have the disadvantage that usually complex and expensive structures are required in order to obtain a useful range of variation for the acoustic parameters. A much more effective and flexible approach to acoustic control is the use of electro-acoustic systems. In this section the electro-acoustic approach to acoustic control will be discussed.
An electro-acoustic system can be used to enhance the primary sound by recording the sound of the sources with some microphones, mixing these microphone signals together and using an amplifier and a loudspeaker to radiate a replica of the source signals into the hall (see figure 1.5.3). Usually two loudspeakers are used, one at each side of the stage.
A problem with this simple setup is that the loudspeaker sound arrives at many listeners prior to the sound from the sources. This means that the listeners will locate the sound sources at the loudspeaker positions instead of at their true positions on stage, because of the law of the first wave front or 'Haas-effect' (Haas,1951). Applying a delay to the loudspeaker signals will solve this problem, provided that the loudspeaker sound and the source sound are not too different with respect to direction and loudness (Ahnert, 1986).
A problem with this kind of amplification system arises when the sound sources are moving around the stage. For a moving source, the delay times required for the loudspeakers vary with time. Only a complicated system that continually adapts the delays according to the momentary source position can make this system work properly. Some mechanism to trace the moving sources on stage should be provided.
A better approach to primary sound control would be to build a system that creates a

replica of the wave fronts generated by the sound sources on stage. This way both the sound waves from the sources and their amplified replicas contain the same directional information, so no localisation problems will occur. The concept of wave field synthesis was introduced by Berkhout (1988). An up to date overview can be found in Berkhout et al. (1993).

The wave field generation technique can also be used to synthesise the direct wave field of an orchestra in the orchestra pit of an opera house. This synthesised wave field can be radiated into the hall as a replacement for the absent direct sound. This way a more natural orchestra sound can be obtained. In the same way, the direct sound of the orchestra can be generated on stage, such that the actors can also hear the orchestra well.

Another application of a wave front generating system is the generation of early reflections, since the wave front of a point source S reflected in a room boundary can be described as the direct wave front of an image source S' at the other side of the wall, the position of S' being the geometrical image of source S mirrored in the boundary plane of the room (see figure 1.5.4). Thus, by calculating the geometrical images of all sources in the room boundaries (including multiple reflections), a wave front generating system can be used to generate the early reflections by adding the (synthesised) wave fields of all image sources.

Although reverberation can also be described in terms of image sources a statistical description is more appropriate for the design of an electro-acoustic system generating reverberation. A loudspeaker distribution throughout the hall, generating a decaying

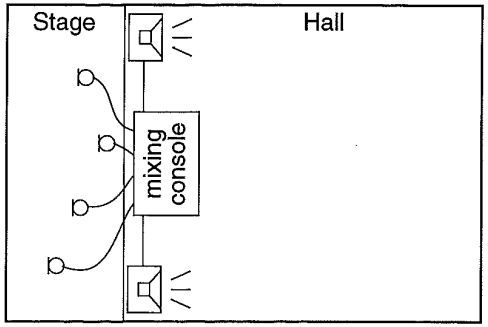

Figure 1.5.3: *Standard setup for direct sound amplification.*

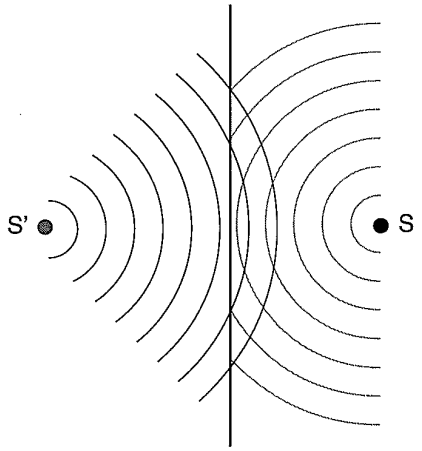

Figure 1.5.4: *The wave front of a point source S reflected against a room boundary can be described as the wave front of a point source S', which is the geometrical image of S in the reflecting surface.*

sound field with a low amount of colouration at each listening position will create the desired effect. In practice electronic circuits with an impulse response consisting of an exponentially decaying impulse series are used to generate a reverberant field with a variable decay time.

1.5.3 Outline of this thesis

In chapter 2 of this thesis a short overview all relevant wave theory is given. In chapter 3 this theory is used to derive the basic equations of wave field synthesis. All simplifications necessary to arrive at a physically realisable system are discussed. In chapter 4 the design of a wave field synthesis system is given, with both an objective and a subjective evaluation of the results.

In chapter 5 the behaviour of an electro-acoustic system for reflection generation and

reverberation enhancement is discussed. A complete modelling scheme, including all relevant hall transfer functions and acoustic feedback is given. The results are compared with measurements in a hall equipped with an electro-acoustic system. Finally, chapter 6 gives an overview of the results and conclusions of the previous chapters.

2. THEORY

2.1 Wave Theory

In a fluid at equilibrium, not influenced by any external mechanisms, a pressure distribution will be present which is constant in time. Usually this static pressure will depend on the position in the medium.
When some external source starts acting on the fluid, the static pressure distribution in the near vicinity of the source will be disturbed. These disturbances in turn are passed to neighbouring parts of the fluid, moving away from the source with a speed determined by the density and the compressibility of the medium. This way, a time-variant pressure field is built up in the fluid. The difference between this time-variant pressure and the static pressure is called the acoustic pressure. Usually the acoustic pressure will depend both on time and on position.
For a source-free part of the medium, the linear acoustic pressure in the space-time domain is described by the well known acoustic wave equation:

$$\rho(\mathbf{r})\,\nabla\cdot\left(\frac{1}{\rho(\mathbf{r})}\nabla p(\mathbf{r},t)\right)-\frac{1}{c^2(\mathbf{r})}\frac{\partial^2}{\partial t^2}p(\mathbf{r},t)=0\,. \qquad (2.1.1)$$

In this equation $\rho(\mathbf{r})$ denotes the static medium density at position $\mathbf{r}=(x,y,z)$, $c(\mathbf{r})$ is the propagation velocity of acoustic waves at this position and $p(\mathbf{r},t)$ is the time-dependent pressure at this point. For a homogeneous medium both $\rho(\mathbf{r})$ and $c(\mathbf{r})$ are independent

of position, so in that case equation (2.1.1) can be simplified to:

$$\nabla^2 p(\mathbf{r},t) - \frac{1}{c^2}\frac{\partial^2}{\partial t^2} p(\mathbf{r},t) = 0 , \qquad (2.1.2)$$

the constant c denoting the acoustic wave velocity of the medium. In room acoustics the medium is air, which can be assumed to be homogeneous under normal conditions. Therefore equation (2.1.2) will be used as the basic equation of this thesis.
When an acoustic point source (monopole) is situated at position $r_i=(x_i,y_i,z_i)$ in the medium, equation (2.1.2) will be valid everywhere except at the position of the source. It can be shown (Berkhout, 1987) that adding a spatial delta-pulse, multiplied by the source signal $s_i(t)$ to the right hand side of equation (2.1.2) will make this equation valid at the source position too:

$$\nabla^2 p(\mathbf{r},t) - \frac{1}{c^2}\frac{\partial^2}{\partial t^2} p(\mathbf{r},t) = -4\pi s_i(t)\,\delta(\mathbf{r}-\mathbf{r}_i) , \qquad (2.1.3)$$

in which $s_i(t)$ is the time signal generated by the source and $\delta(\mathbf{r})$ is the spatial delta pulse.
When more sources are present in the medium, a delta-pulse should be added for each individual point source:

$$\nabla^2 p(\mathbf{r},t) - \frac{1}{c^2}\frac{\partial^2}{\partial t^2} p(\mathbf{r},t) = -4\pi \sum_i s_i(t)\,\delta(\mathbf{r}-\mathbf{r}_i) . \qquad (2.1.4)$$

Sources of a more complex shape than a monopole can be accounted for by describing them in terms of a monopole distribution.
In wave theory an analysis in terms of frequency components is often more appropriate. Applying a Fourier transformation to equation (2.1.4) yields:

$$\nabla^2 P(\mathbf{r},\omega) + k^2 P(\mathbf{r},\omega) = -4\pi \sum_i S_i(\omega)\,\delta(\mathbf{r}-\mathbf{r}_i) , \qquad (2.1.5)$$

in which k is the wave number defined by $k=\omega/c$, $P(\mathbf{r},\omega)$ is the Fourier transform of the sound field $p(\mathbf{r},t)$, and $S_i(\omega)$ is the Fourier transform of the source function $s_i(t)$. For a source free medium equation (2.1.5) reduces to the well known Helmholtz equation:

$$\nabla^2 P(\mathbf{r},\omega) + k^2 P(\mathbf{r},\omega) = 0 . \qquad (2.1.6)$$

2.2 The Kirchhoff representation integral

According to the Huygens principle, the propagation of a wave front through a particular medium can be described by recursively adding the contribution of a number of secondary point sources distributed along the wave front (see figure 2.2.1). Thus, for a source free volume V inside an arbitrary medium, the wave field at an internal point A, caused by some external source distribution, can be determined by calculating the wave field of the distribution of secondary sources over the surface S (figure 2.2.2). In order to calculate the wave field at point A, the acoustic transmission paths from the surface S towards A must be known.
For a homogeneous medium, the acoustical transmission path from a surface point to point A is the same as the acoustical transmission path from point A to that point. Thus, in this case the medium properties required to calculate the response of an external source distribution at some point A inside V can be determined by calculating the

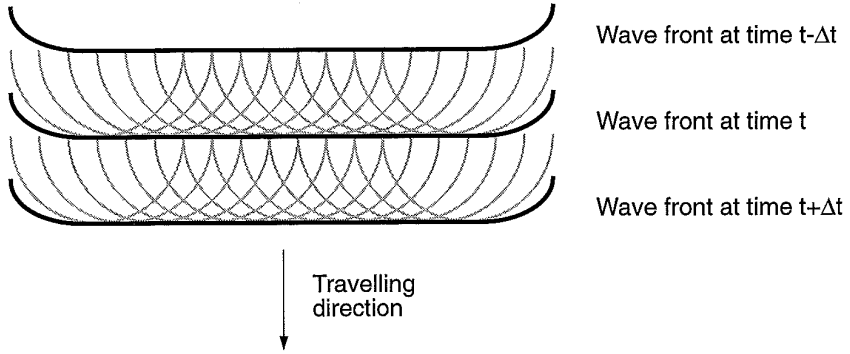

Figure 2.2.1: *Illustration of the Huygens principle of wave propagation: each point of the momentary wave front is viewed as a secondary point source that radiates spherical waves. The new wave front is formed by the envelope of all secondary wave fronts.*

response at the surface S of a point source in A (see figure 2.2.3). This response can be interpreted as the spatial impulse response from A to the surface S. A mathematical proof of the qualitative statements above will be given in the next part of this section. Consider the situation depicted in figure 2.2.2 again: A wave field $P(\mathbf{r},\omega)$ is generated by a primary source distribution located outside volume V. Inside volume V this wave field will obey the Helmholtz equation (2.1.6). Next consider the situation of figure 2.2.3 again: A monopole source is positioned at a point A somewhere inside volume V. Assuming that the source function generated by this monopole source is independent of frequency, i.e. $S(\omega)=1$, the wave field generated by this source should obey the equation:

$$\nabla^2 G(\mathbf{r},\omega) + k^2 G(\mathbf{r},\omega) = -4\pi\delta(\mathbf{r}-\mathbf{r}_A) \ . \qquad (2.2.1)$$

The function $G(\mathbf{r},\omega)$ in equation (2.2.1) is called Green's function. Combination of equation (2.2.1) with the Helmholtz equation (2.1.6) yields:

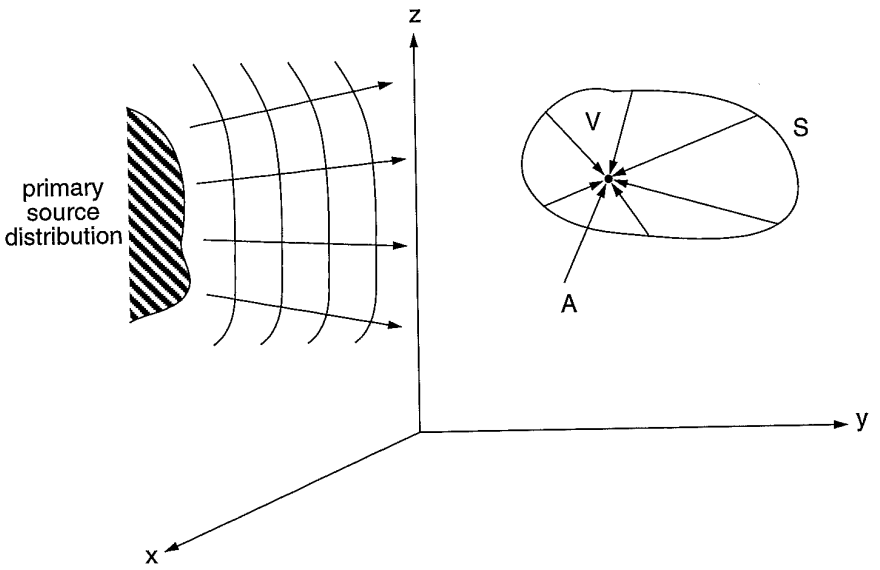

Figure 2.2.2: *An arbitrary source distribution outside volume V generates a wave field. The value of this wave field inside V can be calculated from data measured at the surface S of volume V.*

$$P(\mathbf{r},\omega)\nabla^2 G(\mathbf{r},\omega) - G(\mathbf{r},\omega)\nabla^2 P(\mathbf{r},\omega) = -4\pi\delta(\mathbf{r}-\mathbf{r}_A)P(\mathbf{r},\omega) \ . \qquad (2.2.2)$$

Integration of equation (2.2.2) over volume V gives:

$$-\frac{1}{4\pi}\int_V (P(\mathbf{r},\omega)\nabla^2 G(\mathbf{r},\omega) - G(\mathbf{r},\omega)\nabla^2 P(\mathbf{r},\omega))\,dV = P(\mathbf{r}_A,\omega) \ , \qquad (2.2.3)$$

in which $P(\mathbf{r}_A,\omega)$ denotes the Fourier transformed pressure at position A.

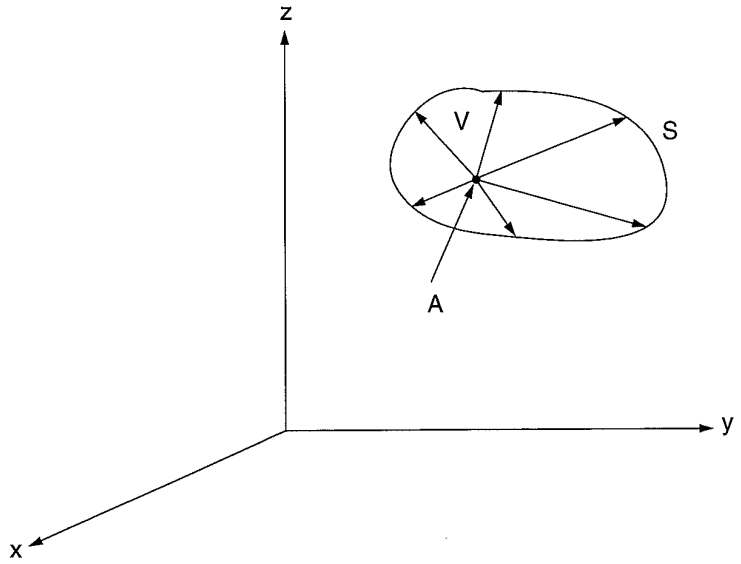

Figure 2.2.3: *The wave field at the surface S of volume V caused by a monopole source in point A can be calculated when the acoustical transmission paths from A towards every point of S is known. For a homogeneous medium the acoustical transmission path from A towards the surface is the same as the acoustical transmission path in the reverse direction.*

Using Green's theorem:

$$\int_V (P\nabla^2 G - G\nabla^2 P)\,dV = -\int_S (P\nabla G - G\nabla P)\cdot \mathbf{n}dS\,, \qquad (2.2.4)$$

in which **n** is an inward pointing normal vector on surface S, it is found that:

$$P(\mathbf{r}_A, \omega) = \frac{1}{4\pi}\int_S (P(\mathbf{r}, \omega)\nabla G(\mathbf{r}, \omega) - G(\mathbf{r}, \omega)\nabla P(\mathbf{r}, \omega))\cdot \mathbf{n}dS\,. \qquad (2.2.5)$$

Using the above assumption that $G(\mathbf{r},\omega)$ is the wave field of a monopole with a source function independent of frequency:

$$G(\mathbf{r}, \omega) = \frac{e^{-jk\Delta r}}{\Delta r}\,, \qquad (2.2.6)$$

in which $\Delta r = |\,\Delta\mathbf{r}\,| = |\,\mathbf{r}_A - \mathbf{r}\,|$ is the distance from the source position to the observation point **r**:

$$\Delta r = \sqrt{(x_A - x)^2 + (y_A - y)^2 + (z_A - z)^2}\,, \qquad (2.2.7)$$

equation (2.2.5) can be rewritten as:

$$P(\mathbf{r}_A, \omega) = \frac{1}{4\pi}\int_S \left(P(\mathbf{r}, \omega)\frac{1 + jk\Delta r}{\Delta r}\cos\varphi\frac{e^{-jk\Delta r}}{\Delta r} - \frac{\partial P(\mathbf{r}, \omega)}{\partial n}\frac{e^{-jk\Delta r}}{\Delta r}\right)dS\,, \qquad (2.2.8)$$

φ being the angle between vector $\Delta\mathbf{r}$ and the inward pointing surface normal vector **n** (see figure 2.2.4). Equation (2.2.8) proves the statement that the acoustic pressure $P(\mathbf{r}_A,\omega)$ at an arbitrary point A inside volume V can be found from data measured only at the surface S that bounds volume V.
Finally, using the equation of motion it can be shown that:

$$\frac{\partial P(\mathbf{r}, \omega)}{\partial n} = -j\omega\rho V_n(\mathbf{r}, \omega)\,, \qquad (2.2.9)$$

V_n being the normal component of the particle velocity in the wave field. Substituting

equation (2.2.9) in equation (2.2.8) yields:

$$P(\mathbf{r}_A, \omega) = \frac{1}{4\pi}\int_S P(\mathbf{r}, \omega)\frac{1 + jk\Delta r}{\Delta r}\cos\varphi\frac{e^{-jk\Delta r}}{\Delta r}dS + \frac{1}{4\pi}\int_S j\omega\rho V_n(\mathbf{r}, \omega)\frac{e^{-jk\Delta r}}{\Delta r}dS\,. \qquad (2.2.10)$$

Equation (2.2.10) is called the Kirchhoff representation integral for homogeneous media. The first term in equation (2.2.10) represents a dipole source distribution over surface S, the strength of each dipole being given by the pressure $P(\mathbf{r},\omega)$ of the incident wave field, while the second term represents a monopole source distribution over surface S, the strength of each monopole source being given by the normal component of the particle velocity $V_n(\mathbf{r},\omega)$ of the incident wave field. The total wave field is the superposition of these two source distributions.

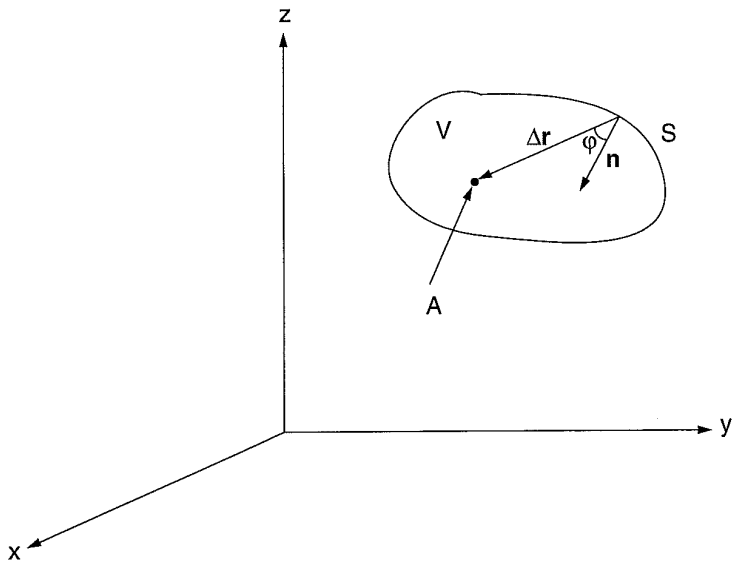

Figure 2.2.4: *Definition of the angle φ between the vector $\Delta\mathbf{r}$ pointing from the surface S towards point A and the inward-pointing surface normal vector* **n**.

2.3 The Rayleigh representation integrals

In the derivation of equation (2.2.5) the only assumption made about the wave field $G(\mathbf{r},\omega)$ was that it should obey equation (2.2.1) inside volume V. The wave field given by expression (2.2.6) fulfills this condition, but any other wave field $H(\mathbf{r},\omega)$ generated by sources outside volume V can be added to $G(\mathbf{r},\omega)$, because inside volume V the function $H(\mathbf{r},\omega)$ will satisfy

$$\nabla^2 H(\mathbf{r},\omega) + k^2 H(\mathbf{r},\omega) = 0 . \qquad (2.3.1)$$

It would be interesting to find a function $H(\mathbf{r},\omega)$ such that either

$$\forall(\mathbf{r} \in S) : \nabla (G(\mathbf{r},\omega) + H(\mathbf{r},\omega)) \cdot \mathbf{n} = 0 , \qquad (2.3.2a)$$

or

$$\forall(\mathbf{r} \in S) : G(\mathbf{r},\omega) + H(\mathbf{r},\omega) = 0 \qquad (2.3.2b)$$

is fulfilled. It is very difficult to derive a closed form expression for wave field $H(\mathbf{r},\omega)$ for a general surface S, but in the special case that S is a plane surface an expression for $H(\mathbf{r},\omega)$ can be found.
Consider the situation depicted in figure 2.3.3: A wave field $P(\mathbf{r},\omega)$ is generated by sources in the half space $z<0$. Volume V is determined by the plane $z=0$ and a hemisphere of radius R in the half space $z>0$. Because all sources are located in the half space $z<0$, volume V will be source free for all values of R.
According to the Sommerfeld radiation criterion (see e.g. Bleistein, 1984) the contribution of the surface integral over the hemisphere cancels when radius R becomes infinite. In that case only the integral over the plane $z=0$ is left. The remaining problem is to find a wave field $H(\mathbf{r},\omega)$ such that either condition (2.3.2a) or condition (2.3.2b) is fulfilled in the entire plane $z=0$. This problem will be solved in the next subsections.

2.3.1 The Rayleigh I representation integral

In order to satisfy equation (2.3.2a) in the plane $z=0$, $H(\mathbf{r},\omega)$ must be a wave field generated by sources in the half space $z<0$ that causes a particle velocity distribution in

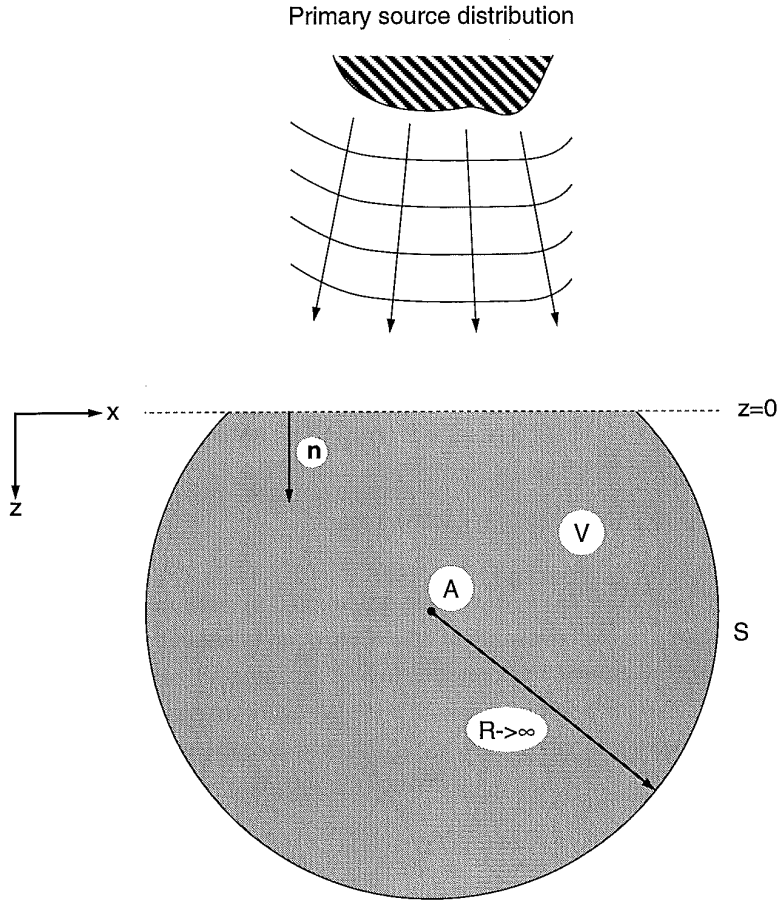

Figure 2.3.1: *The volume used in the derivation of the Rayleigh representation integrals is determined by the plane z=0 and a hemisphere with radius R in the half space z>0*

the plane z=0 the normal component of which is equal in magnitude, but opposite in sign to the normal component of the particle velocity of a monopole source in point A. It is clear that a monopole at A', the image of point A mirrored in the plane z=0, will generate such a wave field, because the distance from a point in the plane z=0 to A is equal to the distance of this point to A', while the waves from the sources in A and A' arrive at the plane z=0 from opposite directions.
Thus H(**r**,ω) is given by:

$$H(\mathbf{r}, \omega) = \frac{e^{-jk\Delta r'}}{\Delta r'} , \tag{2.3.3}$$

with $\Delta r' = |\Delta \mathbf{r}'| = |\mathbf{r}_{A'} - \mathbf{r}|$ (see figure 2.3.4).
Substituting G+H instead of G in the expression for the Kirchhoff integral (2.2.5) and using equation (2.3.2a) yields:

$$P(\mathbf{r}_A, \omega) = -\frac{1}{4\pi} \int_{z=0} ((G(\mathbf{r}, \omega) + H(\mathbf{r}, \omega)) \nabla P \cdot \mathbf{n}) \, dxdy . \tag{2.3.4}$$

From equations (2.2.6) and (2.3.3) it follows that:

$$G(\mathbf{r}, \omega) = H(\mathbf{r}, \omega) \text{ for } z = 0. \tag{2.3.5}$$

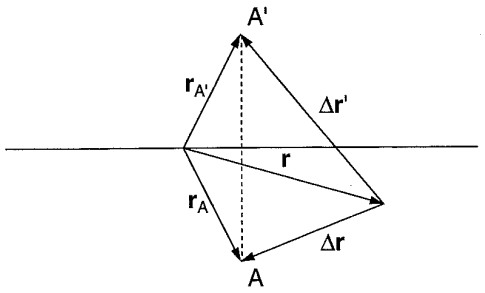

Figure 2.3.2: *Point A and its image A' mirrored in the plane z=0*

Hence, equation (2.3.4) can be written as:

$$P(\mathbf{r}_A, \omega) = -\frac{1}{2\pi} \int_{z=0} G(\mathbf{r}, \omega) \nabla P(\mathbf{r}, \omega) \cdot \mathbf{n} dxdy , \tag{2.3.6}$$

or, using equation (2.2.6) and equation (2.2.9):

$$P(\mathbf{r}_A, \omega) = \frac{1}{2\pi} \int_{z=0} j\omega\rho V_n(\mathbf{r}, \omega) \frac{e^{-jk\Delta r}}{\Delta r} dxdy . \tag{2.3.7}$$

Equation (2.3.7) is called the Rayleigh I representation integral. It states that the wave field in the half space z>0 can be synthesised by a virtual monopole distribution over the plane z=0, the strength of each monopole being given by the normal component of the particle velocity of the wave field measured at the position of this particular monopole in the plane z=0.

2.3.2 The Rayleigh II representation integral

In order to satisfy equation (2.3.2b) at the plane z=0, a pressure field must be found that is equal in magnitude but opposite in sign to the wave field of a monopole source at position A. Because the pressure field of a monopole depends on the distance from the source position only, the wave field of a monopole source at position A', the image of point A mirrored in the plane z=0, which generates the signal of the monopole source in A in counterphase, will yield zero pressure in the plane z=0.
Thus, H(**r**,ω) is given by:

$$H(\mathbf{r}, \omega) = -\frac{e^{-jk\Delta r'}}{\Delta r'} , \tag{2.3.8}$$

with $\Delta r' = |\Delta \mathbf{r}'| = |\mathbf{r}_{A'} - \mathbf{r}|$.
Substituting G+H instead of G in the expression for the Kirchhoff integral (2.2.5) and using (2.3.2b) yields:

$$P(\mathbf{r}_A, \omega) = \frac{1}{4\pi} \int_{z=0} P(\mathbf{r}, \omega) \nabla (G(\mathbf{r}, \omega) + H(\mathbf{r}, \omega)) \cdot \mathbf{n} dxdy . \tag{2.3.9}$$

From equations (2.2.6) and (2.3.8) it follows that

$$\nabla G(\mathbf{r}, \omega) \cdot \mathbf{n} = \nabla H(\mathbf{r}, \omega) \cdot \mathbf{n} \text{ for } z = 0 . \tag{2.3.10}$$

Thus, equation (2.3.9) can be rewritten as:

$$P(\mathbf{r}_A, \omega) = \frac{1}{2\pi} \int_{z=0} P(\mathbf{r}, \omega) \nabla G(\mathbf{r}, \omega) \cdot \mathbf{n} dxdy , \tag{2.3.11}$$

or, substituting equation (2.2.6):

$$P(\mathbf{r}_A, \omega) = \frac{1}{2\pi} \int_{z=0} P(\mathbf{r}, \omega) \frac{1+jk\Delta r}{\Delta r} \cos\varphi \frac{e^{-jk\Delta r}}{\Delta r} dxdy . \tag{2.3.12}$$

Equation (2.3.12) is called the Rayleigh II representation integral. It states that the wave field in the half space z>0 can be synthesised by a virtual dipole distribution in the plane z=0, the strength of each dipole being given by the pressure of the incident wave field measured at its particular position.

2.3.3 The Rayleigh III representation integral

Equation (2.3.7) and (2.3.12) describe the calculation of pressure data from particle velocity data and from pressure data respectively. It is also possible to calculate the components of the particle velocity in point A by using equation (2.3.12) in combination with the equation of motion:

$$\nabla P = -j\omega\rho \mathbf{V} . \tag{2.3.13}$$

From equation (2.3.12) it is found that

$$\nabla_A P(\mathbf{r}_A, \omega) = \frac{1}{2\pi} \int_{z=0} P(\mathbf{r}, \omega) \nabla_A \left(z_A \frac{1+jk\Delta r}{\Delta r^3} e^{-jk\Delta r} \right) dxdy , \tag{2.3.14}$$

in which ∇_A denotes the operator $(\frac{\partial}{\partial x_A}, \frac{\partial}{\partial y_A}, \frac{\partial}{\partial z_A})$.

Thus it is found that

$$\mathbf{V}(\mathbf{r}_A, \omega) = \frac{-(j\omega\rho)^{-1}}{2\pi} \int_{z=0} P(\mathbf{r}, \omega) \mathbf{Q} \frac{e^{-jk\Delta r}}{\Delta r} dxdy , \tag{2.3.15}$$

the vector $\mathbf{Q}=(Q_x,Q_y,Q_z)$ being given by

$$Q_x = (x_A - x) \frac{k^2\Delta r^2 - 3(1+jk\Delta r)}{\Delta r^3} \cos\varphi , \tag{2.3.16a}$$

$$Q_y = (y_A - y) \frac{k^2\Delta r^2 - 3(1+jk\Delta r)}{\Delta r^3} \cos\varphi , \tag{2.3.16b}$$

$$Q_z = \frac{(1+jk\Delta r)(1-3\cos^2\varphi) + k^2\Delta r^2\cos^2\varphi}{\Delta r^3} . \tag{2.3.16c}$$

Equation (2.3.15) is called the Rayleigh III representation integral. Comparison of this expression with the Rayleigh II integral shows that the calculation of particle velocity data from pressure measurements in the plane z=0 is much more complex than the calculation of pressure data from the same measurements. For a recursive use of the Rayleigh integrals, only the normal component of the particle velocity at each depth level needs to be known. Hence, from equations (2.3.16a), (2.3.16b) and (2.3.16c) the last one is of main importance.

2.3.4 The Rayleigh IV representation integral

To transform particle velocity measurements into particle velocity data at another depth level, the equation of motion should be used in combination with the Rayleigh I integral. Combining equations (2.3.13) and (2.3.7) yields for the particle velocity at point A:

$$\mathbf{V}(\mathbf{r}_A, \omega) = -\frac{1}{2\pi} \int_{z=0} V_n(\mathbf{r}, \omega) \nabla_A \left(\frac{e^{-jk\Delta r}}{\Delta r} \right) dxdy . \tag{2.3.17}$$

Using the definition of the operator ∇_A, equation (2.3.17) can be written as

$$\mathbf{V}(\mathbf{r}_A, \omega) = \frac{1}{2\pi} \int_{z=0} V_n(\mathbf{r}, \omega)\, \hat{\mathbf{Q}} \frac{1+jk\Delta r}{\Delta r} \frac{e^{-jk\Delta r}}{\Delta r} dxdy\,, \tag{2.3.18}$$

the vector $\hat{\mathbf{Q}} = (\hat{Q}_x, \hat{Q}_y, \hat{Q}_z)$ being given by

$$\hat{Q}_x = \frac{x - x_A}{\Delta r}\,, \tag{2.3.19a}$$

$$\hat{Q}_y = \frac{y - y_A}{\Delta r}\,, \tag{2.3.19b}$$

$$\hat{Q}_z = \frac{z_A}{\Delta r} = \cos\varphi\,. \tag{2.3.19c}$$

Note that the expression for the normal component of the particle velocity (which is the z-component) has the same form as the Rayleigh II integral. Because of this fact equation (2.3.18) is usually not given a special name, but it might be called the Rayleigh IV representation integral.

2.4 2D wave theory

The wave equation discussed in section 2.1 describes the propagation of acoustic waves through a three-dimensional medium. Solving this equation for a particular situation yields a wave field description at each point of the medium under consideration. In some situations, e.g., waves at a water surface or sound waves between two parallel plates with an intermediate distance less than half the wave length of the sound, the wave phenomena depend on two spatial coordinates only. Because of the more simple geometry involved, these kind of phenomena are easier to understand and more simple to calculate. The theory that should be used to describe these situations is the 2D wave theory.
In 2D wave theory the wave field is independent of one of the three geometrical coordinates. Assuming independence of the y-coordinate, wave equation (2.1.2) becomes

$$\frac{\partial^2 p(\mathbf{r}, t)}{\partial x^2} + \frac{\partial^2 p(\mathbf{r}, t)}{\partial z^2} = \frac{1}{c^2} \frac{\partial^2 p(\mathbf{r}, t)}{\partial t^2}\,. \tag{2.4.1}$$

Equation (2.4.1) can be used directly for the description of compressional waves in membranes and plates. In order to use it for an acoustic situation no quantity that enters the description of the wave field may depend on the value of the y-coordinate. This means that point sources cannot exist in 2D wave theory, and should be replaced by line sources parallel to the y-axis.
Equations from 3D wave theory can be transformed to the corresponding 2D equation by integrating along the y-axis from $-\infty$ to $+\infty$. As an example consider the Rayleigh I and the Rayleigh II integral. Integration of equation (2.3.7) over y, assuming the integrand is constant over y yields (Berkhout, 1987)

$$P(\mathbf{r}_A, \omega) = \frac{1}{2} \int_{z=0} j\omega\rho V_n(x, \omega)\, H_0^{(2)}(k\Delta r)\, dx\,, \tag{2.4.2}$$

in which $H_0^{(2)}(k\Delta r)$ represents the zeroth-order Hankel function of the second kind and Δr is now given by

$$\Delta r = \sqrt{(x - x_A)^2 + z_A^2}\,. \tag{2.4.3}$$

In the far field, characterised by $k\Delta r >> 1$, the Hankel function can be approximated by an exponential (Abramowitz et al., 1965), thus giving

$$P(\mathbf{r}_A, \omega) = \rho c \sqrt{\frac{jk}{2\pi}} \int_{z=0} V_n(x, \omega) \frac{e^{-jk\Delta r}}{\sqrt{\Delta r}} dx \text{ for } k\Delta r \gg 1\,. \tag{2.4.4}$$

Equation (2.4.2) and (2.4.4) are the 2D versions of the Rayleigh I representation integral and its far field approximation respectively.
Applying the same integration procedure to the 3D Rayleigh II integral (2.3.12) yields

$$P(\mathbf{r}_A, \omega) = \frac{jk}{2} \int_{z=0} P(x, \omega) \cos(\varphi)\, H_1^{(2)}(k\Delta r)\, dx\,, \tag{2.4.5}$$

in which $H_1^{(2)}(k\Delta r)$ denotes the first order Hankel function of the second kind. The far

field approximation of equation (2.4.5) is given by

$$P(\mathbf{r}_A, \omega) = \sqrt{\frac{jk}{2\pi}} \int_{z=0} P(x, \omega) \cos(\varphi) \frac{e^{-jk\Delta r}}{\sqrt{\Delta r}} dx \text{ for } k\Delta r \gg 1. \qquad (2.4.6)$$

Equation (2.4.5) and (2.4.6) are the 2D versions of the Rayleigh II representation integral and its far field approximation respectively.
In this thesis 2D wave theory will be used in several examples because of the much simpler computations involved.

2.5 Applications of the Rayleigh integrals

In the previous sections the Rayleigh integrals have been derived. In this section several applications of this theory will be discussed.

2.5.1 Wave field extrapolation

The expressions for the Rayleigh integrals derived in sections 2.3 and 2.4 all describe the wave field at an arbitrary point A in terms of a wave field registration at some plane surface S. The only assumption made in the derivation of the Rayleigh integrals is that all sources are located at one side of surface S, while point A is positioned at the opposite side. This means that once the registration of a wave field at a suitably chosen surface is available, this data can be used to calculate the wave field at any position in the source free half space.
As an example consider the 2D situation shown in figure 2.5.1: a monopole line source of sound at position $(0,-z_0)$ generates a wave field that is measured at the plane z=0. The pressure distribution found at this plane is in the far field given by

$$P(x, z=0, \omega) = S(\omega) \frac{e^{-jkr}}{\sqrt{r}}, \qquad (2.5.1)$$

with r given by

$$r = \sqrt{x^2 + z_0^2}. \qquad (2.5.2)$$

This data registration can be used to extrapolate the wave field towards some level $z=z_1$. Combining equation (2.5.1) with the 2D Rayleigh II integral (2.4.6) yields:

$$P(\xi, z=z_1, \omega) = \sqrt{\frac{jk}{2\pi}} \int_{z=0} S(\omega) \frac{e^{-jkr}}{\sqrt{r}} \cos(\varphi) \frac{e^{-jk\Delta r}}{\sqrt{\Delta r}} dx, \qquad (2.5.3)$$

with

$$\Delta r = \sqrt{(x-\xi)^2 + z_1^2}. \qquad (2.5.4)$$

It is a difficult task to find an analytic solution of equation (2.5.3) at each point of the extrapolation plane, but it is possible to solve it by numeric integration. As an example the wave field generated by a monochromatic (1000 Hz) line source will be extrapolated from a distance of 5 meters from the source (recording level) to a distance of 10

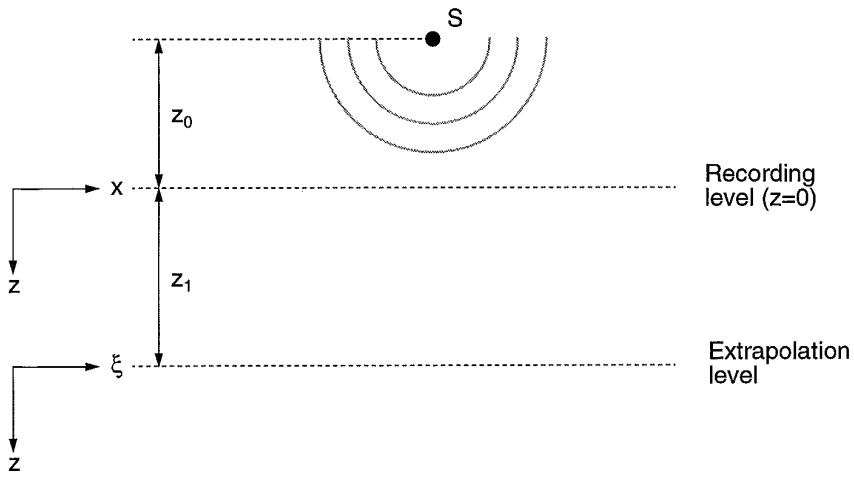

Figure 2.5.1: *The wave field of monopole source S can be extrapolated to depth level $z=z_1$ using the data recorded by the microphones at depth level z=0.*

meters from the source (extrapolation level). The results of the extrapolation process are given in figure 2.5.2.
Figure 2.5.2 a and b show the amplitude and phase of the source wave field at the recording level $z=z_0$. Note the $1/\sqrt{r}$-decrease of the wave field amplitude. Figure 2.5.2 c and d show the amplitude and phase of the source wave field at the extrapolation level $z=z_1$, while figure 2.5.2 e and f show the amplitude and phase of the extrapolated wave field at the extrapolation level. It is clear from these graphs that there is a perfect match between the true and the extrapolated wave field.
Note that the data calculated at $z=z_1$ can be used as the input for a next extrapolation step, thus creating a recursive wave field extrapolation algorithm. A special form of this recursive algorithm, adapted for the description of inhomogeneous media, is widely used by exploration geophysicists to describe the propagation of seismic waves through the earth's subsurface. In their models the earth subsurface is usually described by a layered medium, each layer being characterised by its own acoustic parameters, like density and wave propagation velocity. Starting just below the seismic source at the surface, the wave field is extrapolated in depth, layer by layer, towards the area of interest (target zone). At each layer interface, part of the wave energy is reflected and part of the energy is transmitted towards the next depth level, the ratio of the reflected energy to the transmitted energy being determined by the contrast in acoustic impedance of the two adjacent layers. From the reflected waves measured at the earth's surface it is possible to calculate a detailed model of the structure of the earth's subsurface, either by fitting the theoretical wave field extrapolation data to the seismic measurements or by applying an inverse wave field extrapolation procedure to the measured data, as discussed in the next section.

2.5.2 Inverse wave field extrapolation

The Rayleigh integrals describe the propagation of a wave field from a depth level z_0 to a next depth level z_1 in terms of a distribution of secondary sources. It is also possible to use the extrapolated field at depth level z_1 to find the strength of the secondary sources at depth level z_0, thus extrapolating the wave field in reverse direction. This technique is called backward or inverse extrapolation (figure 2.5.3).
To arrive at the equations that describe the inverse extrapolation process a description of the wave field extrapolation theory in the spatial frequency domain is more appro-

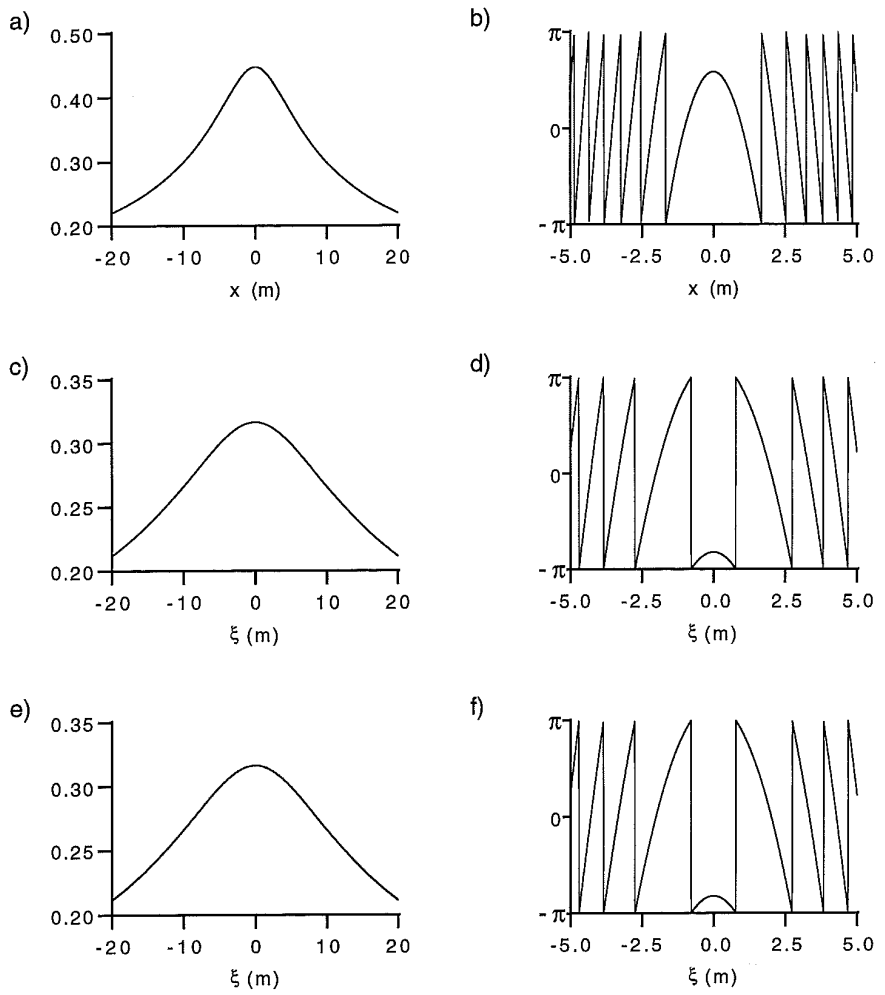

Figure 2.5.2: *Amplitude (left) and phase (right) of a monochromatic (1000 Hz) 2D monopole source wave field*
a,b) true wave field at 5 meter distance
c,d) true wave field at 10 meter distance
e,f) wave field at 5 meter distance extrapolated to 10 meter distance

priate. In order to arrive at such a description, a two-dimensional spatial Fourier transformation, defined by

$$\tilde{P}(k_x, k_y, z, \omega) = \int_{-\infty}^{\infty}\int_{-\infty}^{\infty} P(x, y, z, \omega)\, e^{-jk_x x} e^{-jk_y y} dx dy \,, \qquad (2.5.5)$$

should be applied to the Rayleigh integrals. For the Rayleigh II integral this procedure leads to

$$\tilde{P}(k_x, k_y, z_A, \omega) = \tilde{W}(k_x, k_y, z_A, \omega)\, \tilde{P}(k_x, k_y, z=0, \omega) \,, \qquad (2.5.6)$$

the extrapolator $\tilde{W}$ being given by

$$\tilde{W}(k_x, k_y, z_A, \omega) = e^{-jz_A\sqrt{k^2 - (k_x^2 + k_y^2)}} \text{ for } k_x^2 + k_y^2 \le k^2 \,, \qquad (2.5.7a)$$

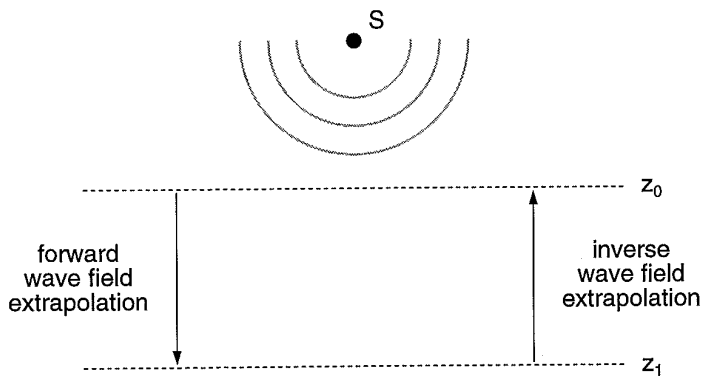

Figure 2.5.3: *Forward extrapolation describes wave propagation away from the source, inverse extrapolation describes wave propagation towards the source.*

and

$$\tilde{W}(k_x, k_y, z_A, \omega) = e^{-z_A\sqrt{(k_x^2 + k_y^2) - k^2}} \text{ for } k_x^2 + k_y^2 > k^2 \,. \qquad (2.5.7b)$$

Note that the spatial convolution procedure described by equation (2.3.12) is in the spatial frequency domain replaced by a multiplication operation. For $k_x^2 + k_y^2 \le k^2$ the multiplication operator describes the phase shift of the waves in travelling from the plane z=0 towards depth level $z=z_A$. For $k_x^2 + k_y^2 > k^2$ the multiplication operator describes waves that do not radiate from the plane z=0 into the medium, but are damped exponentially for increasing z coordinate. These near field waves are called evanescent waves and play a role at less than two wavelengths distance from the radiating surface only.
From equation (2.5.6) the operator $\tilde{F}$ that describes inverse wave field extrapolation is easily found:

$$\tilde{P}(k_x, k_y, z=0, \omega) \equiv \tilde{F}(k_x, k_y, z_A, \omega)\, \tilde{P}(k_x, k_y, z_A, \omega) \,, \qquad (2.5.8)$$

with

$$\tilde{F}(k_x, k_y, z_A, \omega) = \frac{1}{\tilde{W}(k_x, k_y, z_A, \omega)} \qquad (2.5.9)$$

In figure 2.5.4a the amplitude of the multiplication operator $\tilde{W}$ is sketched. From this graph it is clear that the operator decreases rapidly for $k_x^2 + k_y^2 > k^2$. In order to have a perfect inversion procedure, the inverse operator $\tilde{F}$ should increase in this range, as sketched in figure 2.5.4b. In a practical situation this unbounded growth of the inverse extrapolation operator is unacceptable, as it would blow up any noise in the region $k_x^2 + k_y^2 \le k^2$. Thus usually an approximate inverse operator is used which equals the exact inverse operator in the range $k_x^2 + k_y^2 \le k^2$, and decays exponentially outward this region, as indicated in figure 2.5.4c. In the space domain this procedure is equal to using the complex conjugate of the Green's function in the Rayleigh integral. The inverse extrapolation using this operator is exact for travelling waves only, the evanescent waves are heavily damped.
When the registration at the plane $z=z_A$ contains some evanescent waves, which is possible only when this plane is very near the sources, these wave components can be handled in the inverse extrapolation process too. In the next subsection a technique involving evanescent waves will be discussed.

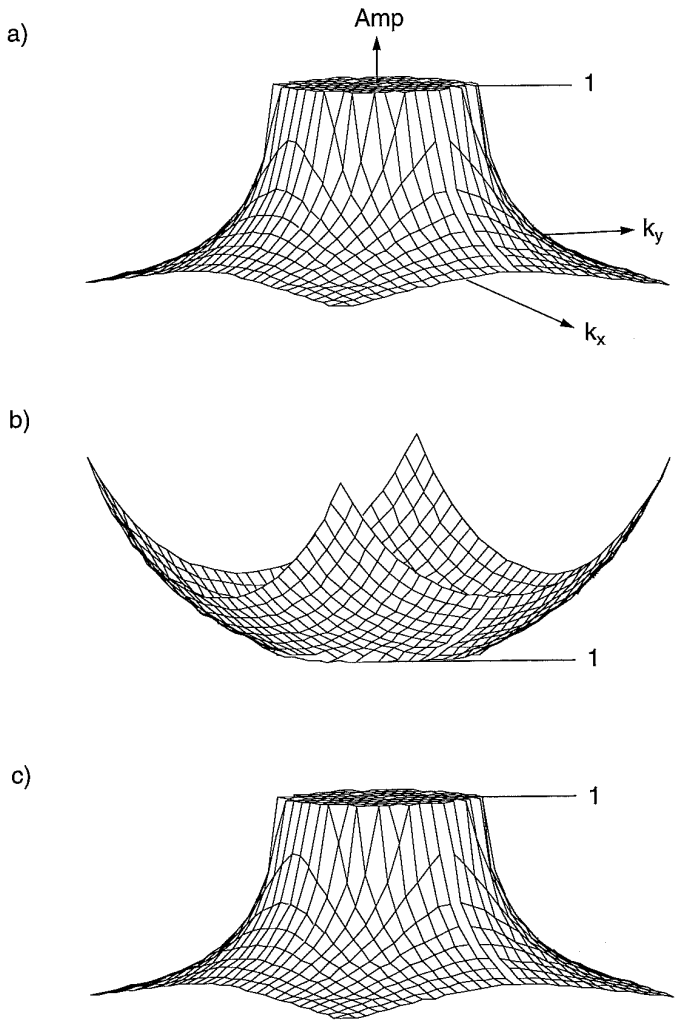

Figure 2.5.4: *Amplitude of wave field extrapolation operators in the k_x-k_y domain.*
a) Forward extrapolation operator $\tilde{W}$
b) Unstable inverse operator $\tilde{F} = \tilde{W}^{-1}$
c) Stabilised inverse operator $\tilde{F} = \tilde{W}^{*}$

2.5.3 Near-field acoustic holography

An important technique taking into account both radiating and evanescent parts of the wave field in the backward extrapolation procedure is near-field acoustic holography (Maynard et al., 1985). In this technique the acoustic wave field generated by a vibrating object (e.g. an automobile engine) is measured over a plane surface at a small distance from the source. Using one of the Rayleigh representation integrals the measured data is either extrapolated forward, i.e. in the direction of wave propagation, or extrapolated backward, i.e. in the direction of the vibrating object (see figure 2.5.5). In the inverse extrapolation, part of the evanescent waves present in the wave field recorded at the scan plane is taken into account as well.

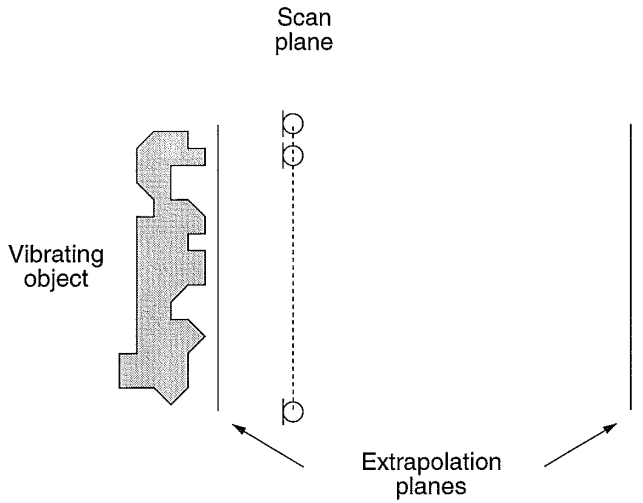

Figure 2.5.5: *The data at the scan plane can be extrapolated towards the source using near-field acoustic holography (NAH), or away from the source using the Rayleigh representation integrals. This way the measurements at the scan plane are sufficient for a complete characterisation of the wave field generated by the source.*

By using near-field acoustic holography it is possible to obtain detailed information about the vibrational amplitudes of an object, without the need for measuring at the surface (which might be hot or wet). This way the most noisy parts of a complicated machine can be located quite accurately. In order to use as much of the information in the evanescent waves as possible, the scan plane should be very close to the vibrating object.
A further refinement of the NAH technique is called spatial transformation of sound fields (Hald,1988), in which the cross spectrum of a reference microphone is used in combination with the data of a microphone scanning over the registration plane, to arrive at a time invariant description of the wave field. This way, the holographic techniques can be used without the need for a large number of simultaneous measurements at the acquisition plane.

2.5.4 Holographic wave field synthesis

In section 2.3 it was pointed out already that the Rayleigh I representation integral and the Rayleigh II representation integral describe a secondary monopole source distribution and a secondary dipole source distribution respectively, over the acquisition plane. This means that a real distribution of monopole sources or dipole sources over a plane can be used to generate a desired wave field by driving each source with the appropriate signal as defined by the Rayleigh integral. Note that although the Rayleigh integrals describe a continuous source distribution, for band limited signals the integrals can be replaced by summations, thus discretizing the source distributions.
As an example consider the following (2D) situation: a monopole line source S located at position (0,0) emits a sound pulse starting at time t=0. This sound pulse propagates away from the source, producing cylindrical wave fronts. In figure 2.5.6 the pressure field generated by source S is shown for a time value t of 20, 30, 40 and 50 ms after the emission. In these (x,z) diagrams the cylindrical wave fronts of the line source are clearly visible as circles.
Next, the same wave field is generated by a loudspeaker array parallel to the x-axis, at 0.5 meter distance from source S. The wave field generated by the loudspeaker array is shown in figure 2.5.7 for times corresponding to the graphs in figure 2.5.6. Comparison of both figures shows that the reconstructed wave field is in perfect agreement with the true wave field generated by source S.

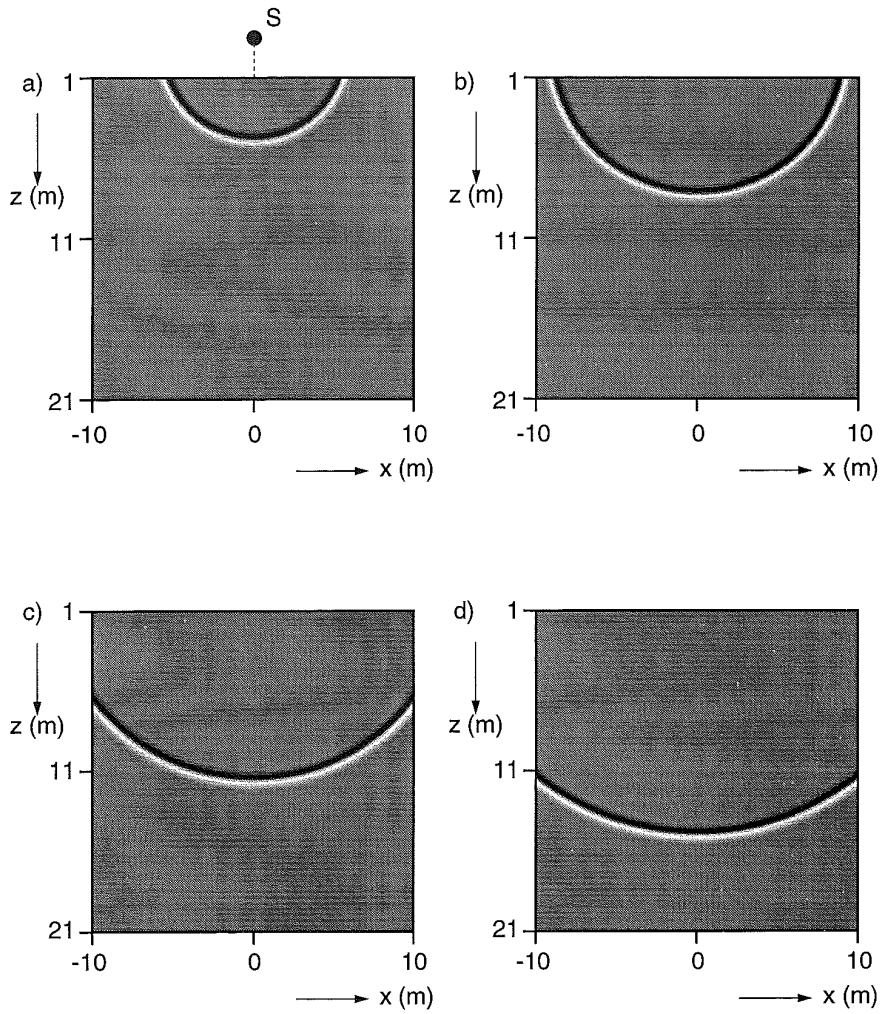

Figure 2.5.6: *The wave field of a monopole source S is calculated in a square region of 20 x 20 meter. The source is positioned at 2 meter distance from the registration area. Snapshots are shown for times of a) 20 ms, b) 30 ms, c) 40 ms and d) 50 ms after the emission of the sound pulse.*

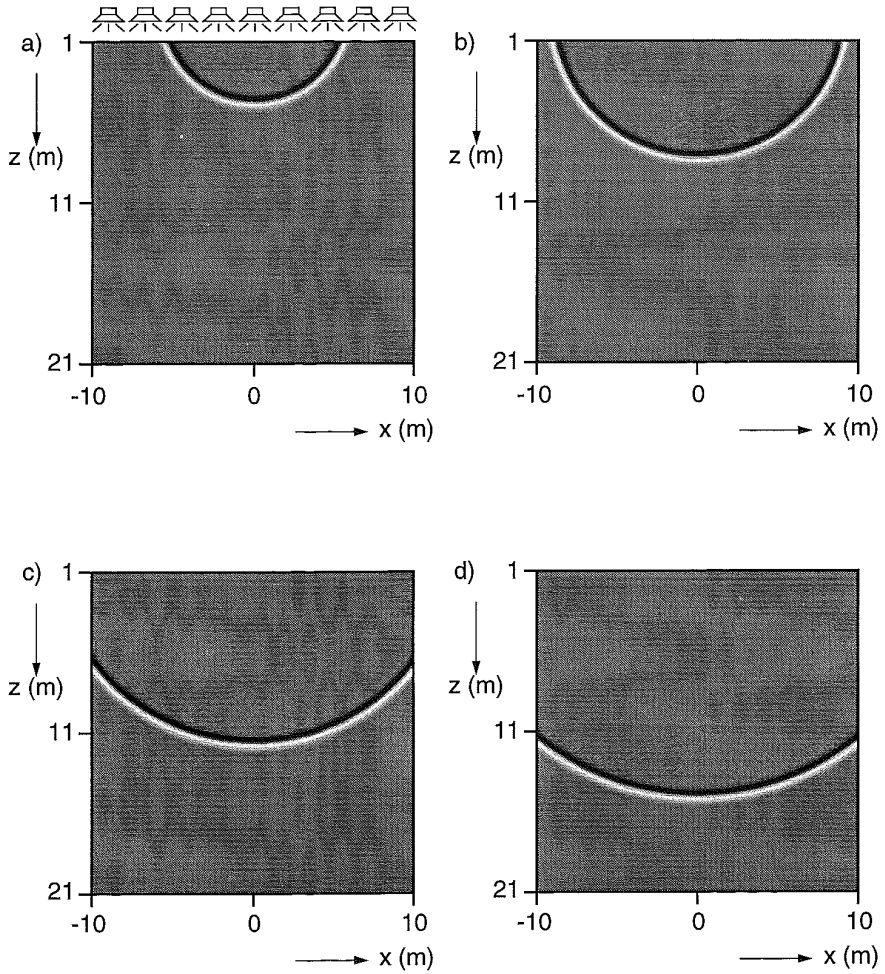

Figure 2.5.7: *The wave field of the monopole source of figure 2.5.6 reconstructed using a loudspeaker array. Snapshots are shown for times of a) 20 ms, b) 30 ms, c) 40 ms and d) 50 ms after the emission of the sound pulse.*

A more thorough discussion of this wave field generation technique, which forms the basis for all electro-acoustic applications described in this thesis, is given in chapter 3 of this thesis.

2.6 Acoustic holography versus optic holography

The acoustic wave field synthesis technique described in section 2.5.3 should be compared with optic wave field synthesis by means of holography. In acoustic wave field synthesis a source distribution over a plane is used, each source being driven by the appropriate signal. From equation (2.3.7) or (2.3.12) it can be seen that these source signals are given by the value of the wave field to be reconstructed, measured at the source plane. Once the value of this wave field is known over the entire source plane (both in amplitude and in phase) a perfect reconstruction of the wave field can be obtained, as was shown in section (2.5). Note that the wave field synthesis is essentially a two-step process: first the wave field at the source plane should be determined, either by measurement or by calculation, and afterwards these wave field values are used to drive the reconstruction sources.
In optic wave field reconstruction (usually called holography) the same two-step process can be recognised: first the wave field to be reconstructed is recorded over a plane, and afterwards a distribution of light sources with the appropriate amplitude and phase characteristics is placed at this plane, which reconstructs the original wave field. A problem encountered in the practical evaluation of optic holography is the very short wavelength of visible light (about 400-800 nm) which makes a very dense distribution of light sources over the reconstruction plane necessary. This problem can be solved by recording the interference pattern of the original wave field with a reference beam on a photographic plate, as is shown in figure 2.6.1. By some chemical processing, the photo resist layer on the photographic plate shrinks, the amount of shrinkage being determined by the light intensity during the recording time. In this way a transparent plate is created with an almost continuously varying thickness. This plate is called the hologram. The phase shift for a light ray passing through a hologram is proportional to the local thickness of the plate, so the shape of a light wave front passing through a hologram will be changed. A special situation arises when the hologram is illuminated by the reference beam used during the recording, as depicted in figure 2.6.2. Because the phase shift caused by the hologram is proportional to the phase difference between

the incident wave field and the reference beam during the recording, the diffracted beam leaving the hologram will have the same phase distribution as the original wave field. Thus the original wave field is reconstructed by illuminating the hologram with the reference beam.

Note that the use of reference beam for recording the hologram and for reconstructing the original wave field is only an aid in the creation of the required source distribution. Any other sufficiently fine source distribution driven by the appropriate signals will in principle yield the same results. The idea that the use of reference beams is an essential part of holography is a misunderstanding of the underlying wave theory.

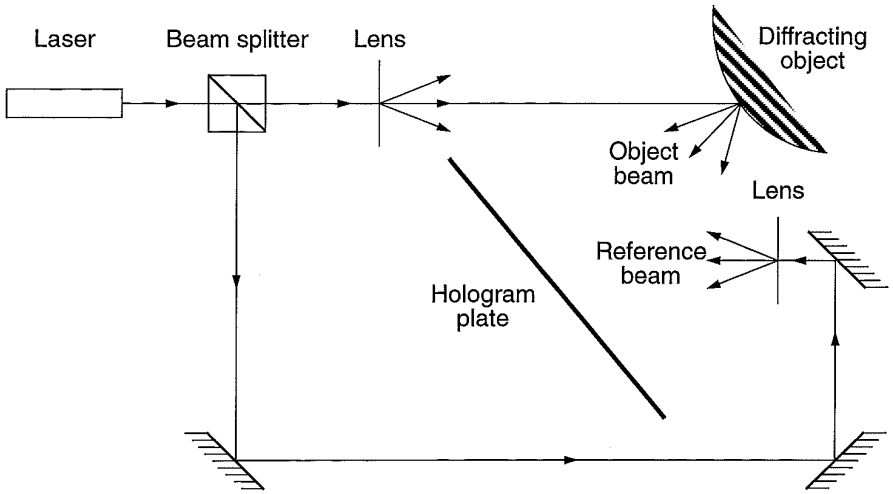

Figure 2.6.1: *Setup for the recording of a hologram. The laser beam is split-up into two parts, one of which illuminates the hologram plate (photographic plate) directly (the reference beam), the other is diffracted by an object first (the object beam). The interference pattern of both beams is recorded on the hologram plate.*

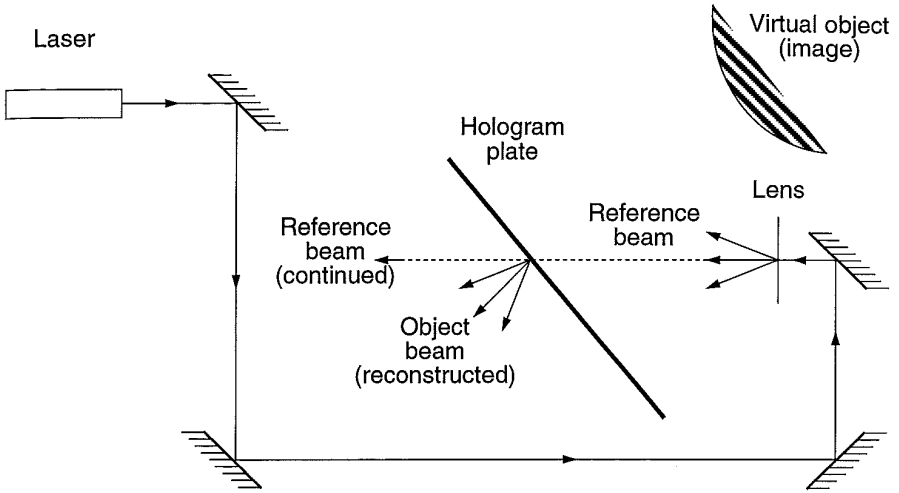

Figure 2.6.2: *Reconstruction of the image recorded on the hologram by illuminating the hologram plate with the reference beam only.*

3. HOLOGRAPHIC WAVE FIELD SYNTHESIS

In section 2.5.4 it was discussed that the theory of the Rayleigh representation integrals can be used to find a method for wave field synthesis. In this chapter these ideas are discussed more thoroughly, together with the limitations encountered when the theory is applied in a practical situation.

3.1 Synthesis of an arbitrary wave field

In section 2.5.4 it was shown that a monopole wave field can be synthesised using an array of loudspeakers. The same procedure can be used to generate an arbitrary wave field. As an example, the wave field of five impulsive point sources S_1-S_5 will be considered. The wave field generated by these sources is shown in figure 3.1.1a-d, for a time of 20, 30, 40 and 50 ms respectively after the emission of the first sound pulse. Note that source S_3 and S_4 generate a wavelet with a larger frequency bandwidth than the other sources.
In order to synthesise a replica of the wave field shown in figure 3.1.1 using a loudspeaker array positioned at z=0, a registration of the wave field should be available at each loudspeaker position. These time registrations of the wave field are shown in figure 3.1.2. Note that the individual sources show up as hyperbolas in the x-t domain registration, the curvature of each hyperbola being determined by the distance of the

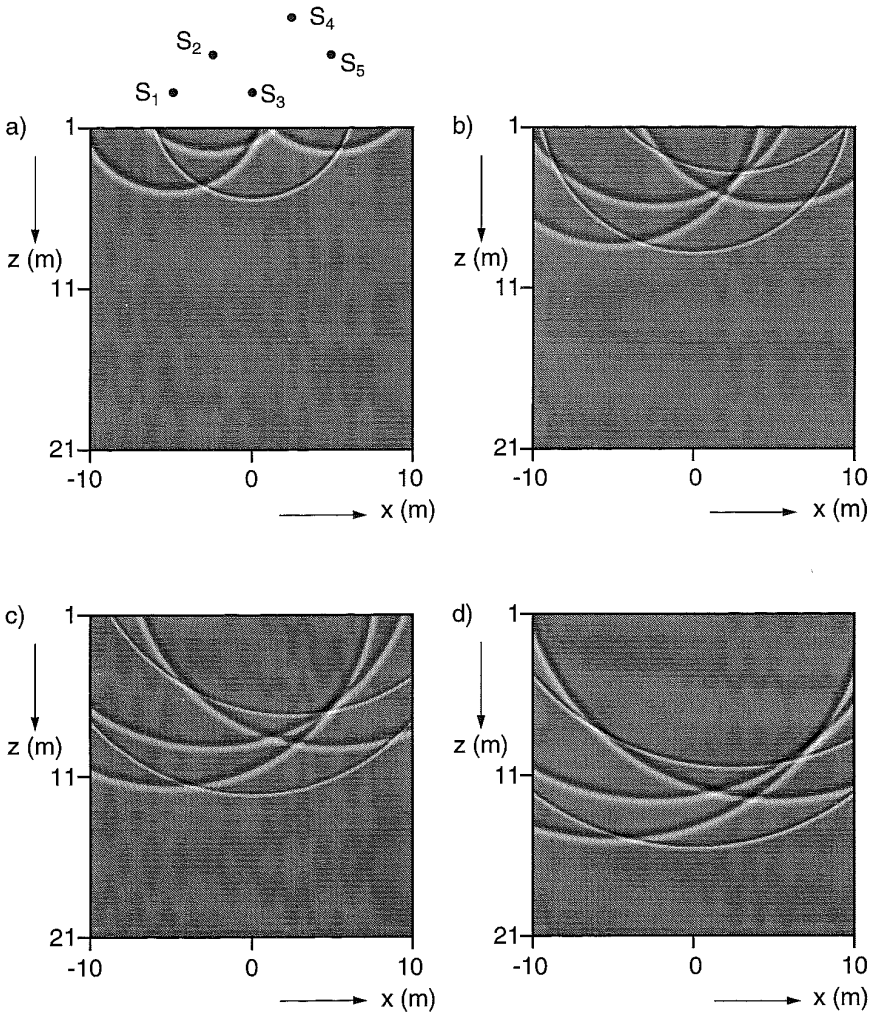

Figure 3.1.1: *The wave field generated by five impulsive monopole sources.*
a) snapshot at 20 ms *b) snapshot at 30 ms*
c) snapshot at 40 ms *d) snapshot at 50 ms*

corresponding source to the x-axis.
The incident field at the position of the loudspeaker array shown in figure 3.1.2 forms the basis of the wave field reconstruction. The wave data shown in figure 3.1.2 is a pressure recording, which means that an array of dipole loudspeakers driven by this pressure data will create the desired pressure field in the half space z>0. Figure 3.1.3a-d show the reconstructed pressure field for the same time instants as the snapshots of figure 3.1.1. Comparison of figure 3.1.1 and figure 3.1.3 shows that there is a perfect match between the direct and the synthesised wave field.

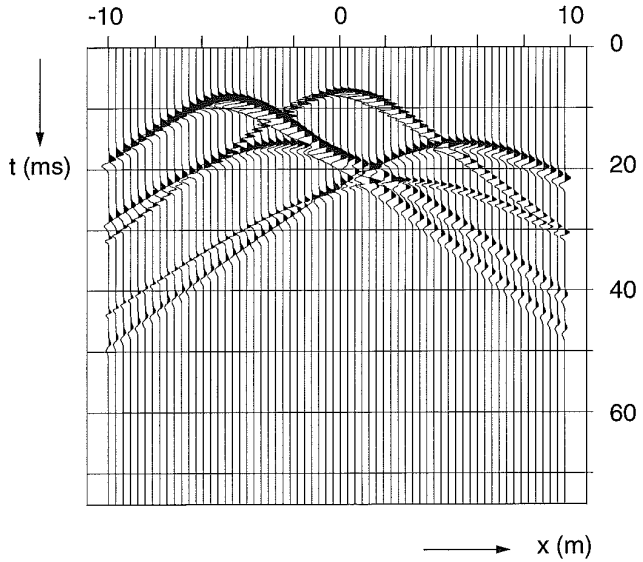

Figure 3.1.2: *Wave field of five impulsive monopole sources, recorded by an array of microphones at z=0. For each microphone the time domain registration is shown.*

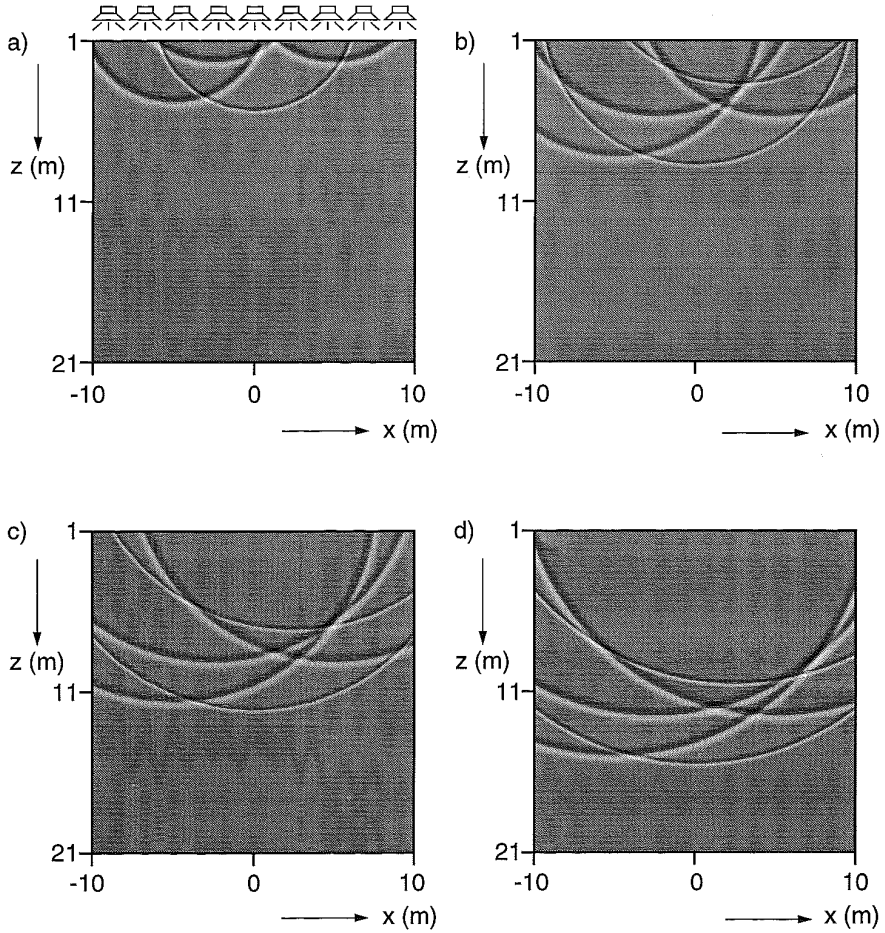

Figure 3.1.3: *Wave field of five impulsive monopole sources synthesised by an array of dipole loudspeakers at the line z=0.*
a) snapshot at 20 ms *b) snapshot at 30 ms*
c) snapshot at 40 ms *d) snapshot at 50 ms*

3.2 Space domain sampling

The Rayleigh representation integrals describe wave field synthesis by means of continuous secondary source distributions. In practical situations these secondary source distributions will be approximated by a regularly spaced array of point sources. This discretisation of the source distribution is allowed, provided that the spatial anti-aliasing criteria are fulfilled.
For time domain sampling, the anti-aliasing criterion says that the sampling interval Δt should be less than one half of the period T_{min} of the highest frequency component in the signal:

$$\Delta t < \frac{T_{min}}{2} . \qquad (3.2.1)$$

The maximum angular frequency that can be distinguished for a given sample interval Δt, usually referred to as the Nyquist frequency ω_N, is given by

$$\omega_N = \frac{\pi}{\Delta t} . \qquad (3.2.2)$$

For sampling in the space domain, the same principle says that the spatial sampling interval Δx should be less than one half of the smallest apparent wavelength in the x-direction $\lambda_{x,min}$ of the wave field under consideration:

$$\Delta x < \frac{\lambda_{x,\,min}}{2} , \qquad (3.2.3)$$

while the spatial Nyquist frequency $k_{x,N}$ is given by

$$k_{x,\,N} = \frac{\pi}{\Delta x} , \qquad (3.2.4)$$

with similar criteria for the sampling interval in the other spatial directions.
In order to better understand the meaning of the apparent wavelength, consider the simple 2D situation depicted in figure 3.2.1a: a monochromatic plane wave propagating in the x-direction, recorded at a certain time instant t_0. In this case, the wavelength in the x-direction λ_x equals the wavelength λ of the plane wave. When the plane wave fronts make an angle θ with the x-axis, the distance between two wave crests meas-

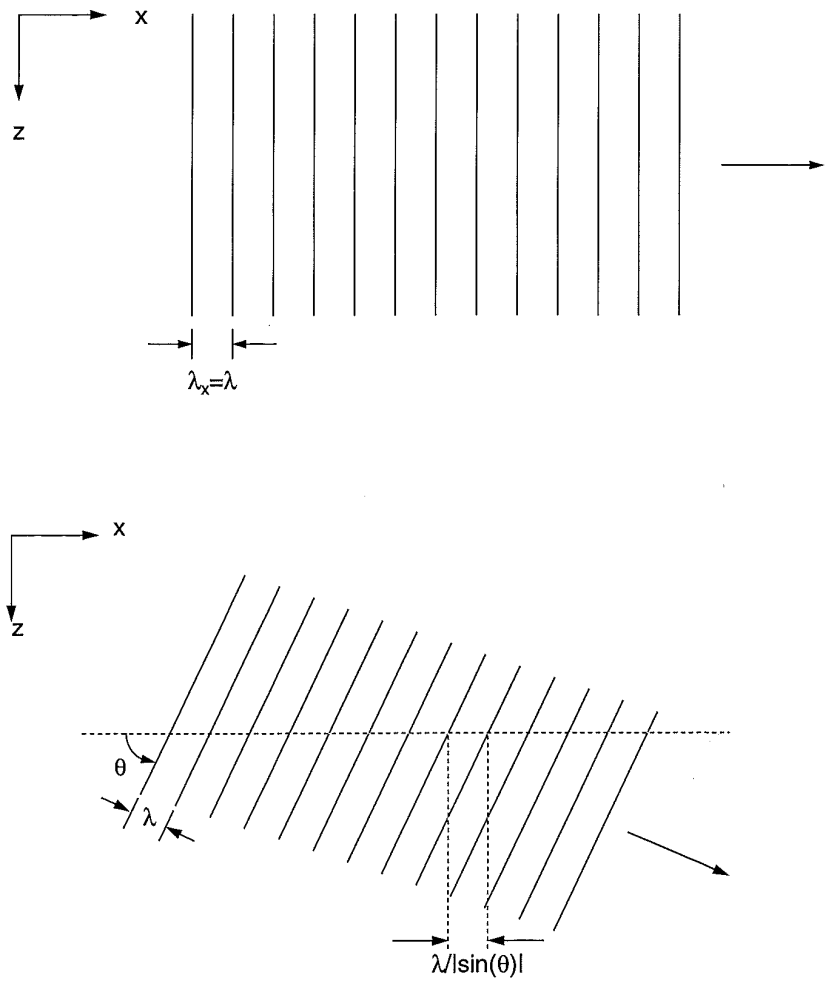

Figure 3.2.1: *a) Plane wave travelling in the x-direction. The maximum sampling distance in the x-direction is given by λ/2.*
b) Plane wave travelling under an angle θ with the x-axis. The maximum sampling distance in the x-direction is given by $^1/_2$ λ/|sin(θ)|.

ured along the x-axis becomes larger by a factor 1/sin(θ) (see figure 3.2.1b):

$$\lambda_x = \frac{\lambda}{\sin(\theta)} . \tag{3.2.5}$$

From equation (3.2.5) it is clear that a plane wave making an angle with the sampling direction can be sampled at a larger interval, without violating the anti-aliasing criterion. In the extreme case θ=0 (a plane wave with wave fronts in parallel with the x-axis), the maximum sample interval in the x-direction becomes infinite, as expected for a wave field that is constant over the entire x-axis.
Important information about time domain signals can be obtained by transforming them to the (temporal) frequency domain using a Fourier transformation along the time axis. It appears to be advantageous to use the same procedure in the analysis of space domain signals. Applying a Fourier transform along the x-axis to a wave field registration yields a data description in the spatial frequency domain. Usually, the data is also transformed to the temporal frequency domain by applying a Fourier transform along the time axis. By these two Fourier transformations a signal p(x,t) is transformed into a signal $\tilde{P}(k_x, \omega)$ given by

$$\tilde{P}(k_x, \omega) = \int_{-\infty}^{\infty}\int_{-\infty}^{\infty} p(x,t)\, e^{-j\omega t} e^{jk_x x} dx dt , \tag{3.2.6}$$

in which k_x denotes the spatial frequency (dimension m^{-1}), which is the spatial equivalent of the temporal frequency ω (dimension s^{-1}).
Equation (3.2.6) describes the transformation from the x-t domain towards the k_x-ω domain. The inverse transformation is given by

$$p(x,t) = \frac{1}{(2\pi)^2}\int_{-\infty}^{\infty}\int_{-\infty}^{\infty} \tilde{P}(k_x, \omega)\, e^{-jk_x x} e^{j\omega t} dk_x d\omega . \tag{3.2.7}$$

Equation (3.2.7) can be considered as a synthesis of the wave field p(x,t) in terms of monochromatic plane waves $e^{j(\omega t - k_x x)}$, the weight of each plane wave given by $\tilde{P}(k_x, \omega)$. Hence, equation (3.2.7) is a decomposition of the wave field p(x,t) into monochromatic plane waves. The apparent (or phase) velocity c_x in the x-direction of these

plane waves is given by

$$c_x = \frac{\omega}{k_x} . \qquad (3.2.8)$$

From equation (3.2.5) it is found that the phase velocity of a plane wave making an angle θ with the x-axis is given by

$$c_x = \frac{c}{\sin(\theta)} . \qquad (3.2.9)$$

Combining equations (3.2.8) and (3.2.9) and introducing the wave number $k=\omega/c$ yields:

$$k_x = k\sin(\theta) . \qquad (3.2.10)$$

Thus, each component in the k_x-ω domain description of the wave field represents a monochromatic plane wave of frequency ω, travelling under an angle θ with the x-axis. Limiting the maximum k_x value in the wave field (spatial filtering) will decrease the amount of high frequency waves travelling under large angles with the x-axis. Limiting the angles present in a wave field to values of θ around 0 to increase the required sample interval will play an important role in section 3.7.

Note that the integral relations (3.2.6) and (3.2.7) describe both travelling waves ($|k_x| \leq \omega/c$) and evanescent waves ($|k_x| > \omega/c$). The presence of evanescent waves in the near field will decrease the maximum sampling distance for a wave data recording close to a sound source. In this thesis it will be assumed that the effect of evanescent waves can be neglected at the recording position of the wave field.

As an example of the use of the wave field description in the k_x-ω domain, consider a plane wave in the x-z domain, the wave fronts making an angle θ with the x-axis (figure 3.2.2a). This plane wave can be described mathematically by

$$p(x,z,t) = s\left(t - \frac{x}{c_x} + \frac{z}{c_z}\right) , \qquad (3.2.11)$$

in which s(t) describes the shape of the source wavelet, and $c_x = c/\sin(\theta)$ and $c_z = c/\cos(\theta)$ are the apparent velocities of the wave along the x- and z-axis respectively.

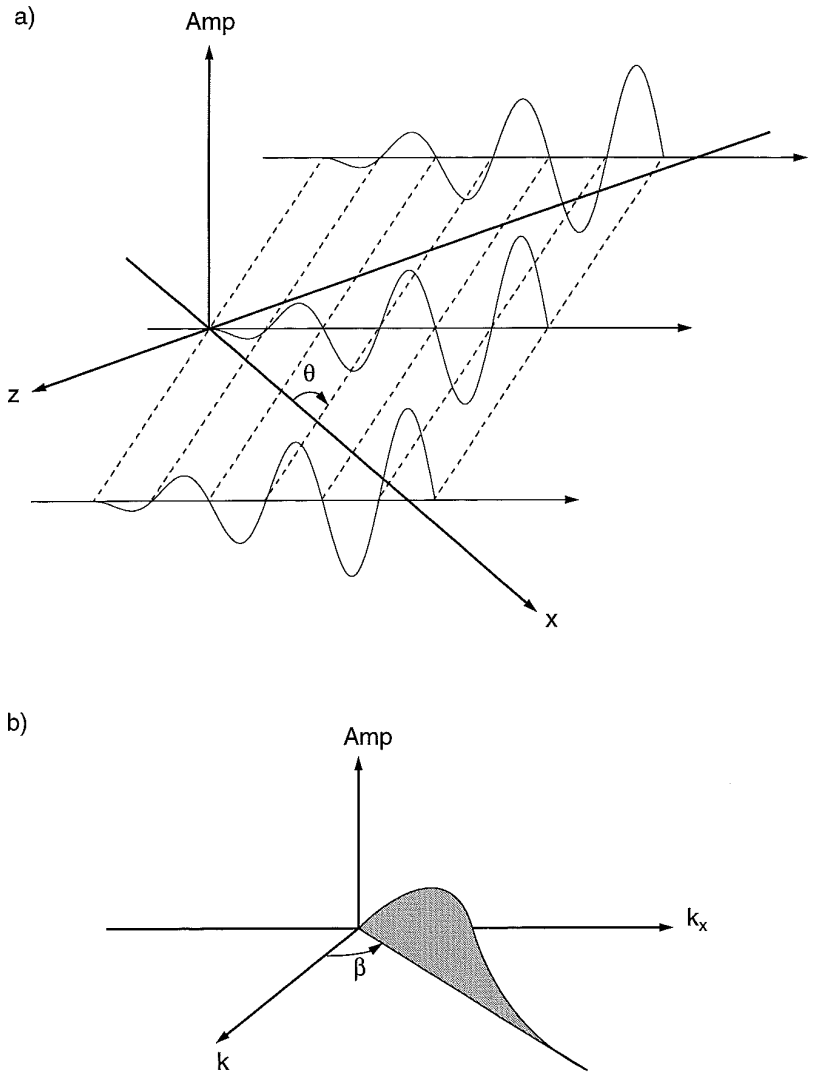

Figure 3.2.2: *A plane wave travelling under an angle θ with the x axis in the x-z domain (a), and in the k_x-k domain (b). The k_x-k domain representation vanishes everywhere, except on the line $k_x=k\sin(\theta)=k\tan(\beta)$.*

Applying a Fourier transformation from time to frequency to equation (3.2.11) yields

$$P(x, z, \omega) = S(\omega)\, e^{-j\omega x/c_x} e^{j\omega z/c_z} . \qquad (3.2.12)$$

Making a registration of this wave field along the x-axis (z=0) and applying a second Fourier transformation from space coordinate to spatial frequency yields:

$$\tilde{P}(k_x, 0, \omega) = 2\pi S(\omega)\, \delta\left(k_x - \frac{\omega}{c_x}\right) , \qquad (3.2.13)$$

where S(ω) is the Fourier transform of the source function s(t).
Thus, the k_x-ω domain representation of a plane wave recording is zero, except on the line $k_x=\omega/c_x$, the amplitude along this line being determined by the spectral shape S(ω) of the source function. This means that the (broadband) plane wave is decomposed into a number of monochromatic plane waves, each frequency component making an angle θ with the x-axis.
In order to obtain axes with comparable units and scales in both directions of the k_x-ω diagram, the temporal frequency ω is usually replaced by the wave number k=ω/c. This way, the k_x-ω domain is replaced by the k_x-k domain. Thus, equation (3.2.13) can be rewritten as

$$\tilde{P}(k_x, 0, k) = 2\pi S(k)\, \delta(k_x - k\sin(\theta)) . \qquad (3.2.14)$$

The k_x-k diagram for the plane wave example is shown in figure 3.2.2b. The angle β of the k_x-k domain representation of the plane wave is directly related to the angle θ of the plane wave in the x-z domain via the relation

$$\tan(\beta) = \frac{k_x}{k} = \sin(\theta) . \qquad (3.2.15)$$

As a second example the double Fourier transform of a more complex wave field will be calculated. Consider the configuration of figure 3.2.3a: two monopole sources generating the same band limited impulse signal are situated in the half space z<0. In figure 3.2.3b the wave field generated by these two sources is shown in the x-z domain, at a time of 40 ms after the emission of the sound pulses. The maximum frequency present in the source signals is 2000 Hz, thus giving a minimum wave length in air of approximately 170 mm.

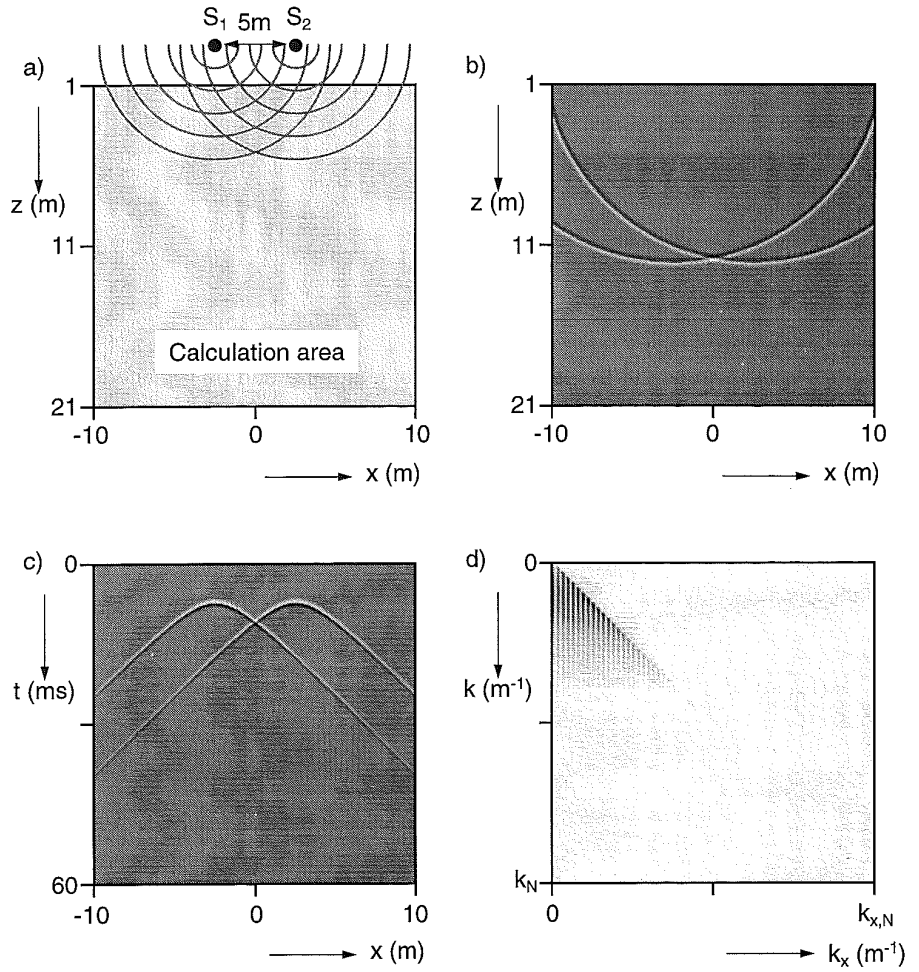

Figure 3.2.3: *The wave field of two monopole sources is calculated in a square region of 20 x 20m.*
a) Configuration *b) snapshot at t = 40 ms*
c) x-t registration *d) k_x-k domain representation*

A registration is made of this wave field along a line parallel to the x-axis, at a distance of 2 meters from the sources. This x-t registration is shown in figure 3.2.3c. Applying a double Fourier transformation to this registration yields the k_x-k diagram shown in figure 3.2.3d. Because of symmetry only the positive spatial frequency part ($k_x \geq 0$)is shown in this graph. From figure 3.2.3 it is clear that in this case the main part of the wave energy, indicated in the graph by the greyness-level, is contained in the region $|k_x|<k$, with a maximum near the lines $k_x=k$ and $k_x=-k$.

3.3 Discretisation of the Rayleigh integrals

For band limited signals the Rayleigh integrals of chapter 2 can be replaced by summations. The discrete version of the 3D Rayleigh I integral is given by

$$P(\mathbf{r}_A, \omega) = \frac{1}{2\pi} \sum_{m=-\infty}^{\infty} \sum_{n=-\infty}^{\infty} j\omega\rho V_n(x_m, y_n, \omega) \frac{e^{-jk\Delta r_{mn}}}{\Delta r_{mn}} \Delta x \Delta y \,, \qquad (3.3.1)$$

while the discrete Rayleigh II integral reads:

$$P(\mathbf{r}_A, \omega) = \frac{1}{2\pi} \sum_{m=-\infty}^{\infty} \sum_{n=-\infty}^{\infty} P(x_m, y_n, \omega) \cdot \frac{1+jk\Delta r_{mn}}{\Delta r_{mn}} \cos(\varphi_{mn}) \frac{e^{-jk\Delta r_{mn}}}{\Delta r_{mn}} \Delta x \Delta y. \qquad (3.3.2)$$

In equations (3.3.1) and (3.3.2) $\mathbf{r}_{mn}=(x_m,y_n,z=0)$ is the position vector of the secondary source with indices m and n, Δr_{mn} is the distance from this source to the observation point A and φ_{mn} is the angle between the line from this source to the observation point and the negative z-axis (see figure 3.3.1a). Equations (3.3.1) and (3.3.2) are also important from a computational point of view, because solving the Rayleigh integrals on a computer is usually done by numeric integration.
In 2D, discretisation of the far field approximation of the Rayleigh I integral leads to

$$P(\mathbf{r}_A, \omega) = \rho c \sqrt{\frac{jk}{2\pi}} \sum_{m=-\infty}^{\infty} V_n(x_m, \omega) \frac{e^{-jk\Delta r_m}}{\sqrt{\Delta r_m}} \Delta x \,, \qquad (3.3.3)$$

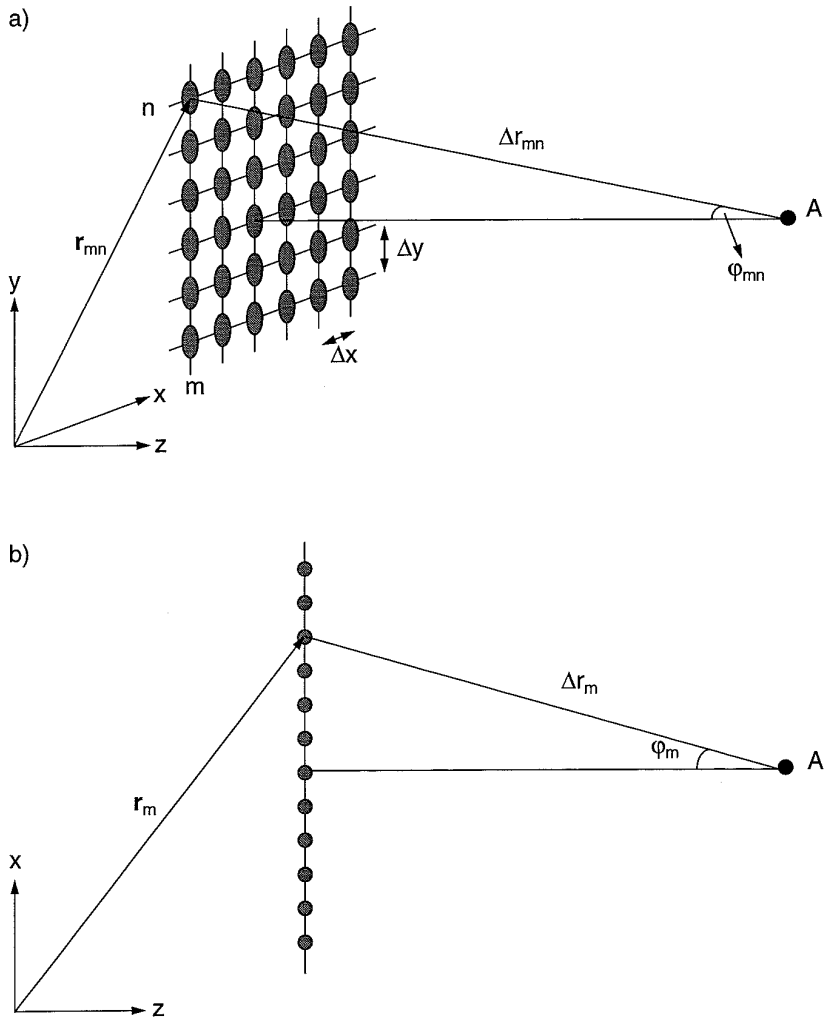

Figure 3.3.1: *a) The discrete 3D Rayleigh integrals (equations (3.3.1) and (3.3.2)) describe a planar array of secondary sources.*
b) The discrete 2D Rayleigh integrals (equations (3.3.3) and (3.3.4)) describe a linear array of secondary sources.

while the 2D discrete far field Rayleigh II integral becomes

$$P(\mathbf{r}_A, \omega) = \sqrt{\frac{jk}{2\pi}} \sum_{m=-\infty}^{\infty} P(x_m, \omega) \cos(\varphi_m) \frac{e^{-jk\Delta r_m}}{\sqrt{\Delta r_m}} \Delta x \,. \qquad (3.3.4)$$

In equations (3.3.3) and (3.3.4) $\mathbf{r}_m=(x_m,z=0)$ is the position vector of the secondary source with index m, Δr_m is the distance from this source to the receiver and φ_m is the angle between the line from this source to the receiver and the negative z-axis (see figure 3.3.1b).

From spectral analysis it is known that discretising a time signal by sampling leads to a periodic signal in the frequency domain (see figure 3.3.2). When undersampling in the time domain occurs, the individual spectra in the frequency domain representation of the signal start to overlap (aliasing), as can be seen in figure 3.3.2 d,h. Thus, it is expected that discretising a wave field along one of the spatial coordinates will cause a periodic spectrum in the spatial frequency domain, while spatial undersampling will cause overlapping spectra in this domain (spatial aliasing).

To illustrate this effect, the 2D two-source example discussed in section 3.2 (figure 3.2.3) will be reconsidered here. The wave field generated by these two sources will be synthesised by a loudspeaker array with a sample distance of 80 mm. As the minimum wavelength in the wave field is 170 mm (neglecting evanescent waves), the synthesised field should be aliasing-free. In figure 3.3.3a the synthesised wave field is shown. Comparison of this graph with figure 3.2.3b shows that the synthesised wave field is a good replica of the original field.

A doubling of the sampling distance will cause a violation of the anti-aliasing criterion. The resulting wave field after reconstruction with this sample interval is shown in figure 3.3.3b. Note that the wave front is still clearly visible, but due to the spatial aliasing the sum of all the loudspeaker contributions does not add up to zero behind the reconstructed wave front. Another doubling of the sampling interval yields a severe distortion of the wave field, as is shown in figure 3.3.3c.

More insight in the spatial aliasing effects can be obtained by an analysis in the k_x-k domain. For the situation of figure 3.3.3a a k_x-k domain diagram of the true monopole wave field at the loudspeaker array is shown in figure 3.3.4a. The k_x-k domain diagram of the wave field synthesised by the loudspeaker array at any position can be obtained by multiplying this incident field by the transfer function from the loudspeaker array to the detection position. This transfer function is shown in figure 3.3.4b for a detection level at 1 meter from the loudspeaker array. Note the periodicity of the transfer function

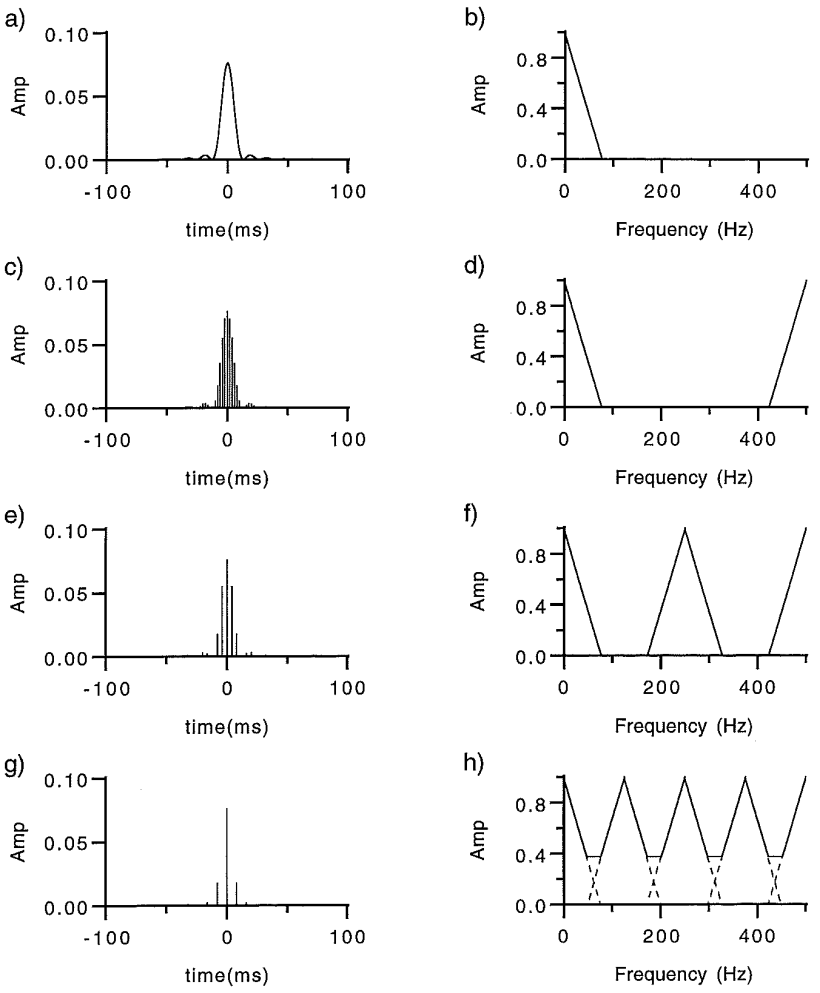

Figure 3.3.2: *Sampling in the time domain causes periodicity in the frequency domain. When the sample interval is too large overlapping spectra occur (aliasing).*

a) Continuous wave *b) spectrum of a)*
c) Oversampled wave *d) spectrum of b), periodic*
e) Correctly sampled wave *f) spectrum of e), periodic*
g) Undersampled wave *h) spectrum of g), aliased*

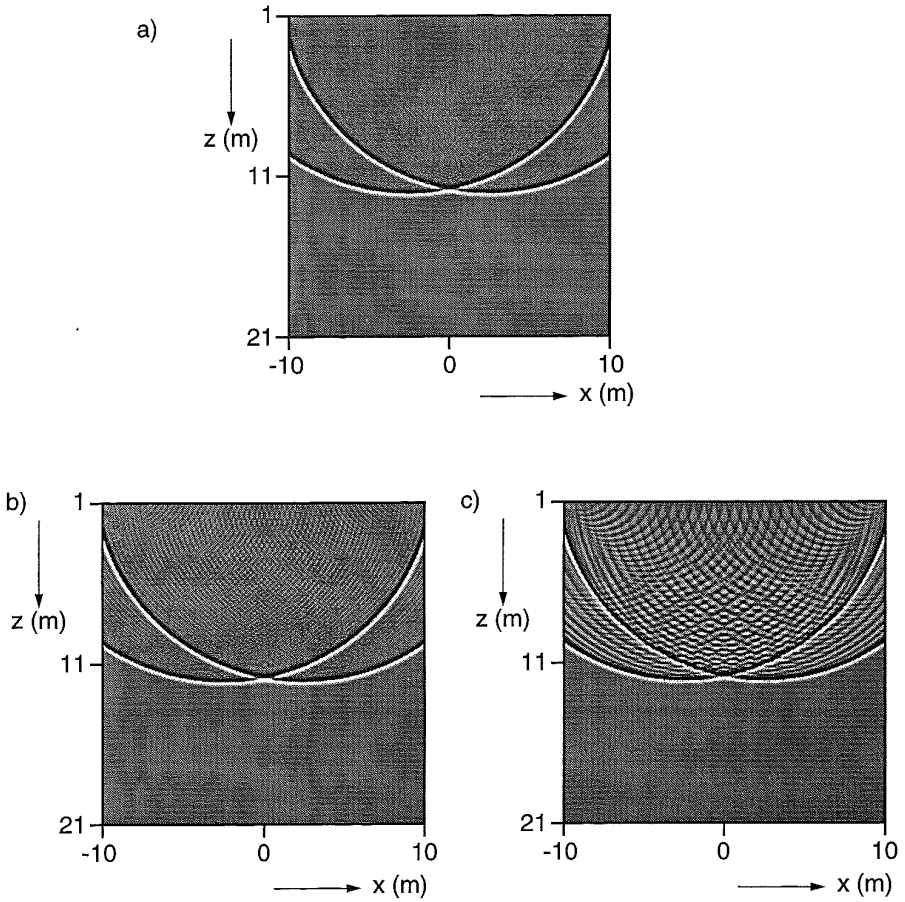

Figure 3.3.3: *Wave field of two monopole sources, synthesised by a loudspeaker array, for three different loudspeaker sample intervals Δx. The maximum source frequency is 2000 Hz, thus the minimum wavelength in the wave field is 170 mm.*
a) Δx = 80 mm, no aliasing
b) Δx = 160 mm, little aliasing
c) Δx = 320 mm, severe aliasing

in the k_x-direction, caused by the loudspeaker distance of 80 mm. The synthesised wave field is shown in the k_x-k domain in figure 3.3.4c and in the x-t domain in figure 3.3.4d. Note that there is no overlap between the incident field and the overlapping parts of the transfer function, so no spatial aliasing is found in this situation.
Figure 3.3.5 and figure 3.3.6 show the same graphs, using a loudspeaker distance of 160 mm and 320 mm respectively. Note the decreasing period of the transfer function for increasing loudspeaker distance and the overlapping spectra in the higher frequency regions, both in the transfer function and in the synthesised field.

3.4 Finite transducer arrays

The loudspeaker array used to synthesise a wave field will always have finite length. This means that the infinite summations described by the discrete versions of the Rayleigh integrals are approximated by the sum of a finite number of terms. For example, equation (3.3.2) will be replaced by

$$P(\mathbf{r}_A, \omega) = \frac{1}{2\pi} \sum_{m=-M}^{M} \sum_{n=-N}^{N} P(x_m, y_n, \omega) \cdot \frac{1 + jk\Delta r_{mn}}{\Delta r_{mn}} \cos(\varphi_{mn}) \frac{e^{-jk\Delta r_{mn}}}{\Delta r_{mn}} \Delta x \Delta y \,, \quad (3.4.1)$$

and equation (3.3.4) by

$$P(\mathbf{r}_A, \omega) = \sqrt{\frac{jk}{2\pi}} \sum_{m=-M}^{M} P(x_m, \omega) \cos(\varphi_m) \frac{e^{-jk\Delta r_m}}{\sqrt{\Delta r_m}} \Delta x \,, \quad (3.4.2)$$

in which M and N denote the number of array loudspeakers in the x- and y-direction respectively.
The error $\varepsilon(\omega)$ in the reconstructed field given by equation (3.4.2), due to the use of a

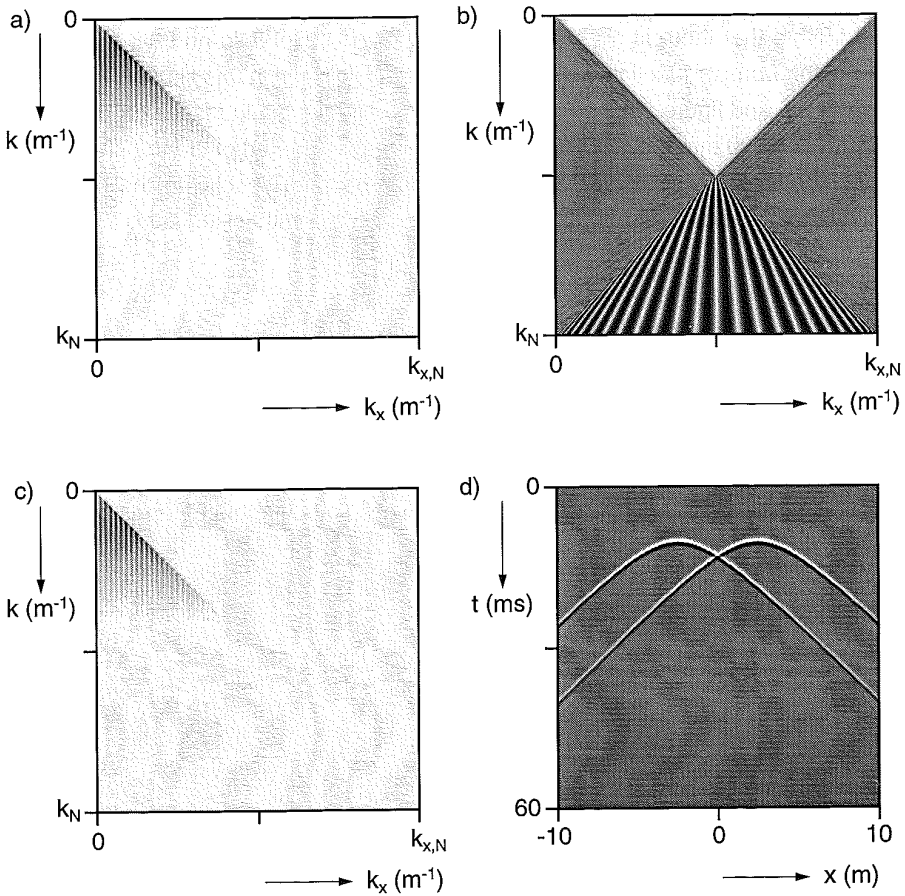

Figure 3.3.4: *Wave field of two monopole sources synthesised by a loudspeaker array with an intermediate loudspeaker distance of 80 mm.*
a) Incident field at the loudspeaker array, k_x-k domain
b) Transfer function from array to detection level, k_x-k domain
c) Synthesised field at the detection level, k_x-k domain
d) Synthesised field at the detection level, x-t domain

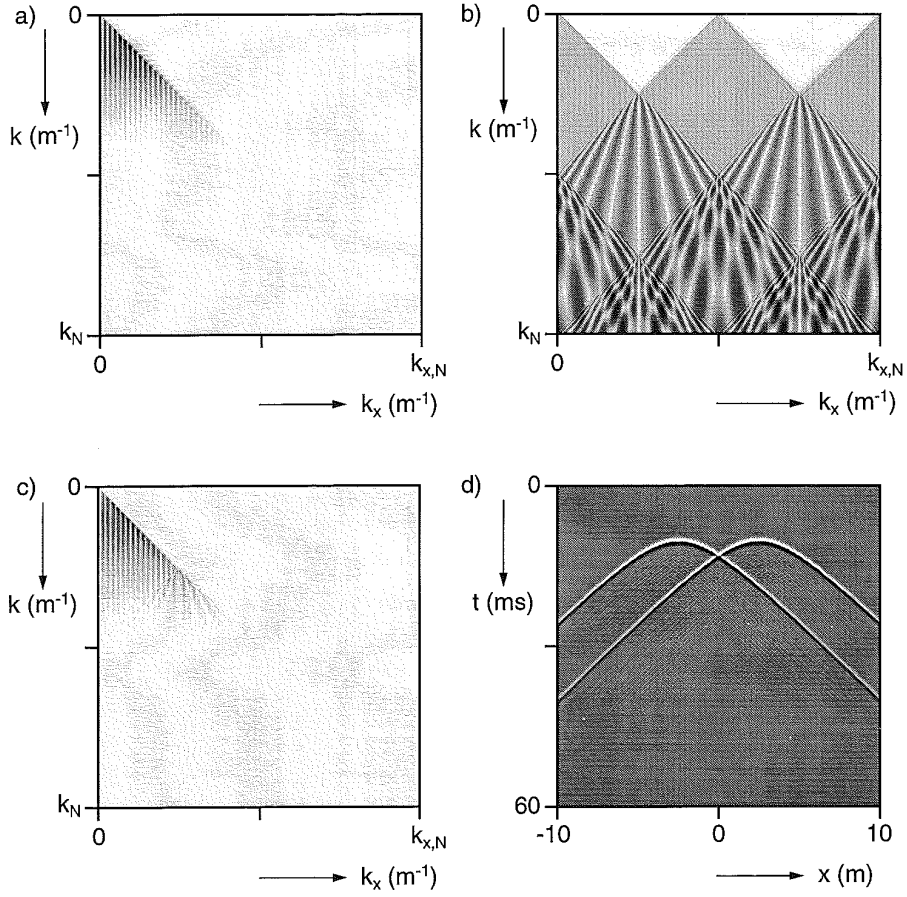

Figure 3.3.5: *Wave field of two monopole sources synthesised by a loudspeaker array with an intermediate loudspeaker distance of 160 mm.*
a) Incident field at the loudspeaker array, k_x-k domain
b) Transfer function from array to detection level, k_x-k domain
c) Synthesised field at the detection level, k_x-k domain
d) Synthesised field at the detection level, x-t domain

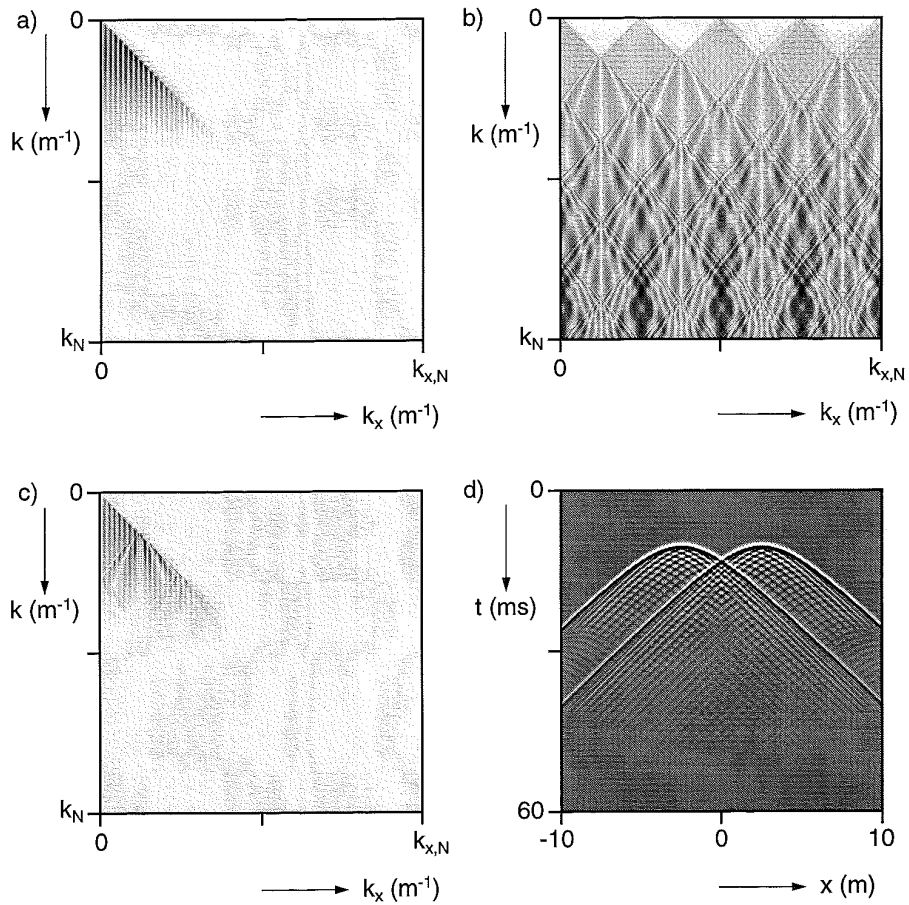

Figure 3.3.6: *Wave field of two monopole sources synthesised by a loudspeaker array with an intermediate loudspeaker distance of 320 mm.*
a) Incident field at the loudspeaker array, k_x-k domain
b) Transfer function from array to detection level, k_x-k domain
c) Synthesised field at the detection level, k_x-k domain
d) Synthesised field at the detection level, x-t domain

finite length loudspeaker array amounts to

$$\varepsilon(\omega) = \sqrt{\frac{jk}{2\pi}} \sum_{m=-\infty}^{-(M+1)} P(x_m, \omega) \cos(\varphi_m) \frac{e^{-jk\Delta r_m}}{\sqrt{\Delta r_m}} \Delta x + \sqrt{\frac{jk}{2\pi}} \sum_{m=M+1}^{\infty} P(x_m, \omega) \cos(\varphi_m) \frac{e^{-jk\Delta r_m}}{\sqrt{\Delta r_m}} \Delta x \,. \qquad (3.4.3)$$

The error described by the first term in equation (3.4.3) can be neglected provided that either the wave field at position (-(M+1)Δx,0) and all positions with lower index m is very small or the reconstruction sources at (-(M+1)Δx,0) and all positions with lower index m are located far from the receiver position. This means that the area where the reconstruction sources are located should extend far beyond both the source area and the receiver area. Because of symmetry, the same requirements hold for the second term in equation (3.4.3).

In practice the number of available reconstruction sources will usually be limited. Thus, usually the error term described by equation (3.4.3) will be significant. As an example consider the situation of figure 3.4.1: the wave field of a monopole line source is recorded at a distance z_0 = 5 m from the source. The recorded signals are amplified and then used to drive an array of dipole loudspeakers (line sources) that reconstructs the original wave field. The length of the loudspeaker array is limited to 10 meters. The wave field generated by the monopole source is shown in the x-z domain in figure 3.4.2a, the x-t domain registration of the wave field at position z=0 is shown in figure 3.4.2b. The corresponding graphs for the wave field generated by the finite length loudspeaker array are shown in figure 3.4.2 c and d. Note that the wave front in the reconstructed field has the right shape, but two additional wave fronts, centred around the edges of the loudspeaker array can be seen. When these secondary wave fronts arrive at the receiver more than about 50 ms after the first wave front, they will be heard as separate echoes, otherwise an audible colouration of the sound field might occur because of comb filter effects. Bilsen et al. (1970) showed that for a time delay of 5 ms the human ear is most sensitive for this colouration effect. To avoid colouration at this time delay value the secondary wave fronts should be attenuated by more than 20 dB relative to the primary wavelet.

In order to get more insight in the process of wave field reconstruction by means of a loudspeaker array it is helpful to consider the contribution of a few parts of the array separately, as indicated in figure 3.4.3. Only the right half of the array will be consid-

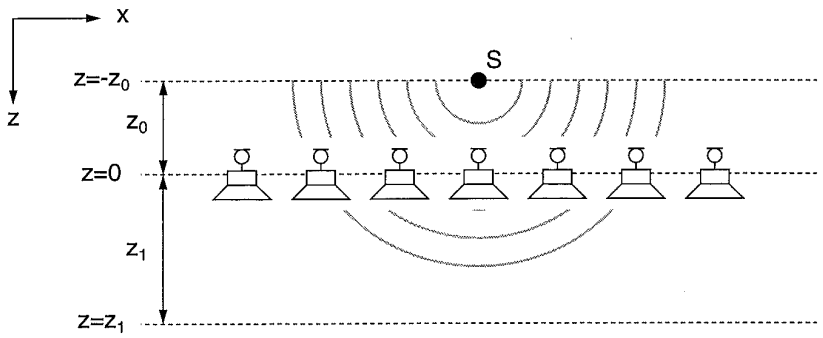

Figure 3.4.1: *The wave field of monopole source S is recorded by a microphone array at a distance z_0 and reconstructed by a loudspeaker array of finite length. The reconstructed wave field is compared to the direct wave field at a distance z_1 from the loudspeaker array.*

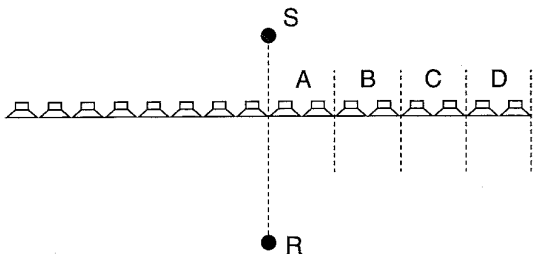

Figure 3.4.3: *To obtain insight in the procedure of wave field synthesis by a loudspeaker array, the contributions of four equally wide parts of the array to the synthesised monopole field at the receiver R are calculated. The four parts of the array are denoted by A, B, C and D respectively.*

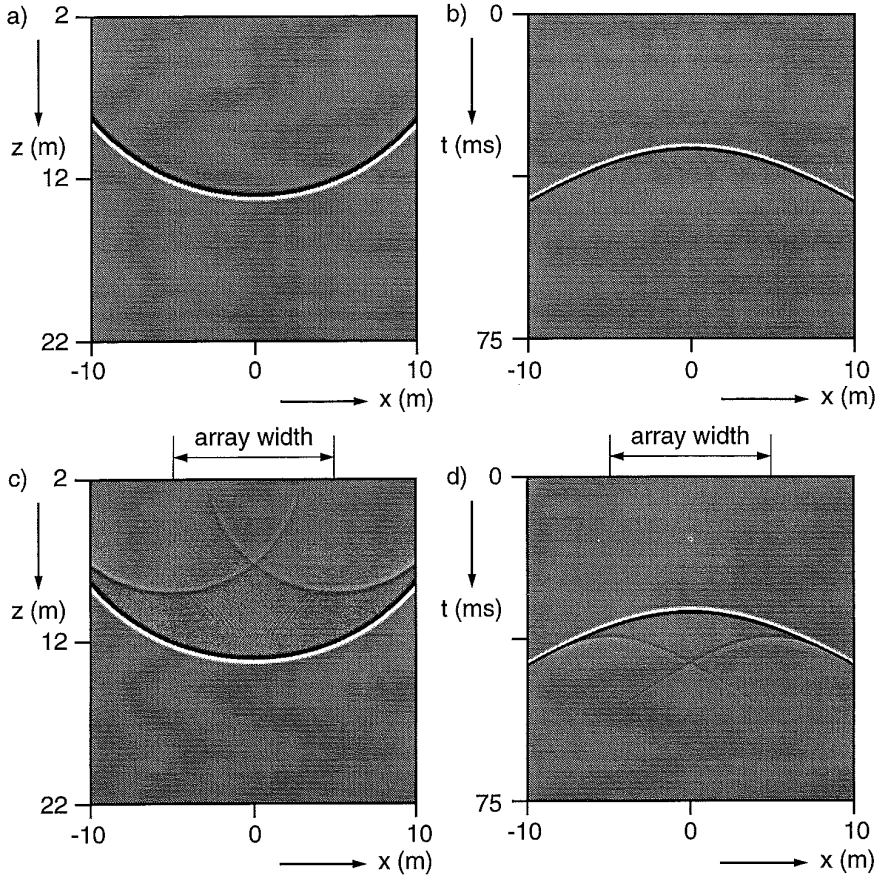

Figure 3.4.2: *Wave field of a monopole source, 10 dB clipped*

a) True wave field, x-z domain

b) True wave field, x-t domain

c) Wave field generated by a finite length loudspeaker array, x-z domain

d) Wave field generated by a finite length loudspeaker array, x-t domain

ered here, since because of symmetry the contribution of the other half is the same for a central source and receiver. In figure 3.4.4 a, c, e and g the contribution to the wave field at the receiver is shown for the four parts A, B, C and D of the array, as defined in figure 3.4.3. Figure 3.4.4 b, d, f and h show the cumulative sum of these wave field contributions. It can be seen from these graphs that each contribution consists of a primary pulse that is a delayed version of the source function, followed by a secondary pulse in counterphase. Each next part of the array adds a signal to the wave field that eliminates this secondary impulse, but adds another one a short time instant later and with a slightly smaller amplitude. Because of this slow decrease in amplitude of the secondary impulse, a lot of reconstruction sources will be needed in order to arrive at a negligible level of this pulse.

Another way to reduce the risk of audible echoes or colouration in the reconstructed signal is by smearing out the energy in the secondary pulse over a larger time interval. This can be accomplished by applying a decreasing weight to the loudspeaker signals near the edge of the loudspeaker array, the weighting function reaching zero at loudspeaker M+1. The effect of this weighting function will be that each next loudspeaker will eliminate much, but not all of the secondary impulse, while introducing a new secondary impulse which, because of the weighting coefficient, has a much lower amplitude. Thus, after the true impulse there will be some sound energy, but the spread over time assures that no separate echoes will be perceived by a listener.

The effect of applying a weighting function can be seen in figure 3.4.5, which shows the same wave field as figure 3.4.2, but now using a one-sided cosine window over the last 10% of the reconstruction sources at both sides of the array. Note that the secondary wavelets have almost disappeared, especially within the width of the array, whereas the effect of smearing out its energy is too small to be visible.

The effect of weighting the loudspeaker contribution can also be described in the spatial frequency domain. The sharp cutoff at the array edges (i.e. multiplication of the data in the space domain with a box-window) can in the spatial frequency domain be described by convolution with a sinc (or sin(x) / x) function, thus introducing a large amount of energy at high spatial frequencies. In the previous section it was shown that high spatial frequencies correspond to waves at large angles with the loudspeaker array. This means that the sharp cutoff will increase the amount of wave energy moving nearly parallel to the array, as can be seen also by comparing figure 3.4.2 with figure 3.4.5. Smoothing the sharp cutoff will decrease the energy at high spatial frequencies. This high frequency energy is contained mainly in the secondary impulses, thus the amplitude of these pulses will be reduced.

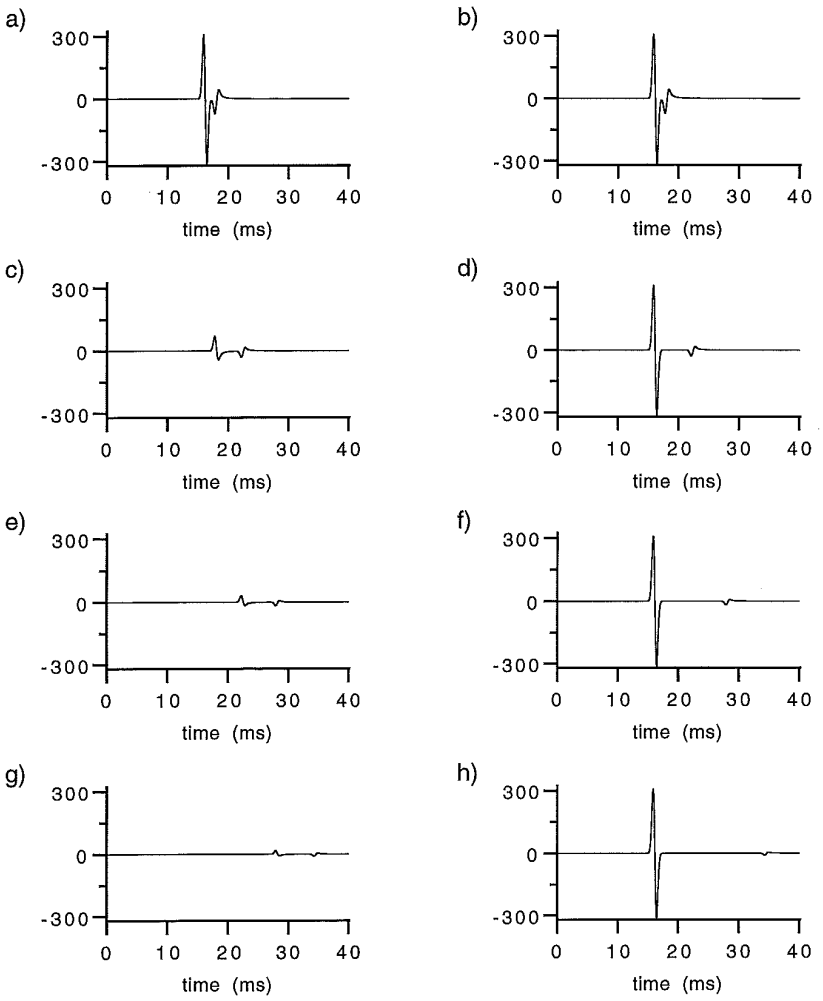

Figure 3.4.4: *Wave field generated by the four parts of the loudspeaker array shown in figure 3.4.3:*

a) part A *b) part A*
c) part B *d) part A + B*
e) part C *f) part A + B + C*
g) part D *h) part A + B + C + D*

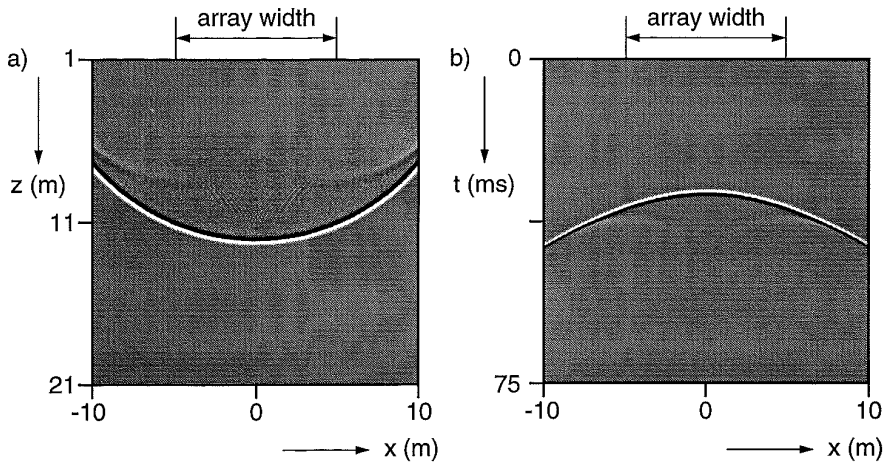

Figure 3.4.5: *Monopole wave field synthesised by a finite length loudspeaker array, weighted with a one-sided cosine window over the last 10% of loudspeakers at both sides.*
a) x-z domain *b) x-t domain*

3.5 3D synthesis with linear transducer arrays

According to the Rayleigh integrals (2.3.7) and (2.3.12) a planar distribution of transducers is needed to synthesise a 3D wave field. Thus, in order to reconstruct the wave field of some arbitrary sound source on the stage of a theatre, a planar distribution of loudspeakers should be placed between the source and the audience. This will not be a very useful situation because such a loudspeaker distribution would visually hide the stage from the audience.
The 2D Rayleigh representation integrals (2.4.2) and (2.4.5) require a linear transducer array only, but using 2D extrapolation operators for a 3D wave field will not generate the required result. Thus the question arises whether an extrapolation operator exists that produces the true 3D wave field at the listening positions by means of a linear array of monopole or dipole loudspeakers.

In order to find such an operator, a simple example will be considered (figure 3.5.1): the 3D wave field of a monopole source at position $(0,0,-z_0)$ is extrapolated using a linear array of loudspeakers positioned at the line given by y=0 and z=0. The receiver position is $(\xi,0,z_1)$. The y-coordinate is zero for both the source, the loudspeaker array and the receiver, so in the remainder of this section it will be omitted in order to keep the notation simple.
The wave field at the receiver is given by

$$P(\xi, z_1, \omega) = S(\omega) \frac{e^{-jk\hat{r}}}{\hat{r}}, \tag{3.5.1}$$

with $\hat{r}$ determined by

$$\hat{r} = \sqrt{\xi^2 + (z_0 + z_1)^2}. \tag{3.5.2}$$

Assuming firstly an array of monopole loudspeakers, the wave field at the receiver generated by the loudspeaker array will be written as a general integral equation:

$$P(\xi, z_1, \omega) = \int_{-\infty}^{\infty} a_m(x)\, e^{-jkr} \frac{e^{-jk\Delta r}}{\Delta r} dx, \tag{3.5.3}$$

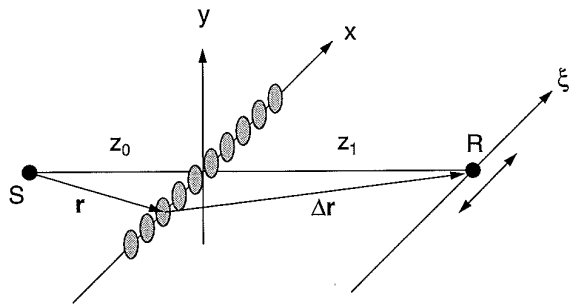

Figure 3.5.1: *The 3D wave field of a monopole source can be synthesised at the listening positions using a linear array of loudspeakers.*

in which $a_m(x)$ is a weighting function which must be determined such that equations (3.5.1) and (3.5.3) yield the same result for the wave field at the receiver. Note that the phase terms in equation (3.5.3) are in accordance with the extrapolation theory of Huygens, Kirchhoff and Rayleigh. Equating (3.5.1) to (3.5.3) yields:

$$\int_{-\infty}^{\infty} \frac{a_m(x)}{\Delta r} e^{-jk(r+\Delta r)} dx = S(\omega) \frac{e^{-jk\hat{r}}}{\hat{r}} . \qquad (3.5.4)$$

In order to solve integral equation (3.5.4) the integral on the left hand side must be evaluated. This can be accomplished using a mathematical concept called the 'stationary phase approximation' (Erdélyi, 1956), which states that an integral I of the form

$$I = \int_{-\infty}^{\infty} f(x)\, e^{jk\varphi(x)} dx \qquad (3.5.5)$$

can, for large values of k (high frequencies), be approximated by

$$I \approx \sqrt{\frac{2\pi}{k|\varphi''(x_0)|}} f(x_0)\, e^{jk\varphi(x_0)} e^{j\,\mathrm{sign}(\varphi''(x_0))\pi/4} . \qquad (3.5.6)$$

In this equation x_0 is the stationary point of the phase function $\varphi(x)$ and $\varphi''(x)$ denotes the second derivative of function $\varphi(x)$. Comparison of the integral in equation (3.5.4) with equation (3.5.5) yields that in this case:

$$\varphi(x) = -(r+\Delta r) , \qquad (3.5.7a)$$

$$\varphi'(x) = -\left(\frac{x}{r} + \frac{x-\xi}{\Delta r}\right) , \qquad (3.5.7b)$$

$$\varphi''(x) = -\left(\frac{z_0^2}{r^3} + \frac{z_1^2}{\Delta r^3}\right) , \qquad (3.5.7c)$$

and

$$f(x) = \frac{a_m(x)}{\Delta r} . \qquad (3.5.7d)$$

The stationary point x_0 of the phase function $\varphi(x)$ can be found by equating the right hand side of equation (3.5.7b) to zero and solving for x:

$$x_0 = \frac{z_0}{z_0 + z_1}\xi . \qquad (3.5.8)$$

Note that the stationary point is found at the intersection point of the line from source to receiver with the loudspeaker array (see figure 3.5.5).
Substituting the value of x_0 in equations (3.5.7a) and (3.5.7c) yields

$$\varphi(x_0) = -\hat{r} , \qquad (3.5.9a)$$

and

$$\varphi''(x_0) = -\frac{z_0^2 + z_0^3/z_1}{r_0^3} , \qquad (3.5.9b)$$

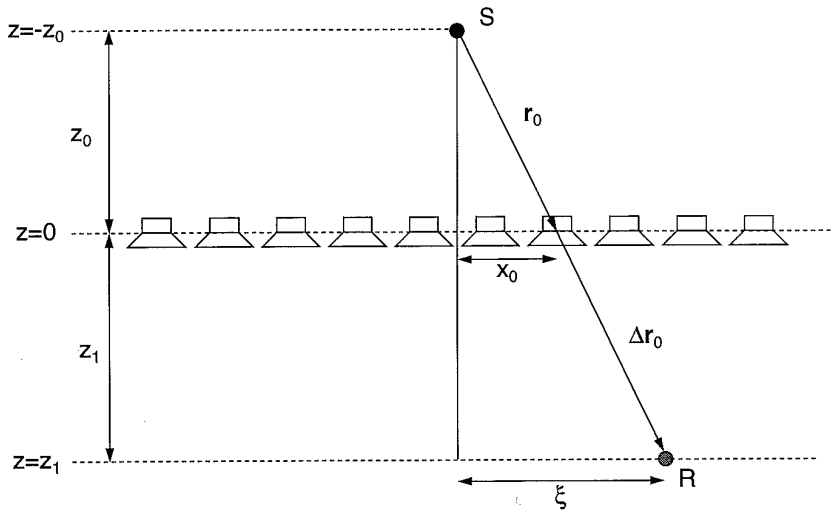

Figure 3.5.5: *The stationary point x_0 of the phase term of integral equation (3.5.4) is found at the intersection point of the line from source to receiver and the loudspeaker array.*

with

$$r_0 = \sqrt{x_0^2 + z_0^2}. \tag{3.5.9c}$$

Using the stationary phase approximation (3.5.6) together with equations (3.5.9a) and (3.5.9b) to solve equation (3.5.4) for $a_m(x)$ yields

$$a_m(x_0) = \Delta r_0 S(\omega) \sqrt{\frac{jk}{2\pi}} \sqrt{\frac{z_0}{z_0 + z_1}} \sqrt{\frac{z_0^3}{z_1 r_0^5}}, \tag{3.5.10}$$

with Δr_0 given by

$$\Delta r_0 = \sqrt{(\xi - x_0)^2 + z_1^2}. \tag{3.5.11}$$

Using the relation between r_0 and Δr_0:

$$\Delta r_0 = \frac{z_1}{z_0} r_0, \tag{3.5.12}$$

equation (3.5.10) can be rewritten as

$$a_m(x_0) = S(\omega) \sqrt{\frac{jk}{2\pi}} \sqrt{\frac{z_0}{z_0 + z_1}} \sqrt{\frac{z_0 z_1}{r_0^3}}. \tag{3.5.13}$$

From equation (3.5.8) it is clear that each value of ξ defines a unique value x_0 and while ξ ranges from $-\infty$ to $+\infty$ every value of x_0 is reached. Thus equation (3.5.10) may be generalised:

$$a_m(x) = S(\omega) \sqrt{\frac{jk}{2\pi}} \sqrt{\frac{z_0}{z_0 + z_1}} \sqrt{\frac{z_0 z_1}{r^3}}. \tag{3.5.14}$$

Thus, the wave field synthesis integral for a linear array of monopole sources is given by

$$P(\xi, z_1, \omega) = S(\omega) \sqrt{\frac{jk}{2\pi}} \sqrt{\frac{z_0^2 z_1}{z_0 + z_1}} \int_{-\infty}^{\infty} \frac{e^{-jkr}}{\sqrt{r^3}} \frac{e^{-jk\Delta r}}{\Delta r} dx, \tag{3.5.15}$$

or, introducing the incident wave field at the loudspeaker positions P(x,z=0,ω)

$$P(\xi, z_1, \omega) = \sqrt{\frac{jk}{2\pi}} \sqrt{\frac{z_0^2 z_1}{z_0 + z_1}} \int_{-\infty}^{\infty} \frac{P(x, z=0, \omega)}{\sqrt{r}} \frac{e^{-jk\Delta r}}{\Delta r} dx. \tag{3.5.16}$$

Along the same lines a wave field synthesis integral for a linear array of dipole sources can be derived. In this case the integral equation to be solved is given by

$$P(\xi, z_1, \omega) = \int_{-\infty}^{\infty} a_d(x)\, jk \frac{z_1}{\Delta r} \frac{e^{-jk\Delta r}}{\Delta r} e^{-jkr} dx. \tag{3.5.17}$$

Solving equation (3.5.17) for the weighting function for dipole sources $a_d(x)$ yields

$$a_d(x) = S(\omega) \sqrt{\frac{1}{jk2\pi}} \sqrt{\frac{z_1}{z_0 + z_1}} \sqrt{\frac{1}{r}}. \tag{3.5.18}$$

Thus for wave field synthesis using an array of dipole loudspeakers the appropriate integral is given by

$$P(\xi, z_1, \omega) = S(\omega) \sqrt{\frac{1}{jk2\pi}} \sqrt{\frac{z_1}{z_0 + z_1}} \int_{-\infty}^{\infty} \frac{jkz_1 e^{-jk\Delta r}}{\Delta r^2} \frac{e^{-jkr}}{\sqrt{r}} dx, \tag{3.5.19}$$

or, introducing the incident wave field at the loudspeaker positions P(x,z=0,ω)

$$P(\xi, z_1, \omega) = \sqrt{\frac{1}{jk2\pi}} \sqrt{\frac{z_1}{z_0 + z_1}} \int_{-\infty}^{\infty} \frac{jkz_1 e^{-jk\Delta r}}{\Delta r^2} \sqrt{r} P(x, z=0, \omega)\, dx. \tag{3.5.20}$$

Extrapolation of a 3D wave field using equation (3.5.3) or equation (3.5.17) is usually referred to as $2^1/_2$D extrapolation, because the method is an intermediate form between 3D extrapolation (1/r-attenuation) and 2D extrapolation (linear transducer arrays). Note that the wave field out of the plane y=0 is not taken into account in the derivation of the $2^1/_2$D operator. As a consequence, the wave field at these positions will be incorrect, but the listeners (all positioned in the plane y=0) will not notice this effect. It can be shown (Berkhout et al., 1993) that when the loudspeaker array is at some height y>0 equations (3.5.16) and (3.5.20) can still be used, provided that the true distances from the source to the array and from the array to the listener are used.

3.6 Reduction of the number of microphones

In all extrapolation formulas discussed in the previous sections, the wave field at a receiver position was expressed in terms of the values of the wave field at the position of the loudspeaker array. Thus, the wave field at the position of the loudspeaker array must be known. These data can be obtained by sampling the wave field at the position of the loudspeaker array, or by sampling the wave field at some plane between the sources and the loudspeaker array and extrapolating these data to the loudspeaker plane. Both methods have the disadvantage that the wave field must be sampled at small spatial intervals, which means that a very large number of microphones is required.

The number of required microphones can be reduced considerably when the position of the sources is known a priori. As an example consider the situation of figure 3.6.1: a monopole source S is positioned at a distance d of a microphone M. The wave field

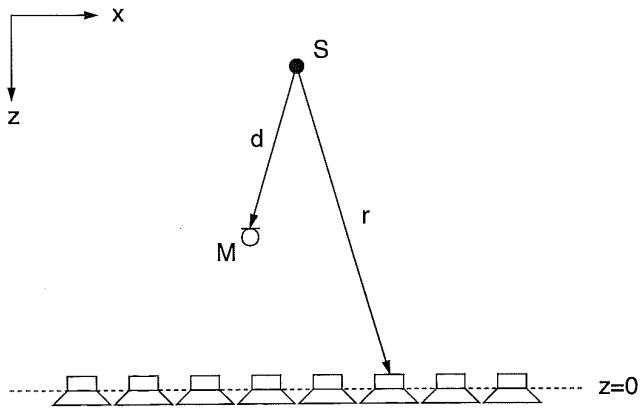

Figure 3.6.1: *When a microphone records a source of which the position is known, the wave field at the loudspeaker array can be extrapolated easily by using equation (3.6.2).*

M(ω) recorded by the microphone is given by

$$M(\omega) = S(\omega)\frac{e^{-jkd}}{d}. \qquad (3.6.1)$$

When the position of the source and the position of the microphone are known it is easy to extrapolate the microphone signal to the plane z=0:

$$P(x, z=0, \omega) = S(\omega)\frac{e^{-jkr}}{r} = M(\omega)\frac{d}{r}e^{jk(d-r)}. \qquad (3.6.2)$$

For a lecturer in an auditorium using a microphone-provided lectern, both source and microphone position are known quite accurately. Thus, in this situation equation (3.6.2) can be applied directly.

A more complicated situation arises when the sources move around in some finite area, e.g., the stage in a theatre. In this case the source position, and thus the distance from source to microphone is not a constant. This means that equation (3.6.2) becomes time variant. This problem can be solved by dividing the source area into a number of small parts, each part being illuminated by its own (highly-) directional microphone (see figure 3.6.2). Now for each microphone equation (3.6.2) can be applied, using the central spot of the microphone beam as the source position. This source position will be called the notional source position for the microphone.

The synthesised wave field will be built up from a number of notional sources, one for each microphone, positioned at the central spots of the microphone beams. The number of microphones needed is determined by the spatial resolution required. Usually, the spatial resolution required is such that a large reduction in microphone count can be obtained, in comparison with spatial sampling of the wave field, in which case the microphone distribution should fulfil the anti-aliasing requirements.

In order to avoid the notional source jumping from one position to another when the true source moves over the boundary of two adjacent sub-areas, there must be some overlap of the microphone beams, such that at the boundary two notional sources of the same amplitude exist, the centre of gravity of which coincides with the true source position. This way a listener will hear a notional source which moves smoothly over the source area.

a) Recording

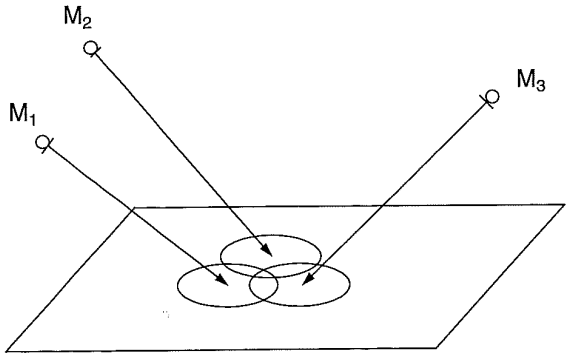

b) Reconstruction

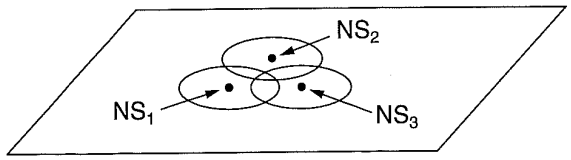

Figure 3.6.2: *By illuminating the stage area with a number of (highly-) directional microphones, the whole stage area can be addressed with a limited number of microphones (a). The synthesised wave field will be built up of notional point sources, one for each microphone, positioned at the central spot of the microphone beam (b). To prevent a source jumping from one microphone to another when moving around the stage, some overlap between the microphone beams is required.*

3.7 Reduction of the number of loudspeakers

Due to the short wave lengths encountered in audio-range acoustics, the sampling interval of a loudspeaker array capable of synthesizing arbitrary wave fields must be very small. For example, to synthesise the wave field of a point source that generates frequencies up to 5 kHz in an aliasing-free way, a loudspeaker array with a spatial sample interval of less than 34 mm is required. As a consequence, only very small loudspeakers can be used to build up the array.

In a practical situation, the number of loudspeakers to be used should be as small as possible, both because of cost and because of system complexity. The use of linear loudspeaker arrays instead of plane arrays as described in section 3.5 yields an enormous reduction of the required number of loudspeakers, but to span 10 meters with a spatial sample distance of 34 mm still about 300 loudspeakers are needed. Thus a further reduction is needed.

As a typical example consider the situation of figure 3.7.1: a loudspeaker array is used to synthesise a wave field at the audience area in an auditorium. It is clear from this figure that there is no need to generate waves (nearly) parallel to the loudspeaker array. Thus, the range of angles present in the synthesised wave field can be reduced. It was shown in section 3.3 that reduction of the range of angles in a wave field will reduce its spatial bandwidth (spatial filtering). This means that a wave field with a limited range of angles can be synthesised by an array with a larger sampling distance than would be required when all possible angles have to be reproduced. As an example consider the situation shown in figure 3.7.2: the wave field of a monopole source is reconstructed by means of a loudspeaker array. The area of interest is chosen such that only a limited range of angles in the wave field is of importance.

Figure 3.7.3a shows the wave field generated by the source, figure 3.7.3b the wave field generated by the loudspeaker array without any spatial filtering. It is clear that some aliasing is present in the wave field of figure 3.7.3b. Applying a spatial filter to reduce the high angle energy in the synthesised wave field yields the graph of figure 3.7.3c. In this case the spatial aliasing has disappeared, but the amplitude of the wave field decreases rapidly outside the area of interest.

The theory discussed in this chapter can be used to design a wave field synthesis system. In the next chapter the design and implementation of such a system will be discussed.

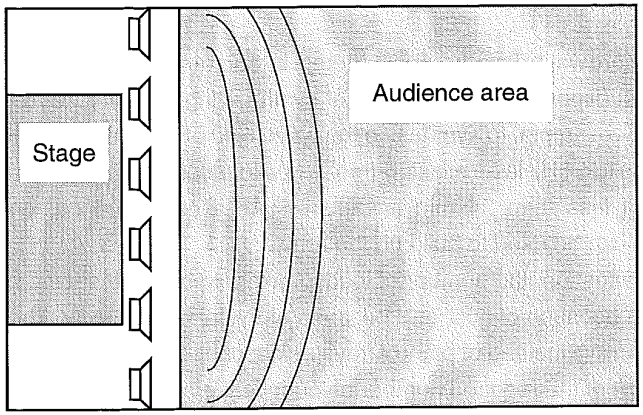

Figure 3.7.1: *In most halls the audience is located such that most listeners receive sound energy only from a small range of angles around normal incidence. Thus a wave front generating system needs to generate plane wave components in this range of angles only.*

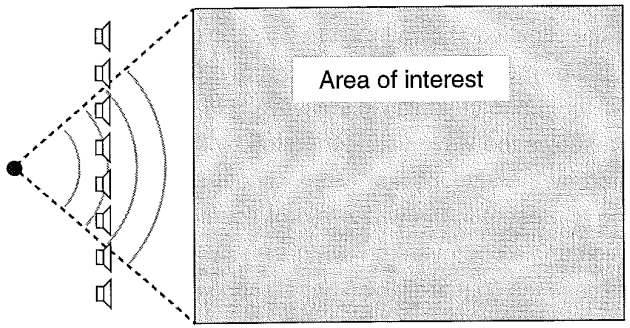

Figure 3.7.2: *Example of a wave front synthesis system which needs to generate a wave field for a limited range of angles only.*

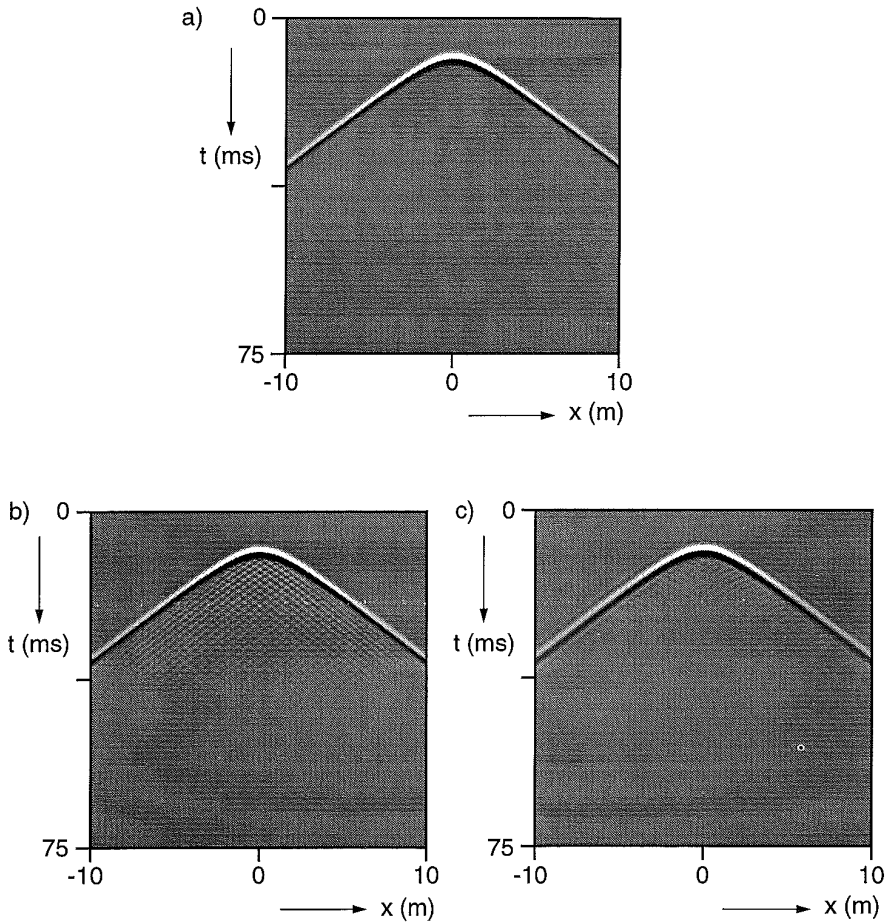

Figure 3.7.3: *The effect of spatial filtering on aliasing. Registrations in the x-t domain.*
a) direct wave field
b) synthesised wave field with aliasing
c) spatially filtered synthesised wave field: aliasing suppressed

4. DESIGN OF A WAVE FIELD SYNTHESIS SYSTEM

In the previous chapters the theory of wave field synthesis has been discussed. In the current chapter this theory will be used for the design of a wave field generating system. The first part of the chapter (sections 4.1, 4.2 and 4.3) describes a laboratory setup (3 inputs x 12 outputs) to test the basic principles of wave field synthesis, the implementation of the required extrapolation operators on a digital signal processor (DSP) and some listening experiments for a perceptual evaluation of the results. The second part of the chapter (sections 4.4, 4.5 and 4.6) describes the design of a prototype system (6 inputs x 48 outputs) and an objective and subjective evaluation of the results obtained with it. Finally, the last part of the chapter discusses the use of wave front generating systems in equipment designed for acoustic control within an enclosure.

4.1 Wave field extrapolation in the time domain

The wave field extrapolation formulas given in chapter 2 and chapter 3 describe the extrapolation process in the (temporal) frequency domain. For a real time wave field synthesis system however, a time domain description is more appropriate. Thus, the extrapolation theory must be transformed to the time domain.
To cover all extrapolation operators simultaneously, a general matrix formulation will

be used here:

$$\mathbf{R}(\omega) = \mathbf{H}_{RL}(\omega)\,\mathbf{W}(\omega)\,\mathbf{H}_{LS}(\omega)\,\mathbf{S}(\omega)\ , \tag{4.1.1}$$

in which $\mathbf{S}(\omega)$ is a vector containing all (notional) source functions, $\mathbf{R}(\omega)$ is a vector containing the wave field at a set of receiver positions, $\mathbf{H}_{LS}(\omega)$ is a matrix describing the transfer from the sources towards the loudspeakers, $\mathbf{W}(\omega)$ is a matrix operator that transforms the incident field into the appropriate driving signals for the loudspeakers and $\mathbf{H}_{RL}(\omega)$ is a matrix describing the transfer from the loudspeakers towards the receivers (see figure 4.1.1).
As an example of equation (4.1.1) the situation of a single monopole source and a single receiver will be considered. In this case the source vector $\mathbf{S}(\omega)$ and the receiver vector $\mathbf{R}(\omega)$ both reduce to a scalar, $\mathbf{H}_{LS}(\omega)$ becomes a column vector and $\mathbf{H}_{RL}(\omega)$ becomes a row vector. The transfer from the source to loudspeaker n is given by the monopole transfer function:

$$H_{L_nS}(\omega) = S(\omega)\frac{e^{-jkr_n}}{r_n}\ , \tag{4.1.2}$$

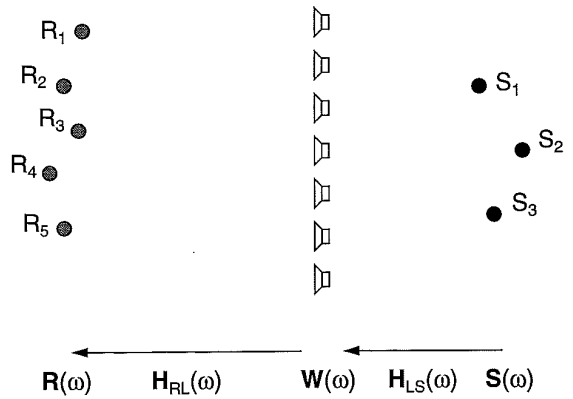

Figure 4.1.1: *The wave field extrapolation process can be described in terms of a matrix multiplication.*

in which $H_{L_nS}(\omega)$ is the n^{th} element of the source-loudspeaker transfer function vector and r_n is the distance from the source to loudspeaker n (see figure 4.1.2). The transfer from loudspeaker n to the receiver can, at least in the far field, be described by

$$H_{RL_n}(\omega) = Q(\Delta\mathbf{r}_n, \omega)\frac{e^{-jk\Delta r_n}}{\Delta r_n}\ , \tag{4.1.3}$$

in which $H_{RL_n}(\omega)$ is the n^{th} element of the loudspeaker-receiver transfer function vector, $Q(\Delta\mathbf{r}_n,\omega)$ is a weighting function that describes the frequency and directivity properties of the loudspeaker. For monopole sources, $Q(\Delta\mathbf{r}_n,\omega)$ equals unity, while for dipole sources this weighting function amounts to

$$Q(\Delta\mathbf{r}_n, \omega) = jk\cos(\varphi) = jk\frac{z_1}{\Delta r_n}\ . \tag{4.1.4}$$

The weighting matrix $\mathbf{W}(\omega)$ depends on the loudspeaker type used. For monopole sources, the weighting matrix $\mathbf{W}_{monopole}(\omega)$ is a diagonal matrix with weighting coeffi-

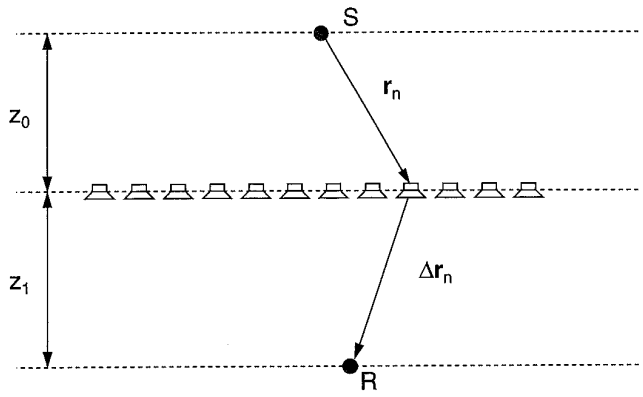

Figure 4.1.2: *The distance from source S to loudspeaker n is denoted by $\mathbf{r}_n$, the distance from loudspeaker n to the receiver R is denoted by $\Delta\mathbf{r}_n$.*

cients $W_{n,monopole}(\omega)$ given by

$$W_{n,\,monopole}(\omega) = \sqrt{\frac{jk}{2\pi}}\sqrt{\frac{z_0^2 z_1}{z_0+z_1}}\sqrt{\frac{1}{r_n}}\,, \tag{4.1.5}$$

as can be seen from equation (3.5.16). For dipole sources the elements $W_{n,dipole}(\omega)$ of the diagonal weighting matrix $\mathbf{W}_{dipole}(\omega)$ are given by

$$W_{n,\,dipole}(\omega) = \sqrt{\frac{1}{jk2\pi}}\sqrt{\frac{z_1}{z_0+z_1}}\sqrt{r_n}\,, \tag{4.1.6}$$

as can be seen from equation (3.5.20).
In a practical situation the incident wave field will be recorded at some distance from the loudspeakers, by a number of (highly) directive microphones. The wave field recorded by these microphones should be extrapolated to the loudspeaker positions:

$$P(\mathbf{r}_n, \omega) = M(\omega)\, H_{MS}^{-1}(\omega)\, H_{L_nS}(\omega)\,, \tag{4.1.7}$$

in which $M(\omega)$ is the microphone signal, $H_{MS}(\omega)$ is the source-microphone transfer function and $H_{L_nS}(\omega)$ describes the transfer from the source to loudspeaker n.
For a monopole source at a distance d from the microphone, the source-microphone transfer function is given by

$$H_{MS}(\omega) = \frac{e^{-jkd}}{d}\,, \tag{4.1.8}$$

the source-loudspeaker transfer is given by

$$H_{L_nS}(\omega) = \frac{e^{-jkr_n}}{r_n}\,, \tag{4.1.9}$$

so that the extrapolation process can be described by (see figure 4.1.3)

$$P(\mathbf{r}_n, \omega) = M(\omega)\,\frac{d e^{-jk(r_n-d)}}{r_n}\,. \tag{4.1.10}$$

By transforming equation (4.1.10) to the time domain, the exponential term is replaced by a time delay, while the multiplication by the scalar factor d/r_n remains unchanged:

$$p(\mathbf{r}_n, t) = \frac{d}{r_n} m(t-\tau_n) = \frac{d}{r_n} m\left(t-\frac{r_n-d}{c}\right)\,, \tag{4.1.11}$$

in which m(t) is the inverse Fourier transform of the microphone signal $M(\omega)$.
The next step in the extrapolation process is formed by the weighting matrix $\mathbf{W}(\omega)$. The most simple situation arises when $\mathbf{W}(\omega)$ is a diagonal matrix, independent of frequency. In that case, only a multiplication factor for each loudspeaker is needed. When $\mathbf{W}(\omega)$ is non-diagonal, and frequency independent, the wave field calculated at each loudspeaker position is smeared out over the complete loudspeaker array (see figure 4.1.4).
If $\mathbf{W}(\omega)$ is diagonal, and frequency dependent, the matrix multiplication process in the frequency domain description leads to a convolution procedure in the time domain. In this case, the incident wave field at each loudspeaker position should be convolved with an amplitude shaping function $w_n(t)$.
In the most general situation, $\mathbf{W}(\omega)$ is neither diagonal nor frequency independent. In this case the incident wave field at each loudspeaker position is, by the **W** matrix, distributed over all loudspeakers, with a unique convolution filter $w_{jk}(t)$ for each possible transfer. A complete implementation of this procedure requires a lot of computational power.

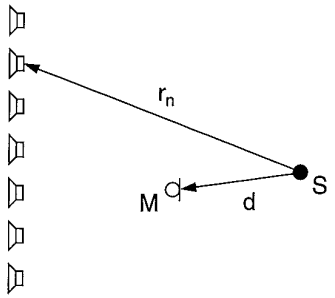

Figure 4.1.3: *The wave field recorded by microphone M can be extrapolated towards loudspeaker n by applying a time delay $\tau_n=(r_n-d)/c$ and multiplying by d/r_n.*

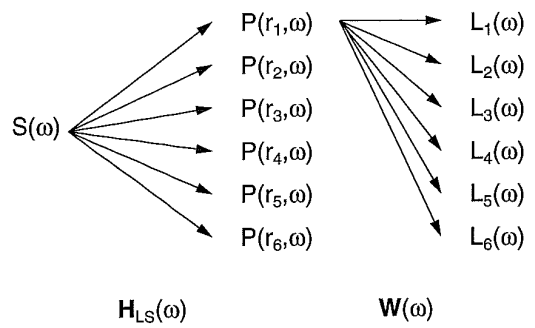

Figure 4.1.4: *When **W**(ω) is a non-diagonal matrix, the wave field calculated at each loudspeaker position is distributed over all loudspeaker driving functions.*

From equations (4.1.5) and (4.1.6) it is clear that for monopole and dipole loudspeakers **W**(ω) is a frequency dependent diagonal matrix. This means that in order to calculate the loudspeaker driving function from the incident wave field at the loudspeakers, a convolution is required. The filter that should be applied ($\sqrt{jk}$ for monopoles and $\sqrt{1/jk}$ for dipoles) must be implemented in the form of a FIR filter.
In summary, the time domain procedure for the wave field synthesis process can be described as follows. The time delays for the extrapolation process are in accordance with Huygens's principle and independent of the loudspeaker type used. These time delays determine the shape of the wave front, the amplitude term influences the energy distribution along the wave fronts only. In practice usually an approximation of the amplitude weighting function **W**(ω) is used. This way, the loudspeaker array produces wave fronts of the right shape, but with the wave energy distributed over the wave fronts in an incorrect way. Whether the approximation for **W**(ω) is allowed or not should be evaluated by means of theoretical analysis, simulation, measurement and listening experiments for each particular situation.

4.2 Laboratory setup of a wave field synthesis system

In figure 4.2.1 a sketch is given of the laboratory setup for wave field synthesis used in

the current research project. It consists of 3 analog input channels, 12 analog output channels and a digital signal processing system. The processing system is based on a digital signal processor (DSP) that gets its input from a set of AD converters, calculates the required output signals and sends these signals to a set of DA converters.
The DSP used is an integer type processor (Texas Instruments TMS320C25) with an instruction cycle of 100 ns. This processor is capable of calculating 12 weighted delays for each input channel at a sampling frequency of 13 kHz per channel. No time is then left to calculate the convolution process described by weighting matrix **W**(ω).
During most tests the laboratory setup was placed in an anechoic chamber. In order to use the available width of the anechoic chamber optimally, the interval between the loudspeakers is chosen to be 45 cm, giving a total array width of 5 meter (see figure 4.2.2). According to equation (3.2.3), an array with this loudspeaker interval will produce wave fronts free from spatial aliasing for frequencies up to 380 Hz, if all radiation angles (-90° to +90°) play a reievant role.
It is clear that this laboratory setup for wave field synthesis is a compromise between cost and complexity at the one hand and satisfaction of the wave field extrapolation theory at the other. The remaining part of this section will discuss the effects of the simplifications and approximations made in the design of the laboratory setup.
First the effect of omitting the convolution procedure as described by weighting matrix **W**(ω) will be discussed. The exact form of this amplitude shaping function depends on the loudspeaker type used. For monopole loudspeakers the appropriate amplitude

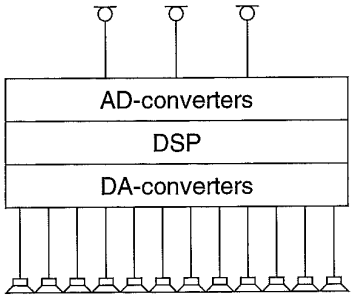

Figure 4.2.1: *The laboratory setup for wave field synthesis consists of 3 analog inputs and 12 analog outputs. A DSP is used for the required signal processing.*

shaping function is given by equation (4.1.5). The frequency dependent part of this weighting function is given by $\sqrt{jk}$, which is a high pass filter with a slope of 3 dB/oct. Omitting this filter in the wave field synthesis process will cause a wave field with a spectrum that drops by 3 dB/oct relative to the spectrum of the original wave field.
As an illustration some 3D simulations will be discussed. First, consider the wave field of a monopole source, recorded by an array of microphones (see figure 4.2.3), in fact representing a row of monaural listeners. Figure 4.2.4a shows the signals received by the microphones as a function of time. Note that the monopole response shows up as a hyperbola in this x-t plot. In figure 4.2.4b the signal received by the microphone at the centre of the detector array is shown in order to reveal the shape of the source function, which is chosen to be a minimum phase wavelet with a gaussian frequency distribution with a cut-off frequency of 1000 Hz, as can be seen in figure 4.2.4c.
Figure 4.2.5 a, b and c show the same plots, but now for a synthesised monopole wave

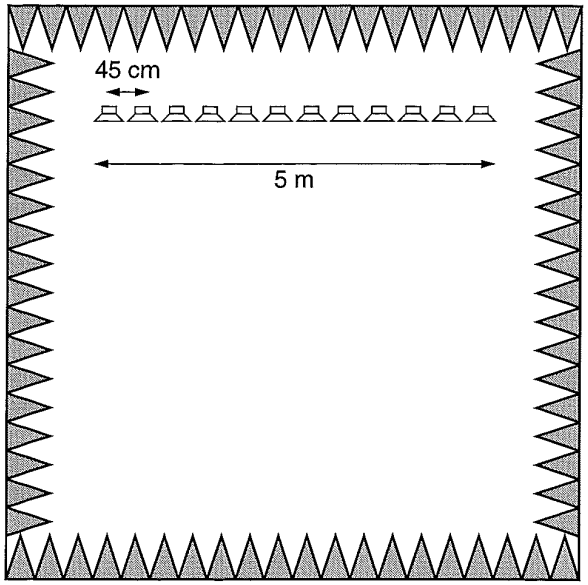

Figure 4.2.2: *The wave front synthesis system in an anechoic chamber environment*

field using the amplitude shaping function as described by equation (4.1.5), thus including the $\sqrt{jk}$ term. Note that there is a perfect match between the true and the synthesised wave field.
The plots in figure 4.2.6 a, b and c show the synthesised wave field again, but omitting the $\sqrt{jk}$ term in the amplitude shaping. From these plots it is clear that the hyperbolic shape of the x-t registration remains the same, but the energy of the source wavelet is smeared out in time, as expected for a synthesis system that implicitly applies a low pass filter to the input signal.
The amplitude shaping filter for dipole loudspeakers is given by equation (4.1.6). The frequency dependent part of this amplitude shaping function is given by $\sqrt{1/jk}$, thus showing low-pass behaviour with an amplitude decrease of 3 dB/oct. Omitting this term in the synthesis process is equivalent to applying a high-pass filter with a slope of 3 dB/oct to the wave field.
In figure 4.2.7 a, b and c the synthesised monopole wave field is shown again, but now using dipole loudspeakers without amplitude shaping in the synthesis process. Note that the ratio between the signals of figure 4.2.7b and figure 4.2.6b is in the frequency domain given by a factor jk, meaning that the signal of figure 4.2.7b is the time derivative of the signal in figure 4.2.6b.
From the previous examples it can be concluded that omitting the convolution filter in the wave field synthesis system will cause a colouration of the synthesised wave field, while the spatial properties like wave front curvature (x-z domain) or hyperbola shape

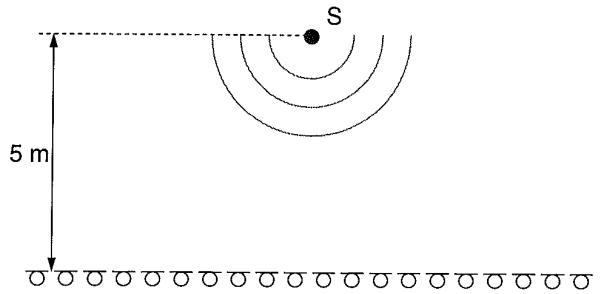

Figure 4.2.3: *The wave field of a monopole source S is recorded by an array of microphones*

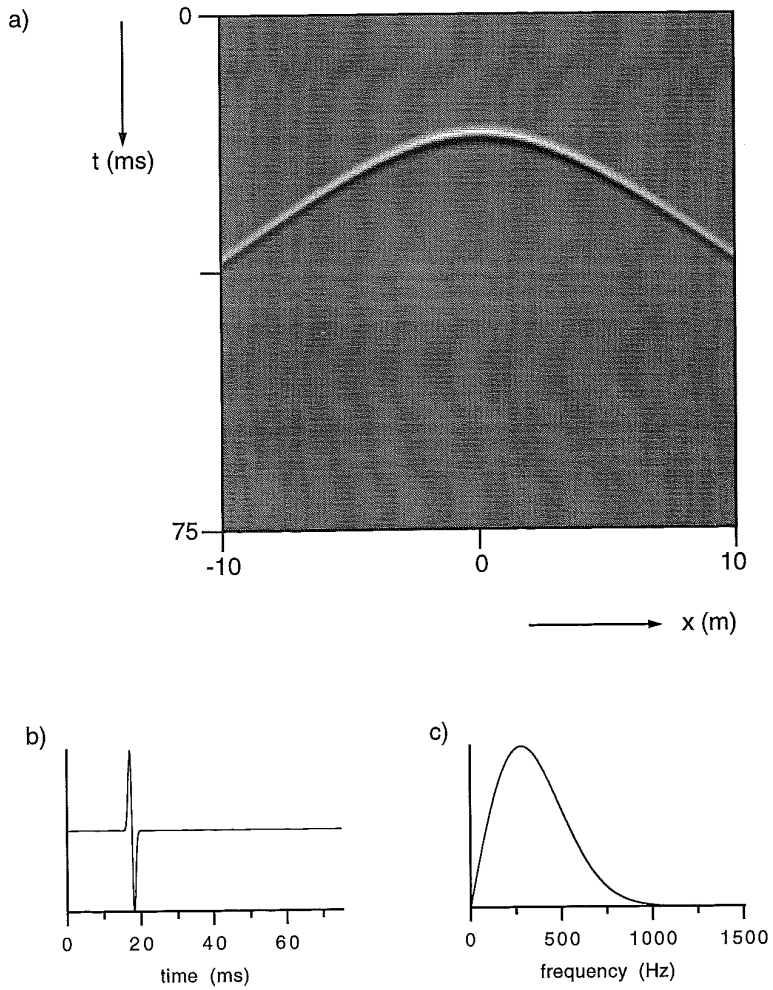

Figure 4.2.4: *The wave field of a monopole source recorded by a microphone array (a), the signal at the central microphone (b), and the spectrum at the central microphone (c).*

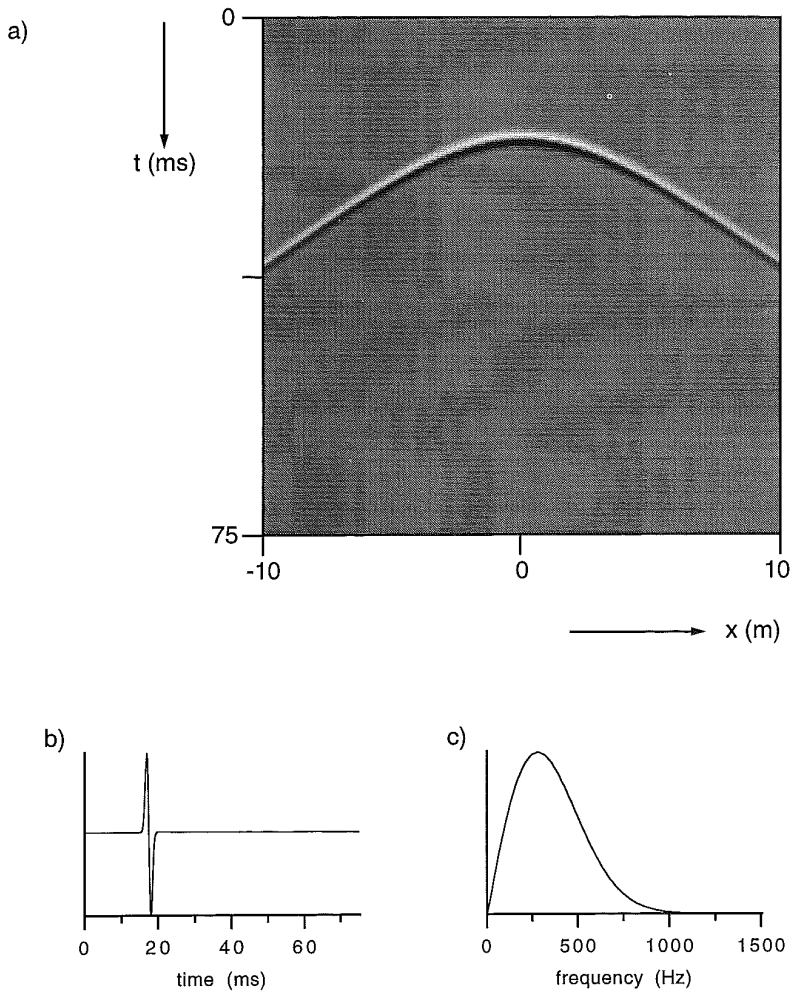

Figure 4.2.5: *Correctly synthesised monopole wave field using monopole loudspeakers, recorded by a microphone array (a), the signal at the central microphone (b), and the spectrum at the central microphone (c).*

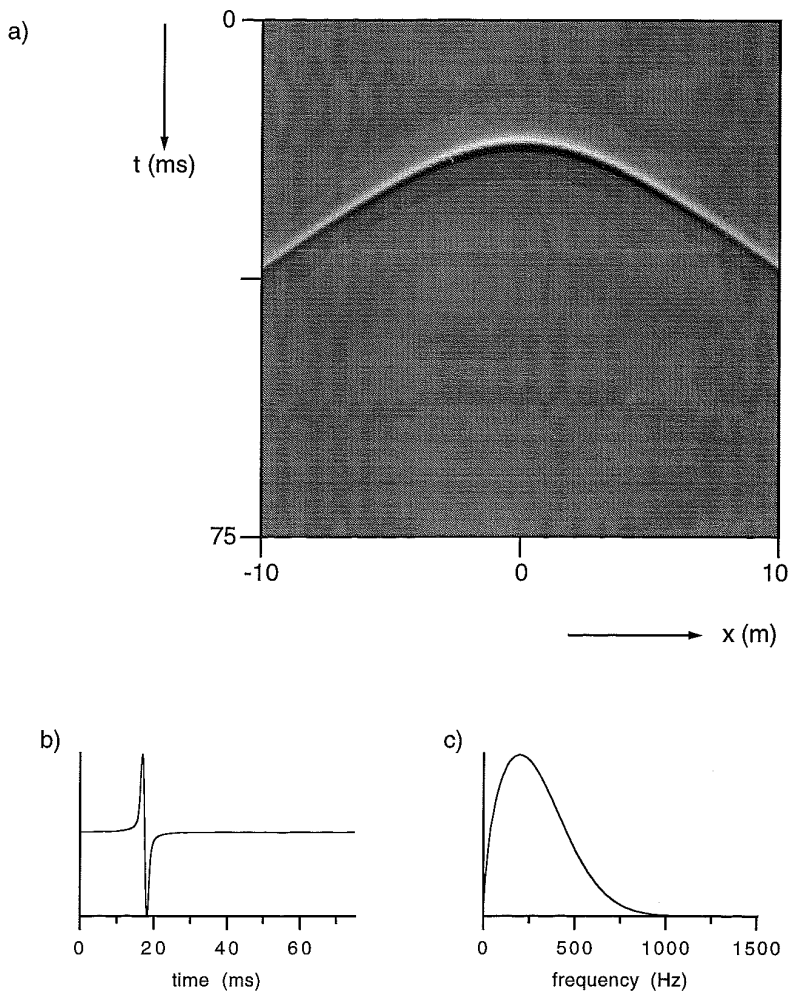

Figure 4.2.6: *Synthesised monopole wave field using monopole loudspeakers without amplitude shaping filter, recorded by a microphone array (a), the signal at the central microphone (b), and the spectrum at the central microphone (c).*

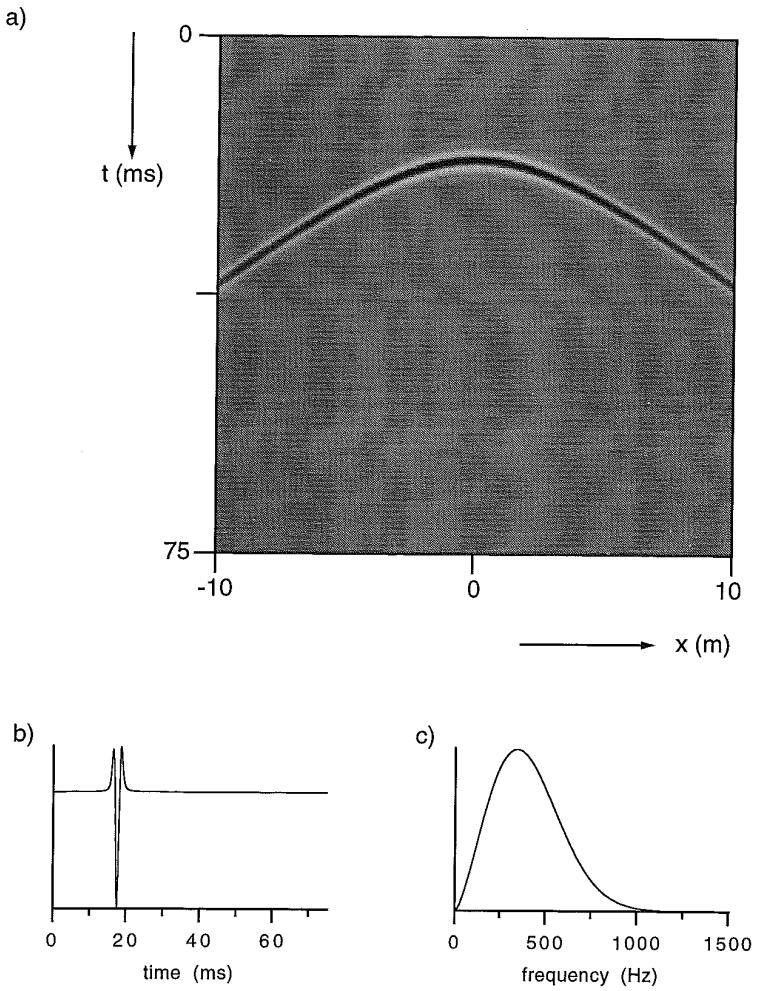

Figure 4.2.7: *Synthesised monopole wave field using dipole loudspeakers without amplitude shaping filter recorded by a microphone array (a), the signal at the central microphone (b), and the spectrum at the central microphone (c).*

(x-t domain) remain unchanged. The colouration effects might be compensated for by using a tone control system on the input circuit.

Another important discrepancy between theory and practice is the loudspeaker distance used in the wave front synthesis system. The lowest frequency at which spatial aliasing occurs is about 380 Hz, which means that a reproduced speech signal will contain aliased components.

As was shown in Section 3.3, spatial aliasing viewed in the x-t domain shows up as additional wave energy after the required wavelet. In figure 4.2.8a a synthesised wave field is shown with a maximum frequency of 1000 Hz and a loudspeaker interval of 0.31 m. Thus, some spatial aliasing is present in the synthesised field, which is clear especially from the central microphone signal shown in figure 4.2.8b and c. When the loudspeaker distance is doubled, the amount of wave energy arriving after the required impulse largely increases, as can be seen from figure 4.2.9a, b and c.

For very sharp impulses the response of the wave front synthesis system will be built up from a set of discrete impulses, one for each loudspeaker in the array. In the frequency domain these impulses lead to a flat part in the frequency response from DC up to the spatial aliasing frequency, provided that the correct amplitude shaping filter is applied. Above the spatial aliasing frequency the frequency response shows a rather irregular behaviour, as can be seen from figure 4.2.10, where the frequency response at the centre of a (very long) array of point sources is shown for several values of the spatial interval between the sources. Note that the amplitude shaping filter causes an increase in the average frequency response above the spatial aliasing frequency.

From the previous discussion it can be concluded that omitting the amplitude shaping filter in the synthesis process will cause a smooth change in the frequency response, which might be compensated for by using a simple tone control system or equaliser. The effect of spatial aliasing, however, is a wild frequency response behaviour in the frequency range above the spatial aliasing frequency, leaving a flat spectrum in the lower frequency regions only. This effect can not be compensated for in a simple way. In the laboratory setup for wave field synthesis both effects are present simultaneously. The monopole field generated by this system has both been simulated and measured, using a band limited impulse (300 Hz - 3 kHz) as a source signal. In figure 4.2.11 these responses are shown as x-t plots. The contribution of each loudspeaker can be seen as a separate hyperbola, which means that a large amount of spatial aliasing is present in the synthesised field.

The monopole source field synthesised by the laboratory setup will have a well defined low frequency part and a less clear high frequency part. The subjective localisation of

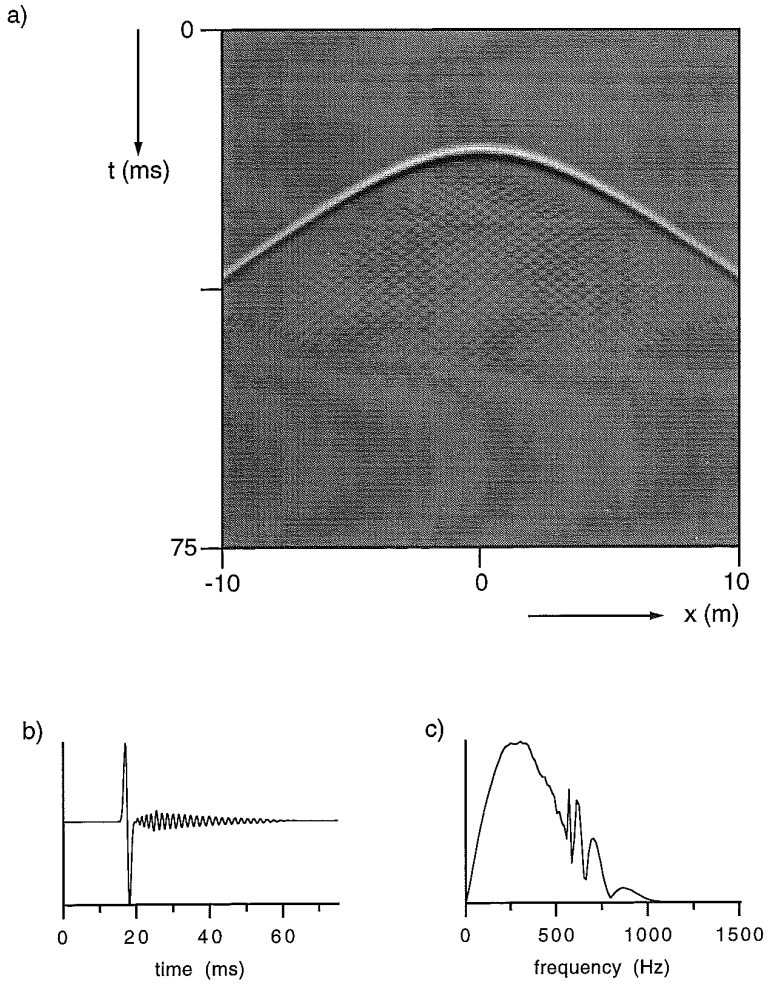

Figure 4.2.8: *Synthesised monopole wave field with some spatial aliasing, recorded by a microphone array (a), the signal at the central microphone (b), and the spectrum at the central microphone (c).*

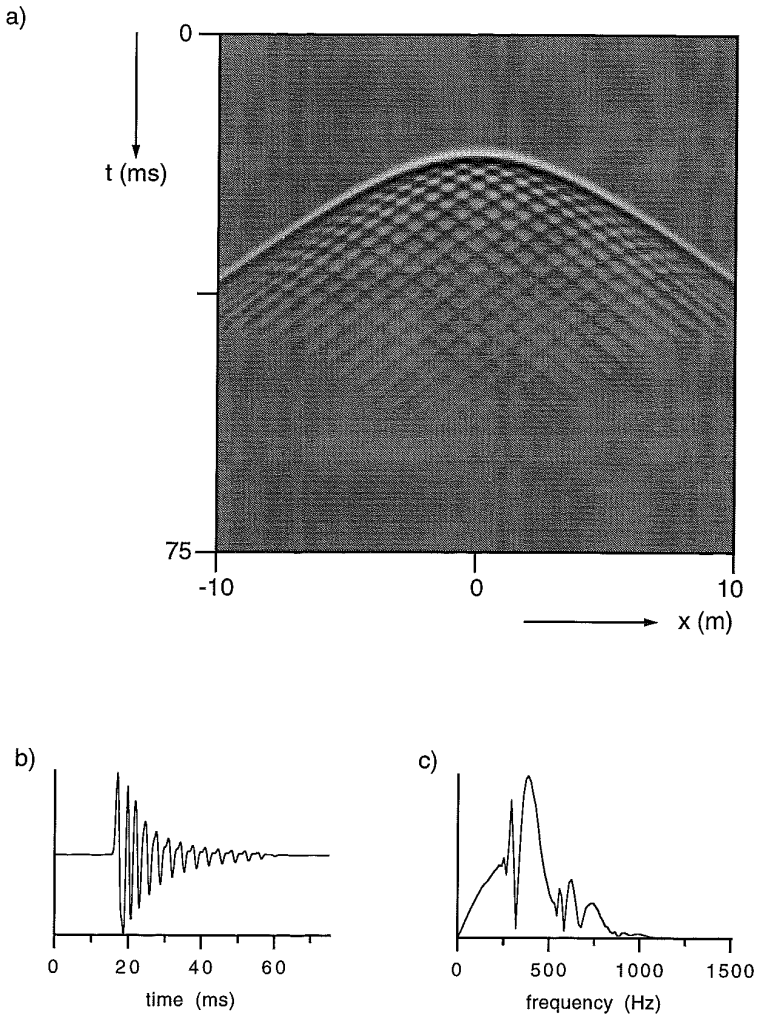

Figure 4.2.9: *Synthesised monopole wave field with severe spatial aliasing, recorded by a microphone array (a), the signal at the central microphone (b), and the spectrum at the central microphone (c). The loudspeaker interval is doubled relative to the interval used in figure 4.2.8.*

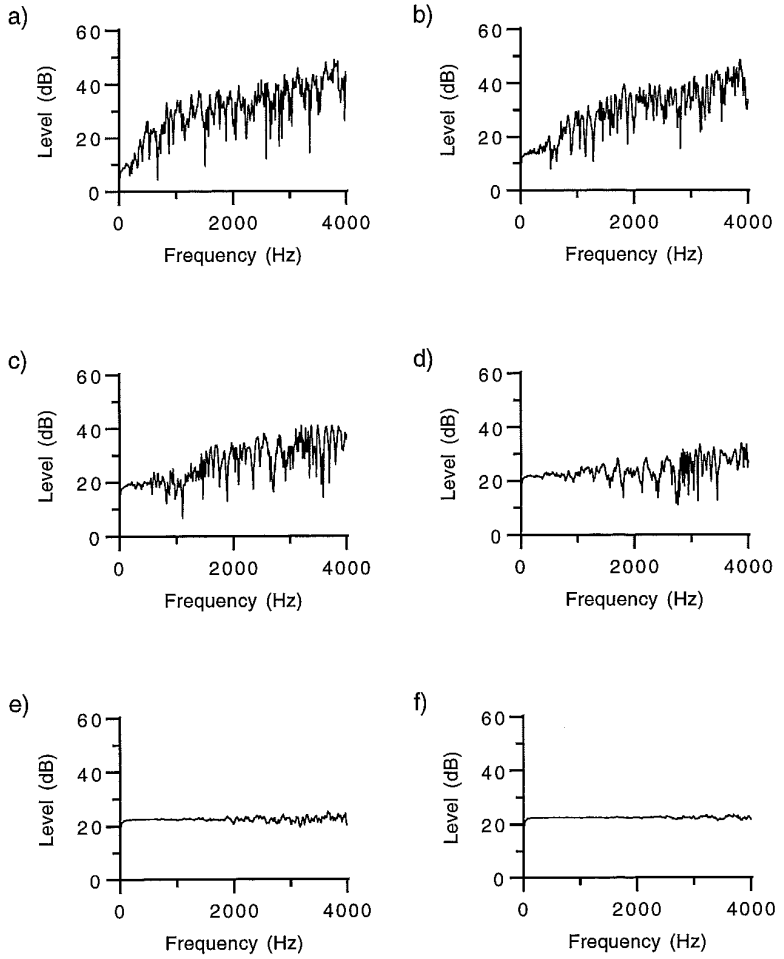

Figure 4.2.10: *The frequency response for a wave front synthesis system for several values of the loudspeaker interval Δx. Spatial aliasing occurs for frequencies above c/2Δx. Correct amplitude shaping is applied.*
a) Δx = 1 m, b) Δx = 0.5 m, c) Δx = 0.25 m,
d) Δx = 0.125 m, e) Δx = 0.063 m, f) Δx = 0.031 m.

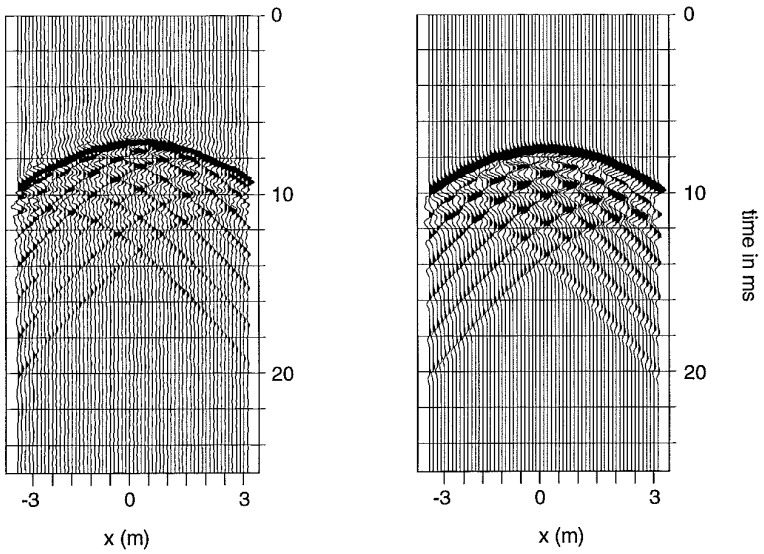

Figure 4.2.11: *Monopole wave field synthesised by the laboratory setup for wave field synthesis: measured (left) and simulated (right). The spatial aliasing in the wave field is clearly visible in both results.*

the image source can be predicted neither from a theoretical analysis nor from the psycho-acoustical literature. To obtain information about the perception of the image source, listening experiments are required. In the next section these listening experiments will be discussed.

4.3 Listening experiments

To obtain some insight in the perceptual properties of the wave field synthesised by the wave field generating system several listening experiments have been carried out. In this section these experiments will be described and a discussion of the results will be given.

The arrangement for the listening experiments is shown in figure 4.3.1. The loudspeaker array is placed in an anechoic chamber, with the listener positioned in front of

the loudspeaker array, at 4 meter distance from the central loudspeaker. A hand-held computer terminal is available to the listener to type in the responses during the experiment. The DSP processor equipment, the PC that controlled the listening experiment and the experiment leader were placed in an adjacent control room.

As speech amplification was the main goal of the research project, a speech stimulus was used in the listening experiments. An audio tape with a male voice reading a novel fragment was used. In order to simulate a notional monopole source, this tape signal was sent to each loudspeaker with a time delay and attenuation corresponding to the distance of the notional source to the particular loudspeaker. Only the synthesised wave field was presented to the subjects, so no visual cues about the source position were available.

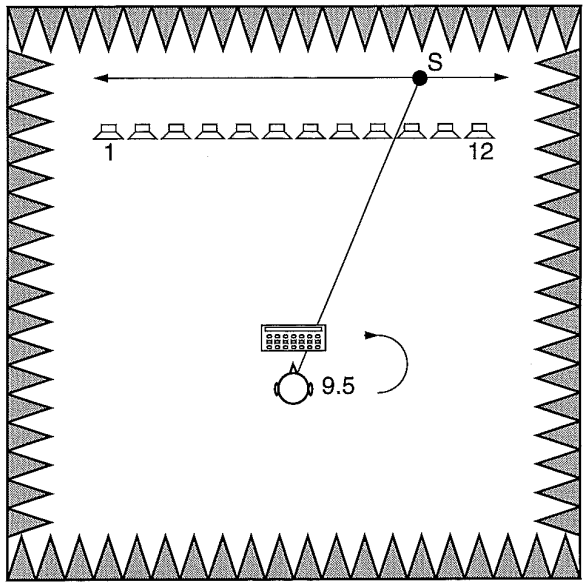

Figure 4.3.1: *In a listening test several subjects were asked to indicate the position of a synthesised monopole source S. The complete setup was placed in an anechoic chamber.*

In the first listening experiment a synthesised monopole field was presented to the subjects, who were asked to type in the position of the simulated monopole source on the computer terminal, in terms of the intersection coordinate of the line from the notional source to the listener and the loudspeaker array (see figure 4.3.1). During each session 25 stimuli were presented to the subject, with a source position chosen randomly from a set of 15 sources. Each session was repeated 3 times for each subject.

In figure 4.3.2 the results of a single session are shown for 4 different subjects. The answers given by the subjects are represented by small circles with a best linear fit given by the solid line. The ideal response curve (answer = simulated source position) is given by the dotted line in the graph. It can be concluded that the answers given by the subjects correlate well with the simulated source position.

As discussed in section 3.6, in practice the sources on stage will be recorded by a set of directional microphones. The synthesised wave field consists of a number of monopole sources (notional sources), positioned at the microphone beam centres. If a single source on stage is positioned such that it is 'seen' by two microphones, it may occur that the impression of two notional sources arises, one at the central spot of each microphone beam (see figure 4.3.3). In a listening experiment this situation has been simulated. The intermediate distance between the two notional sources is chosen to be one meter. The level of the secondary notional source in the synthesised wave field is varied, in order to represent microphone directivity factors.

The results of this listening experiment are shown in figure 4.3.4 for 4 different levels of the secondary notional source S" (0, -3, -6 and -12 dB relative to the level of notional source S'). It is clear that the answers of the subjects are shifted in the direction of the secondary notional source, as long as the level of this source is12 dB or less below the primary source level. To minimise this effect high microphone directivity is required.

A simple extension of the previous experiment is the addition of another secondary notional source S"' at the other side of the primary source S'. This is a more realistic situation, because in practice all microphone areas, except those at the edges of the stage, will be flanked by several adjacent microphone areas, in order to obtain a uniform sound recording level throughout the stage.

The results of this listening experiment are shown in figure 4.3.5. Note that source positions left to the centre of the array are localised by the listeners at the right of the true position while sources right to the centre are shifted to the left. This is caused by the fact that the wave front of the (notional) source that reaches the listener first determines the localisation of the signal (Haas, 1951). E.g., for a true source position S' at the left side of the loudspeaker array notional source S" is nearest to the listener, so

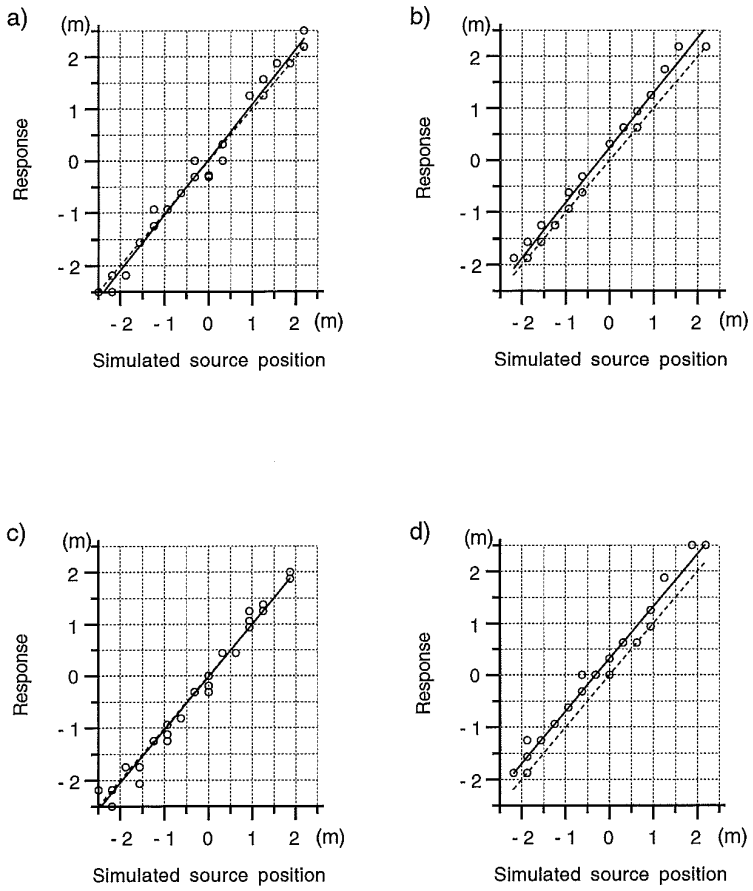

Figure 4.3.2: *Results of the listening experiments for a synthesised monopole wave field for 4 different subjects. Measured data (circles), line fit (solid) and the position of notional source S' (dashed).*
a) Subject A *b) Subject B*
c) Subject C *d) Subject D*

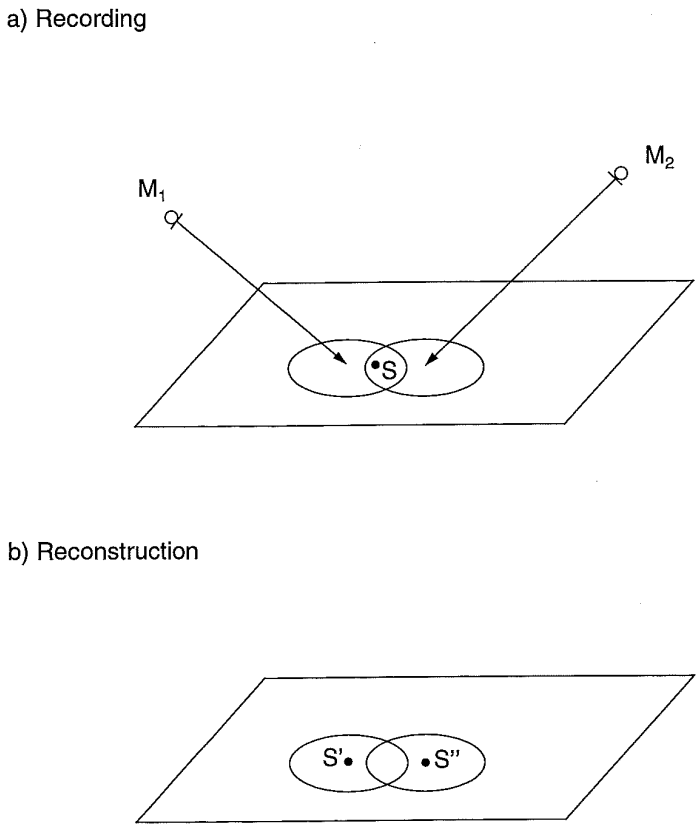

Figure 4.3.3: *A source S recorded by two directive microphones with overlapping apertures (a) may give rise to the perception of two notional sources S' and S" (b)*

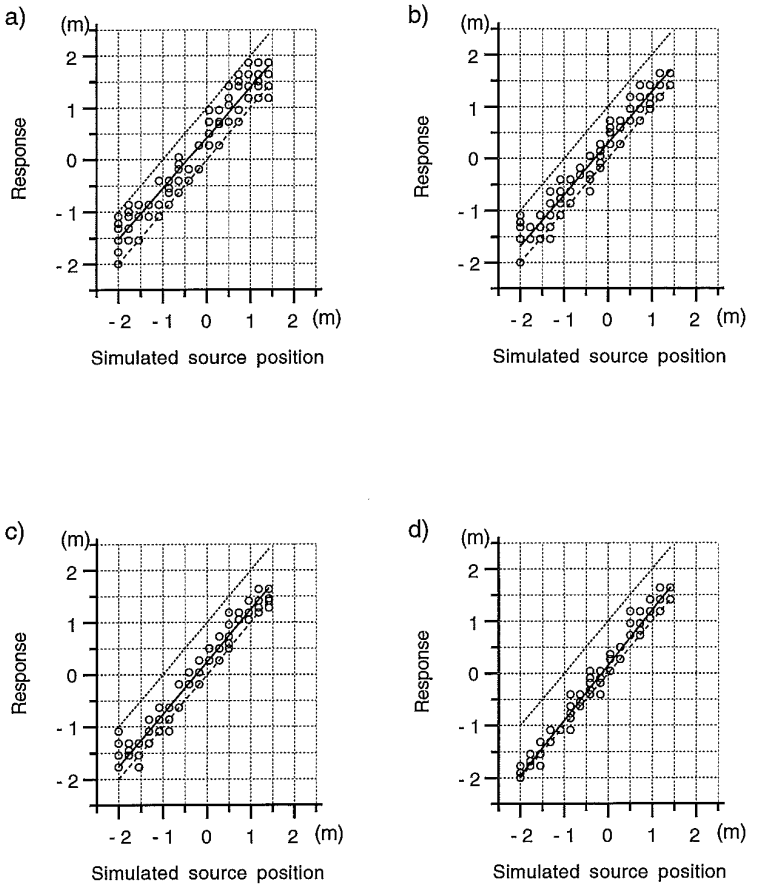

Figure 4.3.4: *The results for the listening experiment with an extra notional source S" caused by microphone overlap, for different levels of this secondary source. Measured data (circles), line fit (solid), position of notional source S' (dashed) and position of notional source S" (dotted), pooled for four subjects.*

a) $L_{S"} = 0$ *dB,* *b)* $L_{S"} = -3$ *dB*

c) $L_{S"} = -6$ *dB,* *d)* $L_{S"} = -12$ *dB*

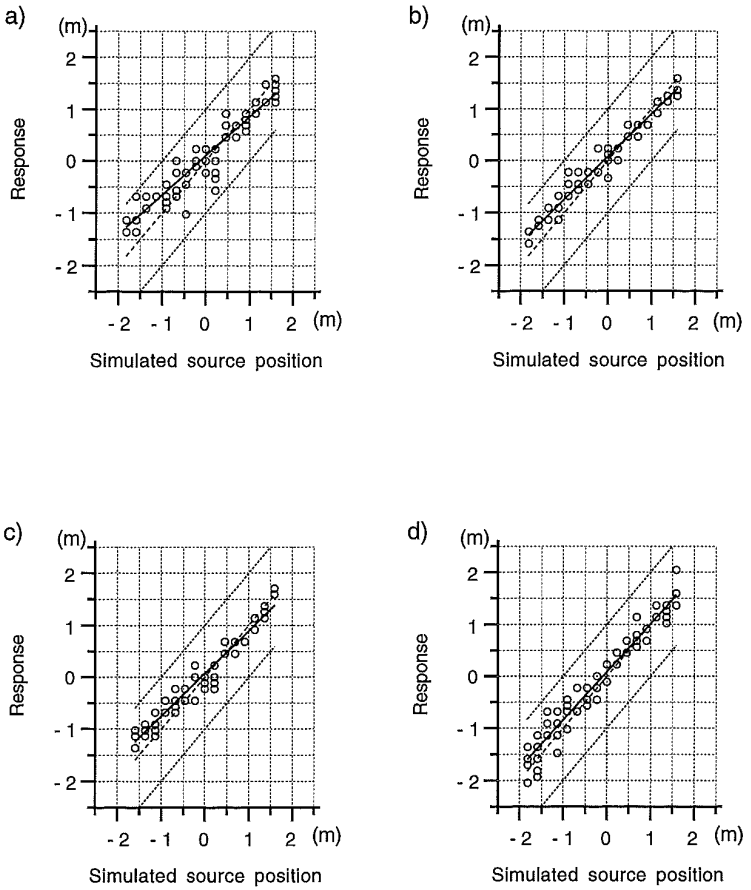

Figure 4.3.5: *Results of the listening experiments with 3 notional sources for different levels of the secondary sources. Measured data (circles), line fit (solid), position of notional source S' (dashed) and position of notional sources S" and S"" (dotted), pooled for four subjects.*
a) $L_{S"}=L_{S""}=0dB$ *b)* $L_{S"}=L_{S""}=-3dB$
c) $L_{S'} = L_{S"}= -6$ *dB,* *d)* $L_{S'} = L_{S"}= -12$ *dB.*

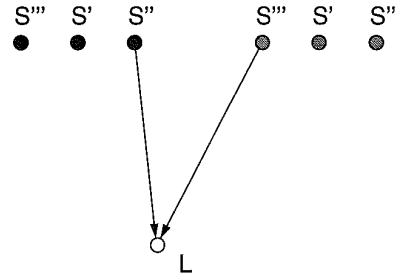

Figure 4.3.6: *When notional source S' is located left of listener L, the secondary notional source S" is nearest to the listener, so the localization will shift in the direction of S", caused by the Haas effect. When notional S' is located right of listener L, the localization shifts in the direction of secondary source S"".*

this source will determine the localisation of the source image (see figure 4.3.6). From the listening experiments discussed above it can be concluded that the wave fields synthesised by the laboratory setup for wave field generation contain the desired directional information. The spatial aliasing in the simulated wave fields does not disturb this information. When listening to (pink or white) noise signals however, a strong position-dependent colouration of the signal can be perceived. This colouration is caused by the spatial aliasing, so it is expected that a loudspeaker array built up of a large number of small loudspeakers will yield much better results in this respect. In the next section the design of such an improved system will be discussed.

4.4 Design of a wave field synthesis prototype system

Based on the laboratory setup discussed in the previous sections a prototype system for wave field synthesis has been designed. The main goal of the new setup was to create a more flexible system for studying the effects of spatial aliasing, aperture angle

control etc. For this purposes an array consisting of a large number of small loudspeakers is required.
For the new array setup 48 loudspeakers with a width of 11 cm have been built, thus creating an array length of about 5 meter when placed closely against each other. All loudspeakers of the array can be addressed individually.
The central processing unit for the new system is formed by 3 coupled floating point DSP processor boards (Motorola DSP96002). The processor boards are plugged into a PC486 and each one is coupled to a 16 channel DA converter board. For microphone input the on-board analog inputs of the DSP processor boards are used. A schematic diagram of the processor setup is shown in figure 4.4.1. Note that each input channel can be routed to all output channels via the multi-processor interface.
Programming and control of the DSP system is possible over the PC data bus. The extrapolation operator parameters (amplitudes and delay times) are placed in a memory area shared by the PC and the DSP's and can be altered during run time of the DSP, thus creating the possibility of smooth operator changes or moving notional

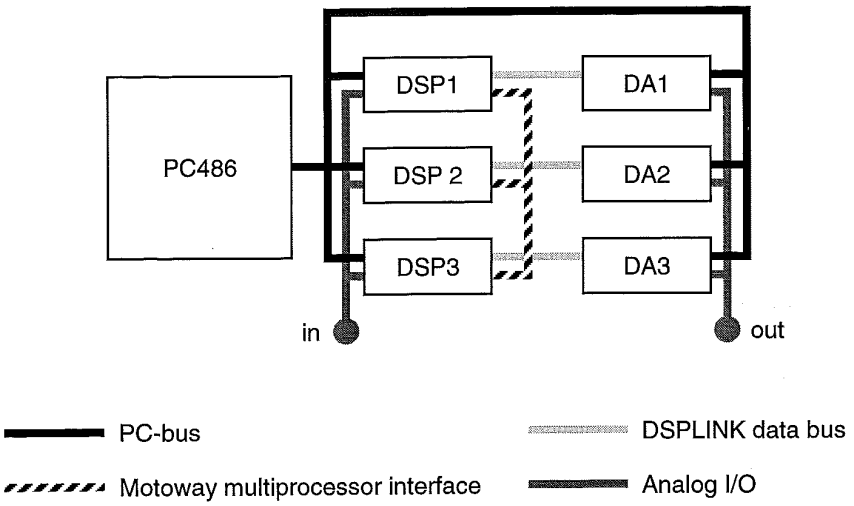

Figure 4.4.1: *Schematic diagram of the DSP hardware of the new wave field synthesis system, with all relevant data communication channels.*

sources.
The input channels are sampled at 16 kHz, so that the frequency bandwidth is sufficient for speech processing. In the current setup no input data filtering is applied, but at the chosen sample interval some computation time is left over in the system, which can be used for applying a FIR filter to the input data. For simple changes in frequency behaviour a tone control system on the microphone pre-amplifiers can be used.
The smallest spatial sample interval that can be used with the current loudspeaker type is 11 cm. The aliasing frequency for full ±90° angle radiation is about 1500 Hz, but for almost all practical situations a less wide radiation angle will be sufficient, thus increasing the maximum aliasing-free frequency.
In figure 4.4.2 several photographs of the prototype system during tests in an anechoic chamber are shown. The signal processing system and the amplifiers are placed in an adjacent control room.

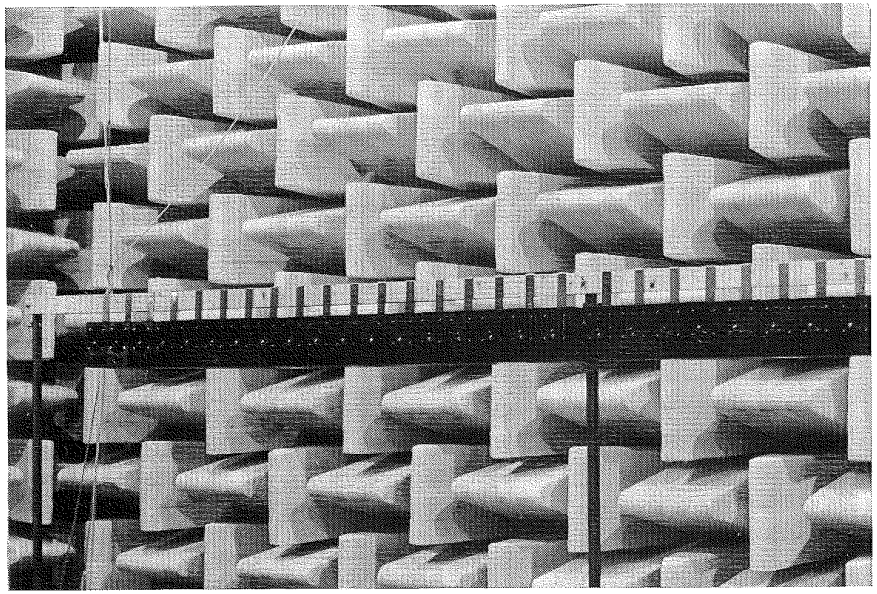

Figure 4.4.2: *The wave field synthesis prototype system in an anechoic chamber.*

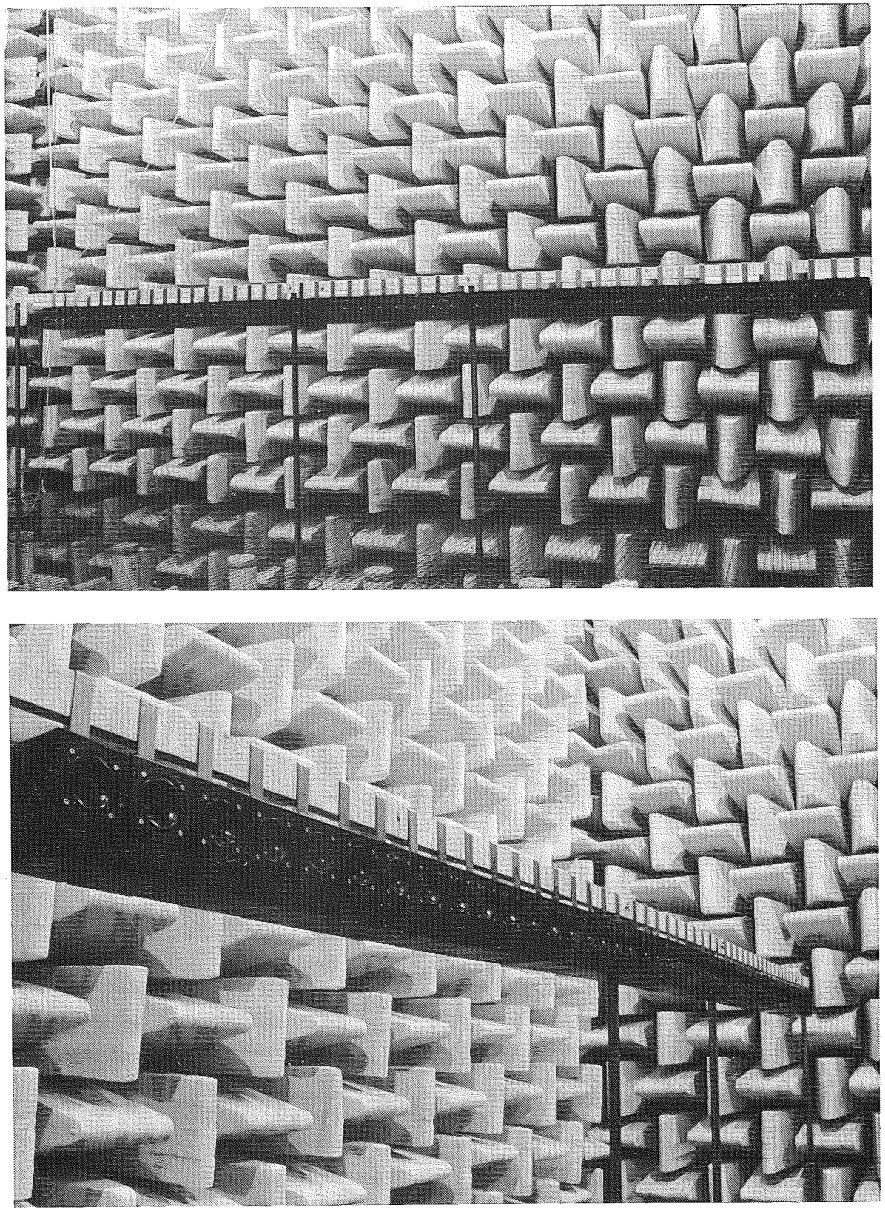

Figure 4.4.2: *(Cont.)*

4.5 Evaluation of the wave field synthesis prototype system

As with the 12 loudspeaker laboratory setup, both objective and subjective tests have been carried out with the 48 loudspeaker prototype system. First, the time response of the system has been measured using an impulsive signal with a frequency range from 300 to 3000 Hz. The time response is measured at a constant distance from the array at intervals of 10 cm. As the spatial aliasing frequency of the array is 1500 Hz it is expected that the wave field will be aliasing-free for an angle range of about ±30° around the normal of the array. The measured wave field (x-t diagram) is shown in figure 4.5.1, together with a simulation. It can be seen from these graphs that some spatial aliasing is present in the wave field, as expected. Measurement and simulation

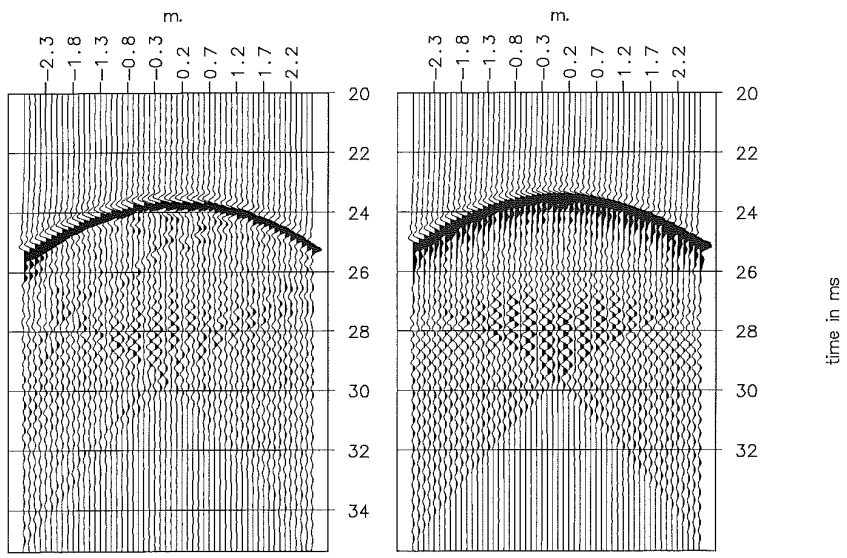

Figure 4.5.1: *Measurement (left) and simulation of a monopole wave field synthesised by an array of 48 loudspeakers. The maximum frequency of the source wavelet (3000 Hz) is above the spatial aliasing frequency (1500 Hz), so that some aliasing effects can be seen in the graphs.*

are in good agreement with each other.
As a second experiment the wave field is measured again, now using an impulsive source signal with a frequency range from 150 to 1500 Hz. This wave field is expected to be aliasing-free for all positions. In figure 4.5.2 both the simulated and the measured results are shown for this experiment. It can be seen that all aliasing effects have disappeared, leaving the diffractions from the array edges only. Again, measurement and simulation are in good agreement.
For comparison with the laboratory setup system discussed before, part of the 48 loudspeakers in the prototype system can be switched off, leaving a system with 12 loudspeakers only. The size of the new prototype system is such that leaving on each fourth loudspeaker only, a system is obtained with the same distribution of loudspeak-

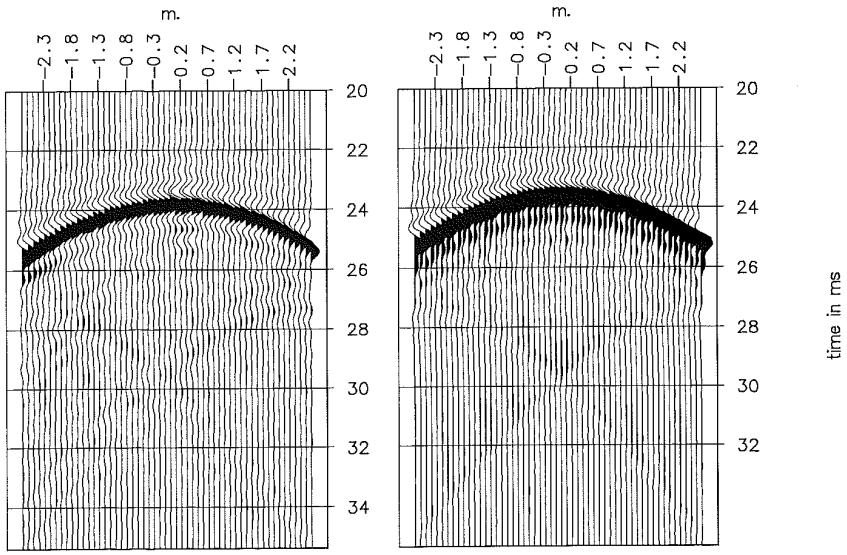

Figure 4.5.2: *Measurement (left) and simulation of a monopole wave field synthesised by an array of 48 loudspeakers. The maximum frequency of the source wavelet (1500 Hz) equals the spatial aliasing frequency, so the wave field is aliasing free.*

ers as the 12 loudspeaker laboratory setup (see figure 4.5.3). The wave field generated by this system is shown in figure 4.5.4 for an impulsive source signal with a maximum frequency of 3000 Hz and in figure 4.5.5 for an impulsive source signal with a maximum frequency of 1500 Hz. In both situations severe aliasing effects can be seen. As the loudspeaker contributions do not cancel after the simulated direct wave, a hyperbola can be seen in the graphs for each of the loudspeakers. The graph of figure 4.5.4 can be directly compared to the graph of figure 4.2.11.
From figure 4.5.1, 4.5.2, 4.5.4 and 4.5.5 it can be concluded that the wave field synthesis prototype system generates wave fields that show much less severe spatial aliasing effects than the 12 loudspeaker laboratory setup. The frequency at which spatial aliasing effects start corresponds well with the theoretical results.
Apart from the time response, the frequency response of the wave field synthesis system is also of great importance. In figure 4.5.6 the third octave band frequency response of the system is shown for several configurations, measured using pink noise as input signal. Figure 4.5.6a shows the frequency response using a single loudspeaker only, figure 4.5.6b shows the response using 12 loudspeakers and figure 4.5.6d shows the response using all 48 loudspeakers of the array.
Figure 4.5.6c shows the level difference when switching from 1 to 12 loudspeakers. It can be seen from this graph that the frequency behaviour of the 12 loudspeaker system is rather irregular above the spatial aliasing frequency of about 370 Hz. In figure 4.5.6e the level difference is shown when switching from 1 to 48 loudspeakers. Note the decrease in level with a slope of about 3 dB/octave, as expected, since the required $\sqrt{jk}$ filter is not implemented in the current version of the system.

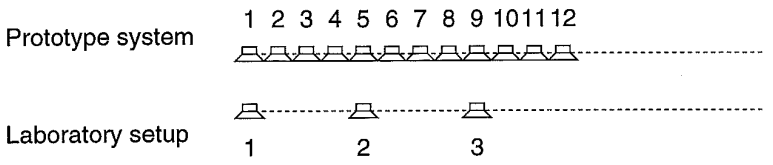

Figure 4.5.3: *The wave field synthesis prototype system can be transformed into an equivalent of the laboratory setup system by switching on only each fourth loudspeaker in the array.*

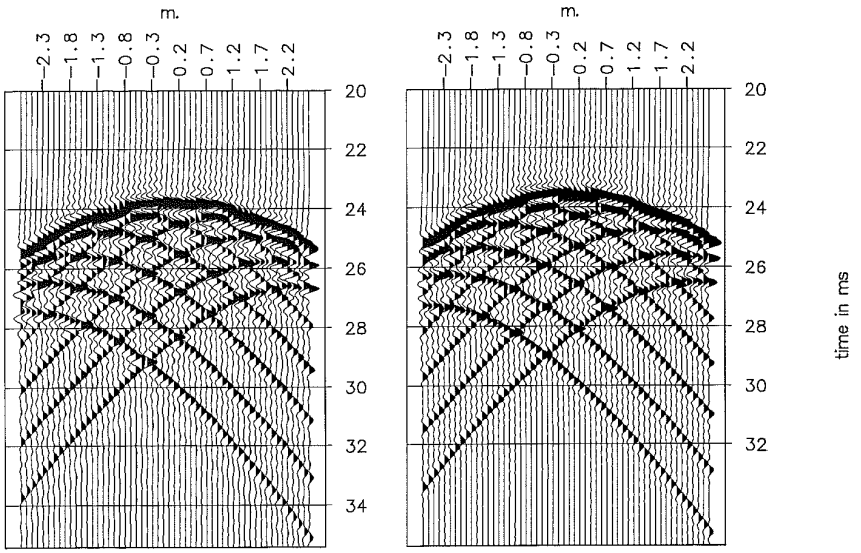

Figure 4.5.4: *Measurement (left) and simulation of a monopole wave field synthesised by an array of 12 loudspeakers. The maximum frequency of the source wavelet (3000 Hz) is far above the spatial aliasing frequency. For each loudspeaker of the array a hyperbola can be seen in the registration. These graphs can be compared directly to the graphs shown in figure 4.2.11.*

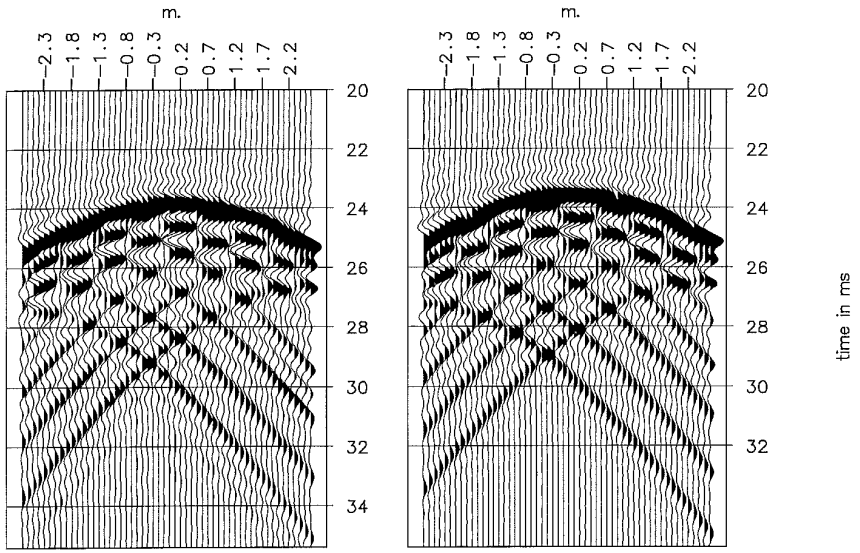

Figure 4.5.5: *Measurement (left) and simulation of a monopole wave field synthesised by an array of 12 loudspeakers. The maximum frequency of the source wavelet (1500 Hz) is still far above the spatial aliasing frequency. For each loudspeaker of the array a hyperbola can be seen in the registration.*

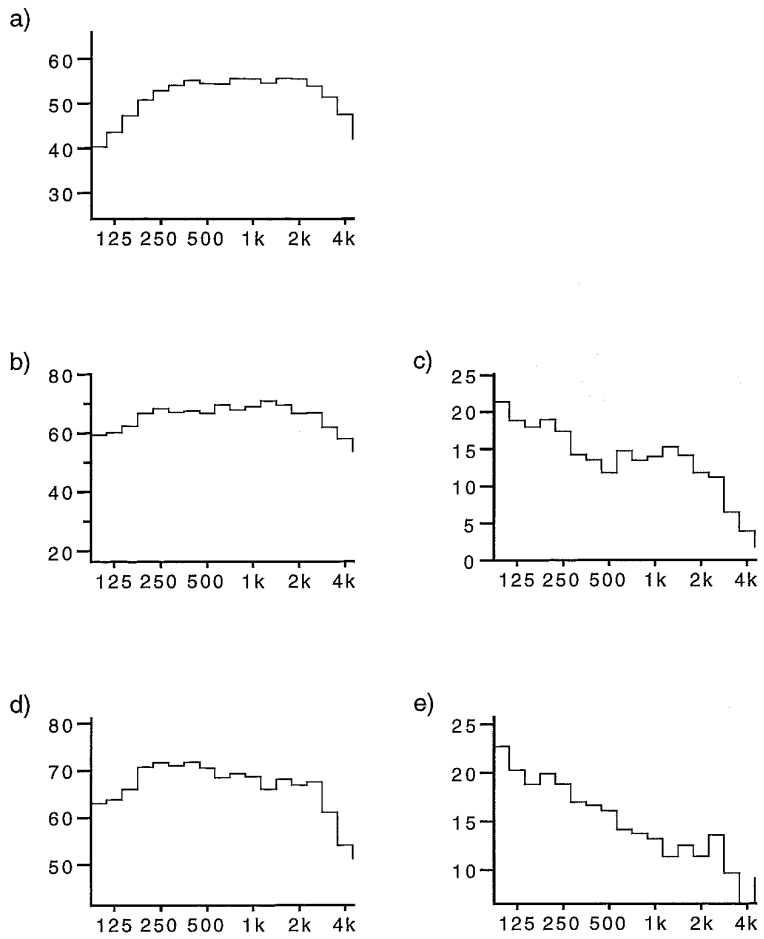

Figure 4.5.6: *Measured third octave band spectra and level increase at the central receiver position of the x-t measurements, for several configurations of the loudspeaker array.*
a) Single loudspeaker
b) 12 loudspeaker array *c) Level increase for 12 loudspeaker array*
d) 48 loudspeaker array *e) Level increase for 48 loudspeaker array*

For comparison the frequency response of the system can also be determined from the measured x-t plots of the system (see figure 4.5.7). These plots are measured using the sweep-method, in which a measured sweep response is transformed into a band limited impulse response by applying a deconvolution filter. A more thorough discussion of this technique is given in appendix A.
The graph shown in figure 4.5.7a is the spectrum of a single loudspeaker response, after the deconvolution process. The source signal used was a linear sweep with a frequency range from 300 to 3000 Hz. Note that the deconvolved frequency response is flat within this range. The spectrum shown in figure 4.5.7b is measured in the same way, now using 12 loudspeakers, while the spectrum shown in figure 4.5.7d is measured using all 48 loudspeakers of the array. As before, figure 4.5.7c and e show the difference plots for the frequency responses. Because of the finer resolution in the higher frequency regions of these graphs, the spatial aliasing effects are more clear than in figure 4.5.6. Note that the frequency scale in figure 4.5.7 is a constant absolute bandwidth scale, yielding a 3 dB/octave level increase up to the aliasing frequency.
The 3 dB/octave decrease in level in the wave field generated by the wave field synthesis system causes a slightly dull sound, especially in direct comparison with the sound of a single loudspeaker. In a future version of the array this effect can be compensated for by applying a filter with a 3 dB/octave increase at each input channel of the system.

4.6 Subjective evaluation of the prototype system

As with the12 loudspeaker laboratory setup, a subjective evaluation of the prototype system has been carried out. To test the spatial properties of the generated wave field, a monopole wave field was synthesised in an anechoic chamber, with the simulated (notional) source at a position chosen randomly from a pre-defined set of 20 possible locations. As before, the source position is simulated by driving each loudspeaker with the source signal, delayed and attenuated in correspondence with the distance from the source to the loudspeaker.
A listener was asked to indicate the perceived position of the source by typing in at a hand-held computer terminal the number of the loudspeaker at the intersection of the line from the simulated source to the listener and the loudspeaker array (see figure 4.6.1). During each session 30 stimuli were presented to the listener. Each session was repeated once to obtain a larger data set.

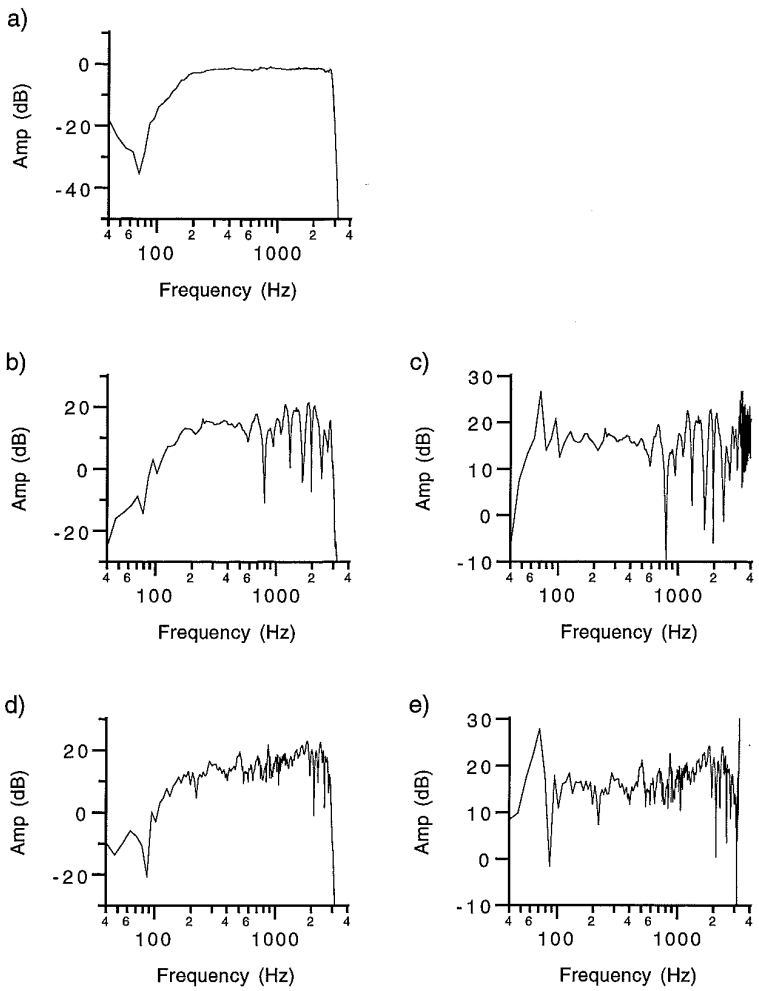

Figure 4.5.7: *Frequency response and level increase at the central receiver position of the x-t measurements of figure 4.5.1 and figure 4.5.4, for several configurations of the loudspeaker array. Source wavelet 300 - 3000 Hz.*
a) Single loudspeaker
b) 12 loudspeaker array *c) Level increase for 12 loudspeaker array*
d) 48 loudspeaker array *e) Level increase for 48 loudspeaker array*

Several source signals have been used during the experiments. As speech amplification was the main goal for the wave field synthesis prototype system, during the first experiments speech was used as a source signal. The speech signal used was an audio tape recording of a novel fragment, read by a male voice. The results obtained using this stimulus are shown in figure 4.6.2a-c, for three different test subjects. The graphs show the pooled results of both measurement sessions. Figure 4.6.2d shows the pooled results for all three subjects. From these graphs it is clear that the answers of the listeners match the simulated source position very well.
The experiment was repeated using band limited pink noise with a maximum frequency of 1500 Hz. As spatial aliasing occurs only for frequencies above the cut-off

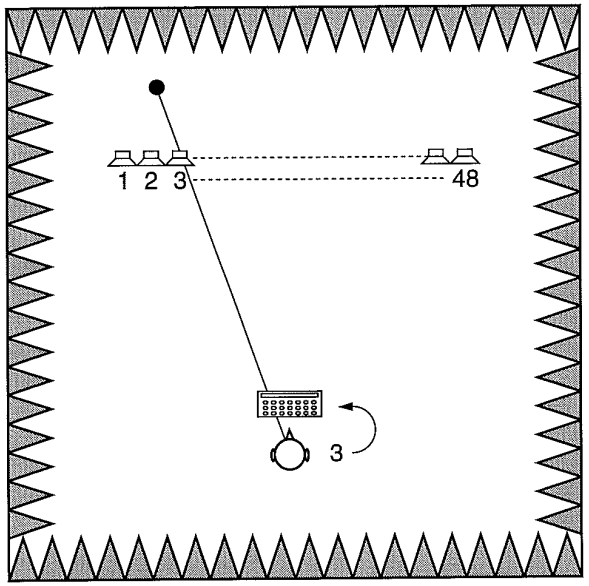

Figure 4.6.1: *During the subjective evaluation of the wave field synthesis prototype system a listener was asked to indicate the (randomly chosen) notional source position by typing in the number of the loudspeaker at the intersection of the line from source to listener and the loudspeaker array at a computer terminal. The loudspeaker array was placed in an anechoic chamber.*

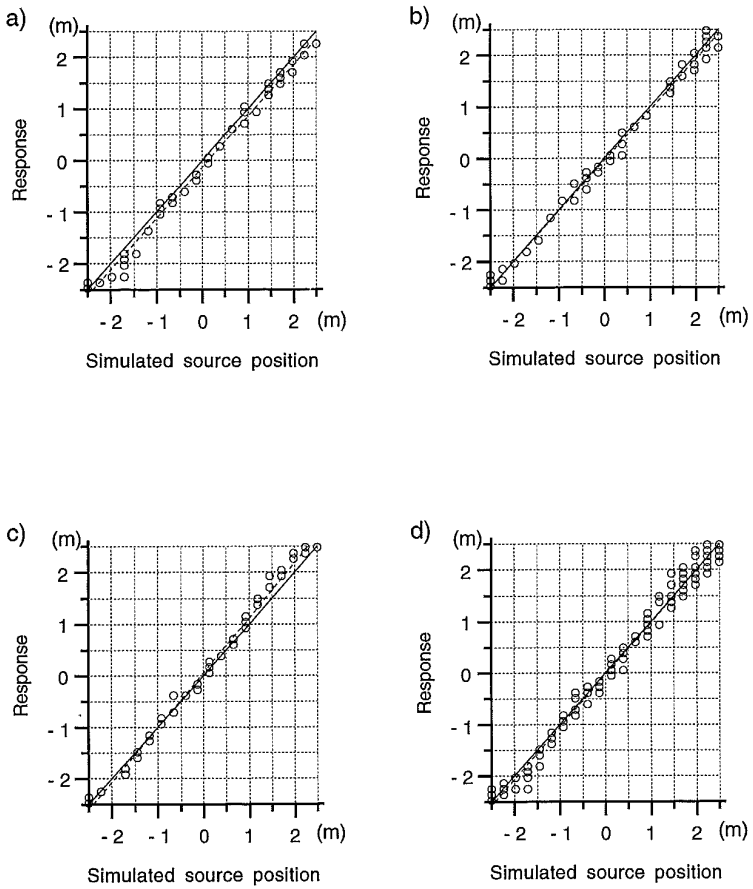

Figure 4.6.2: *Results of the localisation experiment using speech as a source signal. Measured data (circles), line fit (dashed) and ideal response (solid).*
a) Subject A *b) Subject B*
c) Subject C *d) Pooled result*

frequency of the noise the generated wave field will be aliasing free for this situation. The graphs in figure 4.6.3 show that using this source signal the simulated source position and the answers of the test subjects are highly correlated as well.

Next, the experiment was repeated using broad band pink noise as a source signal. Although the perceived source consists of a well localised low-frequency image, surrounded by a broader high frequency image, the answers given by the test subjects still match very well with the simulated position, as can be seen from figure 4.6.4 on page 153.

As listening experiments with the 12 loudspeaker setup turned out, the wide high frequency image using a broadband noise signal is absent for speech signals. This is caused by the fact that all frequency components in a speech signal have a common envelope. When localising a source generating such a modulated signal, the well localised low frequency part is used by the auditory system to obtain information about the source position. As the high frequency part of the source signal is modulated in the same way as the low frequency part, no separate high frequency image is perceived. The same effect can be obtained by modulating the amplitude of a broadband noise signal with a modulating frequency of about 6 Hz. Switching on the modulation gives the effect of a broad source image, shrinking to a well localised point source.

With the new prototype system the same effects can be obtained, but as the aliasing free part of the generated wave field extends to a much higher frequency, the difference in localisation is much smaller. For completeness, the listening experiment has also been carried out using broadband noise, modulated in amplitude with a frequency of 6 Hz. The results of this experiment are shown in figure 4.6.5 on page 154.

The linear curve fits to the measured data, shown in figures 4.6.2 to 4.6.5 by the dotted lines, yield some extra information about the accuracy of the localisation of the simulated source. In table 4.6.1 on page 155 the values for the slope (A) and offset (B) of the fitted line are given, together with their standard deviation (σ_A and σ_B), and the regression coefficient R. It can be concluded from this table that the localisation is very accurate, for all source signals used. For broadband noise only a slight increase in the standard deviation is found.

The larger standard deviation found for the modulated noise signal was not expected on basis of the simple experiment in which the modulation was switched on and off. The difference between modulated noise and speech as a source signal might be caused by the transients in the speech signal that are absent in the modulated noise, indicating that transients are important in the perception of source localisation.

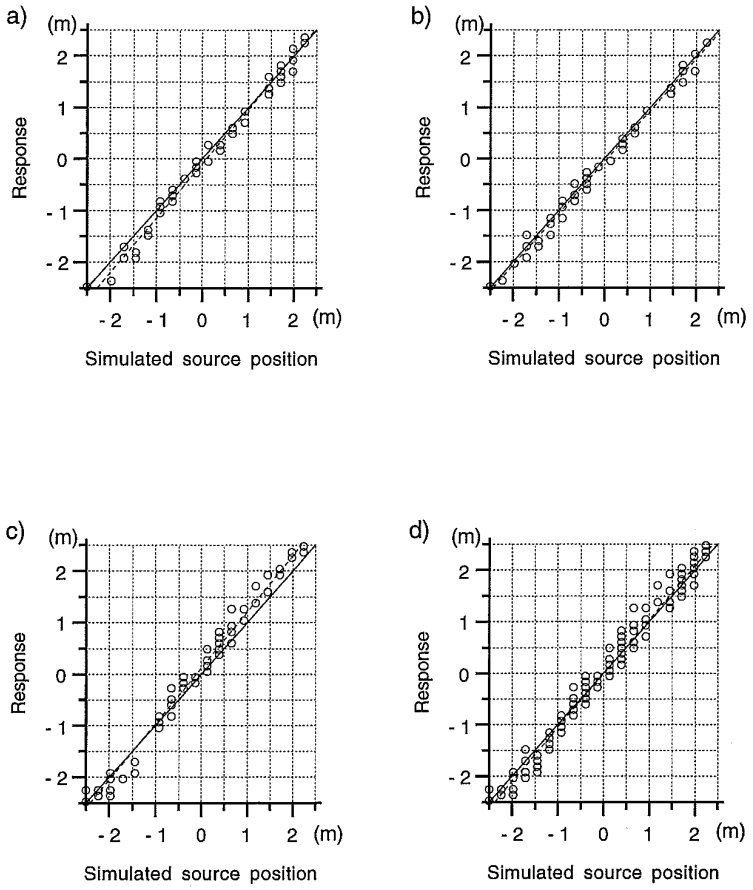

Figure 4.6.3: *Results of the localisation experiment using band limited noise (cut-off frequency 1500 Hz) as a source signal. Measured data (circles), line fit (dashed) and ideal response (solid).*

a) Subject A *b) Subject B*

c) Subject C *d) Pooled result*

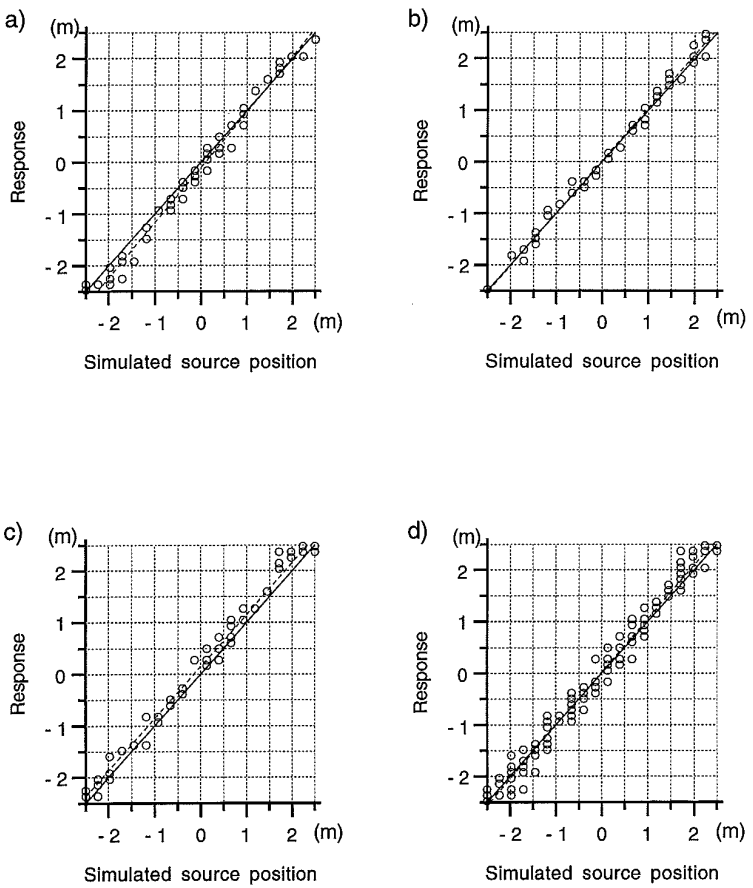

Figure 4.6.4: *Results of the localisation experiment using broad band noise as a source signal. Measured data (circles), line fit (dashed) and ideal response (solid).*

a) Subject A *b) Subject B*

c) Subject C *d) Pooled result*

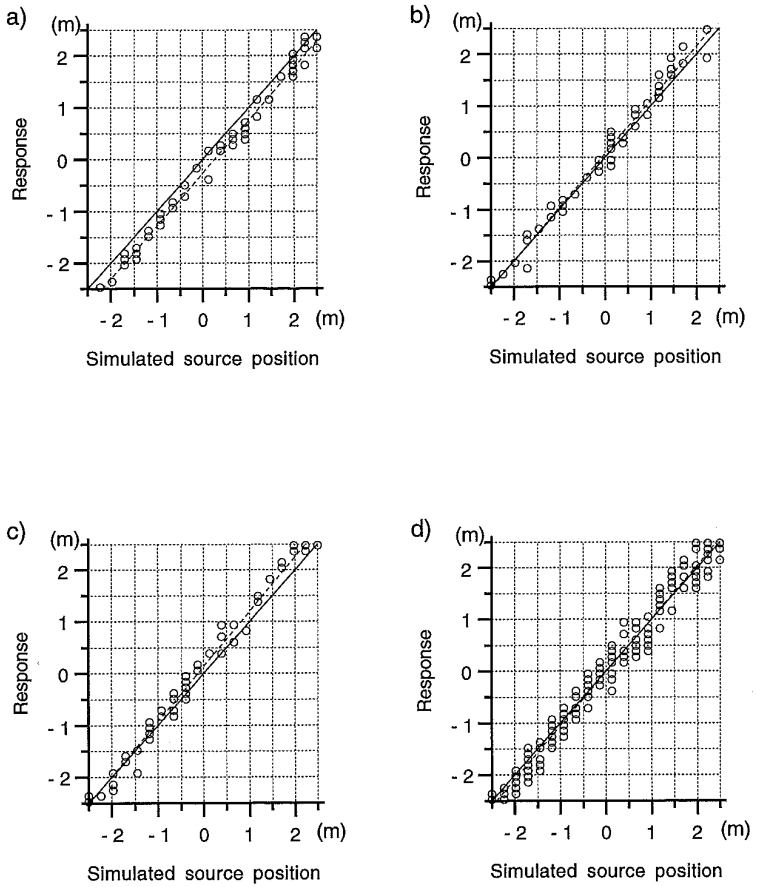

Figure 4.6.5: *Results of the localisation experiment using amplitude modulated noise (modulation frequency 6 Hz) as a source signal. Measured data (circles), line fit (dashed) and ideal response (solid).*
a) Subject A *b) Subject B*
c) Subject C *d) Pooled result*

		A	σ_A	B	σ_B	R
speech	Subject 1	0.993	0.011	-0.133	0.017	0.996
	Subject 2	0.983	0.010	-0.044	0.017	0.997
	Subject 3	1.064	0.011	0.057	0.017	0.996
	Pooled	1.016	0.008	-0.035	0.012	0.995
band limited noise	Subject 1	1.053	0.013	-0.094	0.018	0.996
	Subject 2	1.000	0.011	-0.059	0.015	0.997
	Subject 3	1.087	0.016	0.122	0.023	0.994
	Pooled	1.046	0.009	-0.009	0.013	0.993
broadband noise	Subject 1	1.069	0.014	-0.099	0.022	0.995
	Subject 2	1.021	0.012	0.027	0.017	0.996
	Subject 3	1.007	0.015	0.145	0.023	0.994
	Pooled	1.036	0.009	0.020	0.014	0.993
modulated noise	Subject 1	1.020	0.033	-0.267	0.051	0.971
	Subject 2	1.038	0.017	0.074	0.023	0.993
	Subject 3	1.061	0.014	0.135	0.023	0.995
	Pooled	1.033	0.016	0.020	0.024	0.980

Table 4.6.1: *The statistical parameters obtained by fitting a straight line to the data from the listening experiments. The values given are line slope (A) and offset (B), standard deviation of slope and offset (σ_A and σ_B) and the regression coefficient R.*

4.7 Applications of wave field synthesis

Apart from the speech amplification system, several other applications of wave field synthesis can be thought of. As a wave field can be generated with the required properties, both in time and in space, the wave field of an arbitrary source distribution, real or imaginary, can be synthesised.

In room acoustics, e.g., the wave field synthesis technique can be used to enhance the direct sound of a source on stage. This way a sound enhancement system is created that creates an amplified sound field with the same spatial and temporal properties as the original sound field. A system of this type has recently been installed in the opera house (stadsteater) in Malmö, Sweden. The configuration here consists of 12 microphones to address all locations on stage and an array of 96 loudspeakers, spanning a total width of 24 meter.

The same wave field synthesis technique can be used to generate the wave field of a set of image sources, in order to change the acoustical properties of a hall (figure 4.7.1). The virtual reflections generated by the wave field synthesis system are added to the natural reflections of the hall. Note that the loudspeaker outputs will also be reflected by the physical walls of the hall, thus creating physical images of the virtual sources (figure 4.7.2). This effect will be discussed further in chapter 5.

In order to create a hall with full acoustic control it should be equipped with both a direct sound enhancement array at the front and several reflection generating arrays at the side and back walls (figure 4.7.3). To minimise the influence of the hall itself, the walls and ceiling should be made absorptive. The primary sound and the early reflections should be generated in accordance with the image source model, such that the reflection pattern of a required hall is generated. For the reverberation a statistical approach will be sufficient. The reverberation system, however, can take advantage of the large number of loudspeakers distributed throughout the hall.

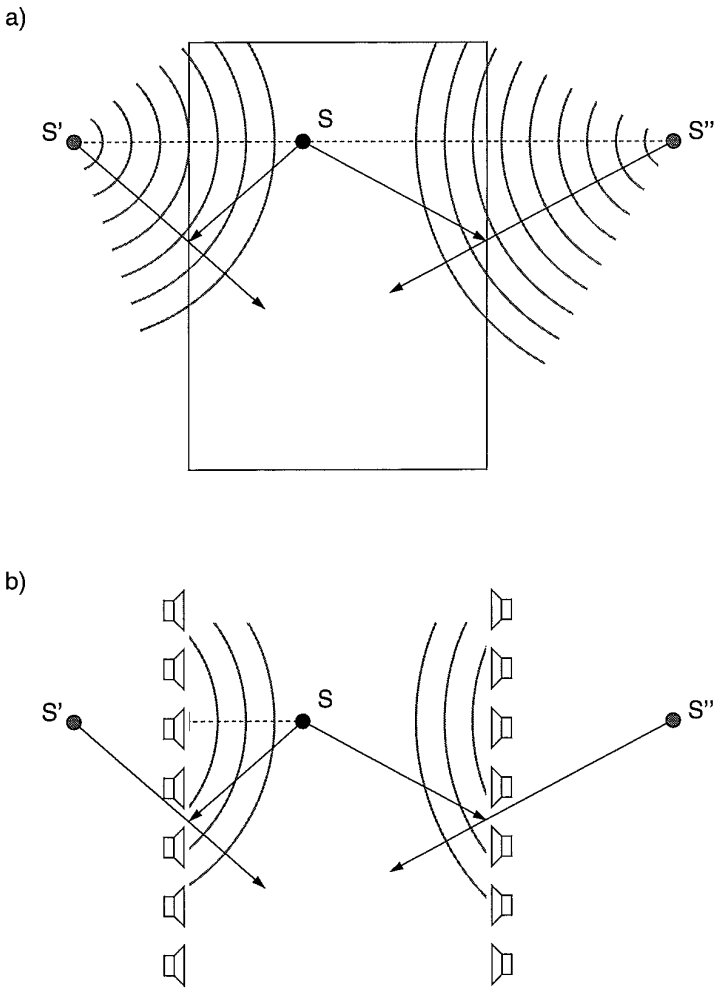

Figure 4.7.1: *The wave field of image sources S' and S" (a) can be generated by loudspeaker arrays at the side walls of the hall (b)*

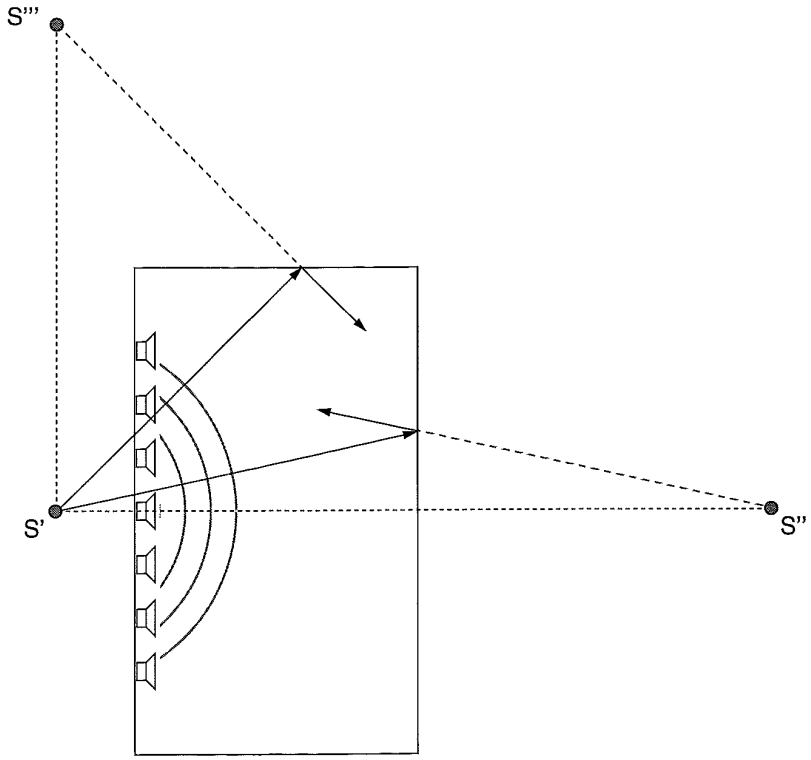

Figure 4.7.2: *Reflection of the synthesised wave field against the room boundaries will give rise to images of the virtual source S'.*

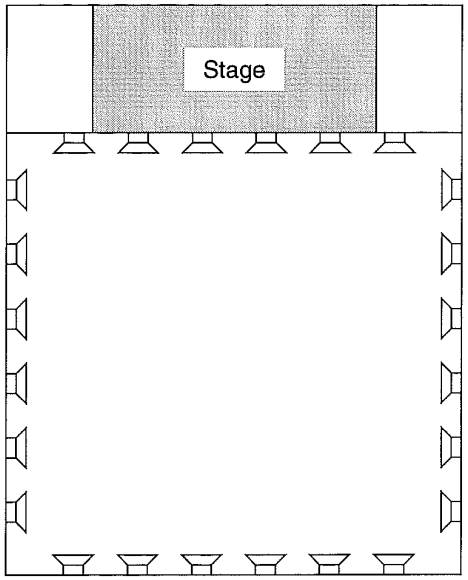

Figure 4.7.3: *A hall equipped with loudspeaker arrays at all sides to obtain full acoustic control. In this situation both the direct sound, the early reflections and the reverberation in the hall can be controlled.*

5. MODELLING A HALL EQUIPPED WITH AN ELECTRO-ACOUSTIC REVERBERATION SYSTEM

If some electro-acoustic system for reflection generation and reverberation enhancement is placed in a hall, the total impulse response of that hall will change. Apart from the hall response, an extra contribution of the system will be found. As both the sound from the sources towards the system microphones and the sound from the system loudspeakers towards the receiver pass through the hall, the corresponding transfer functions should be part of the calculation process. Thus, the calculation of hall responses will be an important part of the simulation model derived in this chapter.
Section 5.1 gives a mathematical description of the simulation model, in section 5.2 some additional signal properties, useful in the analysis of the calculated responses, will be discussed. In section 5.3 the signal properties defined in section 5.2 will be related to the acoustical parameters defined in chapter 1.
A model to calculate the acoustical response of a hall will be discussed in section 5.4. In section 5.5 this model is used to simulate the response of a simply-shaped model hall equipped with an electro-acoustic system. The total response of this hall will be calculated by subsequently taking into account all relevant transfer functions, as discussed by Vogel et al. (1992). In section 5.6 the results of the simulation model will be compared with measurements in a hall equipped with an electro-acoustic system for which the simulated configuration is representative. Finally, section 5.7 summarises the main conclusions of this chapter.

5.1 Introduction

If a hall is equipped with an electro-acoustic system (EAS) for reflection generation and reverberation enhancement, the reflected part of the sound field in the hall is built up by contributions of both the system and the hall. To quantify the transmission of sound field from the source to the listener, from the source to the EAS microphones and from the EAS loudspeakers to the listener, the appropriate hall transfer functions should be taken into account.
As an example consider the situation of figure 5.1.1: a rectangular room with a single sound source at position S, a one channel EAS consisting of a microphone M and a loudspeaker L and a listener at receiver position R. The wave field $p_R(t)$ at the receiver position can be described by

$$p_R(t) = h_{RS}(t) * s(t) \ , \tag{5.1.1}$$

in which s(t) is the signal generated by the sound source S and $h_{RS}(t)$ is the source-receiver transfer function. This transfer function is built up of two parts: the (original) hall transfer function $h_{RS,hall}(t)$ and the system transfer function $h_{RS,sys}(t)$:

$$h_{RS}(t) = h_{RS,\,hall}(t) + h_{RS,\,sys}(t) \ . \tag{5.1.2}$$

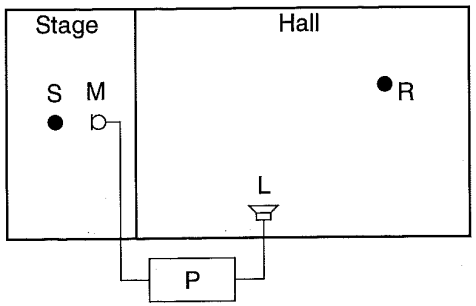

Figure 5.1.1: *A simple EAS in a hall consisting of one microphone M, one loudspeaker L and a processor P.*

The system transfer function can be written as a convolution:

$$h_{RS,\,sys}(t) = h_{RL}(t) * h_{EAS}(t) * h_{MS}(t) \ , \tag{5.1.3}$$

in which $h_{MS}(t)$ is the source-microphone transfer function, $h_{RL}(t)$ is the loudspeaker-receiver transfer function and $h_{EAS}(t)$ is the system transfer function. In summary, the complete simulation model is described by

$$p_R(t) = [h_{RS,\,hall}(t) + h_{RL}(t) * h_{EAS}(t) * h_{MS}(t)] * s(t) \ . \tag{5.1.4}$$

For a multi-channel EAS with several microphones and loudspeakers (see figure 5.1.2) an extended version of equation (5.1.4) should be used:

$$p_R(t) = \left[h_{RS,\,hall}(t) + \sum_{m=1}^{M} \sum_{n=1}^{N} h_{RL_n}(t) * h_{EAS_{mn}}(t) * h_{M_m S}(t) \right] * s(t) \ , \tag{5.1.5}$$

in which M denotes the number of microphones and N denotes the number of loudspeakers. Note that for an EAS consisting of a number of single-channel systems in parallel, M and N will be equal and the matrix of system transfer functions $h_{EAS}(t)$ will have diagonal elements only.
For generation of early reflections the system transfer functions $h_{EAS}(t)$ should be cho-

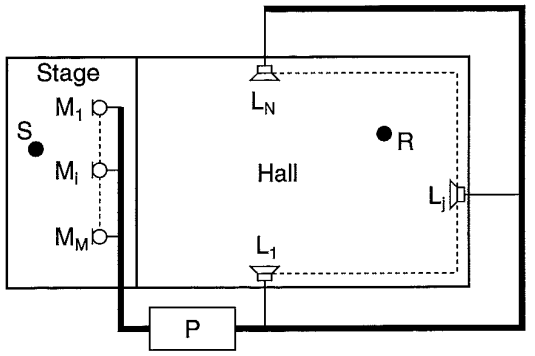

Figure 5.1.2: *Hall with a multi-channel EAS with M microphones, N loudspeakers and a processor (matrix) P.*

sen such that all loudspeakers together generate the required image source wave field, as discussed in the previous chapters. For generation of late reflections (reverberation enhancement) a statistical approach is allowed, in which system transfer functions consisting of a decaying pulse sequence are commonly used.
In order to incorporate in the simulation model the acoustic feedback term, which describes the sound transfer from the EAS loudspeaker back to the EAS microphone, an extra term should be added to the right hand side of equation (5.1.5). The output of each loudspeaker is picked up by all microphones and, because of the EAS system matrix, each microphone signal is (after some processing) re-radiated by all loudspeakers. Thus, the extended calculation model, including acoustic feedback, is given by

$$p_R(t) = \left[h_{RS}(t) + \sum_{m=1}^{M} \sum_{n=1}^{N} h_{RL_n}(t) * h_{EAS_{mn}}(t) * h_{M_mS}(t) \right] * s(t) +$$

$$\sum_{i=1}^{N} \left[\sum_{m=1}^{M} \sum_{n=1}^{N} h_{RL_n}(t) * h_{EAS_{mn}}(t) * h_{M_mL_i}(t) \right] * s_{L_i}(t) \ , \qquad (5.1.6)$$

in which $s_{L_i}(t)$ denotes the signal generated by loudspeaker i and $h_{M_mL_i}(t)$ is the transfer function from loudspeaker i to microphone m. Using only the first order feedback, neglecting all higher order terms, this loudspeaker signal is given by

$$s_{L_i}(t) = s(t) * \sum_{j=1}^{M} h_{M_jS}(t) * h_{EAS_{ji}}(t) \ , \qquad (5.1.7)$$

so that the complete model, including first order feedback, can be written as

$$p_R(t) = s(t) * \left[h_{RS}(t) + \sum_{m=1}^{M} \sum_{n=1}^{N} h_{RL_n}(t) * h_{EAS_{mn}}(t) * h_{M_mS}(t) + \right.$$

$$\left. \sum_{j=1}^{M} \sum_{i=1}^{N} \sum_{m=1}^{M} \sum_{n=1}^{N} h_{RL_n}(t) * h_{EAS_{mn}}(t) * h_{M_mL_i}(t) * h_{EAS_{ji}}(t) * h_{M_jS}(t) \right] . \qquad (5.1.8)$$

From equation (5.1.8) it is clear that the wave field at the receiver can be calculated by convolving the source signal s(t) with a transfer function composed of the EAS response and several hall transfers, which means that the effect of a particular EAS

will depend on the environment it is placed in.
In this chapter equation (5.1.8) will be used as a starting point for the analysis of the behaviour of an EAS inside a hall. The evaluation of the results will be based on several parameters, both from the field of signal theory and from the field of room acoustics. In the next section the required signal properties will be introduced, the acoustical parameters were introduced in chapter 1 already.

5.2 Signal properties

When the source signal s(t) in equation (5.1.8) is replaced by a Dirac delta pulse the signal at the receiver $p_R(t)$ will be the total impulse response of both hall and system. This impulse response can be used to calculate the acoustical parameters defined in chapter 1.
In addition to these acoustical parameters several parameters from signal theory will be helpful to give a global characterisation of the hall response. The signal properties that will be used here are the energy E(x) of a causal signal x(t), defined as

$$E(x) = \int_0^\infty x^2(t)\,dt \ , \qquad (5.2.1)$$

its first order moment $M_1(x)$, defined as

$$M_1(x) = \int_0^\infty t x^2(t)\,dt \ , \qquad (5.2.2)$$

its second order moment $M_2(x)$, defined as

$$M_2(x) = \int_0^\infty t^2 x^2(t)\,dt \ , \qquad (5.2.3)$$

its first order length $L_1(x)$, defined as

$$L_1(x) = \frac{\int_0^\infty t x^2(t)\,dt}{\int_0^\infty x^2(t)\,dt} = \frac{M_1(x)}{E(x)}, \qquad (5.2.4)$$

and its second order length $L_2(x)$, defined as

$$L_2(x) = \frac{\int_0^\infty t^2 x^2(t)\,dt}{\int_0^\infty x^2(t)\,dt} = \frac{M_2(x)}{E(x)}. \qquad (5.2.5)$$

In the next section the relation of these general signal properties with the acoustical parameters defined in chapter 1 will be discussed.

5.3 The relation between signal properties and acoustical parameters

5.3.1 Signal properties of a hall impulse response

The acoustical parameters defined in chapter 1 were all described in relation with the hall impulse response. Therefore, the signal properties introduced in the previous section will also be applied to the hall impulse response h(t). Some of these properties have a direct equivalent in the set of acoustical measures. The energy in the impulse response, e.g., is defined as

$$E(h) = \int_0^\infty h^2(t)\,dt, \qquad (5.3.1)$$

a definition used both in acoustics and in signal theory.

The first order length of the impulse response $L_1(h)$ is given by

$$L_1(h) = \frac{\int_0^\infty t h^2(t)\,dt}{\int_0^\infty h^2(t)\,dt}, \qquad (5.3.2)$$

a quantity in acoustics usually referred to as the "Schwerpunktszeit" (Eng.: centre time), as can be seen by comparison with equation (1.3.16).
The other signal properties have no direct equivalent in acoustics, but it is clear that there is a strong correlation between, e.g., the first and second order length of a hall impulse response and its reverberation time. This correlation, however, can not be expressed by a simple mathematical relation, due to the irregular shape of a typical hall impulse response.

5.3.2 Signal properties of a decay curve

A signal related to the impulse response, and also used frequently in room acoustics, is the decay curve. The decay curve is a recording of the root mean square (rms) sound pressure in a hall as a function of time, after switching off a stationary sound source. In appendix A the measurement of decay curves is discussed. The relation between the impulse response and the decay curve is discussed in section 1.3.1.
It is possible to apply the signal properties defined in the previous section to characterise the decay curve. It can be shown (Kuttruff, 1979) that in a diffuse sound field, the decaying rms sound pressure $p_{rms}(t)$ can be described by an exponential function (see figure 5.3.1):

$$p_{rms}(t) = p_{rms}(0)\, e^{-cAt/8V}, \qquad (5.3.3)$$

in which it is assumed that the sound source is switched off at time t=0, at which moment the rms sound pressure is given by $p_{rms}(0)$. The constant A in equation (5.3.3) denotes the total absorption of the room.

Using the definition of the reverberation time, the decay curve can also be written as

$$p_{rms}(t) = p_{rms}(0)\, 10^{-3t/T_{60}}, \tag{5.3.4}$$

in which the constant T_{60} denotes the room's reverberation time.
Combining equation (5.3.3) and equation (5.3.4) yields Sabine's well known reverberation time formula:

$$T_{60} = \frac{6\ln(10)\cdot 4V}{cA} \approx \frac{1}{6}\frac{V}{A} \tag{5.3.5}$$

It can be shown (Barron, 1988) that in most halls the decay curve is almost exponential a short time after switching off the sound source. Thus the derivation of the signal properties starting from equation (5.3.4) will be valid as an approximation for most real situations. In this section only the results of the calculation will be given, the complete derivations can be found in appendix D.

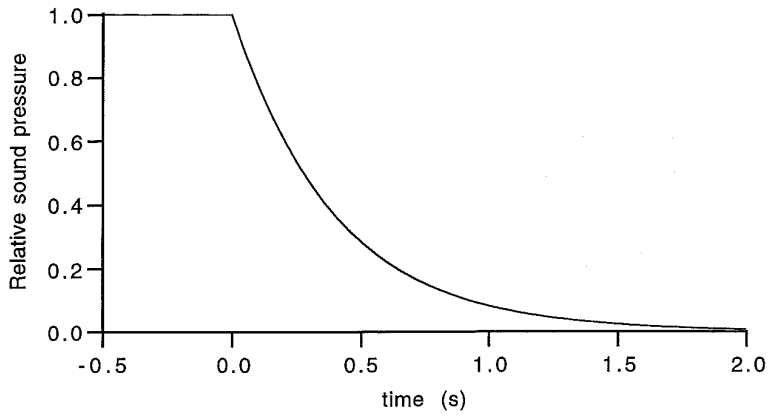

Figure 5.3.1: *In a diffuse sound field the rms sound pressure decays exponentially after switching off the sound source at time t=0.*

The energy in the decay curve $E(p_{rms})$ is given by

$$E(p_{rms}) = p_{rms}^2(0)\frac{T_{60}}{6\ln(10)}, \tag{5.3.6}$$

and its first order moment $M_1(p_{rms})$ is given by

$$M_1(p_{rms}) = p_{rms}^2(0)\left(\frac{T_{60}}{6\ln(10)}\right)^2. \tag{5.3.7}$$

The first order length of the decay curve is the ratio of its first order moment and its energy. Hence, for a diffuse field the first order length of the decay curve $L_1(p_{rms})$ is given by

$$L_1(p_{rms}) = \frac{T_{60}}{6\ln(10)}. \tag{5.3.8}$$

Equation (5.3.8) can be considered as a more general definition of the reverberation time, and can also be used for non-exponential decay curves.
The second order moment of the decay curve $M_2(p_{rms})$ is given by

$$M_2(p_{rms}) = 2p_{rms}^2(0)\left(\frac{T_{60}}{6\ln(10)}\right)^3, \tag{5.3.9}$$

and its second order length $L_2(p_{rms})$ is found as the ratio of the second order moment and the energy, and is thus given by

$$L_2(p_{rms}) = 2\left(\frac{T_{60}}{6\ln(10)}\right)^2, \tag{5.3.10}$$

which can be thought of as another definition of the reverberation time. Note that the energy and the moments of the decay curve depend on the energy of the source signal, while the length measures do not.
For a non-exponential decay, found in rooms with coupled volumes, and in halls equipped with an electro-acoustic reverberation enhancement system, the normal method of reverberation time determination over a specified decay range yields inaccurate results. Using equation (5.3.8) or equation (5.3.10) as a general definition for the reverberation time can solve this problem, as the reverberation time is this way

defined in terms of a uniquely defined property of the decay curve that takes the complete decay process into account. In this thesis, when dealing with non-linear decay curves two new definitions for the reverberation time will be used:

$$T_{60}(L_{1,r}) \equiv 6\ln(10)\, L_1(p_{rms}) \ , \tag{5.3.11}$$

and

$$T_{60}(L_{2,r}) \equiv 6\ln(10) \sqrt{\frac{L_2(p_{rms})}{2}} \ . \tag{5.3.12}$$

5.3.3 Signal properties of an impulse sequence

Another important signal, often generated by electro-acoustic reverberation systems, is a sequence of impulses. Most generally, such a signal can be described as

$$h(t) = \sum_{m=0}^{\infty} a_m \delta(t-\tau_m) \ . \tag{5.3.13}$$

Note that equation (5.3.11) also describes the impulse response of a system consisting of a set of weighted delay lines.
The impulse sequences generated by most electro-acoustic systems can be described by a globally equidistant sequence with globally exponential decay. A single-channel version of such a system can be approximately described by a simple feedback loop (see figure 5.3.2a). The impulse response h(t) of the feedback loop is given by

$$h(t) = \sum_{m=0}^{\infty} g^m \delta(t-m\tau) \ . \tag{5.3.14}$$

For a loop gain g less than one, the impulse response of such a feedback loop system consists of an exponentially decreasing equidistant impulse series. As a consequence, the frequency response of the system is a comb filter showing peaks at all integral mul-

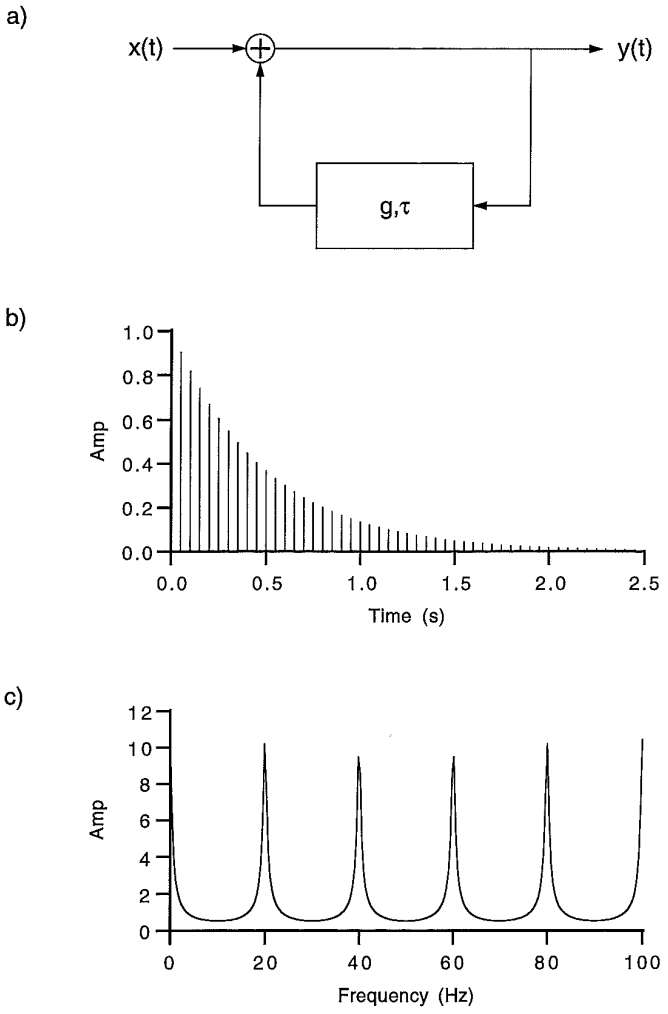

Figure 5.3.2: *Simple feedback loop as a generator of an exponentially decreasing equidistant impulse sequence*
a) Block diagram
b) Impulse response
c) Frequency response

tiples of the fundamental frequency f_b that is the reciprocal of the loop delay τ:

$$f_b = \frac{1}{\tau} . \tag{5.3.15}$$

Figure 5.3.2b and figure 5.3.2c respectively show the impulse response and frequency response of a feedback loop with a delay time τ of 50 ms and a loop gain g of 0.9. Note the spectral peaks at all integral multiples of 20 Hz in figure 5.3.2c. In practical systems much effort is taken to reduce the unwanted spectral peaks in the frequency response of the feedback loop. E.g., Schroeder (1962) discusses a feedback loop configuration with an all pass filter response.

As the impulse response of a system like the feedback loop consists of a number of Dirac delta pulses (with infinite energy), the signal properties defined in section 5.2 can not be used directly to characterise it. However, by using a short impulse with finite length and finite amplitude as input signal, a characteristic energy, length and moment for the system can be defined, as is shown in appendix E.

The characteristic energy $\hat{E}(h)$ of the impulse response is given by

$$\hat{E}(h) = \frac{1}{1-g^2} , \tag{5.3.16}$$

its characteristic first order moment $\hat{M}_1(h)$ by

$$\hat{M}_1(h) = \tau \sum_{m=0}^{\infty} m g^{2m} , \tag{5.3.17}$$

and its characteristic first order length $\hat{L}_1(h)$ by

$$\hat{L}_1(h) = \frac{\tau g^2}{1-g^2} . \tag{5.3.18}$$

The characteristic second order moment $\hat{M}_2(h)$ of the impulse response is given by

$$\hat{M}_2(h) = \tau^2 \sum_{m=0}^{\infty} m^2 g^{2m} , \tag{5.3.19}$$

and its characteristic second order length $\hat{L}_2(h)$ by

$$\hat{L}_2(h) = \tau^2 \sum_{m=0}^{\infty} (2m-1) g^{2m} . \tag{5.3.20}$$

5.4 Modelling of hall transfers

To determine the total hall response as described by equation (5.1.8) several hall transfer functions must be calculated. For a rectangular ('shoe-box type') hall these responses can be simulated easily using the image source technique. In this technique the response is calculated by recursively mirroring the source S in each of the room boundaries and weighting the energy of the image source at each reflection with the appropriate wall reflection coefficient (see figure 5.4.1 on page 174). The hall response is found by adding the contributions of all image sources.

As an example the response of a rectangular hall with a size of 40x25x15m will be calculated. The energy absorption coefficient is taken to be 0.25 for each wall and independent of frequency and incidence angle. In figure 5.4.2 a sketch of this hall with the source and receiver position is shown. Figure 5.4.3a shows the impulse response

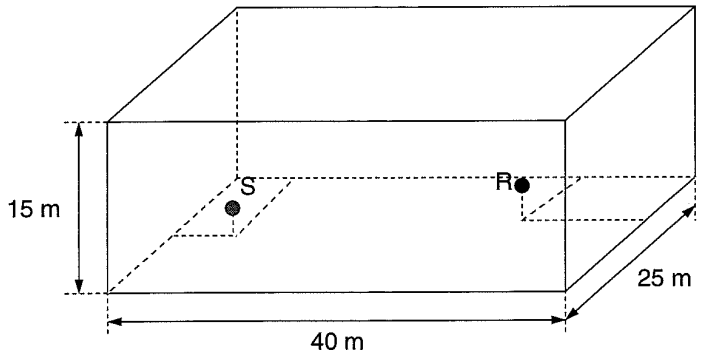

Figure 5.4.2: *The model hall is a large rectangular hall of dimensions 40x25x15m.*

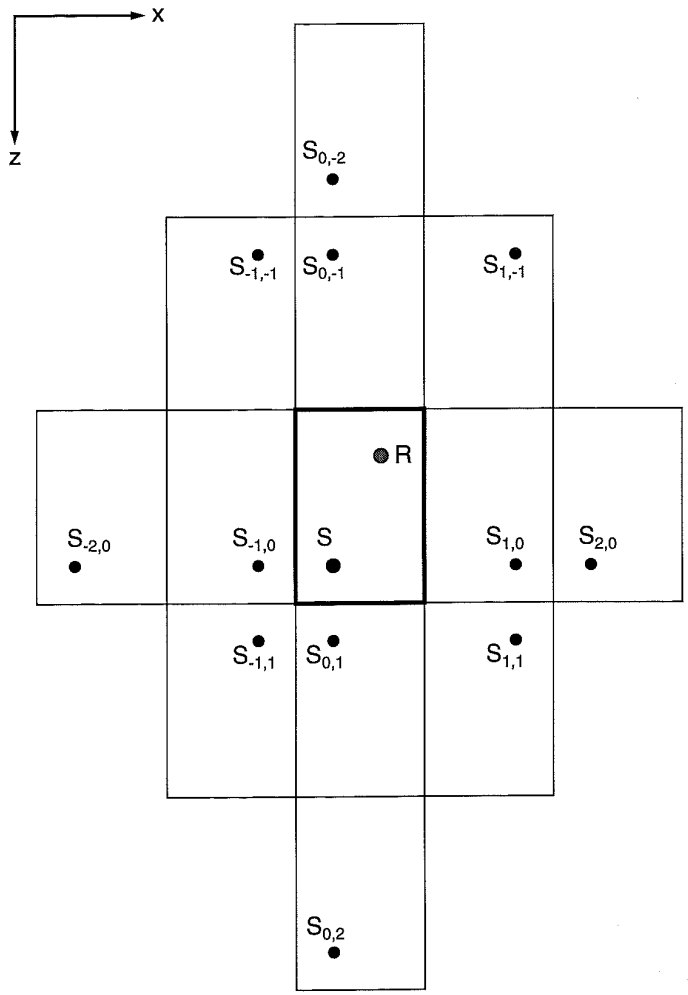

Figure 5.4.1: *Illustration of the image source technique: the source S is recursively mirrored in the room boundaries, thus creating a great number of image sources. For clarity, in this graph only the first and second order images in 2 directions are shown. The indices of the image sources indicate the reflection order for the x and z direction respectively.*

calculated for this room using the image source technique and figure 5.4.3b shows the reverberation curve calculated from the impulse response. Note that the calculated impulse response has infinite bandwidth.

To validate the reverberation time calculated a comparison with some theoretical models is required. In the past several simple models have been derived to calculate the reverberation time of a room from global parameters like volume V, wall surface S and average absorption coefficient $\bar{\alpha}$. As an example Sabine found from an energy balance for the room:

$$T_{60} \approx \frac{6\ln(10)}{c}\frac{4V}{\bar{\alpha}S} = \frac{13.8}{c}\frac{4V}{\bar{\alpha}S} \approx \frac{1}{6}\frac{V}{A}, \qquad (5.4.1)$$

in which A is the total absorption of the room in square meters open window. The total absorption can be found by adding the product of area and absorption coefficient for all parts of the room surface.

Using a ray model for the description of a sound field in a hall, Eyring (1930) found for the reverberation time the formula

$$T_{60} = \frac{24\ln(10)}{c}\frac{V}{S\ln\left((1-\bar{\alpha})^{-1}\right)} \approx \frac{1}{6}\frac{V}{S\ln\left((1-\bar{\alpha})^{-1}\right)}. \qquad (5.4.2)$$

Note that, for $\bar{\alpha} \ll 1$ equation (5.4.2) yields the same results as equation (5.4.1).

Another simple reverberation time formula for an occupied hall with reflective walls and ceiling was derived by Kosten (1966) who found that

$$T_{60} = \frac{1}{6}\frac{V}{S_s\alpha_{eq}}, \qquad (5.4.3)$$

in which S_s is the 'seated area' of the hall and α_{eq} is called the equivalent absorption coefficient, which equals 1.07 averaged over the 500 Hz and 1 kHz octave bands, as was found from the analysis of measurement data for a large number of occupied concert halls.

In table 5.4.1 the reverberation times of the model hall calculated from the decay curve of figure 5.4.3b and from the reverberation time formulae (5.4.1), (5.4.2) and (5.4.3) are given for comparison. From this table it is clear that the image source model overestimates the reverberation time, due to the non-linear shape of the reverberation curve.This non-linear shape of the decay curve shows that the image source model predicts a non-diffuse sound field in the hall.

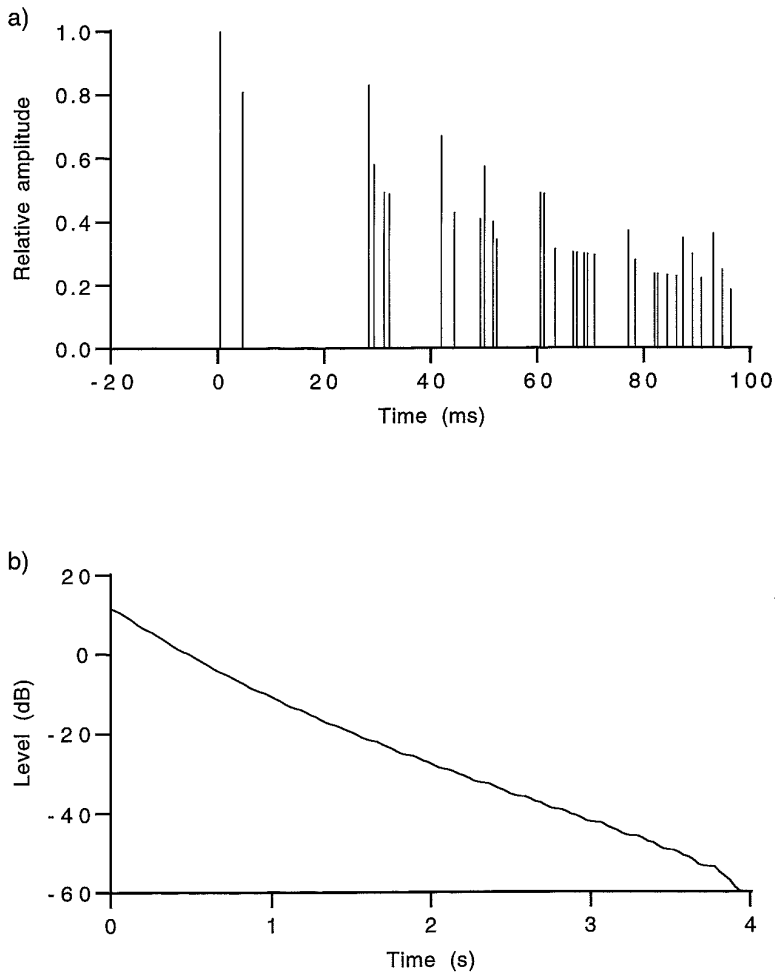

Figure 5.4.3: *Response of a large rectangular hall (40x25x15 m) with uniform absorption over all boundaries, calculated using the image source method.*
a) Impulse response (infinite band width)
b) Reverberation curve

As a second example a rectangular hall of 40x20x15m, with reflecting side walls and ceiling (α=0.05) and an absorbing floor (α=0.80) is taken, the absorption coefficients again being independent of frequency and incidence angle. The total absorption in this hall is the same as the total absorption in the hall of the previous example. In figure 5.4.4a the calculated impulse response for this hall is shown, table 5.4.2 gives the reverberation times for this example. It is clear that for this situation the reverberation time calculated using the image source method is much too high.
In order to find the cause of this error the complete set of image sources must be con-

Calculation model	Reverberation time (s)
Image source	2.8
Sabine	2.6
Eyring	2.3
Kosten	2.3

Table 5.4.1: *Reverberation times for the model hall with uniform absorption, calculated using four different models.*

Calculation model	Reverberation time (s)
Image source	9.0
Sabine	2.6
Eyring	2.3
Kosten	2.3

Table 5.4.2: *Reverberation times for the model hall with non-uniform absorption, calculated using four different models.*

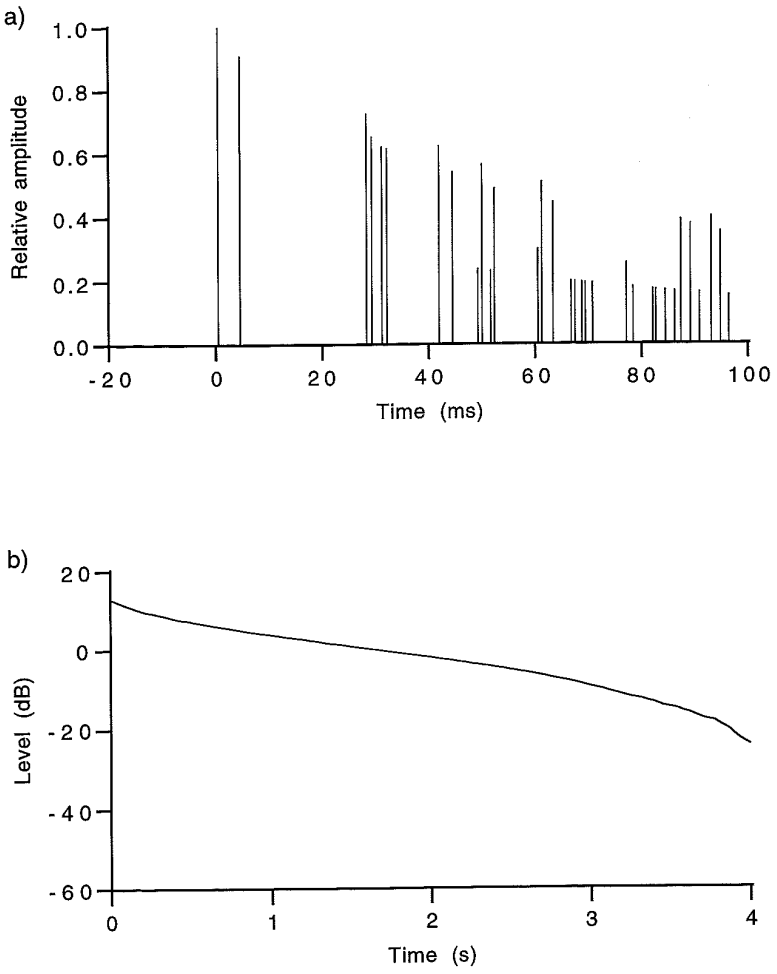

Figure 5.4.4: *Response of a large rectangular hall (40x25x15 m) with absorbing floor and reflecting walls and ceiling, calculated using the image source method.*
a) Impulse response (infinite band width)
b) Reverberation curve

sidered. The image sources in a horizontal plane decay only slowly in amplitude with increasing distance, because of the small absorption coefficients of the side walls. On the other hand, the decrease in amplitude of the image sources in a vertical direction is very rapid. Thus, during the first part of the impulse response both horizontal and vertical image sources will contribute, but after a short time the contribution of the vertical image sources can be neglected, leaving the contribution of the sources in the plane z=0 only. This can be seen from the decay curve for this example (figure 5.4.4b). From this graph it is found that the sound decay in the hall has a rapid start during the first 200 ms, the average slope over this interval being about 15 dB/s, and a very slow decay from 200 ms onward, with an average slope of 4 dB/s.

In practice the very long reverberation times of the previous example are not observed. This is caused by the fact that the specular reflection used in the image source model is only an approximation of the real world situation. A good description of the reflection process at the room boundaries can only be obtained by taking some diffusion into account in the calculation.

To model diffusion a ray-tracing based algorithm is more appropriate. In the model used here the energy radiated by the sound source is evenly distributed over a set of pyramids of equal solid angle around the source centre (see figure 5.4.5). Each pyramid is represented by a single ray at the centre that is traced throughout the room volume for a total travel time of a few seconds. At each reflection of the ray part of the

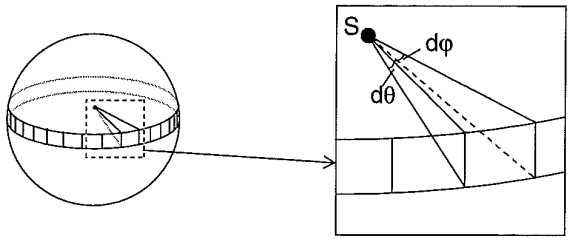

Figure 5.4.5: *The sound energy radiated by the source S is evenly distributed over a set of adjacent cones by dividing a sphere around the source in horizontal layers of constant elevation angle interval dθ. The azimuth angle interval dφ is determined such that all cones have equal solid angle.*

energy is absorbed, part is reflected specularly and the rest is reflected diffusely. The diffuse part of the reflection is modelled by a point source at the wall surface radiating a fraction $\delta_i(1-\alpha_i)$ of the incident energy, evenly distributed over all elements of solid angle around the reflection point. The coefficient δ_i is called the diffusion coefficient of the wall. No multiple reflection of diffuse energy is taken into account, an approximation that is valid for small values of the diffusion coefficients only.
The specularly reflected part of the sound ray energy E_{spec} amounts to

$$E_{spec} = (1-\delta_i)\,(1-\alpha_i)\,E_{inc} \qquad (5.4.4)$$

in which α_i denotes the absorption coefficient of the wall and E_{inc} is the energy of the incoming ray.
In order to encapsulate the image source part of the modelling in the ray tracing algorithm, the source S is also mirrored at each reflection of the ray. When the line from the current source position to the receiver is inside the pyramid that is traced, the contribution of the this source is added to the calculate response. Since the complete set of pyramids forms a non-overlapping coverage of the source radiation area each image source gives a contribution only once. This way the image source model and the diffuse reflection model can be combined into a single algorithm, the schematic diagram of which is shown in figure 5.4.6.
As an illustration of the model discussed above, the response of the hall with non-uniform absorption will be calculated for several values of the diffusion coefficient δ. In figure 5.4.7 the calculated reverberation curves are shown for δ equal to 0, 0.1, 0.2 and 0.3. The corresponding reverberation times are shown in table 5.4.3 on page 183. From figure 5.4.7 and table 5.4.3 it is clear that a value of 0.2 for the diffusion coefficient yields the best results. Thus, in the rest of this thesis the diffuse ray-tracing algorithm with diffusion coefficients around 0.2 will be used for modelling halls.

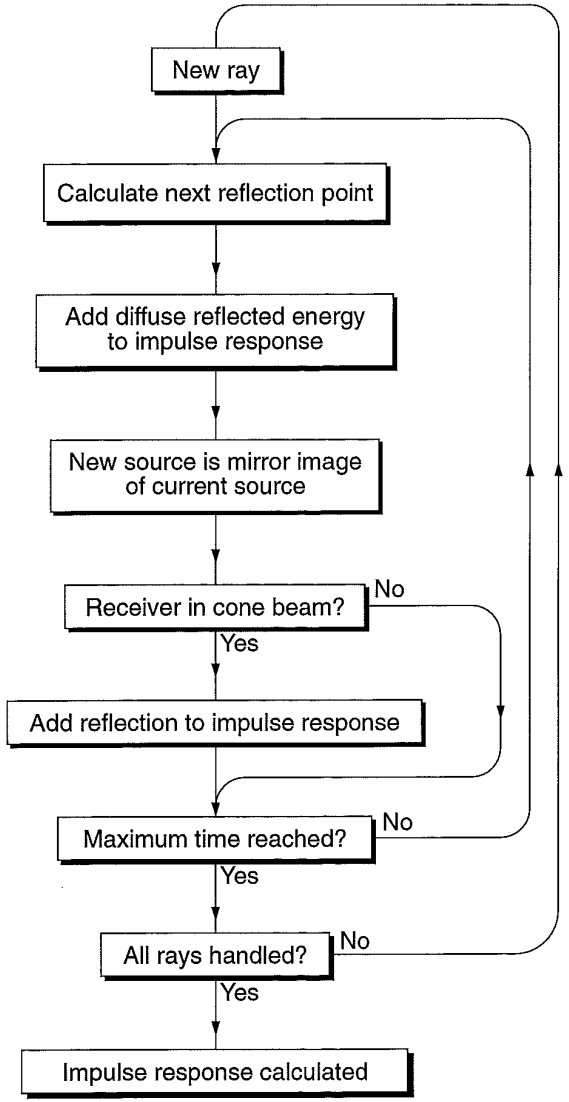

Figure 5.4.6: *Schematic diagram showing the calculation procedure for a hall impulse response combining the image source method with a ray tracing algorithm for the modelling of partly diffuse reflections.*

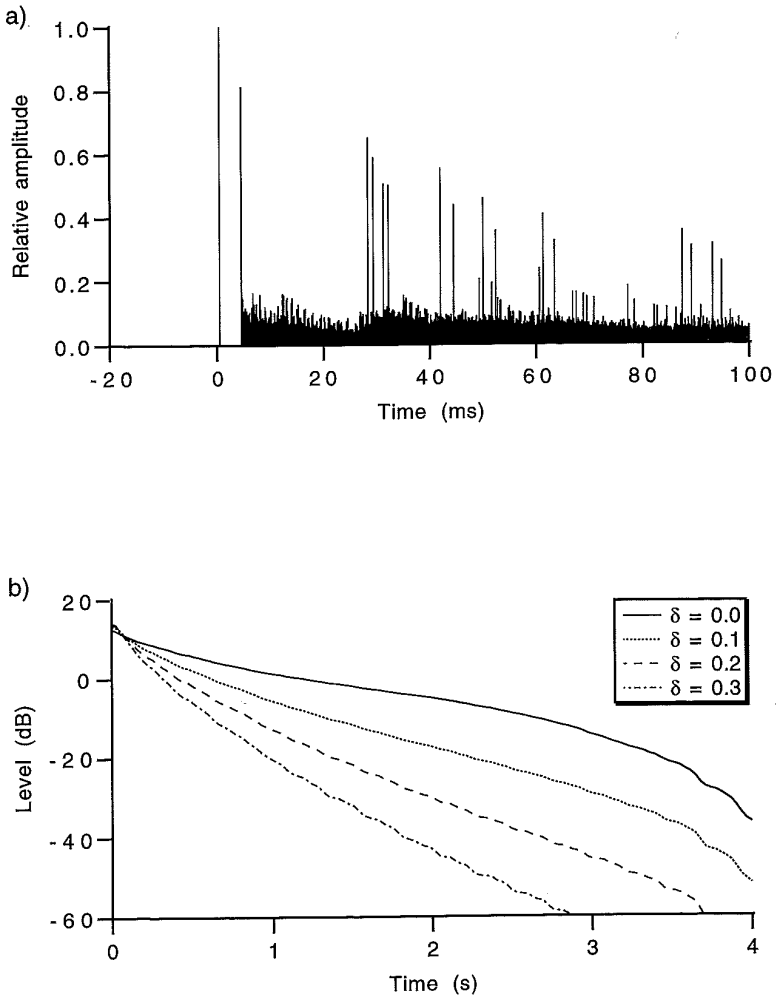

Figure 5.4.7: *Responses of a large rectangular hall (40x25x15 m) with absorbing floor and reflecting walls and ceiling, calculated using the diffuse ray-tracing method.*
a) Impulse response, $\delta = 0.2$
b) Reverberation curves, $\delta = 0.0$, $\delta = 0.1$, $\delta = 0.2$, $\delta = 0.3$

diffusion coefficient δ	reverberation time (s)
0.0	8.0
0.1	4.0
0.2	2.5
0.3	1.7

Table 5.4.3: *Reverberation times for the model hall with non-uniform absorption, calculated using the diffuse ray-tracing model, for four different values of the diffusion coefficient δ. Note that, for δ=0, there is a small difference in the calculated reverberation time for the image source method and the diffuse ray-tracing method, caused by the increasing accuracy of the ray-tracing method for large time values.*

5.5 Modelling example

The calculation model discussed in the previous section can be used to model a hall equipped with an electro-acoustic system. In this section a modelling example will be presented for a simply-shaped hall. In section 5.5.1 a description of the hall used in all examples in the remainder of this chapter is given, and the hall transfer function for the given source and receiver position will be simulated. This hall is chosen such that it is representative for the shape of the auditorium at Delft University, which is equipped with an electro-acoustic system and, besides for public performances, often used for acoustical experiments and measurements.
In section 5.5.2 a single-channel system for early reflection generation will be added to the modelling scheme, in section 5.5.3 a reverberation processor is added to the electro-acoustic system. In section 5.5.4 the acoustic feedback in the electro-acoustic system is also taken into account. In section 5.5.5 and 5.5.6 the same modelling procedure will be used to simulate the response of a hall equipped with a multi-channel electro-acoustic system.

5.5.1 Description of the model hall

The hall used in the modelling procedure is a rectangular hall with dimensions 25x25x12 m, a sketch of which is shown in figure 5.5.1. The values of the absorption coefficients and diffusion coefficients of the room boundaries are given in table 5.5.1. In figure 5.5.2a and figure 5.5.2b the impulse response and the reverberation curve for the model hall are shown. Note that the decay curve has a concave shape caused by the non-uniform absorption distribution in the hall. The first part of the decay curve is shown in figure 5.5.3, from which it is clearly visible that it has a convex start. This is caused by the low reflection density at the start of the hall response. In classical noise-decay measurements this effect is usually invisible, due to the irregular shape of the decay curve. Table 5.5.2 on page 187 gives the numerical values of the energy and the first and second order length of the impulse response, the energy of the decay curve and the reverberation time as determined from the first and second order length of the decay curve, according to equations (5.3.11) and (5.3.12) respectively.

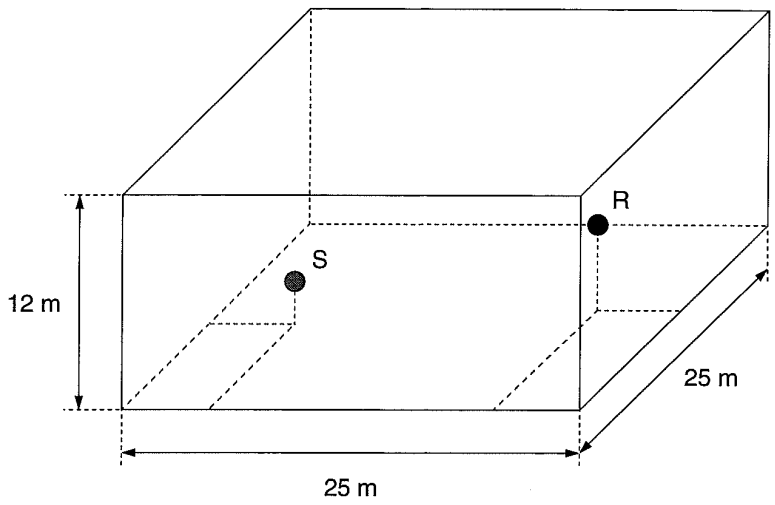

Figure 5.5.1: *The model hall used is a rectangular hall of dimensions 25x25x12 m.*

	α	δ
Front wall	0.1	0.1
Left side wall	0.3	0.2
Right side wall	0.3	0.2
Back wall	0.3	0.2
Floor	0.7	0.3
Ceiling	0.2	0.3

Table 5.5.1: *Absorption coefficients α and diffusion coefficients δ for the boundaries of the model hall.*

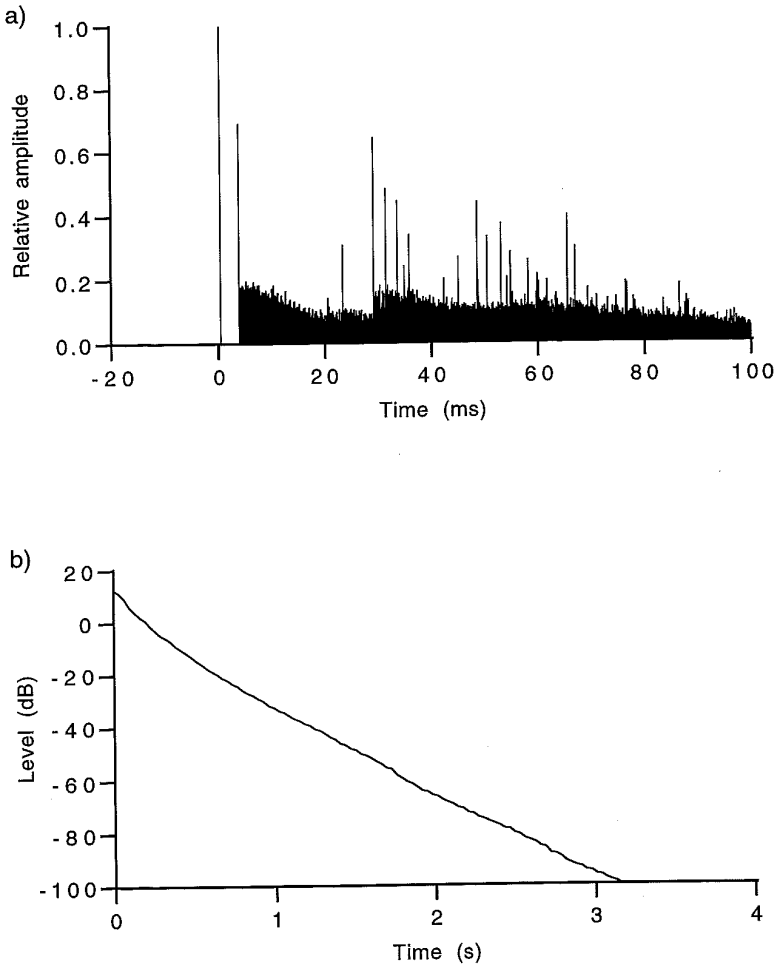

Figure 5.5.2: *Simulated responses of the model hall with the EAS switched off*
a) Impulse response
b) Reverberation curve

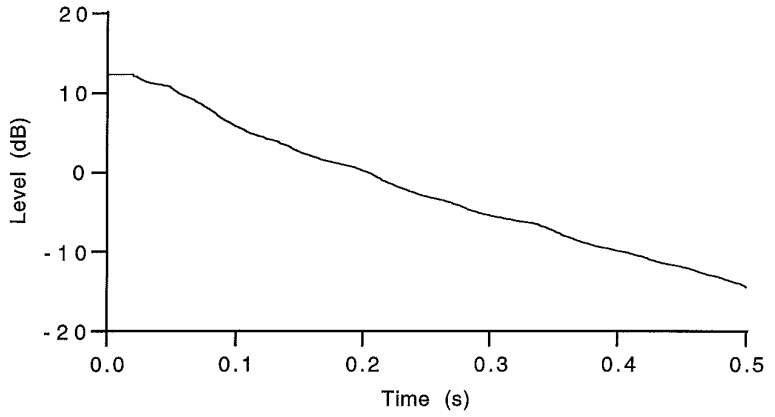

Figure 5.5.3: *First part of the decay curve of the model hall.*

Property	Value	Unit
Impulse response energy E_i	$5.3 \cdot 10^{-4}$	Pa^2s
Impulse response first order length $L_{1,i}$	$8.1 \cdot 10^{-2}$	s
Impulse response second order length $L_{2,i}$	$1.1 \cdot 10^{-2}$	s^2
Reverberation curve energy E_r	1.4	Pa^2s
Reverberation time from rev. curve first order length $T_{60}(L_{1,r})$	1.0	s
Reverberation time from rev. curve second order length $T_{60}(L_{2,r})$	1.0	s

Table 5.5.2: *Signal properties and units for the model hall with the EAS switched off.*

5.5.2 The single-channel early reflection processor

In this section the effects will be evaluated of adding, to the hall described before, a single channel system for generation of early reflections. The system consists of one microphone and one loudspeaker, connected together by an electronic signal processing unit. The system microphone is mounted above the stage, at a height of seven meters. The system loudspeaker is attached to the ceiling and radiates downward to the audience area.
As discussed in section 5.1, the contribution of the system $h_{RS,sys}(t)$ to the total hall response $h_{RS}(t)$ for a given source-receiver combination can be found as the convolution of the source-microphone transfer $h_{MS}(t)$, the processor response $h_{EAS}(t)$ and the loudspeaker-receiver transfer $h_{RL}(t)$:

$$h_{RS,\,sys}(t) = h_{RL}(t) * h_{EAS}(t) * h_{MS}(t) \; . \qquad (5.5.1)$$

The total hall response $h_{RS}(t)$ is the sum of the source-receiver response $h_{RS,hall}(t)$ and the system response $h_{RS,sys}(t)$:

$$h_{RS}(t) = h_{RS,\,hall}(t) + h_{RS,\,sys}(t) \; . \qquad (5.5.2)$$

First, the source-microphone transfer function $h_{MS}(t)$ and the loudspeaker-receiver transfer function $h_{RL}(t)$ will be calculated. These transfer functions are shown in figure 5.5.4a and figure 5.5.4b respectively. As the diffuse ray-tracing model described in section 5.4 is valid only as a statistical result, the diffuse part of the source-microphone response and the loudspeaker receiver response is not taken into account in the convolution described by equation (5.5.1).
The response of the early reflection processor $h_{EAS}(t)$ will be modelled as a pulse sequence, with an average interval between the pulses of 20 ms. The actual pulse intervals are randomised over a ±10% interval. The relative attenuation between consecutive pulses is 3 dB, thus yielding an attenuation of 60 dB after 0.4 second. The processor response of the early reflection system is shown in figure 5.5.5.
The contribution $h_{RS,sys}(t)$ of the early reflection system to the total hall response can be found by convolving the responses shown in figure 5.5.4a, figure 5.5.4b and figure 5.5.5. The result of this convolution procedure is the system response $h_{RS,sys}(t)$ shown in figure 5.5.6. Note the increased reflection density in the resulting response compared with the processor response shown in figure 5.5.5.

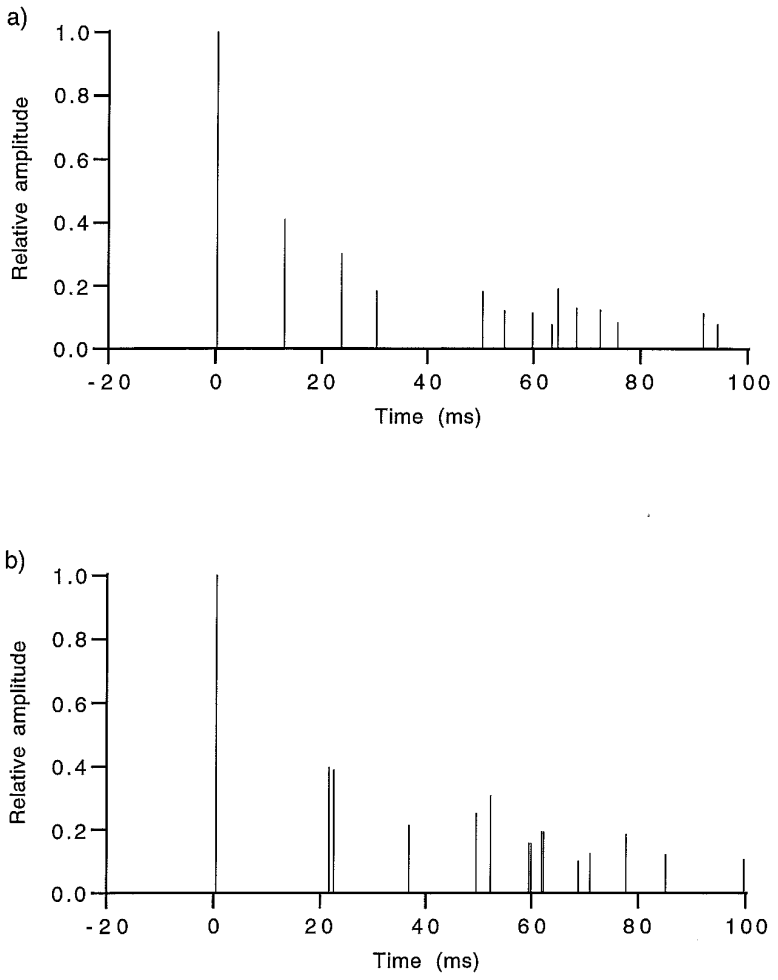

Figure 5.5.4: *Simulated transfer functions for the model hall*
a) Source-microphone transfer $h_{MS}(t)$
b) Loudspeaker-receiver transfer $h_{RL}(t)$

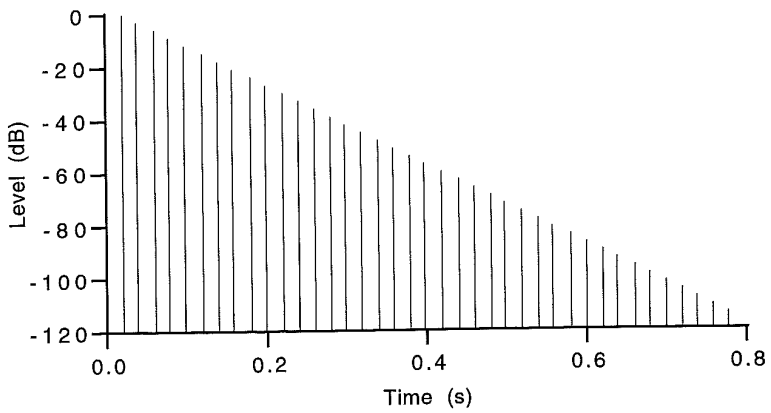

Figure 5.5.5: *The response of the early reflection processor $h_{EAS}(t)$ is a pulse sequence with an average pulse interval of 20 ms and a relative attenuation between two consecutive pulses of 3 dB.*

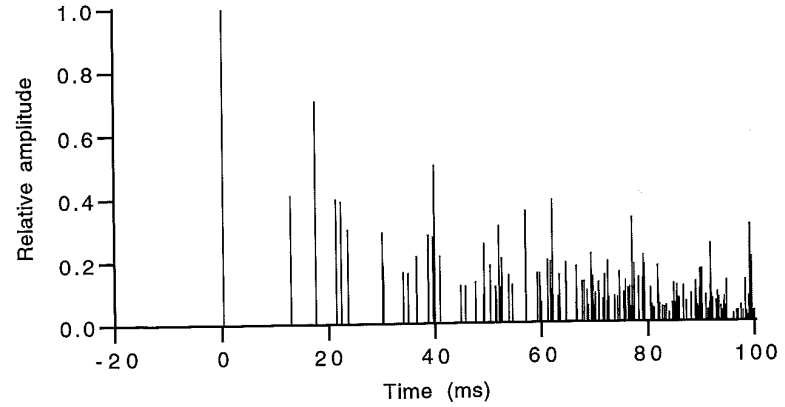

Figure 5.5.6: *The contribution $h_{RS,sys}(t)$ of the early reflection system to the total hall response.*

In figure 5.5.7 the reverberation curve of the early reflection system response shown in figure 5.5.6 is given. Note the typical convex shape of the reverberation curve, caused by the convolution of the processor response of the early reflection processor with the hall transfer functions. It is clear that, due to the convolution process, the decay of the system contribution is no longer exponential, so the reverberation time will strongly depend on the time interval over which the decay is determined. The 60 dB decay time of the system response is much larger than the decay time of the processor transfer function $h_{EAS}(t)$. A more thorough discussion of the effect of convolving (exponentially) decaying impulse responses can be found in appendix F.

Finally, the total response $h_{RS}(t)$ of hall plus system can be found by adding the hall response and the early reflection system response. The relative amplitude of these responses, however, can be chosen arbitrarily. In figure 5.5.8a the response is shown for a system amplitude chosen such that the first reflections of both system and hall have approximately the same magnitude. This level will be used as reference (0 dB) in comparison with other system levels. In figure 5.5.8b the reverberation curve of hall plus system is shown, for the response shown in figure 5.5.8a, for a system amplitude 6 dB higher and for a system amplitude 6 dB lower. For comparison the reverberation

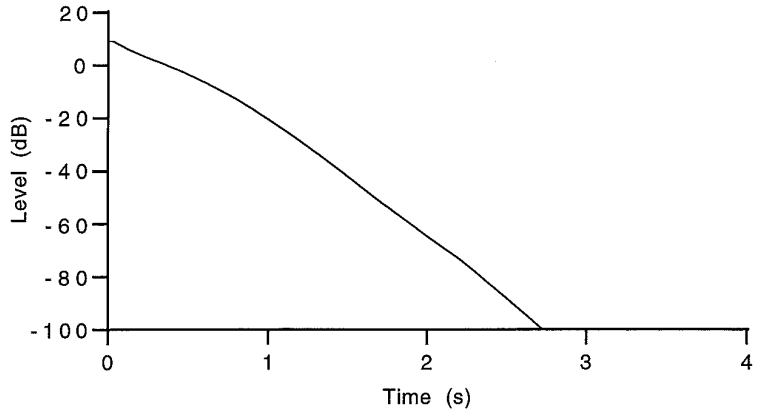

Figure 5.5.7: *Reverberation curve of the early reflection system as recorded at the receiver position. Note the convex shape of the curve, caused by the convolution of the processor response with the hall transfer functions.*

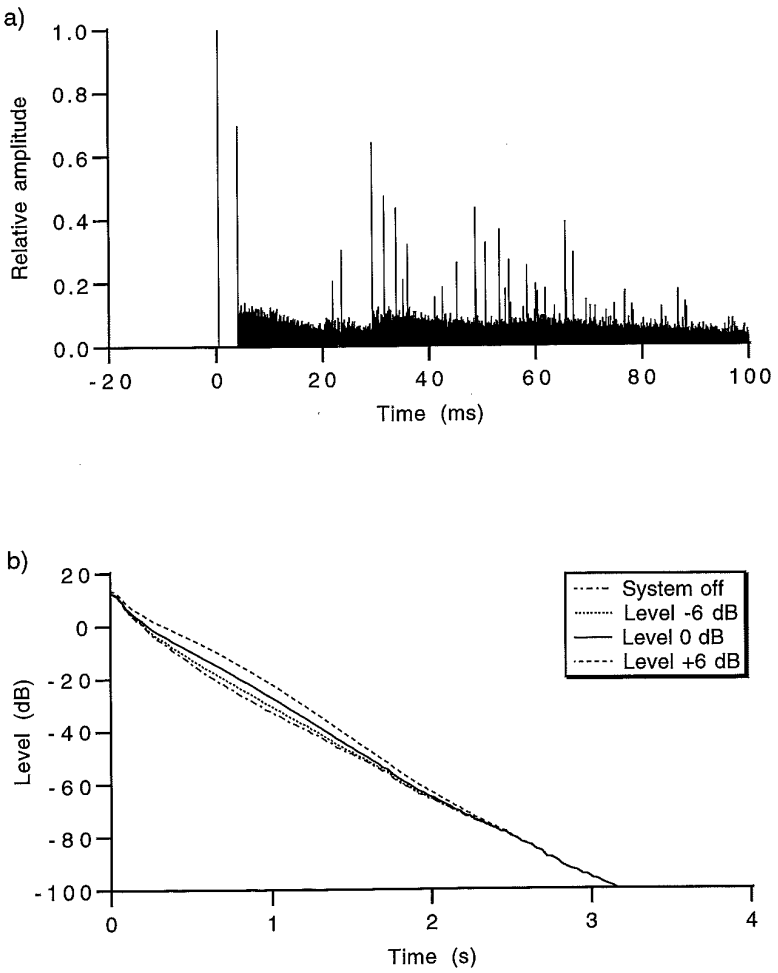

Figure 5.5.8: *Calculated responses of the model hall with the single-channel early reflection system switched on.*
a) Impulse response $h_{RS}(t)$, system level 0 dB
b) Reverberation curve, system level -∞ (off), -6 dB, 0 dB and +6 dB

curve of the hall (system off) is also shown in this graph.
The shape of the decay curve can be accounted for by considering the hall decay curve and the system decay curve together. In figure 5.5.9 both these curves are shown. The total decay curve is found by adding the curves shown in the graph. In regions where the level of the hall decay curve is above the system decay curve, the total level is dominated by the system and vice versa. Changing the output level of the system alters the level of the system decay curve, and thus changes the relative level of hall and system. From figure 5.5.8 it can be seen that raising the system amplitude makes the convex shape of the system response more pronounced in the total response. Lowering the system amplitude decreases the influence of the system on the total response, as expected.
In table 5.5.3 the signal properties of the simulated response as defined in table 5.5.2 on page 187 are shown for all three levels of the early reflection system discussed before. For comparison, the values for the hall with the system off are given too. Note that, when the early reflection system is operated on a high level, the standard reverberation time is not a good measure for the hall response, due to the non-linear behaviour of the decay curve. For this situation, the signal properties yield a more gen-

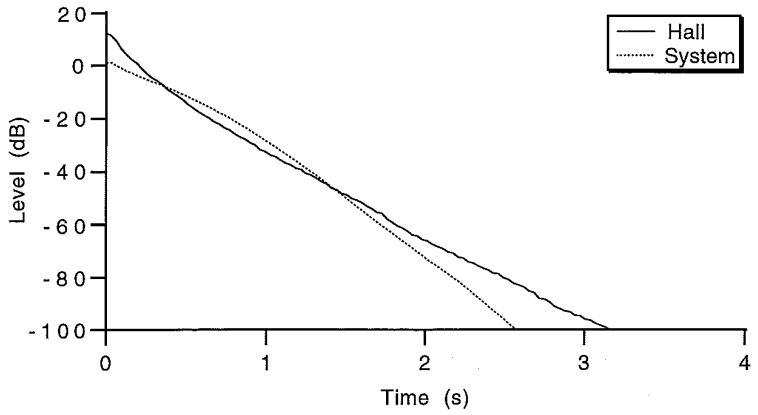

Figure 5.5.9: *Contribution of the hall (system off) and of the system to the total decay curve. The level of the system contribution can be changed.*

eral description of the hall response.
The energy measure is an indicator of the output level of the system. It can be seen from table 5.5.3 that both the energy of the impulse response E_i and the energy of the decay curve E_r increase with increasing system level. Both measures can be used as an indicator of the total sound level in the hall. As the energy of the decay curve is a very sensitive indicator that shows large variations even for small changes in the system parameters, the energy of the impulse response is a more suitable indicator.
As before, the reverberation time as calculated from the first and second order length of the decay curve is also shown in table 5.5.3. Note that both length measures yield comparable results for the reverberation time.

	System level			
Property	off	-6 dB	0 dB	+6 dB
E_i	$5.3 \cdot 10^{-4}$	$5.4 \cdot 10^{-4}$	$5.7 \cdot 10^{-4}$	$6.9 \cdot 10^{-4}$
$L_{1,i}$	$8.1 \cdot 10^{-2}$	$8.3 \cdot 10^{-2}$	$8.7 \cdot 10^{-2}$	$1.0 \cdot 10^{-1}$
$L_{2,i}$	$1.1 \cdot 10^{-2}$	$1.2 \cdot 10^{-2}$	$1.4 \cdot 10^{-2}$	$2.2 \cdot 10^{-2}$
E_r	1.4	1.5	1.6	2.3
$T_{60}(L_{1,r})$	1.0	1.0	1.1	1.4
$T_{60}(L_{2,r})$	1.0	1.1	1.2	1.6

Table 5.5.3: *Signal properties for the model hall, for several output levels of the single-channel early reflection system.*

5.5.3 The single-channel reverberation processor

In this section the single-channel electro-acoustic system discussed before will be extended with a reverberation processor. The positions of the system microphone and the system loudspeaker remain unchanged.
The response of the reverberation processor is a pulse sequence with an average pulse interval of 40 ms and a relative attenuation of 1 dB, thus yielding an attenuation of 60 dB in 2.4 seconds. The randomisation in the pulse interval is ±10%.
The early reflection processor and the reverberation processor of the system can be connected either in parallel or in series, as shown in figure 5.5.10. In figure 5.5.11 the processor response $h_{EAS}(t)$ is shown for the two configurations shown in figure 5.5.10. The output levels of the early reflection processor and the reverberation processor are chosen such that the first reflection of both systems have the same amplitude. Note that in the serial configuration the reflection density in the output of the reverberation processor increases, due to the convolution with the response of the early reflection

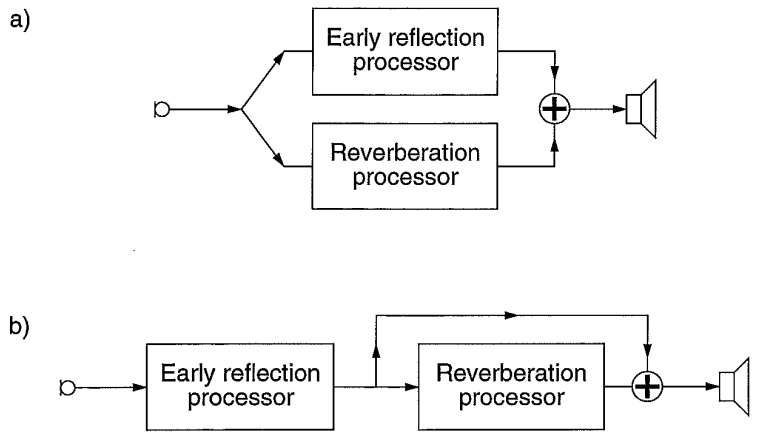

Figure 5.5.10: *Two possible interconnections of the early reflection processor and the reverberation processor of the electro-acoustic system.*
a) Parallel configuration
b) Serial configuration

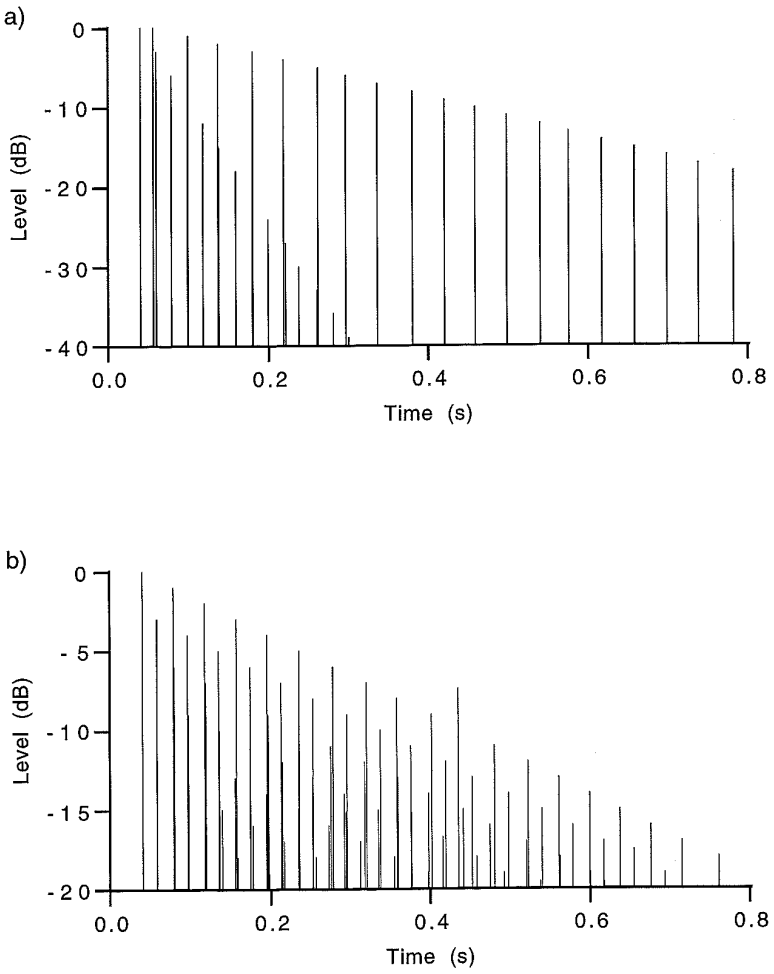

Figure 5.5.11: *Processor response $h_{EAS}(t)$ for the two possible interconnections of the early reflection processor and the reverberation processor shown in figure 5.5.10.*
a) Parallel configuration
b) Serial configuration

processor. In appendix F the effect of serial connection of pulse sequences is discussed in more detail.

The increase of reflection density for the serial configuration is an advantage in situations where the loudspeaker of the electro-acoustic system radiates most of its sound directly to the audience, as in this case the 40 ms pulse interval of the reverberation processor is too large. In the serial configuration the initial delays of both processors add up, which can be advantageous for loudspeakers at the back of the hall.

The total system contribution $h_{RS,sys}(t)$ to the source-receiver response is shown in figure 5.5.12 for the two system configurations shown in figure 5.5.10. As the reflection density increases with time in the serial configuration, the differences in the impulse responses shown in figure 5.5.12 are also increasing with time. For the 100 ms time interval shown in the graph the differences are not yet very large.

The reverberation curves calculated from the two responses of figure 5.5.12 are shown in figure 5.5.13. Note the almost constant level over the first 0.5 seconds of the decay curve in figure 5.5.13b, caused by the convolution of the two processor responses.

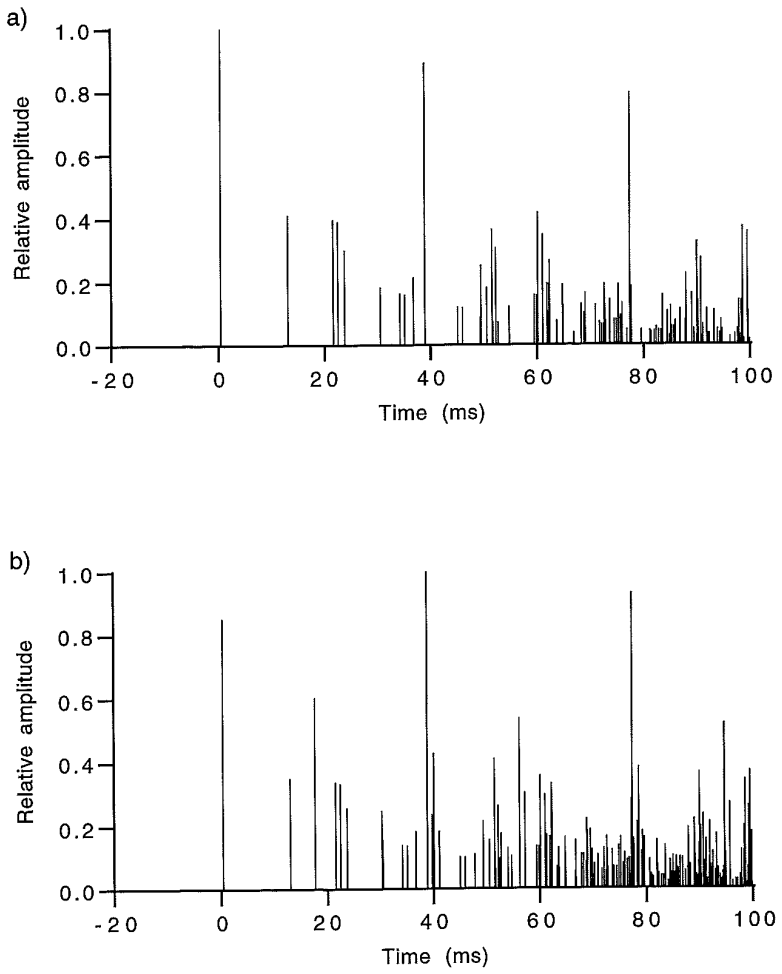

Figure 5.5.12: *Total system response $h_{RS,sys}(t)$ for the two interconnections of the early reflection processor and the reflection processor shown in figure 5.5.10.*
a) Parallel configuration
b) Serial configuration

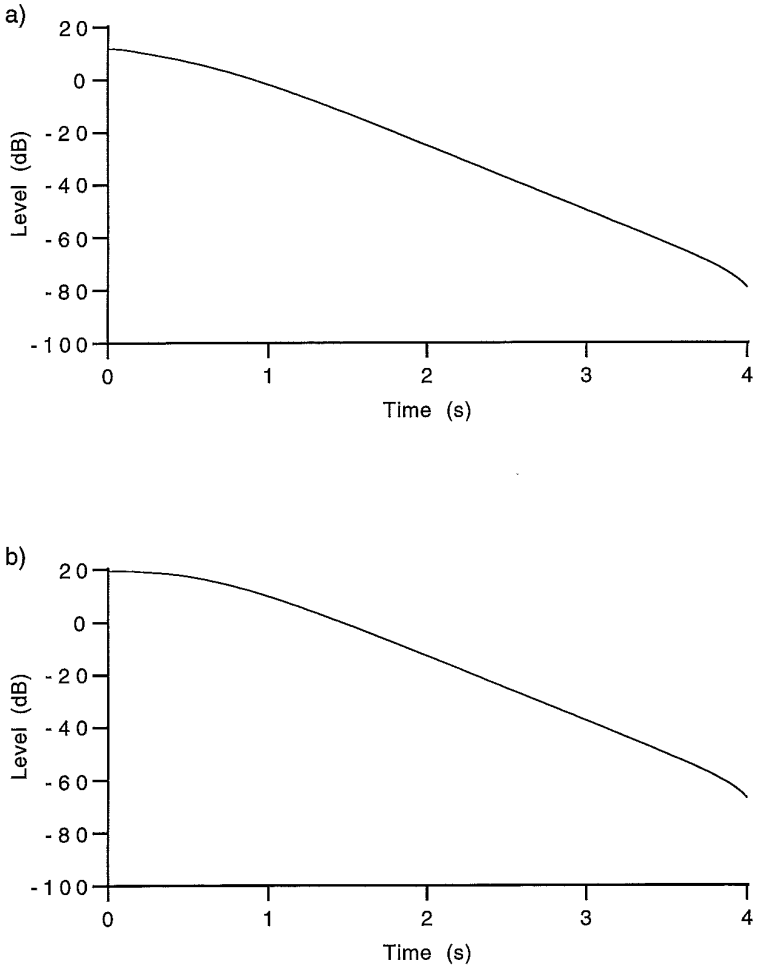

Figure 5.5.13: *Decay curve of the reverberation processor of the electro-acoustic system as recorded at the receiver position, for the two interconnections of the system processors shown in figure 5.5.10.*
a) Parallel configuration
b) Serial configuration

For the parallel configuration figure 5.5.14 shows the total hall response and the reverberation curve for three different output levels of the electro-acoustic system. Note the significant double decay in the low level reverberation curve, the start having the decay of the hall and the end having the decay of the reverberation processor. When the output level of the reverberation processor is increased, the shape of the decay curve is mainly determined by the system decay, as can be seen by comparison with figure 5.5.13a.

In table 5.5.4 the signal properties as defined in table 5.5.2 on page 187 are given for the parallel configuration of the early reflection processor and the reverberation processor. Note that the decay curve is not a straight line over the interval from 5 to 35 dB below the starting level. As a consequence, the standard reverberation time is not well defined for this situation. After about 0.5 second the decay curve has a slope of 25 dB/s, so determining the reverberation time over this part of the decay curve would yield a value of 2.4 seconds, which is the same as the 60 dB decay time of the combined early reflections and reverberation processor decay curve.

	System level			
Property	off	-6 dB	0 dB	+6 dB
E_i	$5.3 \cdot 10^{-4}$	$5.7 \cdot 10^{-4}$	$6.9 \cdot 10^{-4}$	$1.2 \cdot 10^{-3}$
$L_{1,i}$	$8.1 \cdot 10^{-2}$	$1.0 \cdot 10^{-1}$	$1.4 \cdot 10^{-1}$	$2.3 \cdot 10^{-1}$
$L_{2,i}$	$1.1 \cdot 10^{-2}$	$2.4 \cdot 10^{-2}$	$5.4 \cdot 10^{-2}$	$1.1 \cdot 10^{-1}$
E_r	1.4	1.8	3.2	8.5
$T_{60}(L_{1,r})$	1.0	1.7	2.6	3.4
$T_{60}(L_{2,r})$	1.0	2.0	2.8	3.4

Table 5.5.4: *Signal properties for the model hall with the early reflection processor and the reverberation processor in parallel configuration, for several output levels of the system.*

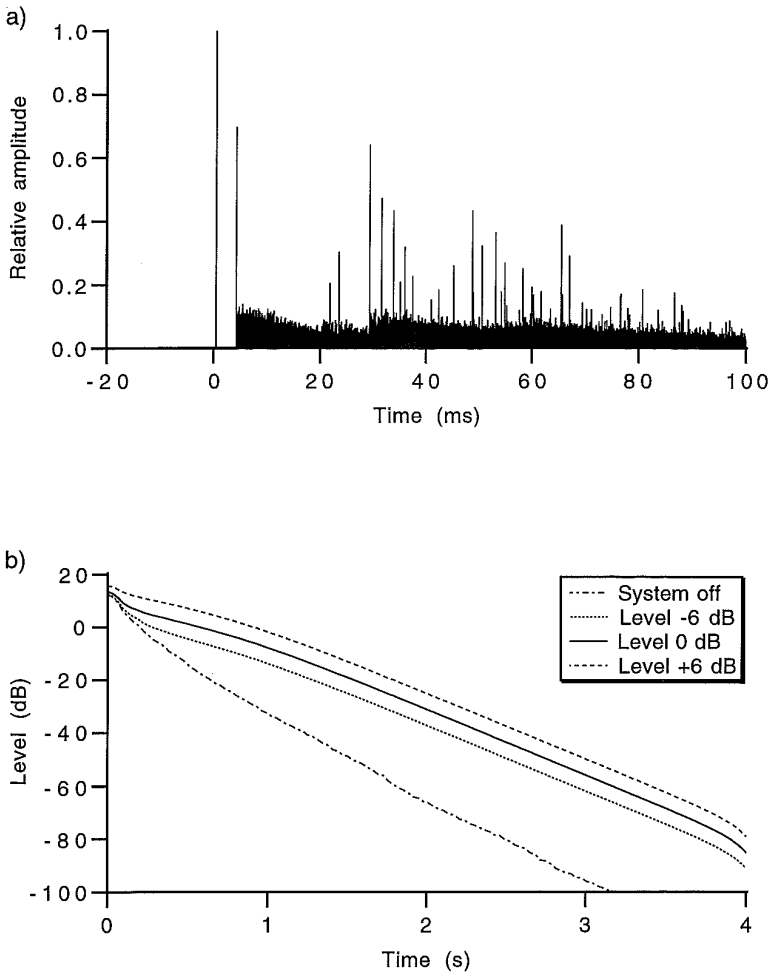

Figure 5.5.14: *Simulated hall responses for the parallel configuration of the early reflection processor and the reverberation processor.*
a) Impulse response $h_{RS}(t)$, system level 0 dB
b) reverberation curve, system level -∞ (off), -6 dB, 0 dB and +6 dB

In figure 5.5.15 the total hall response $h_{RS}(t)$ and the reverberation curve are shown for the serial configuration of the early reflection processor and the reverberation processor, for three different output levels of the system. It can be seen that the resulting reverberation curves are mainly determined by the system response and also show the almost constant level at the start. As was found for the parallel configuration, for high system levels the hall response is almost completely determined by the system response, as can be seen by comparison with figure 5.5.13b.
The calculated reverberation time and signal properties of the simulated responses as defined in table 5.5.2 on page 187 are given in table 5.5.5 for the three system levels used. Due to the constant level at the first part of the decay curve, the standard reverberation time is not a good measure for this situation. After some time, the decay curve has a constant slope of 25 dB/s, so determining the reverberation time over this part of the decay curve would yield a value of 2.4 seconds, which is the same as the 60 dB decay time of the combined early reflections and reverberation processor decay curve.

	System level			
Property	off	-6 dB	0 dB	+6 dB
E_i	$5.3 \cdot 10^{-4}$	$7.1 \cdot 10^{-4}$	$1.2 \cdot 10^{-3}$	$3.3 \cdot 10^{-3}$
$L_{1,i}$	$8.1 \cdot 10^{-2}$	$2.1 \cdot 10^{-1}$	$3.5 \cdot 10^{-1}$	$5.2 \cdot 10^{-1}$
$L_{2,i}$	$1.1 \cdot 10^{-2}$	$1.2 \cdot 10^{-1}$	$2.5 \cdot 10^{-1}$	$3.9 \cdot 10^{-1}$
E_r	1.4	4.7	15	55
$T_{60}(L_{1,r})$	1.0	4.0	4.8	5.1
$T_{60}(L_{2,r})$	1.0	3.9	4.4	4.6

Table 5.5.5: *Signal properties for the model hall with the early reflection processor and the reverberation processor in serial configuration, for several output levels of the system.*

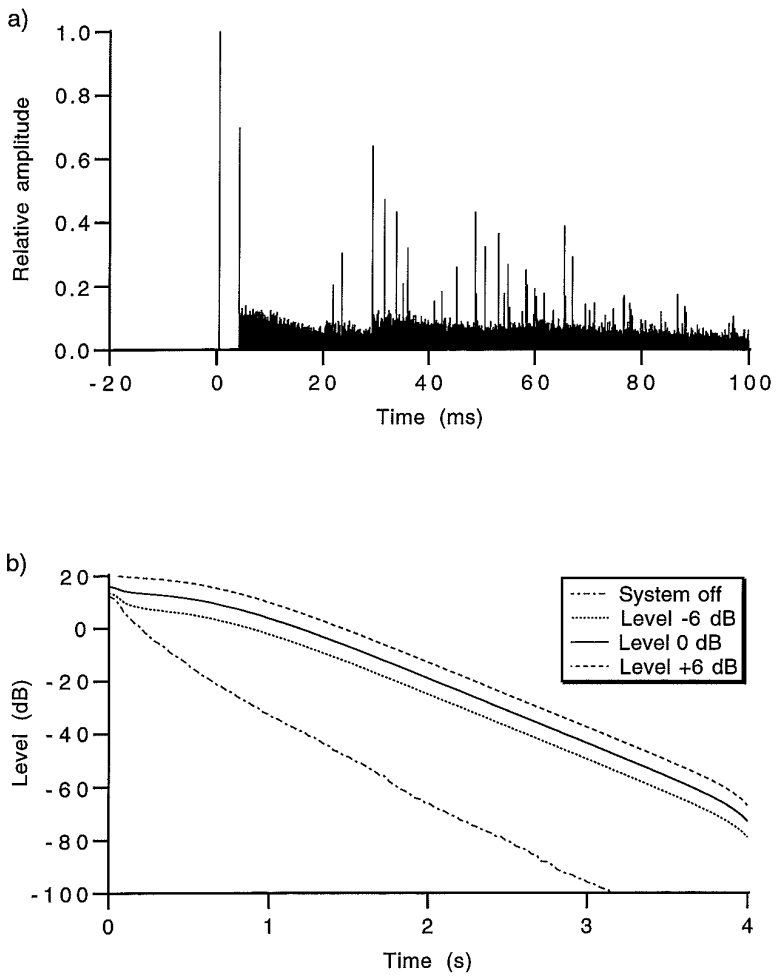

Figure 5.5.15: *Simulated hall responses for the serial configuration of the early reflection processor and the reverberation processor.*
a) Impulse response $h_{RS}(t)$, system level 0 dB
b) reverberation curve, system level -∞ (off), -6 dB, 0 dB and +6 dB

From figure 5.5.14 and figure 5.5.15 it can be concluded that for these situations the reverberation curve is almost completely determined by the system response. From figure 5.5.8b it can be seen that using the early reflection system only yields a decay curve mainly determined by the hall response. These effects indicate that for a large difference in reverberation time between the hall and the system, the response with the longest reverberation time is most important. To analyse this effect some further, similar reverberation curves as shown in figure 5.5.14 and figure 5.5.15 are calculated, but now using a reverberation processor response with an average pulse interval of 40 ms, a randomisation of ±10% and a relative pulse attenuation of 1.5 dB, thus yielding a 60 dB decay time of 1.6 second. As before, the level of the early reflection processor and the reverberation processor are chosen such that the first reflection generated by both responses have the same amplitude.

The simulated reverberation curves of the reverberation processor as recorded at the receiver position are shown in figure 5.5.16. Note the constant level at the first part of the decay curves, especially for the serial configuration. After some time, both decay curves have a constant slope of about 37.5 dB/s, yielding the same 60 dB decay time of 1.6 second as the processor response.

The decay curves of the hall with the system switched on are shown in figure 5.5.17, for several levels of the system and for both the parallel and the serial configuration. The calculated signal properties for this simulation as defined by table 5.5.2 on page 187 are given in table 5.5.6 on page 207.

As before, the decay curve for the serial configuration shows a constant part at the first 0.5 second, a shape that is also found for the decay curve of the hall for a high output level of the reverberation system. Due to this flat part, the standard reverberation time calculated by fitting a straight line to the interval from 5 to 35 dB below the start level does not have a well defined meaning. After one second, the decay of both the parallel configuration and the serial configuration have the same slope of 37.5 dB/s as the system response, thus yielding a 60 dB decay in 1.6 second.

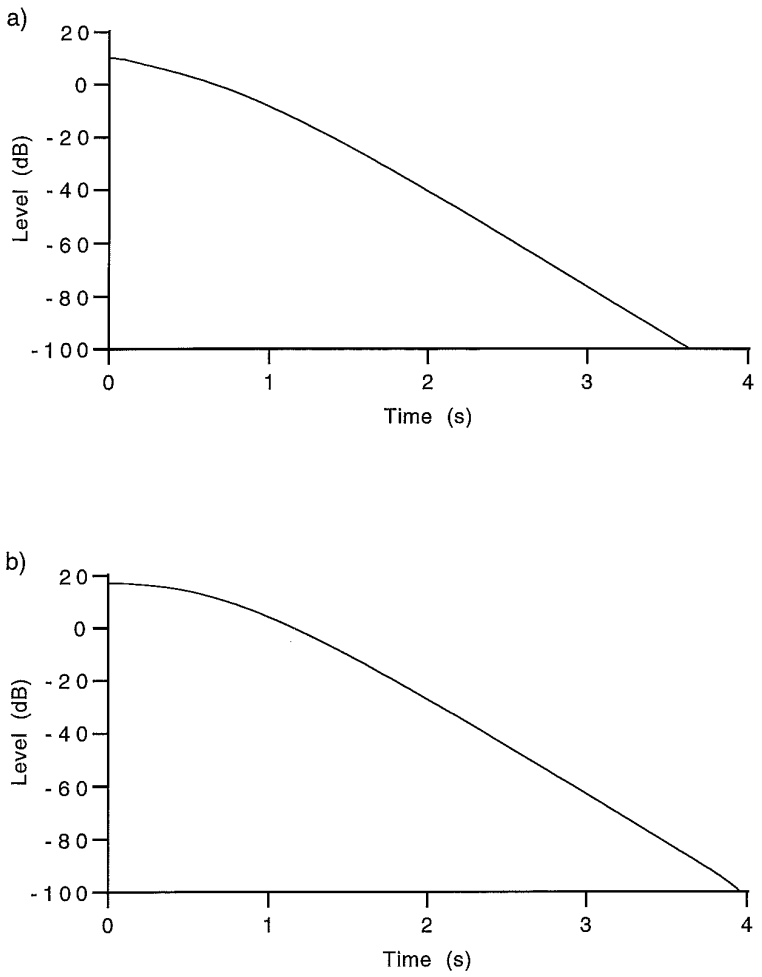

Figure 5.5.16: *Decay curve of the reverberation processor of the electro-acoustic system as recorded at the receiver position, for the two interconnections of the system processors shown in figure 5.5.10. The reverberation processor has 60 dB decay time of 1.6 second.*
a) Parallel configuration
b) Serial configuration

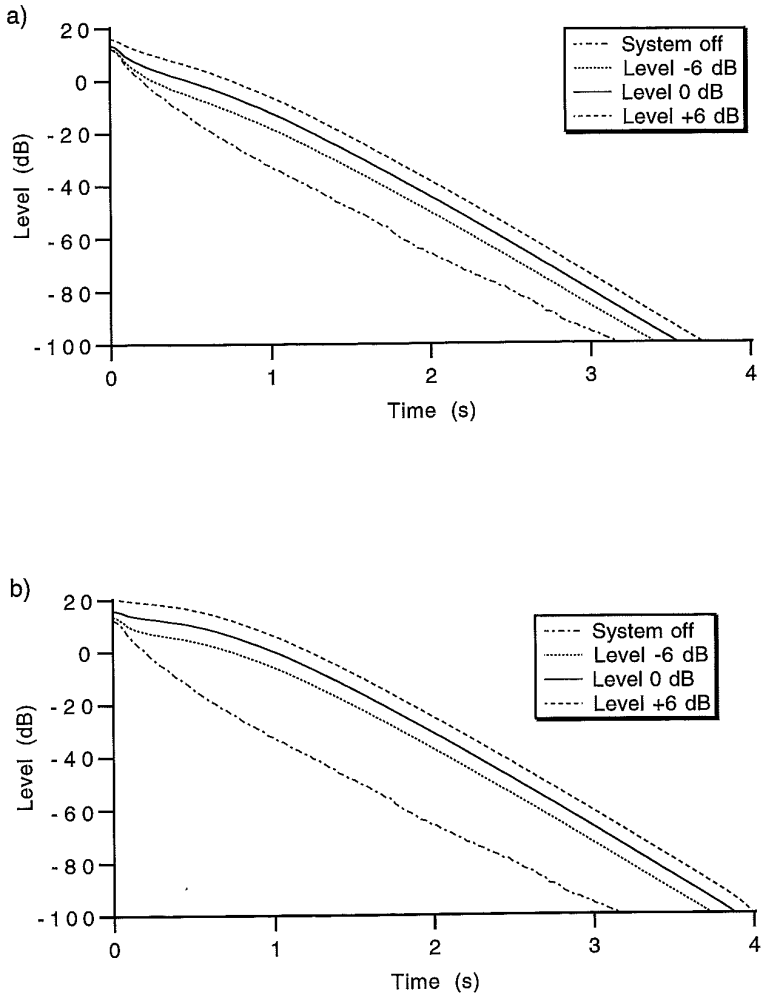

Figure 5.5.17: *Reverberation curves for a processor response with a 60 dB decay time of 1.6 second, for the two interconnections of the electro-acoustic system shown in figure 5.5.10.*
a) Parallel configuration
b) Serial configuration

		System level			
	Property	off	-6 dB	0 dB	+6 dB
Parallel configuration	E_i	$5.3 \cdot 10^{-4}$	$5.6 \cdot 10^{-4}$	$6.5 \cdot 10^{-4}$	$1.0 \cdot 10^{-3}$
	$L_{1,i}$	$8.1 \cdot 10^{-2}$	$9.1 \cdot 10^{-2}$	$1.2 \cdot 10^{-1}$	$1.7 \cdot 10^{-1}$
	$L_{2,i}$	$1.1 \cdot 10^{-2}$	$1.7 \cdot 10^{-2}$	$3.1 \cdot 10^{-2}$	$6.3 \cdot 10^{-2}$
	E_r	1.4	1.7	2.4	5.5
	$T_{60}(L_{1,r})$	1.0	1.3	1.9	2.6
	$T_{60}(L_{2,r})$	1.0	1.5	2.1	2.6
Serial configuration	E_i	$5.3 \cdot 10^{-4}$	$6.4 \cdot 10^{-4}$	$9.7 \cdot 10^{-4}$	$2.3 \cdot 10^{-3}$
	$L_{1,i}$	$8.1 \cdot 10^{-2}$	$1.5 \cdot 10^{-1}$	$2.6 \cdot 10^{-1}$	$3.9 \cdot 10^{-1}$
	$L_{2,i}$	$1.1 \cdot 10^{-2}$	$6.2 \cdot 10^{-2}$	$1.5 \cdot 10^{-1}$	$2.4 \cdot 10^{-1}$
	E_r	1.4	3.1	8.2	29
	$T_{60}(L_{1,r})$	1.0	2.9	3.8	4.2
	$T_{60}(L_{2,r})$	1.0	3.0	3.6	3.8

Table 5.5.6: *Sgnal properties for the model hall for both configurations and several output levels of the system of the system. The response of the reverberation processor has a 60 dB decay time of 1.6 second.*

5.5.4 Single-channel electro-acoustic system with acoustic feedback

In this section the influence of acoustic feedback from the system loudspeaker back to the system microphone will be discussed. For this situation, the source-receiver transfer function $h_{RS}(t)$ is given by

$$h_{RS}(t) = h_{RS,\,hall}(t) + h_{RS,\,sys}(t) + h_{RS,\,FB}(t) \ , \qquad (5.5.3)$$

in which the feedback term $h_{RS,FB}(t)$is given by

$$h_{RS,\,FB}(t) = h_{RL}(t) * h_{EAS}(t) * h_{ML}(t) * h_{EAS}(t) * h_{MS}(t) \ . \qquad (5.5.4)$$

As an illustration the example with the early reflection processor only as discussed in section 5.5.2 is repeated here, now including the feedback term $h_{RS,FB}(t)$ at several levels. The influence of the acoustic feedback is most easily seen by considering the decay curve of the hall. In figure 5.5.18a the decay curve derived from the feedback response described by equation (5.5.4) is shown. The slope at the linear part of this decay curve is about 30 dB/s, which is less steep than the slope of 200 dB/s for the early reflection processor decay and the slope of 50 dB/s of the hall decay. As the feedback part of the system response is the convolution of five transfer functions (three hall transfers and the processor transfer twice) the convex shape of the feedback response decay is more prominent than that of the system response decay.
Figure 5.5.18b shows the decay curve for the source-receiver transfer given by equation (5.5.3), for several levels of the feedback term. The signal properties of the simulated responses as defined in table 5.5.2 on page 187 are given in table 5.5.7 on page 210. When the feedback level is high it dominates the total decay curve, as can be seen by comparing figure 5.5.18a with figure 5.5.18b.

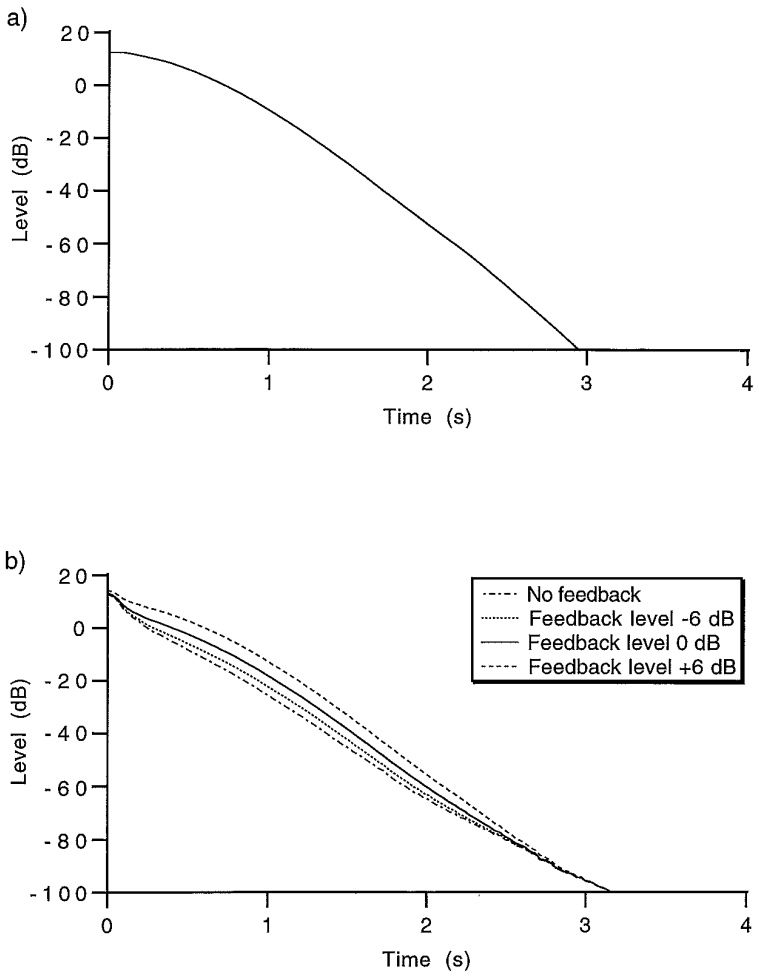

Figure 5.5.18: *The effect of loudspeaker-microphone feedback on the total hall reverberation curve, with only the early reflection system switched on.*
a) Feedback decay curve only
b) Total decay curve for different levels of the feedback

	Feedback level			
Property	-∞	-6 dB	0 dB	+6 dB
E_i	$5.7 \cdot 10^{-4}$	$5.8 \cdot 10^{-4}$	$6.0 \cdot 10^{-4}$	$6.7 \cdot 10^{-4}$
$L_{1,i}$	$8.7 \cdot 10^{-2}$	$9.1 \cdot 10^{-2}$	$9.9 \cdot 10^{-2}$	$1.3 \cdot 10^{-1}$
$L_{2,i}$	$1.4 \cdot 10^{-2}$	$1.6 \cdot 10^{-2}$	$2.0 \cdot 10^{-2}$	$3.6 \cdot 10^{-2}$
E_r	1.6	1.7	1.9	2.7
$T_{60}(L_{1,r})$	1.1	1.2	1.4	2.0
$T_{60}(L_{2,r})$	1.2	1.3	1.6	2.1

Table 5.5.7: *Signal properties for the simulated responses of the hall with the early reflection processor only, including loudspeaker microphone feedback at several levels.*

The effect of feedback when both the early reflection processor and the reverberation processor of the hall are switched on will be considered next. A reverberation processor with a decay slope of 25 dB/s will be used. The results are calculated for the parallel configuration and shown in figure 5.5.19. The slope of the linear part of the processor feedback decay is about 20 dB/s and is thus less steep than the decay of the processor response.

Table 5.5.8 shows the signal properties for the calculated responses as defined in table 5.5.2 on page 187. Note that the decay is mainly determined by the feedback contribution as given by equation (5.5.4). In section 5.5.3 it was found that the decay without feedback is mainly determined by the system response, with the same 25 dB/s slope in the linear part as the reverberation processor. Thus, the decay time is increased by the loudspeaker-microphone feedback.

	Feedback level			
Property	-∞	-6 dB	0 dB	+6 dB
E_i	$6.9 \cdot 10^{-4}$	$7.1 \cdot 10^{-3}$	$7.5 \cdot 10^{-4}$	$9.4 \cdot 10^{-3}$
$L_{1,i}$	$1.4 \cdot 10^{-1}$	$1.6 \cdot 10^{-1}$	$2.0 \cdot 10^{-1}$	$3.2 \cdot 10^{-1}$
$L_{2,i}$	$5.4 \cdot 10^{-2}$	$7.0 \cdot 10^{-2}$	$1.2 \cdot 10^{-1}$	$2.6 \cdot 10^{-1}$
E_r	3.2	3.6	4.8	9.8
$T_{60}(L_{1,r})$	2.6	3.1	4.1	5.5
$T_{60}(L_{2,r})$	2.8	3.4	4.2	5.2

Table 5.5.8: *Signal properties for the simulated responses of the hall with the early reflection processor and the reverberation processor in parallel configuration, including loudspeaker-microphone feedback at several levels.*

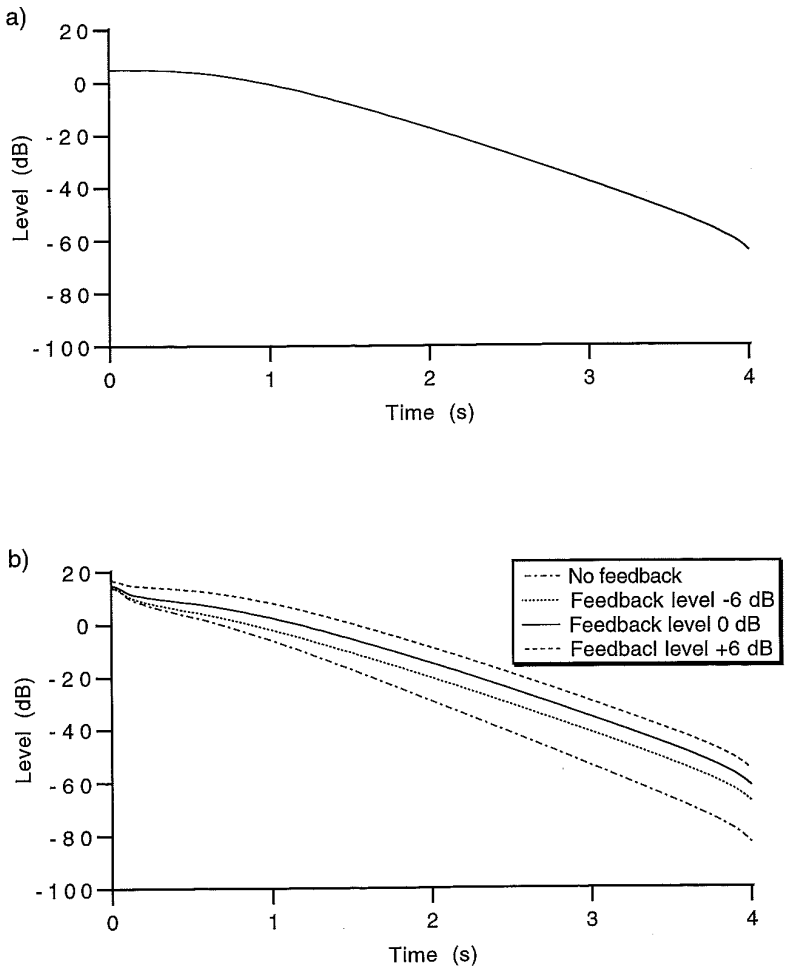

Figure 5.5.19: *The effect of loudspeaker-microphone feedback on the total hall reverberation curve, with the early reflection processor and the reverberation processor in parallel configuration.*
a) Feedback decay curve only
b) Total decay curve for different levels of the feedback

5.5.5 The multi-channel early reflection processor

The electro-acoustic systems used in practice are always multi-channel systems, consisting of several microphones and several loudspeakers. The single-channel systems discussed before are only an approximate model in which the total system response is addressed to a single microphone-loudspeaker channel.
In this section the early reflection processor discussed in section 5.5.2 will be reconsidered, the early reflections now being generated by a set of 24 loudspeakers distributed throughout the hall. In the situation considered here only one source is present on stage. By dividing the stage into several sub-areas, each addressed by a single directive microphone (a technique discussed more thoroughly in section 3.6), this source is recorded by one microphone only. In figure 5.5.20 a top view of the model hall is shown, with the position of the microphone and the loudspeakers indicated.

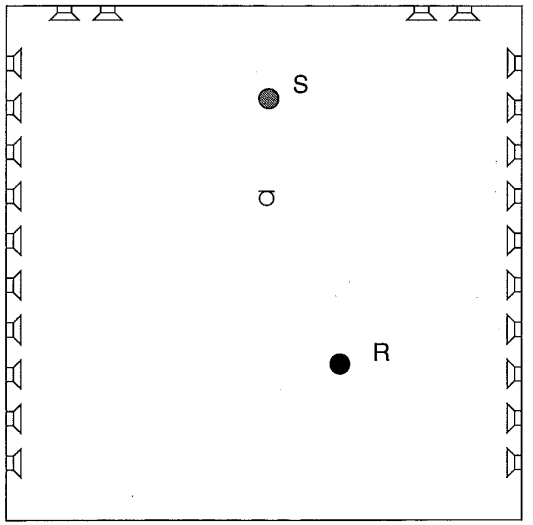

Figure 5.5.20: *Top view of the model hall with the source S, the receiver R, the system microphone and the system loudspeakers indicated.*

The processor response for each loudspeaker channel is chosen such that all loudspeakers together generate the processor response of the single-channel system discussed in section 5.5.2. This means that each loudspeaker of the multi-channel system radiates only 1/24th of the reflections of the single-channel system. As a consequence, the reflection density per channel is much lower than for the single-channel system processor response shown in figure 5.5.5 on page 190.

The reverberation curve for the total early reflection system processor response is shown in figure 5.5.21a. In figure 5.5.21b the reverberation curve is shown for several output levels of the system. Comparing figure 5.5.8 on page 192 with figure 5.5.21 shows that the computed results for the single-channel system and the multi-channel system are almost identical. This means that the single-channel early reflection processor can be used as an approximation of the multi-channel system, thus saving a lot of computation time. The approximation remains valid as long as directional information is not taken into account in the calculation.

In table 5.5.9 the signal properties of the simulated responses as defined in table 5.5.2 on page 187 are given. The numerical values are in good agreement with those in table 5.5.3 on page 194.

	System level			
Property	off	-6 dB	0 dB	+6 dB
E_i	$5.3 \cdot 10^{-4}$	$5.5 \cdot 10^{-4}$	$6.1 \cdot 10^{-4}$	$8.4 \cdot 10^{-4}$
$L_{1,i}$	$8.1 \cdot 10^{-2}$	$8.4 \cdot 10^{-2}$	$9.1 \cdot 10^{-2}$	$1.1 \cdot 10^{-1}$
$L_{2,i}$	$1.1 \cdot 10^{-2}$	$1.2 \cdot 10^{-2}$	$1.5 \cdot 10^{-2}$	$2.1 \cdot 10^{-2}$
E_r	1.4	1.5	1.8	3.0
$T_{60}(L_{1,r})$	1.0	1.0	1.1	1.4
$T_{60}(L_{2,r})$	1.0	1.1	1.2	1.3

Table 5.5.9: *Signal properties for the model hall with the multi-channel early reflection processor at several levels.*

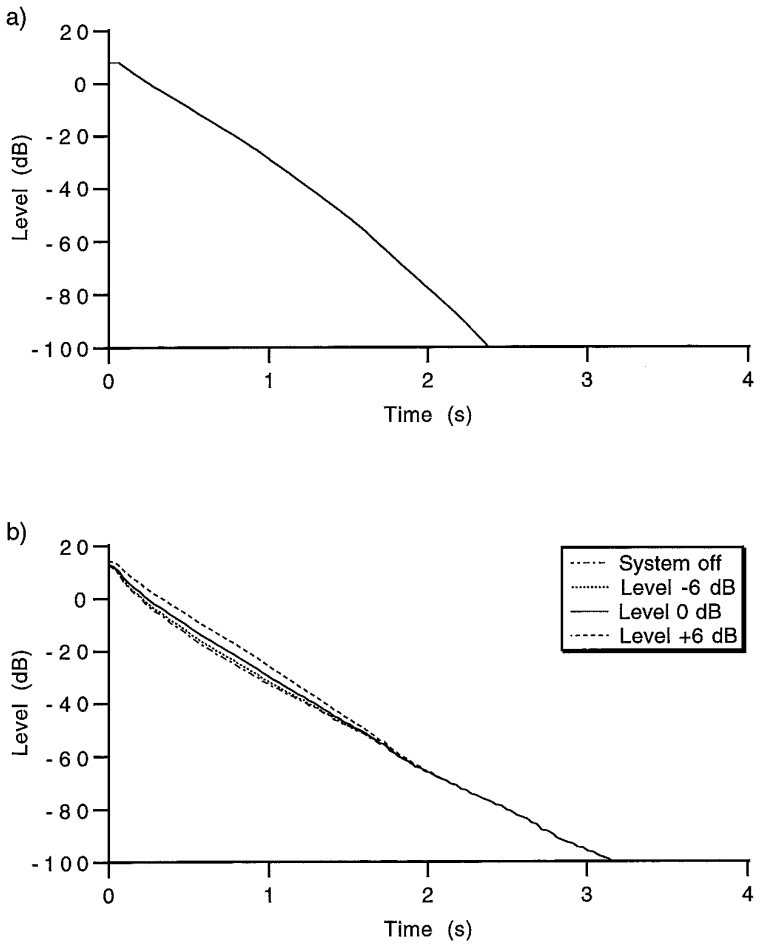

Figure 5.5.21: *Calculated responses of the model hall with the multi-channel early reflection system switched on.*
a) Reverberation curve of the processor response
b) Reverberation curve, system level -∞ (off), -6 dB, 0 dB, +6 dB

5.5.6 The multi-channel reverberation processor

In this section the single-channel reverberation processor discussed in section 5.5.3 will be extended to a multi-channel system. The loudspeaker distribution that will be used for this system is the same as the loudspeaker distribution of the early reflection system discussed in the previous section. Both the parallel configuration and the serial configuration of the early reflection processor and the reverberation processor will be reconsidered here.

As with the early reflection system, the response of the single-channel reverberation processor discussed in section 5.5.3 will be distributed over all 24 loudspeakers. As a consequence, in the parallel configuration the number of reflections per loudspeaker channel is a factor of 24 smaller than for the single channel system. Combining the outputs of all loudspeakers, however, exactly compensates this loss in reflection density, so it is expected that the single channel system and the multi-channel system will yield similar results.

In figure 5.5.22 the reverberation curve of the multi-channel early reflection and reverberation processor in parallel configuration and the hall with system switched on are shown. The graphs are in good agreement with figure 5.5.14 on page 201. Thus, the single-channel system discussed before can be used as a good approximation for the multi-channel system.

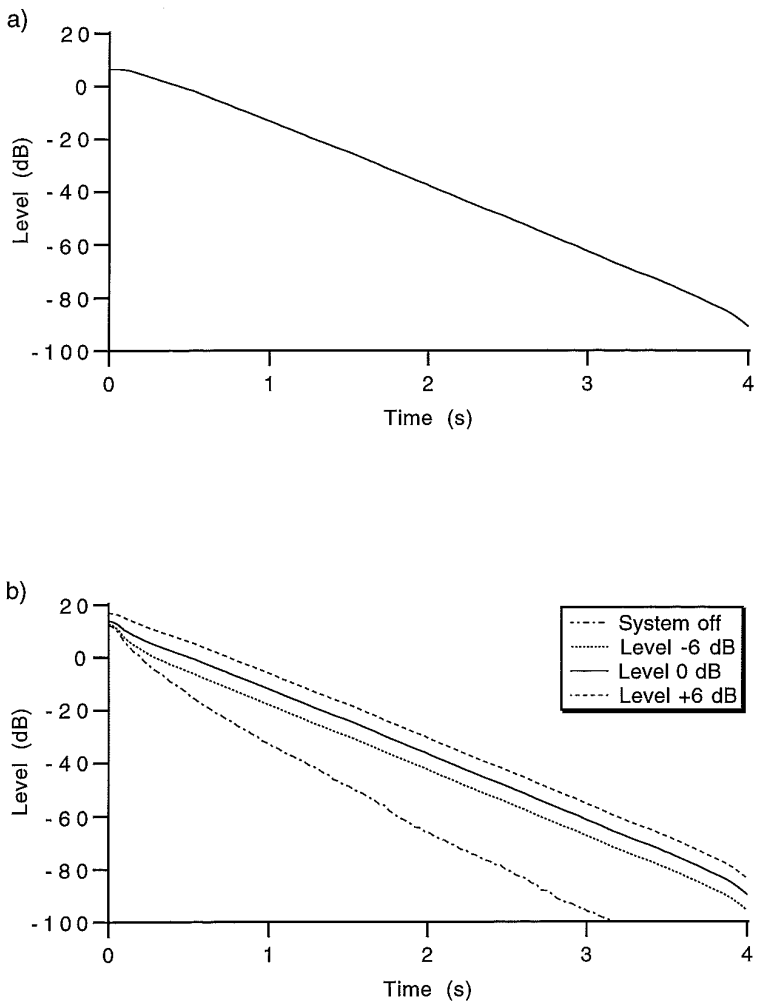

Figure 5.5.22: *Calculated responses of the model hall with the multi-channel reverberation system in parallel configuration switched on.*
a) Reverberation curve of the processor response
b) Reverberation curve, system level -∞ (off), -6 dB, 0 dB, +6 dB

In our model describing a serial configuration of a multi-channel early reflection processor and a multi-channel reverberation processor, each reflection generated by the early reflection processor is convolved with a reverberation processor (see figure 5.5.23). The output of each reverberation processor is distributed over all loudspeakers in the hall, in the same way as was discussed in relation with the early reflection processor. Due to the convolution process, the reflection density in the processor output will be increased, in comparison with the parallel configuration.

Figure 5.5.24a shows the contribution of the multi-channel early reflection and reverberation system in serial configuration to the reverberation curve at the receiver position. In figure 5.5.24b the total reverberation curve at the receiver position is shown. Comparison with the graphs shown in figure 5.5.15 on page 203 shows that the results of the single-channel reverberation system and the multi-channel reverberation system are almost identical. Again, the single-channel system discussed before is a good approximation for the more complex multi-channel model.

Table 5.5.10 on page 220 shows the signal properties of the impulse response and the decay curve as defined in table 5.5.2 on page 187 for both configurations of the reverberation system.

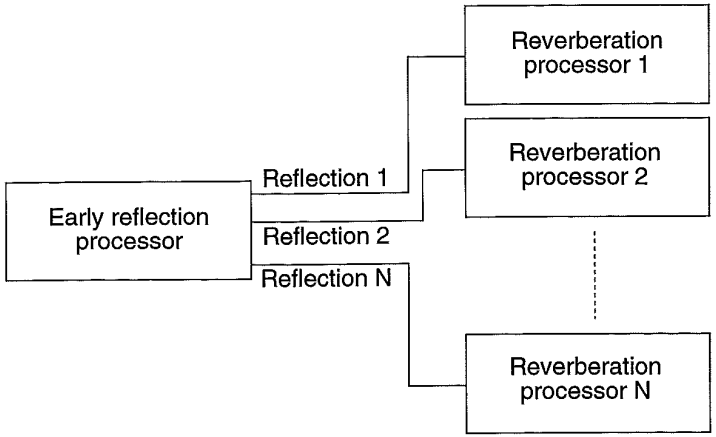

Figure 5.5.23: *In the serial configuration of the multi-channel early reflection processor and reverberation processor each reflection generated by the early reflection processor is convolved with a reverberation processor.*

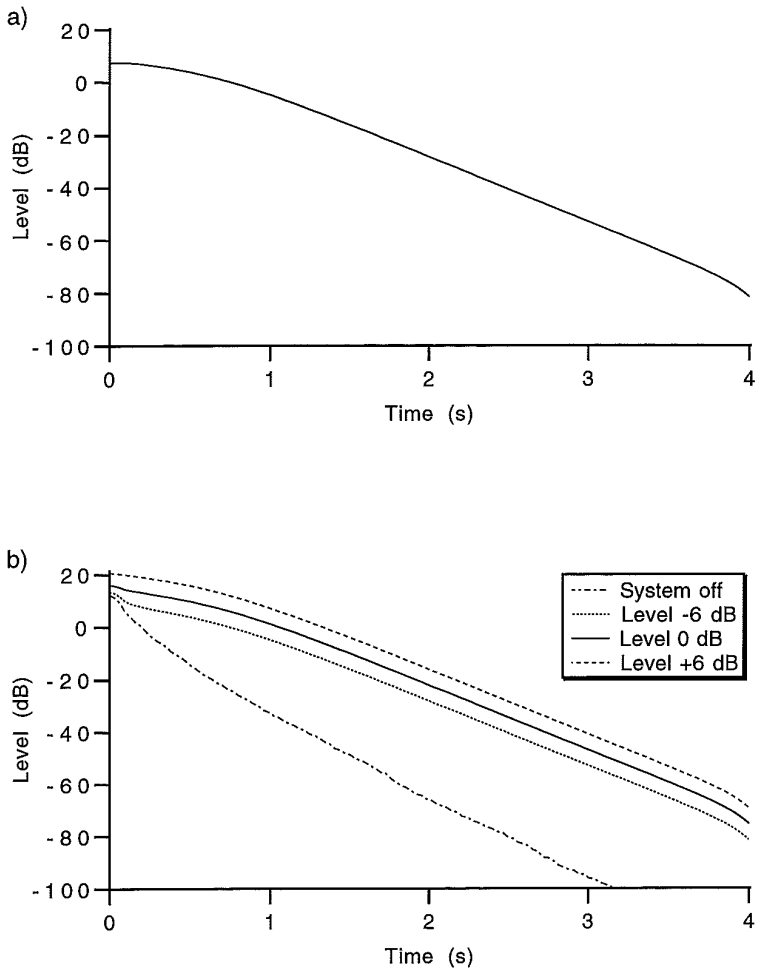

Figure 5.5.24: *Calculated responses of the model hall with the multi-channel reverberation system in serial configuration switched on.*
a) Reverberation curve of the processor response
b) Reverberation curve, system level -∞ (off), -6 dB, 0 dB, +6 dB

		System level			
	Property	off	-6 dB	0 dB	+6 dB
Parallel configuration	E_i	$5.3 \cdot 10^{-4}$	$5.9 \cdot 10^{-4}$	$7.8 \cdot 10^{-4}$	$1.5 \cdot 10^{-3}$
	$L_{1,i}$	$8.1 \cdot 10^{-2}$	$1.0 \cdot 10^{-1}$	$1.4 \cdot 10^{-1}$	$2.0 \cdot 10^{-1}$
	$L_{2,i}$	$1.1 \cdot 10^{-2}$	$2.1 \cdot 10^{-2}$	$4.2 \cdot 10^{-2}$	$7.5 \cdot 10^{-2}$
	E_r	1.4	1.9	3.5	9.9
	$T_{60}(L_{1,r})$	1.0	1.5	2.1	2.6
	$T_{60}(L_{2,r})$	1.0	1.7	2.2	2.6
Serial configuration	E_i	$5.3 \cdot 10^{-4}$	$7.2 \cdot 10^{-4}$	$1.3 \cdot 10^{-3}$	$3.6 \cdot 10^{-3}$
	$L_{1,i}$	$8.1 \cdot 10^{-2}$	$1.8 \cdot 10^{-1}$	$3.1 \cdot 10^{-1}$	$4.1 \cdot 10^{-1}$
	$L_{2,i}$	$1.1 \cdot 10^{-2}$	$8.7 \cdot 10^{-2}$	$1.8 \cdot 10^{-1}$	$2.6 \cdot 10^{-1}$
	E_r	1.4	4.2	13	47
	$T_{60}(L_{1,r})$	1.0	3.3	4.0	4.3
	$T_{60}(L_{2,r})$	1.0	3.4	3.8	4.0

Table 5.5.10: *Signal properties for the model hall with the multi-channel reverberation processor at several levels, both for the parallel and for the serial configuration of the early reflection processor and the reverberation processor.*

5.6 Comparison with measurements

In this section, the simulations of the previous sections will be compared with measurements in the Auditorium of Delft University of Technology. In figure 5.6.1 a sketch of the layout of this hall is shown. The shape is approximately square, with sides of 25 meters each. The maximum height is about 12 meters. The seated parts have a rather steep decline and occupy a large part of the total hall boundary. As a consequence, the reverberation time of the hall is not too large (1.2 second in the mid-frequency range), making it suitable for speech transmission.
The auditorium is equipped with a system for early reflection generation and reverberation enhancement (Acoustic Control Systems, ACS). When not in use for public performances, this hall can be used for acoustic experiments and measurements. At

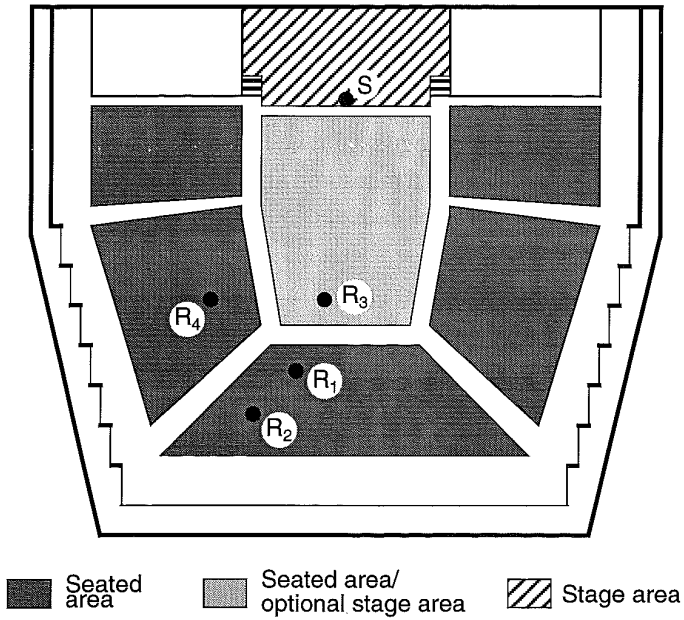

Figure 5.6.1: *Sketch of the layout of the auditorium of Delft University of Technology, used for the acoustic measurements discussed in this section. The measurement positions have been indicated.*

several positions in the hall the acoustical properties have been measured using four different settings of the ACS system. The source position S and the receiver positions R_1-R_4 used for the measurements have been indicated in figure 5.6.1.

At receiver position R_4 the reverberation time has been measured using the classical interrupted noise method (see appendix A for details). The measured reverberation curves are shown in figure 5.6.2 (500 Hz octave band) and figure 5.6.3 (1 kHz octave band) for the four different ACS settings used. Usually the ACS system settings are specified in terms of reverberation time. Table 5.6.1 lists the mid-frequency reverberation time values measured in the hall for the system settings used during the measurements.

With the ACS system switched off the auditorium is suited for speech transmission. Setting 1 (early reflection system only) makes the hall suitable for recitals and chamber music, while setting 4 is used for symphonic music. Due to its long reverberation time setting 7 is usually referred to as the "cathedral setting". This setting is used for demonstration purposes only.

In order to get measured results that can be easily compared with the simulated results of the previous sections, impulse response measurements are required. The impulse response of a hall can be measured using the sweep method discussed in appendix A. Using a sweep signal with a frequency range from 300 to 3000 Hz the impulse response of the auditorium has been measured at all four measurement positions and all four system settings. These impulse responses can be used to calculate both the

ACS setting	Reverberation time (s)
off	1.2
1	1.5
4	2.3
7	5.0

Table 5.6.1: *List of mid-frequency reverberation times of the auditorium of Delft University, for the ACS settings used during the measurements*

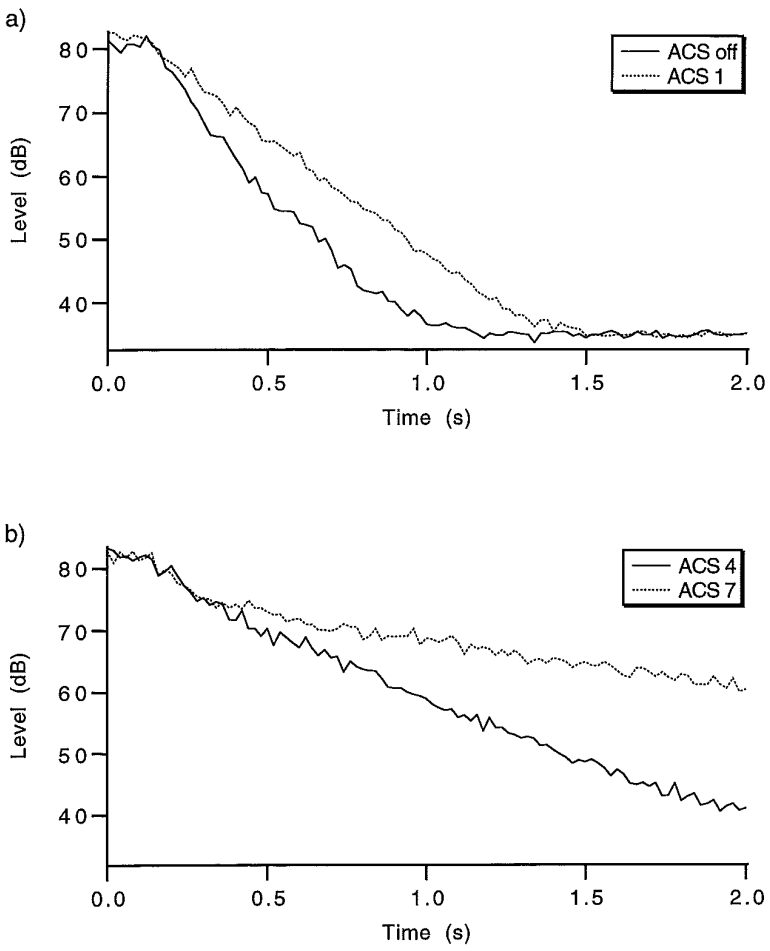

Figure 5.6.2: *Reverberation curves measured in the auditorium of Delft University using the interrupted noise method. 500 Hz octave band.*
a) ACS off and ACS setting 1
b) ACS setting 4 and ACS setting 7

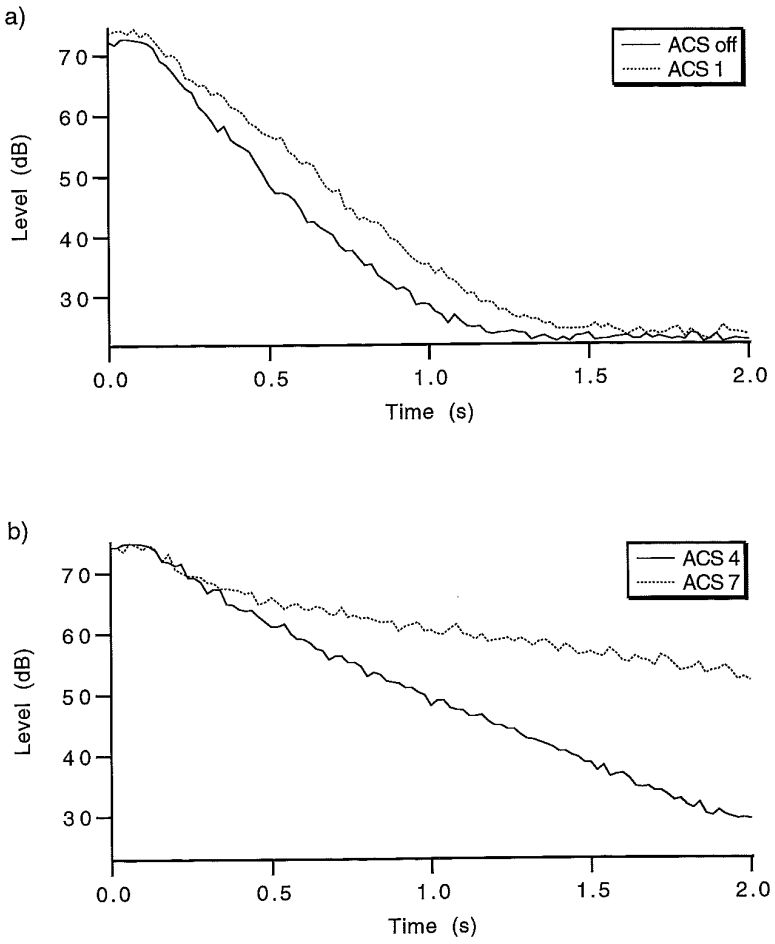

Figure 5.6.3: *Reverberation curves measured in the auditorium of Delft University using the interrupted noise method. 1 kHz octave band.*
a) ACS off and ACS setting 1
b) ACS setting 4 and ACS setting 7

reverberation curve and the signal properties discussed in the previous sections.
Figure 5.6.4 shows the reverberation curves calculated from the impulse responses measured at position R_1 for the four ACS settings used. Note that the dynamic range of the decay curves is rather low, caused by the low dynamic range in the measured impulse responses.
From figure 5.6.4 some effects can be seen that were found earlier in the simulations. The reverberation curve with ACS at setting 1 shows a less steep decay than the hall without the system. As the early reflection processor of the ACS system has a very steep decay, this increase in reverberation time must be caused by the convolution of the processor response with the source-microphone response and the loudspeaker-receiver response. As some early reflection loudspeakers are mounted near the stage, the acoustic feedback will also play some role in the lengthening of the decay time. The decay curve measured with the ACS system at setting 7 clearly shows a double decay, due to the rather low output level that is used for the system in this setting.
In order to simulate the acoustical behaviour of the auditorium, the processor decay times of the system should be known. These values are listed in table 5.6.2 as specified by the manufacturer. The ACS system is always operated in serial configuration.

ACS setting	T_{60}(ER)	T_{60}(REV)
off	-	-
1	0.20	-
4	0.25	1.9
7	0.25	4.8

Table 5.6.2: *ACS early reflection processor decay time (T_{60}(ER)) and ACS reverberation processor decay time (T_{60}(REV)) for the four ACS settings used during the measurements.*

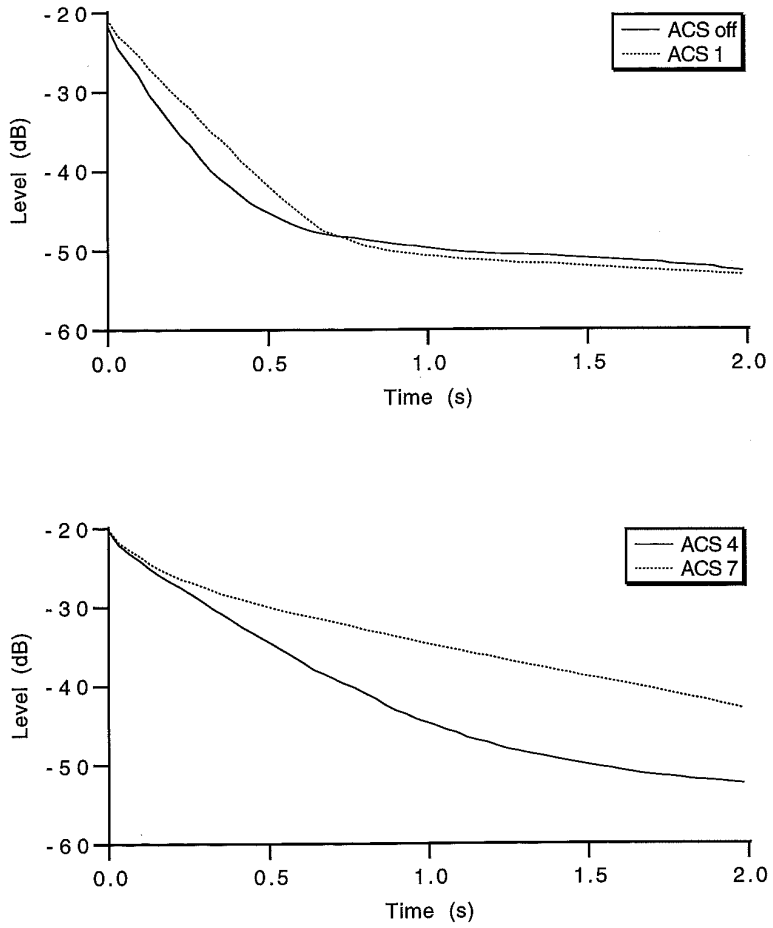

Figure 5.6.4: *Reverberation curves measured in the auditorium*
a) ACS off, ACS setting 1
b) ACS setting 4, ACS setting 7

Using the processor reverberation times specified by the manufacturer, and taking into account the adjusted levels of direct sound, early reflection processor and reverberation processor, a simulation of the Delft system has been made, using the serial multichannel model described in section 5.5.6. Since the energy properties of the simulated signals can be set to any desired value by adjusting the source level, only the reverberation times calculated from the energy independent length properties are used for the comparison between simulations and measurements. Note: both the measured and the simulated reverberation times are calculated from the length of the decay curve.

The comparison between measurements and simulations is given in table 5.6.3. The simulations yield T_{60} values that match very well with the measurements, especially when realising that the simulation model is only a rough approximation to the real world situation. The simulation model will be useful in designing the required processor responses in a specific application of an electro-acoustic system.

	Parameter	measured	simulated
ACS off	$T_{60}(L_{1,r})$	1.0	1.0
	$T_{60}(L_{2,r})$	1.1	1.0
ACS setting 1	$T_{60}(L_{1,r})$	1.4	1.2
	$T_{60}(L_{2,r})$	1.4	1.3
ACS setting 4	$T_{60}(L_{1,r})$	2.3	2.5
	$T_{60}(L_{2,r})$	2.5	2.6
ACS setting 7	$T_{60}(L_{1,r})$	4.9	5.6
	$T_{60}(L_{2,r})$	5.4	5.6

Table 5.6.3: *Measured and simulated reverberation time and signal properties for the auditorium of Delft University.*

5.7 Conclusions

In this chapter it is shown that the acoustical behaviour of a hall equipped with an electro-acoustic system for reflection generation and reverberation enhancement can be described by a convolutional model. Each signal transmission path in the hall or in the system introduces an extra convolution step in the simulation model.
The convolutional model shows that the reverberation curve of a hall equipped with an electro-acoustic system for reflection generation and reverberation enhancement shows a non-exponential decay. Due to the convolution of the processor responses with the source-microphone hall transfer and the loudspeaker-receiver hall transfer a more or less flat start of the decay curve is found, in agreement with the results of appendix F.
Due to this non-exponential decay, the reverberation time determined over a certain dB range, must be concluded to be not the most appropriate measure for the decay phenomenon, since it so strongly depends on the dB range specified. A better alternative is the first or second order length of the impulse response and the first and second order length of the decay curve. As these measures are determined over the full length of the signal, they give a more global description of the decay.
Therefore, in section 5.3 two new definitions for the reverberation time were given, based on the first or second order length of the reverberation curve respectively. For exponential decay curves these measures yield the standard reverberation time, while for non-exponential decays they are defined in a way that takes into account the whole reverberation curve. Comparison between simulations and measurements showed that, indeed, these new definitions -as well as the total computational model- are relevant.

6. CONCLUSIONS AND DISCUSSION

In this chapter the main results and conclusions of the research discussed in this thesis will be summarised. Section 6.1 discusses the wave field synthesis system and section 6.2 discusses the modelling scheme for halls equipped with an electro-acoustic system.

6.1 The wave field synthesis system

In this thesis it has been shown that the wave field synthesis technique discussed in chapter 3 and chapter 4 can be used to create wave fields with pre-specified spatial and temporal properties. Listening tests showed that even a simple system using an array of only 12 loudspeakers, with a sampling distance of about 50 cm, can generate a monopole source wave field with a well defined source localisation.
Due to spatial aliasing a position-dependent colouration of the synthesised wave field is perceived for frequencies above the aliasing frequency. By applying a smaller sampling distance, however, the aliasing frequency can be raised to any desired height. From experiments with a wave field synthesis array of 48 loudspeakers at an intermediate distance of 11 cm, the perceived colouration of the synthesised wave field appeared to be much less than with the simple system mentioned above.
The wave field synthesis systems were all built up using a digital signal processor (DSP) for the required signal processing. The processing system implements a complete matrix of weighted delay lines, connecting all microphone inputs to all

loudspeaker outputs. The fast increase in processor speed over time enables the creation of systems with an ever increasing complexity.
Experiments in the auditorium of the Delft University with a wave field synthesis prototype system for direct sound enhancement showed that a 5 dB(A) level increase of the direct sound was possible, with the source localisation maintained. As with all sound enhancement systems using microphones and loudspeakers in the same room, acoustic feedback limits the maximum amplification that can be obtained. No feedback limiting techniques have been implemented in the system yet. Hence, further increase of the maximum amplification factor can still be obtained.
In the opera house in Malmö, Sweden (Malmö Stadsteater) an extended version of the wave field synthesis prototype system (12 microphones and 96 loudspeakers) has been installed for the enhancement of the opera singers and improvement of their balance with the orchestra. The maximum level increase without noticeable feedback effects that can be obtained with this system is 6 dB(A). Together with an electro-acoustic system for early reflection generation and direct sound enhancement, the wave field system yields a spectacular improvement of the acoustical qualities of this theatre.

6.2 The modeling scheme for a hall equipped with an electro-acoustic system

In chapter 5 of this thesis a modeling scheme was discussed that simulates the response of a hall equipped with an electro-acoustic system. This model takes into account all relevant hall transfer functions: the direct transfer from the source position towards the measurement position, the transfer from the source position towards the system microphones, the transfer from the system loudspeakers to the measurement position and the feedback transfer from the system loudspeakers back to the system microphones.
It was shown that in modeling the appropriate hall transfers, diffusion should be taken into account as well. An algorithm combining the accuracy of the image source method with a ray-tracing model for the diffusion was discussed. This calculation method yields accurate results for the prediction of reverberation curves.
The modelling results were given in terms of the impulse response and the reverberation curve. To compare these responses, several measures were used: the energy, first order length and second order length of the impulse response and the reverberation

time determined from first order length and second order length of the reverberation curve.
As the decay curve of a hall with an electro-acoustic system is usually non-exponential, the standard reverberation time is not a good measure for this situation. The relation derived between the reverberation time and the first order length of the decay curve of a hall with exponential decay, however, can be used as a general definition for the reverberation time valid for a hall with non-exponential decay as well. This way a more reliable definition of the reverberation time is obtained.
The total stationary sound level in the hall is described by the energy of the impulse response. The sound level in a hall for several settings of the electro-acoustic system can be compared by comparing these energy measures.
The decay curve of a hall equipped with an electro-acoustic system can be characterised as follows:

> When the first order length of the system response is smaller than the first order length of the hall response, the system will not change the first order length of the hall response noticeably if the acoustic feedback is at a sufficiently low level. The energy of the hall increases.
>
> When both the system response and the hall response have the same first order length, the first order length of the total response will be larger than the first order length of the hall response.
>
> When the first order length of the system response is larger than the first order length of the hall response, the first order length of the total response will be largely the same as the first order length of the system response, if the acoustic feedback is at a sufficiently low level.
>
> When the level of the system response is low compared with the sound level in the hall and the system decay is less steep than the hall decay, the decay curve will show a double decay with the hall decay in the first part and the system decay in the second part.
>
> When the level of the system response is high compared with the sound level in the hall, the decay curve will show a convex part at the start.

Comparison of the results generated by the modelling scheme with measurements in a hall, equipped with an electro-acoustic system for reflection generation and reverber-

ation enhancement, showed that all effects predicted by the simulation model are also found in practice. The simulation model can predict accurate values for the reverberation time as determined from the length of the decay curve.

Appendix A. ACOUSTIC MEASUREMENT TECHNIQUES

In this appendix several common acoustic measurement techniques will be discussed. After some general considerations in section A.1, the classical method for the measurement of reverberation curves will be discussed in section A.2. In section A.3 the measurement of impulse responses is treated, including a discussion on calculating reverberation times from finite length impulse responses. Finally, in section A.4 a summary of the time delay spectrometry technique is given.

A.1 General considerations

Since the beginning of this century measurements have been performed to quantify the acoustical properties of rooms. In 1900, an article was published which described the measurement of reverberation times in several auditoriums in the United States (Sabine, 1900). Because level meters were not available at that time, Sabine measured the time during which a decaying tone burst was audible in the room.
In later years, electrical equipment offered the opportunity to perform more accurate measurements. Loudspeakers gave the possibility of generating dedicated acoustic test signals like sine waves, sweep signals and noise bursts, while microphones and level recorders replaced the human ear in determining sound pressure levels. Since then, measurement procedures could be standardised, which made comparison of dif-

ferent results much easier.
The introduction of digital electronics and calculators made new measurement techniques available. Because digital post-processing of measured data became possible, more detailed information could be extracted, while special filtering techniques gave the opportunity to eliminate the influence of the measurement equipment from the data. Nowadays, special purpose computer systems are available, designed especially for acoustic measurements.

A.2 Measurement of reverberation curves using interrupted noise

The definition of the reverberation time given in section 1.3.1 suggests that it can be quantified by recording the sound pressure level as a function of time after switching off a stationary sound source in the room under consideration. The result thus obtained is usually called a decay curve or a reverberation curve. For this type of measurement an omni-directional broad band sound source, an omni-directional microphone and a recording device are needed. Figure A.2.1 shows a schematic diagram of this type of measurement system. The band pass filter should be used for measuring the reverberation time in frequency bands (usually octaves or third octaves).
Note that when the definition of the reverberation time is applied strictly, a dynamic range of at least 60 dB is required in the measurements, which means that a rather

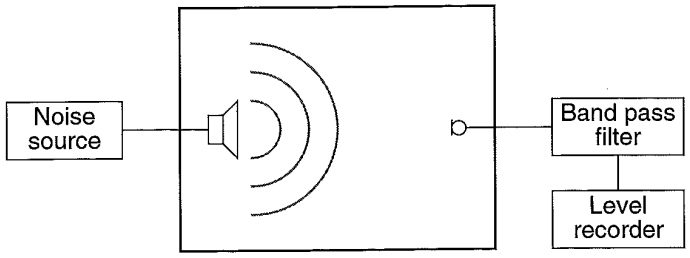

Figure A.2.1: *Setup for the measurement of reverberation curves using the interrupted noise method.*

high power sound source should be used, which produces a sound pressure level of more than 60 dB above the background noise level in the room at all frequency bands of interest. When the sound pressure decays exponentially after switching off the sound source, the sound pressure level will drop linearly with time. The registration of the decaying sound pressure level will thus be a straight line. For this situation a dynamic range of 60 dB is not required because the slope of the curve determines the reverberation time.
Theoretical investigations (see, e.g., Kuttruff, 1979 or Barron et al., 1988) have shown that the sound pressure will decay exponentially in all halls of regular shape with diffusely reflecting walls. This means that in most cases of practical importance the measured reverberation curves are expected to be straight lines. Because noise is used as a driving signal, the reverberation curve will show some random fluctuations about the theoretically predicted straight line.
The reverberation time can be determined from the slope of the line which best fits the measured curve. Usually the best fit is determined by the eyes of the experimenter, so the result can show some error (or even bias towards a desired value), especially in the low frequency bands where the random fluctuations in the measured curves are large, due to the necessary narrow pass band (and thus broad time response) of the filters used. Because most level recorders can record only one frequency band at a time, the measurement sequence must be repeated for each frequency band of interest. To avoid bias and random errors, averaging over at least 3 decay curves should take place.
Since the introduction of fast digital electronics it is possible to build digital frequency analysers that operate in real time, which means that the spectrum of the input signal is available immediately at their output. The principle of this type of analyser is shown in figure A.2.2: after passing through an anti-aliasing filter, the signal is sampled at a rate determined by the maximum frequency of interest and then transferred to a digital filter bank. These filters are implemented in the time domain so that each new sample can be used to update the filter outputs. In this way real time behaviour is obtained. Note that (after an initial start up period) new data samples are used at once in the frequency analysis, in contrast to FFT-techniques in which the frequency analysis is carried out off-line over contiguous data blocks.
A digital real time frequency analyser can be used to measure reverberation times by picking the output of the filter bank at regular time intervals of, say, 20 ms. In this way a data matrix is obtained with the rows showing a complete frequency spectrum at one instant of time and the columns showing the sound pressure level in a particular fre-

quency band as a function of time. Thus the columns of the data matrix are in fact sampled reverberation curves, the sample interval given by the time between consecutive spectra.

The advantages of this method are the simultaneous measurement of all frequency bands and the ability to average several reverberation curves before extracting reverberation times. Because of the digital data representation inside the analyser, it is possible to use a computer algorithm for post-processing the data (e.g. smoothing 'noisy' reverberation curves) and for calculating the reverberation times.

A disadvantage of automatic reverberation time calculation is the usually very simple

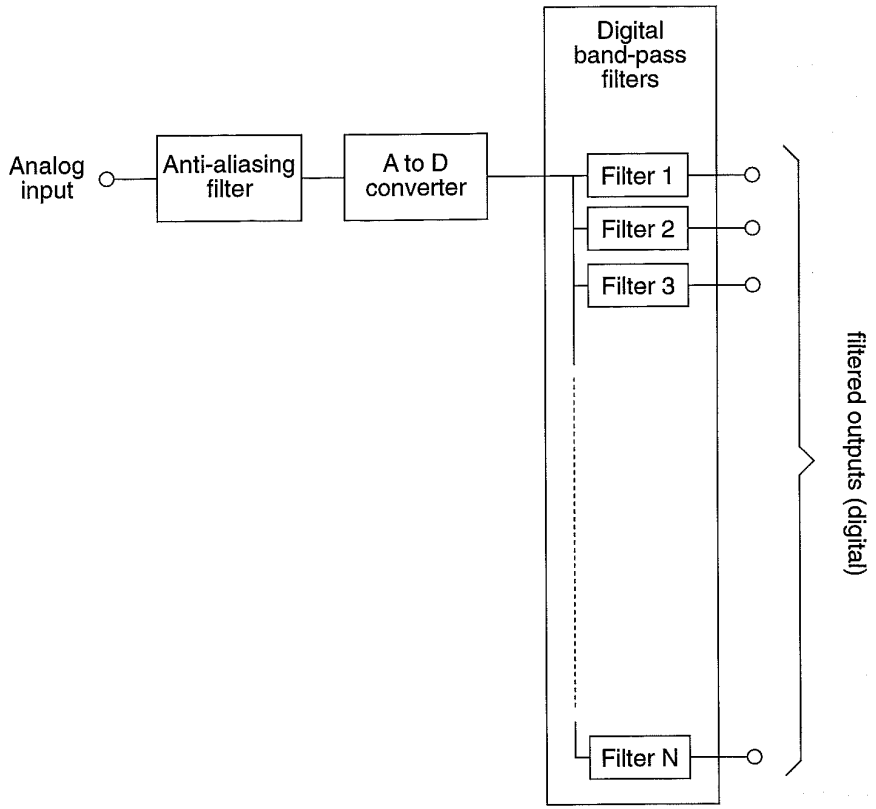

Figure A.2.2: *Schematic diagram of a digital real time frequency analyser.*

algorithm used, ignoring all deviations from linear behaviour of the reverberation curve. Thus it remains necessary to inspect the reverberation curves by eye and to use a more sophisticated reverberation time extracting technique in case of strong non-linearities in the reverberation curves.

A few notes about the reliability of the data obtained in using the interrupted noise method should be made. First consider the band pass filter used in the measurement setup. The octave or third octave filters used in impulse response measurements usually have a steep slope at the beginning, and a less steep slope at the end of their time response (see figure A.2.3). When an interrupted noise signal is input to this type of filter, the response measured at the output will show a decay with a rate determined by the end part of the filter response. Thus, a decay curve measured in an anechoic chamber using this filter will show the decay of the filter, instead of the step-shaped decay of the room.

A sufficient condition to eliminate this disturbing effect of the filter, usually referred to as filter ringing, is given by

$$BT_{60} > 16\ , \qquad \text{(A.2.1)}$$

in which B is the -3 dB bandwidth of the band pass filter and T_{60} is the reverberation

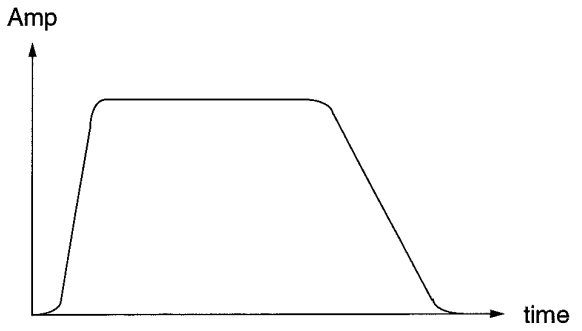

Figure A.2.3: *Amplitude (schematic) of the time domain response of a typical relative band filter (e.g., octave or third octave filter), as used in acoustic measurements. Note the steep slope at the start and the less steep slope at the end of the response.*

time to be measured (Jacobson, 1987).
Because of the steeper slope at the start of the filter response in the time domain, it might be advantageous to record the broad band interrupted noise signal first and then feed it into the band pass filter played backward. For a typical filter used in decay measurements, condition (A.2.1) can then be relaxed to

$$BT_{60} > 4 \,, \tag{A.2.2}$$

so that reverberation times about 4 times shorter can still be measured for a given filter bandwidth (Jacobsen and Rindel, 1987).
Another point of interest is the response of the detector. To eliminate the random behaviour of the driving noise as much as possible, the detector should perform some averaging on the input signal. When the averaging time of the detector is too large however, it will change the slope of the measured decay curve. It can be shown (Jacobsen, 1987) that for forward analysis and exponential averaging the averaging time T_{av} should obey the inequality

$$T_{av} < \frac{T_{60}}{14} \,, \tag{A.2.3}$$

while for reversed measurements (Jacobsen and Rindel, 1987) the condition

$$T_{av} < \frac{8T_{60}}{14} \tag{A.2.4}$$

should be obeyed.
Once the bandwidth and the averaging time have been determined, the minimum number of averages N_{av} necessary for reliable results is given by

$$N_{av} = \frac{1}{BT_{av}} \,, \tag{A.2.5}$$

(Rindel et al., 1989). When all these conditions are met, the measured reverberation curve will show the correct slope, but it might still be rather noisy. Averaging some more measurements can further reduce these random fluctuations.
As an example the reverberation curves of a hall for several octave bands, measured by a real time frequency analyser using the interrupted noise method, are shown in figure A.2.4. The results shown are obtained by averaging five decaying noise bursts.

Note: traditionally, the reverberation time is determined over a pre-specified dynamic range of the decay curve. Thus, only part of the decay curve is used for the decay time measurement. In chapter 5 of this thesis a better definition of the reverberation time is given, that takes into account the complete decay curve.

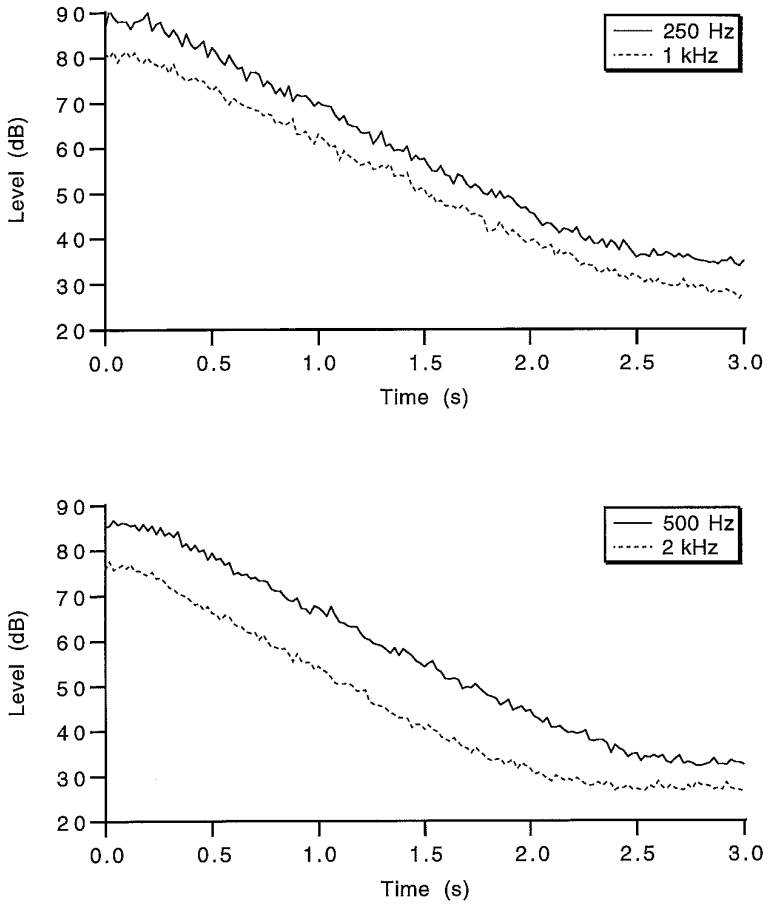

Figure A.2.4: *Reverberation curves measured in a hall with a real time frequency analyser using the interrupted noise method, for four different octave bands (centre frequency 250 Hz, 500 Hz, 1 kHz and 2 kHz).*

A.3 Measurement of impulse responses

A problem in measuring impulse responses is to find a good, reproducible impulsive sound source that radiates enough energy into the hall. All known impulsive sound sources, like exploding balloons and alarm pistols, show a large spread in energy, directivity and frequency contents from one shot to another, so these sources are not very useful in obtaining accurate measurements.
Much better results can be obtained using the method described by Berkhout et al. (1980), which is shown schematically in figure A.3.1: an omnidirectional sound source generates a sweep signal w(t) in the room under consideration. The sound field y(t) recorded by the microphone is given by the impulse response h(t) of the room convolved with the source signal:

$$y(t) = h(t) * w(t) \tag{A.3.1}$$

or, in the frequency domain:

$$Y(\omega) = H(\omega)\, W(\omega) \tag{A.3.2}$$

The frequency responses of the microphone M(ω), the loudspeaker L(ω) and the registration system R(ω) can be included in the analysis by introducing a new source

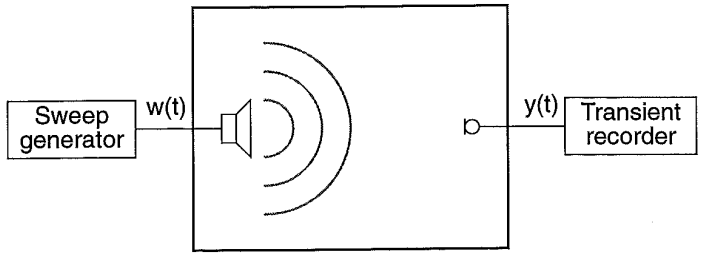

Figure A.3.1: *Measurement setup for the registration of a sweep response. The recorded sweep response can be transformed into a band limited impulse response by applying deconvolution filter (A.3.5).*

signal W'(ω) defined by:

$$W'(\omega) = W(\omega)\, L(\omega)\, M(\omega)\, R(\omega) \tag{A.3.3}$$

Finally, the recorded signal becomes :

$$Y'(\omega) = H(\omega)\, W'(\omega) \ . \tag{A.3.4}$$

When the measurement system is placed in a (perfect) anechoic chamber, which has an impulse response consisting of one single delta pulse or, in the frequency domain, a white transmission spectrum, the output signal equals W'(ω), so the properties of the complete measurement system can be determined by one single measurement.
From this measurement of W'(ω) a deconvolution filter F(ω) can be calculated as follows:

$$F(\omega) = \frac{W'^{*}(\omega)}{|W'(\omega)|^2 + a^2} \ , \tag{A.3.5}$$

in which the asterisk denotes complex conjugation and a^2 is a (real) constant, determined by the signal to noise ratio of the measurements.
Application of deconvolution filter (A.3.5) to the measured signal Y'(ω) yields:

$$X(\omega) = H(\omega) \frac{|W'(\omega)|^2}{|W'(\omega)|^2 + a^2} \ . \tag{A.3.6}$$

From equation (A.3.6) it is clear that X(ω) equals the Fourier transform of the impulse response H(ω) in those frequency regions where the magnitude of W'(ω) is large compared to a, while X(ω) approaches zero in those regions where the signal W'(ω) contains little energy. Thus when the energy in the source signal is large (large signal to noise ratio) the deconvolution filter equals the inverse filter of the wavelet used, and when the energy in the source signal is small (poor signal to noise ratio) the deconvolution filter is forced to zero to prevent noise blow-up.
The signal X(ω) can be viewed as a band limited impulse response, the limitations in frequency being determined by the frequency contents of the source signal W(ω). The impulse responses obtained with this method have a high signal to noise ratio and the reproducibility is very good. In figure A.3.2 the deconvolution procedure is shown in the form of some graphs, starting from the sweep signal in an anechoic chamber up to the impulse response obtained by deconvolving the sweep response measured in a hall.

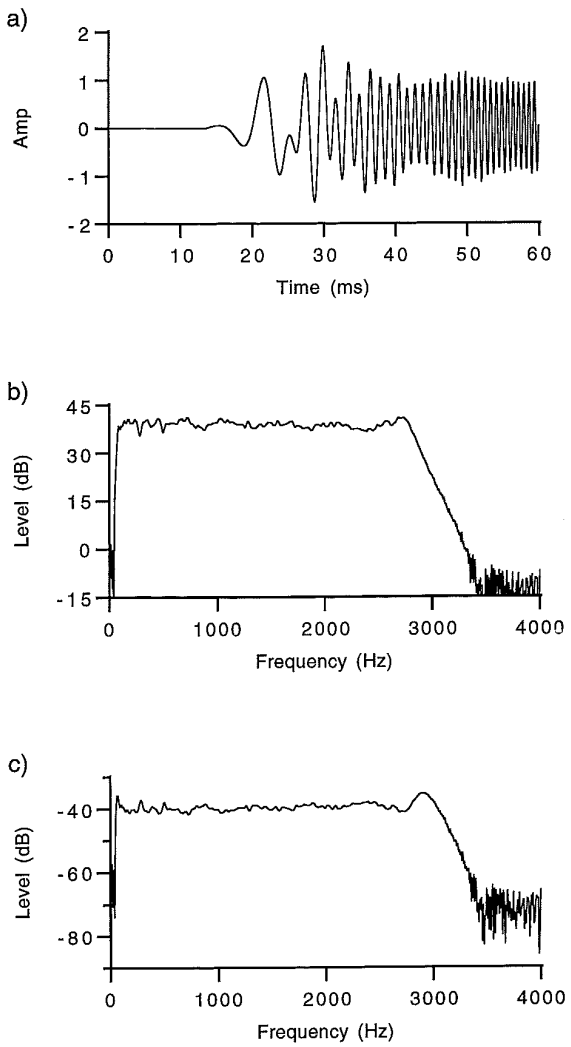

Figure A.3.2: *Illustration of the deconvolution procedure for sweep responses.*

a) Sweep signal, measured in an anechoic chamber

b) Spectrum of measured sweep signal

c) Spectrum of deconvolution filter

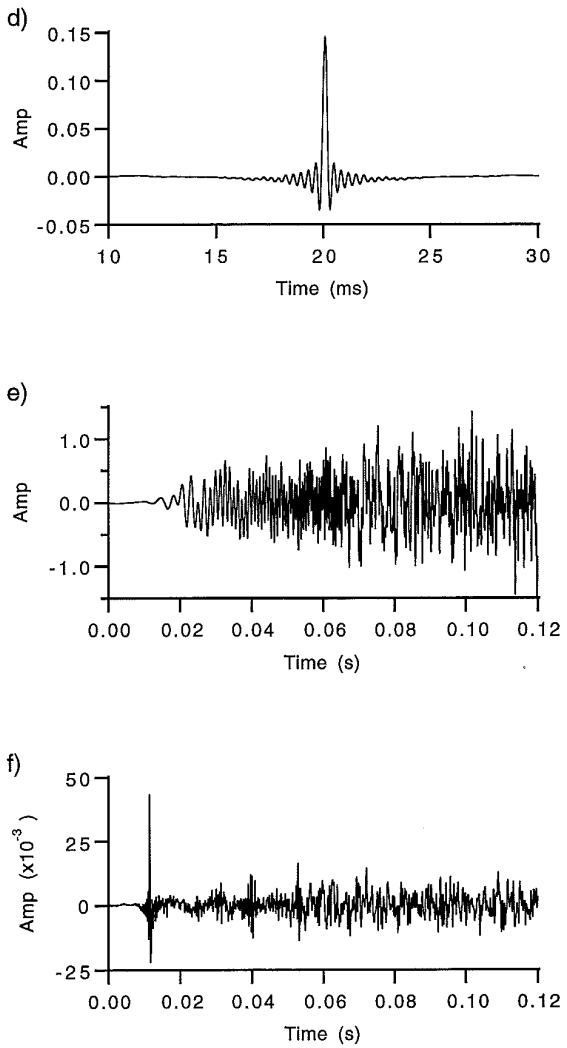

Figure A.3.2: *Continued*

d) Filtered reference sweep (band limited impulse)

e) Measured sweep response

f) Deconvolved sweep response (band limited impulse response)

Once the impulse response is available all quantities discussed in section 1.3 can be calculated from it. For tracking the reverberation curve and calculating parameters like the clarity index, the impulse response should be integrated over an interval reaching to infinity. In practice only a finite recording of the impulse response will be available, so an error will be introduced in the calculated parameters.
To quantify the errors in the calculated results, a description of the sound field in a room in terms of sound rays is a helpful tool. For simplicity, the spherical wave pattern sent out by the source is divided into cones, each represented by a single ray. These rays reflect specularly against the room boundaries, loosing a fraction $\bar{\alpha}$ of their energy at each reflection. The solid angle element cut out by the cone remains constant during the calculation, thus its width increases for increasing time.
At time t, a sound ray leaving the source at time t=0 has travelled a distance of ct meters, c being the velocity of sound. On the average this ray has been reflected ct/ℓ times by one of the walls forming the room boundary, a result valid only for times $t \gg \ell/c$. The constant ℓ used in this expression is the mean free path (the average distance travelled by the sound ray between two consecutive reflections) for this particular room. At each reflection the ray loses a fraction $\bar{\alpha}$ of its energy, while spatial divergence will give an energy attenuation of $1/c^2t^2$. The number of rays hitting the receiver between time t and t+dt is proportional to t^2, so statistically the squared impulse response can be described by:

$$h^2(t) = A(1-\bar{\alpha})^{ct/\ell}, \tag{A.3.7}$$

in which A is a constant determined by the source strength and $\bar{\alpha}$ is the average energy absorption at each reflection against a room boundary. Thus the energy in the impulse response decays exponentially with time.
Calculating the reverberation curve by integrating the impulse response (A.3.7), from time t to infinity yields

$$r^2(t) \equiv \int_t^\infty h^2(\tau)\,d\tau = \frac{-\ell A}{c \ln(1-\bar{\alpha})}(1-\bar{\alpha})^{ct/\ell} \equiv AC(1-\bar{\alpha})^{ct/\ell}, \tag{A.3.8}$$

in which the constant C, defined by

$$C \equiv \frac{-\ell}{c \ln(1-\bar{\alpha})}, \tag{A.3.9}$$

is introduced for notational simplicity.
The approximation $q^2(t)$ of the signal $r^2(t)$ obtained when only a finite length recording of h(t) from t=0 up to some time t=T is available, is given by

$$q^2(t) = \int_t^T h^2(\tau)\,d\tau. \tag{A.3.10}$$

This integral can be rewritten as:

$$\int_t^T h^2(\tau)\,d\tau = \int_t^\infty h^2(\tau)\,d\tau - \int_T^\infty h^2(\tau)\,d\tau, \tag{A.3.11}$$

which can be evaluated using equation (A.3.8):

$$\int_t^T h^2(\tau)\,d\tau = AC\left[(1-\bar{\alpha})^{ct/\ell} - (1-\bar{\alpha})^{cT/\ell}\right]. \tag{A.3.12}$$

Thus the error term ε caused by the finite time integration is found to be

$$\varepsilon \equiv r^2(t) - q^2(t) = AC(1-\bar{\alpha})^{cT/\ell}. \tag{A.3.13}$$

The relative error ε_r at time t is

$$\varepsilon_r(t) \equiv \frac{\varepsilon}{r^2(t)} = (1-\bar{\alpha})^{c(T-t)/\ell} = e^{(t-T)/C}. \tag{A.3.14}$$

From equation (A.3.14) a few important conclusions can be drawn. First note that the relative error approaches zero for infinite recording time T, as expected. Also note that the relative error increases exponentially for increasing time t and constant recording time T, while it decreases exponentially for constant time t and increasing recording time T. For time t equal to T integral (A.3.10) equals zero, so the error term ε is equal to $r^2(t)$, giving a relative error of 100 %, in agreement with equation (A.3.14).
In figure A.3.3 the reverberation curve of a hall, calculated from a measured impulse response is shown, for the 500 Hz and 1 kHz octave bands. Both graphs show a reverberation curve calculated from a measured impulse response of 1 second duration and from a measured impulse response of 3 seconds duration. Note the increasing error in the level of the reverberation curves for increasing time.

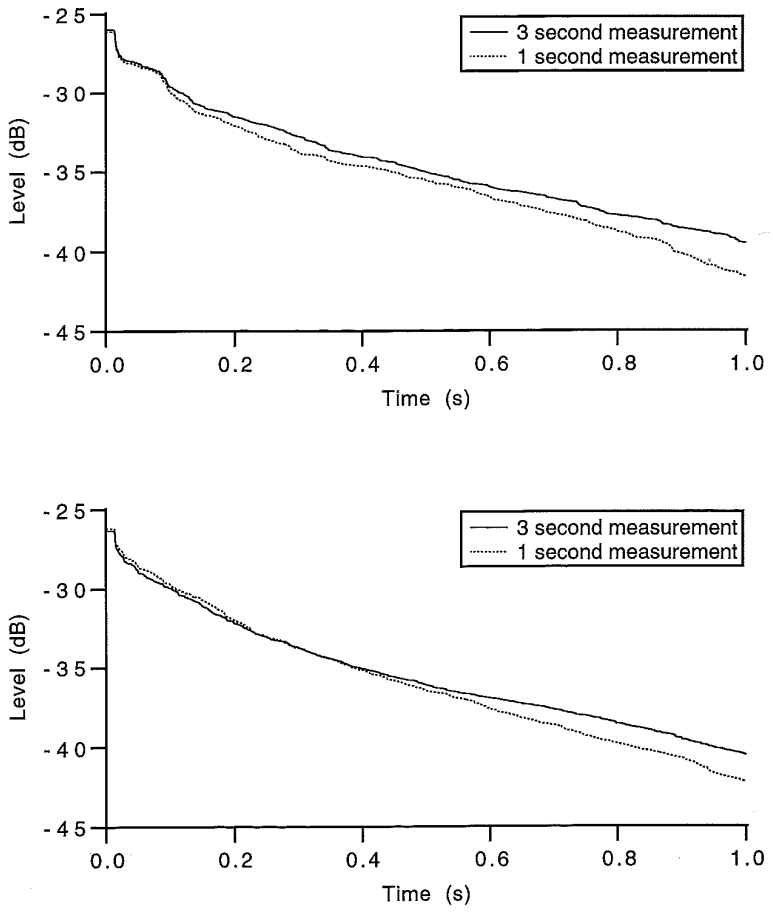

Figure A.3.3: *Reverberation curves calculated from a measured impulse response, for a measurement time of 1 second and a measurement time of 3 seconds.*
a) 500 Hz octave band
b) 1 kHz octave band

The practical use of equation (A.3.14) is best illustrated by a few simple examples.

Example 1:

The clarity index is defined as the ratio of the energy in the first 80 ms of the impulse response and the energy in the impulse response from 80 ms to infinity:

$$C_{80} = 10\log\left(\frac{\int_{0}^{80ms} h^2(t)\,dt}{\int_{80ms}^{\infty} h^2(t)\,dt}\right). \qquad \text{(A.3.15)}$$

For a clarity index measurement to be valid, the error in the denominator of equation (A.3.15) should not be too large. Substituting t = 80 ms and the maximum allowed relative error ε_r (e.g. 1%) in equation (A.3.14) yields an equation in which the recording time T is the only unknown. Thus from this equation the minimum recording time T required can be solved.
As a numerical example consider a rectangular room of dimensions 30 x 30 x 10 meter. Its volume V equals 9000 m^3, while the total wall surface amounts to 3000 m^2. The mean free path ℓ within an enclosure equals 4V/S (Kosten, 1960), so for this particular situation ℓ equals 12 meters. Using an average absorption coefficient of 0.15, the constant C is found to be 0.22. Specifying a maximum allowed error of 1%, the necessary recording time T is found to be 1.1 second.

Example 2:

For the commonly used reverberation time measurement method the situation is more complicated because the reverberation curve is the running integral from time t to infinity of the squared impulse response. This means that the relative error as described by equation (A.3.14) is different for each time instant. Equation (A.3.14) shows that the inaccuracy increases exponentially with increasing time.
When the reverberation time is calculated over a given time interval $t_1<t<t_2$, (the more usual situation of calculating the reverberation time over a dB range is discussed in the next example), the error in the reverberation curve

should remain small over the complete time interval. The error is largest at time $t = t_2$, so it is best to specify a maximum tolerated error for this instant of time. The necessary recording time T can then be found the same way as discussed in example 1.
Using the same numerical parameters as in the previous example and a maximum error of 1% specified at time t_2 equal to 1.5 second, the required recording time T is found to be 2.5 seconds.Thus for accurate reverberation time calculations the required recording time is much longer than for parameters like the clarity index.

Example 3:

Traditionally the reverberation time is calculated over a dB range instead of over a time interval. Using equation (A.3.8) the sound pressure level as a function of time is given by

$$L_p(t) = 10\log\left(\frac{r^2(t)}{r_0^2}\right) = 10\log(AC) + 10\log(1-\bar{\alpha})\frac{ct}{\ell}, \qquad (A.3.16)$$

in which the reference energy r_0^2 is taken to be 1. Note the linear decay of the sound pressure level with time.
From equation (A.3.16) it follows that

$$L_p(0) = 10\log(AC) . \qquad (A.3.17)$$

At time t_0 the level has dropped to $\Delta L_p(t_0)$ dB below the start level. From equation (A.3.16) $\Delta L_p(t_0)$ is found to be

$$\Delta L_p(t_0) \equiv L_p(t_0) - L_p(0) = 10\log(1-\bar{\alpha})\frac{ct}{\ell} . \qquad (A.3.18)$$

This equation can be used to express t_0 in terms of the level $\Delta L_p(t_0)$:

$$t_0 = \frac{\ell \Delta L_p(t_0)}{10c\log(1-\bar{\alpha})} . \qquad (A.3.19)$$

Equations (A.3.19) can be used to calculate the times corresponding to the levels specified as the bounds of the calculation area. Once these times are known, the procedure of example 2 can be followed to obtain the required

recording time.
Using again the same numerical parameters as in the previous examples, the time T_{30} at which the sound pressure level has dropped to 30 dB below the stationary level is found to be 1.5 seconds. From example 2 it can be seen that in this case the required recording time is 2.5 seconds.

A.4 Time delay spectrometry

Another interesting method for measuring impulse responses is called time delay spectrometry (TDS), which is characterised by the fact that a frequency measurement yields information about the time response of a linear system (see figure A.4.1). It can be seen from this figure that the source signal used is a (usually long) linear sweep. By multiplying the response of the system on this sweep signal with the sweep signal itself, an output signal is obtained with a spectrum (frequency domain) that has the same shape as the impulse response (time domain) of the system, as will be shown in this section. Here only a brief discussion of this technique will be given, fully explaining

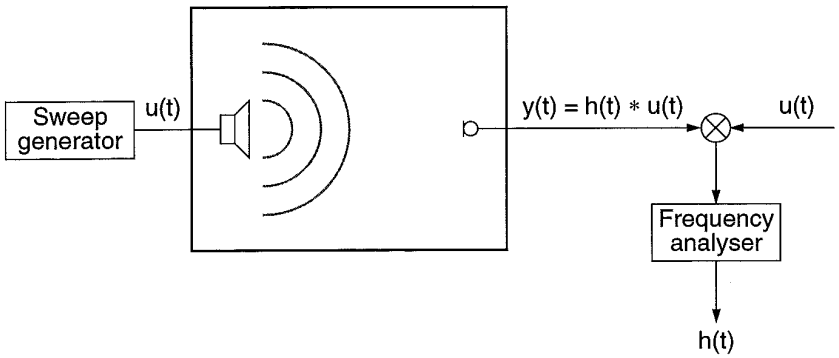

Figure A.4.1: *Setup for the measurement of a room impulse response using time delay spectrometry. Note that the measured impulse response h(t) is the output of a frequency analyser.*

the fundamental principles; a more thorough approach is found in Biering et al. (1983). The source signal used with time delay spectrometry is a linear sweep u(t) defined by

$$u(t) = \cos(\pi S t^2 + 2\pi f_a t + \theta_a) \ , \ 0 \le t \le T_s \ , \tag{A.4.1}$$

S, f_a and θ_a being constants. The meaning of these constants can best be explained by looking at the instantaneous frequency $f_i(t)$ defined by

$$f_i(t) = \frac{1}{2\pi}\frac{d\theta_i(t)}{dt} \ , \tag{A.4.2}$$

in which $\theta_i(t)$ is the instantaneous argument of the cosine function. For the linear sweep u(t) the instantaneous frequency becomes:

$$f_i(t) = St + f_a \ , \tag{A.4.3}$$

from which f_a can be seen to be the start frequency, while S is the sweep rate, the change in frequency per unit time. From equation (A.4.1) the constant θ_a is seen to be the initial phase of the sweep signal. The term linear sweep is based on the fact that the instantaneous frequency is linear in time.
Given the impulse response of a linear time invariant system h(t):

$$h(t) = \sum_{i=0}^{\infty} a_i \delta(t - \tau_i) \ , \tag{A.4.4}$$

the response on the linear sweep u(t) is found by convolving the sweep signal with the impulse response h(t). This yields the signal y(t) given by

$$y(t) \equiv h(t) * u(t) = \sum_{i=0}^{\infty} a_i u(t - \tau_i) \ . \tag{A.4.5}$$

Multiplying the sweep response y(t) by the source signal u(t) leads to a weighted summation of cosine products. Using equation (1.3.23) and the transformation of a cosine

product into a sum of cosines, it is found that

$$u(t)\,u(t-\tau_i) = \frac{1}{2}\cos(2\pi S t^2 + (4\pi f_a - 2\pi S\tau_i)t + \phi_i + 2\theta_a) + \frac{1}{2}\cos(2\pi S t\tau_i - \phi_i) \ , \tag{A.4.6}$$

the constant ϕ_i being defined by

$$\phi_i = 2\pi f_a \tau_i - \pi S \tau_i^2 \ . \tag{A.4.7}$$

The first cosine term in equation (A.4.6) describes a complicated interference pattern between the two sweep signals, which is not desired in the measurement results. Usually the measurement setup can be chosen such that this term is small. If it is not, it can be eliminated by adding two measurements with an initial phase θ_a differing by $\pi/2$. Adding $\pi/2$ to the initial phase will change the sign of the first cosine term, while it does not influence the second term at all. Thus, the interference term can be omitted from the calculations.
Hence, the result of multiplying the sweep response by the source signal leads to the signal z(t) given by

$$z(t) = \frac{1}{2}\sum_{i=0}^{\infty} a_i \cos(2\pi S t\tau_i - \phi_i) \ , \tag{A.4.8}$$

which can be rewritten as

$$z(t) = \frac{1}{4}\sum_{i=0}^{\infty} a_i \left(e^{j(2\pi S t\tau_i - \phi_i)} + e^{-j(2\pi S t\tau_i - \phi_i)}\right) \ . \tag{A.4.9}$$

Transformation of equation (A.4.9) to the frequency domain is simple, the Fourier transform Z(ω) being given by

$$Z(\omega) = \frac{1}{4}\sum_{i=0}^{\infty} a_i \left(e^{-j\phi_i}\delta(\omega - 2\pi S\tau_i) + e^{j\phi_i}\delta(\omega + 2\pi S\tau_i)\right) \ . \tag{A.4.10}$$

Equation (A.4.10) shows that the amplitude of the spectrum Z(ω) has the same shape as the impulse response h(t). Note that the spectrum Z(ω) is two-sided, showing the

same value at both $+\omega$ and $-\omega$, while the time response is not. Either half of the spectrum can be used to obtain the required impulse response.
To change the frequency axis into a time axis a simple transformation can be used. The relation between time and frequency is given by

$$t = \pm\frac{\omega}{2\pi S} . \qquad \text{(A.4.11)}$$

It is this relation between time t and frequency ω from which the term time delay spectrometry is derived. It can be shown (Biering et al., 1983) that the TDS technique yields optimal signal to noise ratio in comparison with other measurement methods.

Appendix B. WAVE FIELD SYNTHESIS SYSTEM, LABORATORY SETUP

In this appendix, the laboratory setup of the wave field synthesis system discussed in chapter 4 is described in detail. In section B.1 an overview of the digital hardware is given, in section B.2 the analog part of the setup is discussed.

B.1 Digital hardware

The central part of the wave field synthesis laboratory setup system was formed by a Texas Instruments TMS320C25 digital signal processor (DSP). This 40 MHz processor was mounted on a PC plug-in board (Loughborough Sound Images TMS320C25 PC short board), that was installed in an IBM PC-AT computer. DSP programs, written in assembly language, could be assembled on the PC and downloaded in DSP memory. Software routines were available for monitoring and controlling the DSP from the PC terminal screen.
The analog to digital converters (Loughborough Sound Images 12 bit, 32 channel AD converter card, type AD32) and digital to analog converters (Loughborough Sound Images 12 bit, 16 channel DA converter card, type DA16) used for the input and output of audio signals, were placed in a separate cabinet, together with the microphone pre-amplifiers and the loudspeaker power amplifiers. Communication between the DSP and the AD and DA boards was over the DSPLink interface bus, a digital commu-

nication system for DSP processing systems and peripheral boards. A separate power supply was used for the AD and DA boards, to prevent digital noise pick-up on the audio signals via the power supply. In figure B.1.1 a sketch of the digital hardware is given.

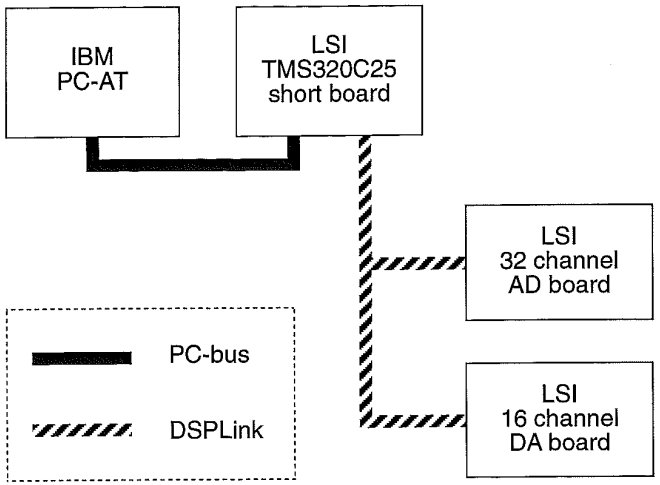

Figure B.1.1: *Schematic diagram of the digital hardware of the wave field synthesis system, laboratory setup.*

B.2 Analog hardware

The analog part of the laboratory setup hardware consisted of a set of microphone pre-amplifiers, a set of anti-aliasing filters and a set of loudspeaker power amplifiers. The input of the anti aliasing filter could be driven either direct (line-level) or via the microphone pre-amps. The output signals of the DA converters were driving the loud-

speaker power amplifiers directly, the output volume being controlled by varying the DA converter reference voltage. In figure B.2.1 a sketch of the analog hardware section is given.

The microphones used in the laboratory setup were AKG type D190E dynamic microphones with a cardioid directivity pattern. In figure B.2.2 the frequency response of this type of microphone is given, in figure B.2.3 the directivity pattern at several frequency bands is shown.

The loudspeakers used were MC1 two-way bass-reflex loudspeakers, with dimensions 20x25x40 cm. The frequency response of this type of loudspeaker is shown in figure B.2.4, in figure B.2.5 the directivity pattern is shown for several frequency bands.

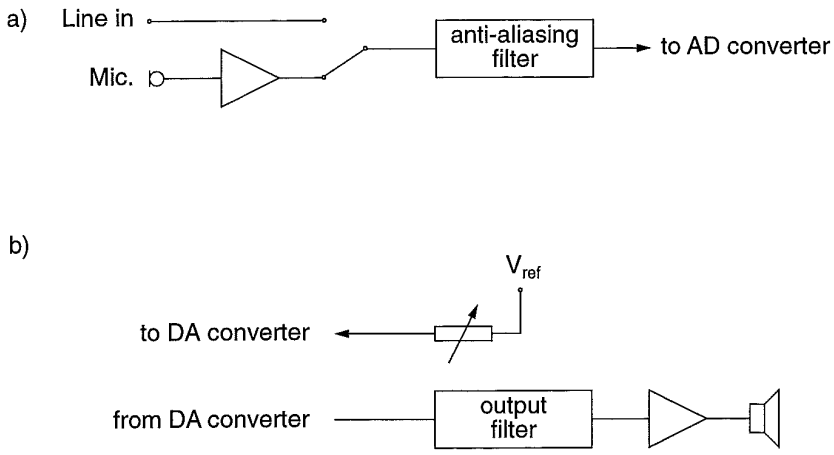

Figure B.2.1: *Schematic diagram of the analog hardware of the wave field synthesis system, laboratory setup.*
a) Input section
b) Output section

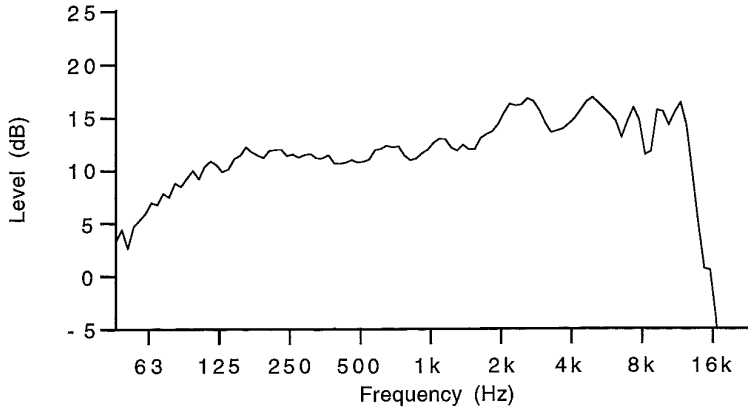

Figure B.2.2:*Frequency response of the AKG D190E microphones used in the laboratory setup wave field synthesis system.*

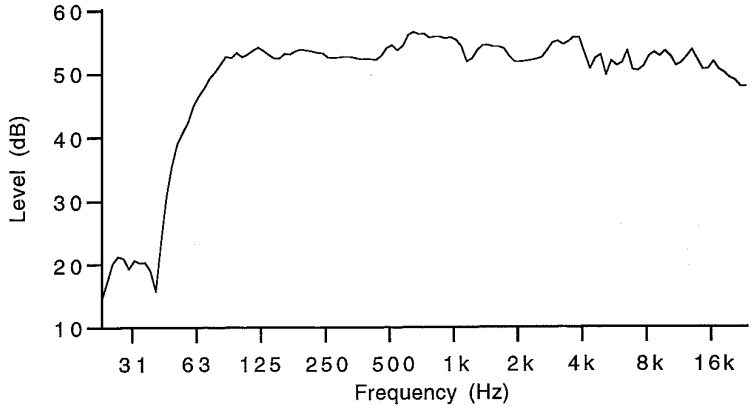

Figure B.2.4:*Frequency response of the MC1 loudspeakers used in the laboratory setup wave field synthesis system.*

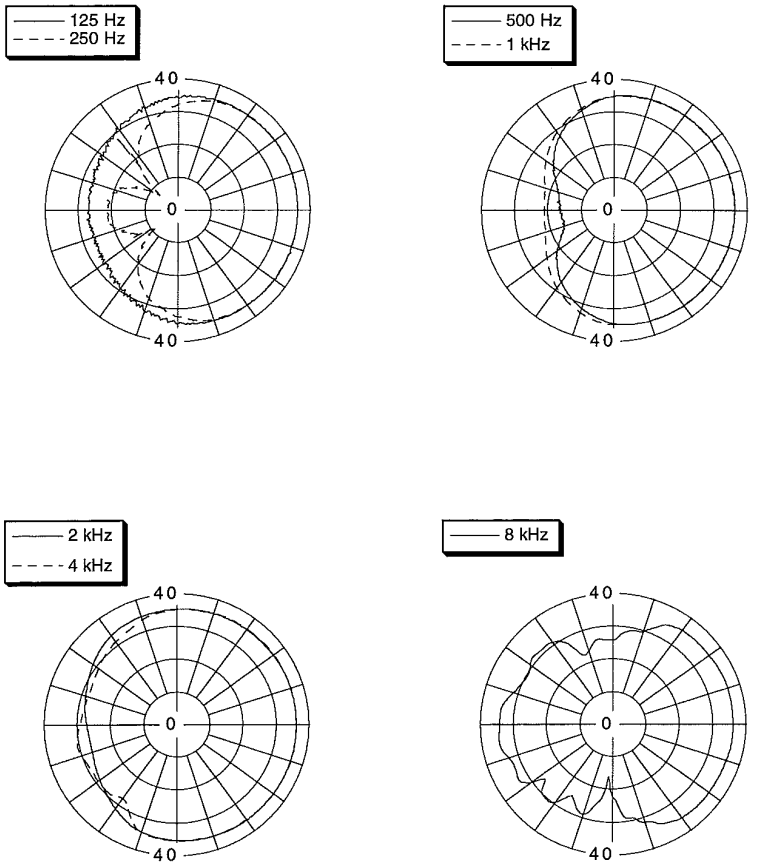

Figure B.2.3:*Directivity pattern of AKG D190E microphone at several frequency bands.*

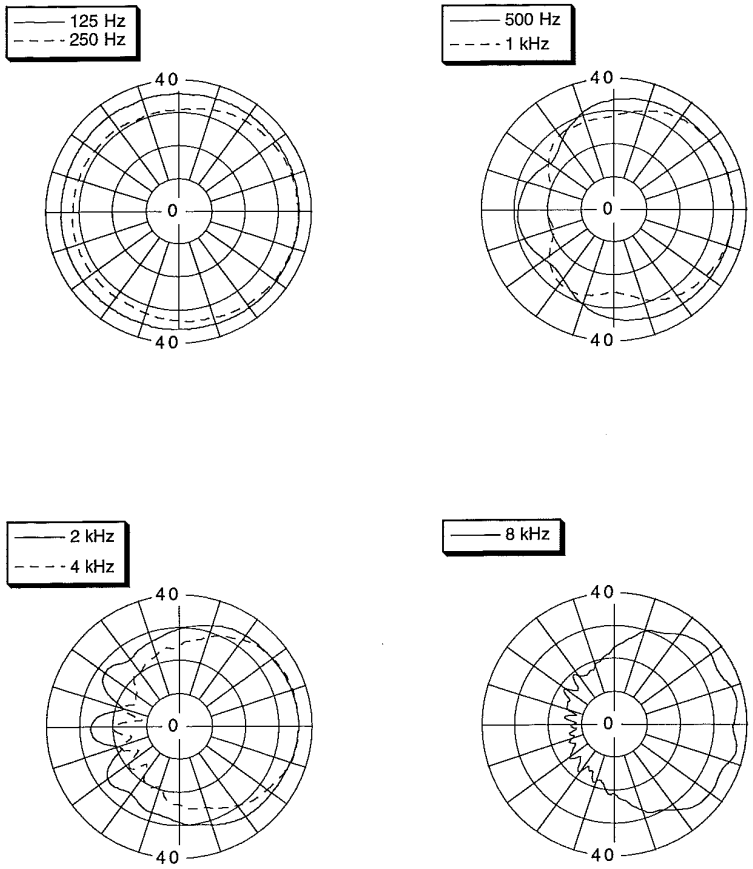

Figure B.2.5:*Directivity pattern of the MC1 loudspeaker at several frequency bands.*

Appendix C. WAVE FIELD SYNTHESIS SYSTEM, PROTOTYPE

In this appendix, the prototype of the wave field synthesis system discussed in chapter 4 is described in detail. In section C.1 an overview of the digital hardware is given, in section B.2 the analog part of the setup is discussed.

C.1 Digital hardware

As the prototype system for wave field synthesis had to drive much more loudspeakers than the simple laboratory setup discussed in appendix B, a more complicated digital hardware was needed. It was decided to use three coupled digital signal processor boards (Loughborough Sound Images M96002PC), each equipped with a Motorola DSP96002 floating point processor. The DSP boards were plugged into a PC486 computer.

The programs for the DSP boards were written in assembly language, assembled on the PC and down loaded in DSP memory over the OnCE port of the DSP96002 chip. Software routines were available for downloading code, monitoring, debugging and controlling the DSP boards from the PC.

Each DSP board was equipped with two 16-bit analog to digital converters and two 16-bit digital to analog converters. The AD converters of the DSP boards were used as inputs, the DA converters were used for monitoring the inputs only. The loudspeakers

were driven by a DA converter board (Loughborough Sound Images 12 bit, 16 channel DA converter card, type DA16), coupled to the DSP board via the DSPLink interface, a digital communication system for DSP processing systems and peripheral boards. Each DSP board had its own DA converter board, thus yielding a total of 48 loudspeaker outputs. A sketch of the digital hardware of the prototype system is shown in figure C.1.1.

To obtain a full 6 inputs x 48 outputs matrix, all 6 input channels had to be available at each DSP board. This could be accomplished using the Motoway multi-processor interface, a digital data bus that makes the memory at port B of each 96000 processor addressable by all boards connected to the bus. When new input data is available,

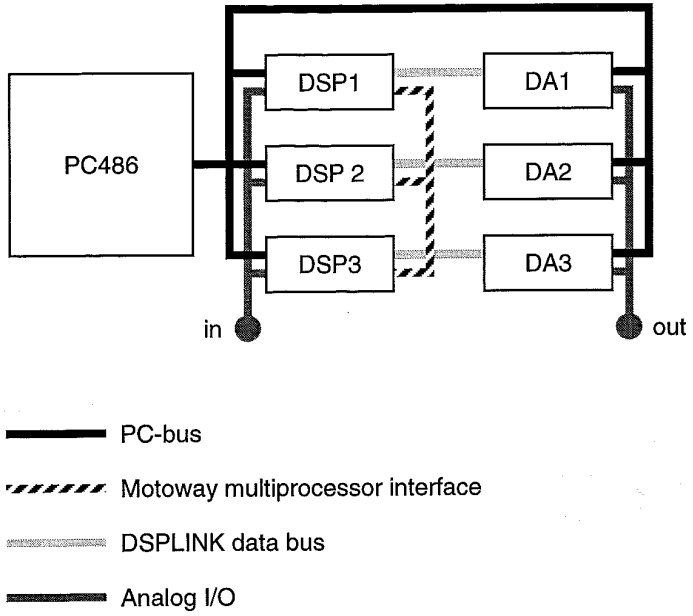

Figure C.1.1: *Schematic diagram of the digital hardware of the wave field synthesis prototype system.*

each DSP board reads its own AD converter data and stores this data value in port B memory. The data from the other AD converters is read from port B memory over the Motoway bus. In figure C.1.2 a sketch of the DSP processors and the communication over the Motoway bus is given.

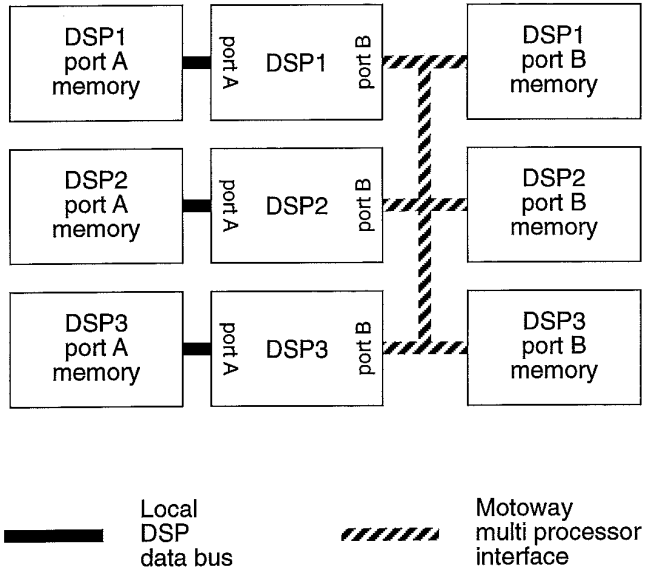

Figure C.1.2: *Sketch of the distribution of local memory (port A) and shared memory (port B) in the DSP hardware of the wave field synthesis prototype system.*

C.2 Analog hardware

The analog part of the prototype system hardware consisted of a six-channel mixing console with built-in microphone pre-amplifiers and phantom power and a set of loud-

speaker power amplifiers. The anti-aliasing filters were part of the AD conversion system on the DSP boards. The inputs could be either direct (line level) or via the microphone pre-amps. The output signals of the DA converters were driving the loudspeaker power amplifiers directly, the output volume being controlled by varying the DA converter reference voltage. In figure C.2.1 a sketch of the analog hardware section is given.

The microphones used in the laboratory setup were Sennheiser type ME40 and ME80 condenser microphones with a super-cardioid directivity pattern. In figure C.2.2 the frequency response of this type of microphone is given, in figure C.2.3 and figure C.2.4 the directivity pattern at several frequency bands is shown.

The loudspeakers used were custom built, with dimensions 11x11x20 cm. The frequency response of this type of loudspeaker is shown in figure C.2.5, in figure C.2.6 the directivity pattern is shown for several frequency bands.

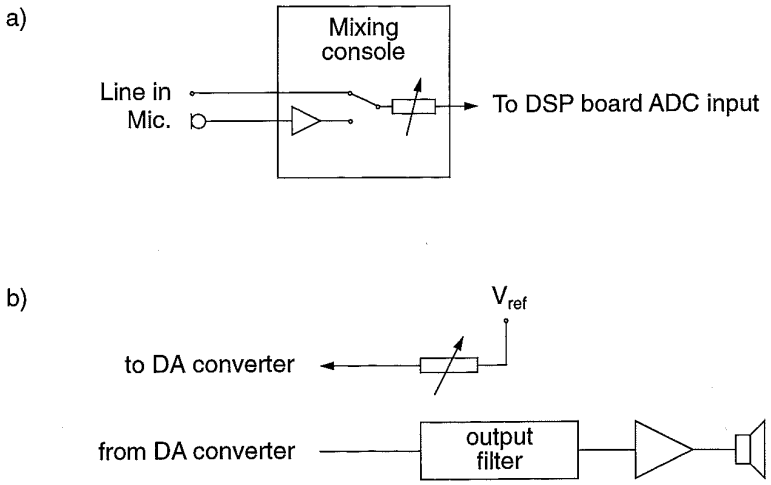

Figure C.2.1: *Schematic diagram of the analog hardware of the wave field synthesis system, laboratory setup.*
a) Input section
b) Output section

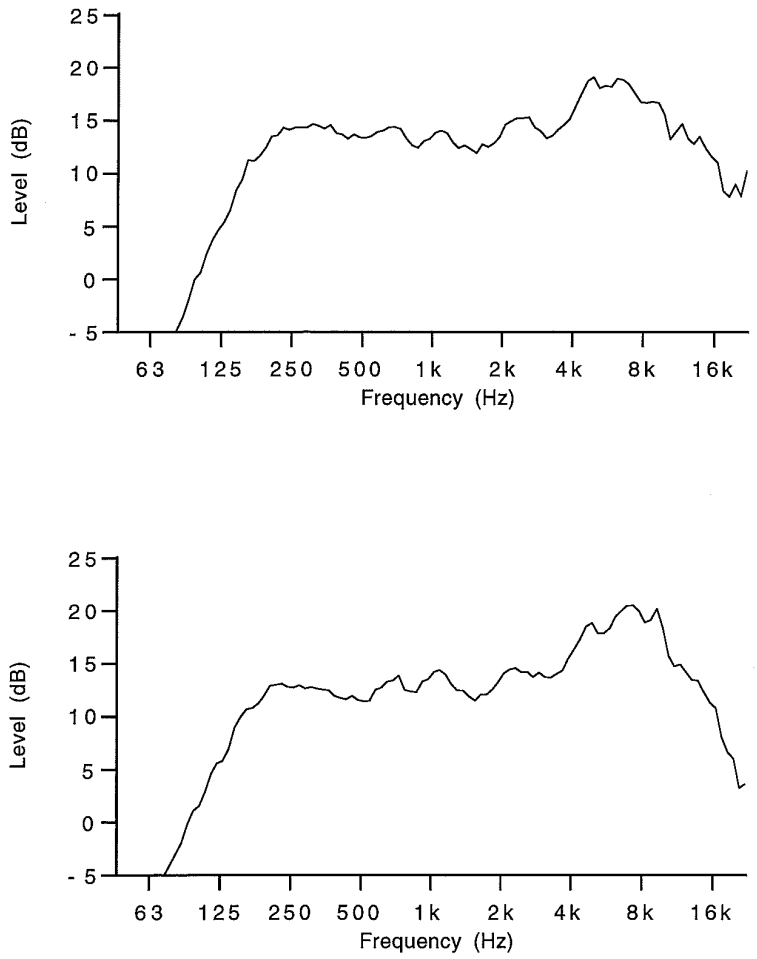

Figure C.2.2: *Frequency response of the microphones used.*
a) Sennheiser ME40
b) Sennheiser ME80

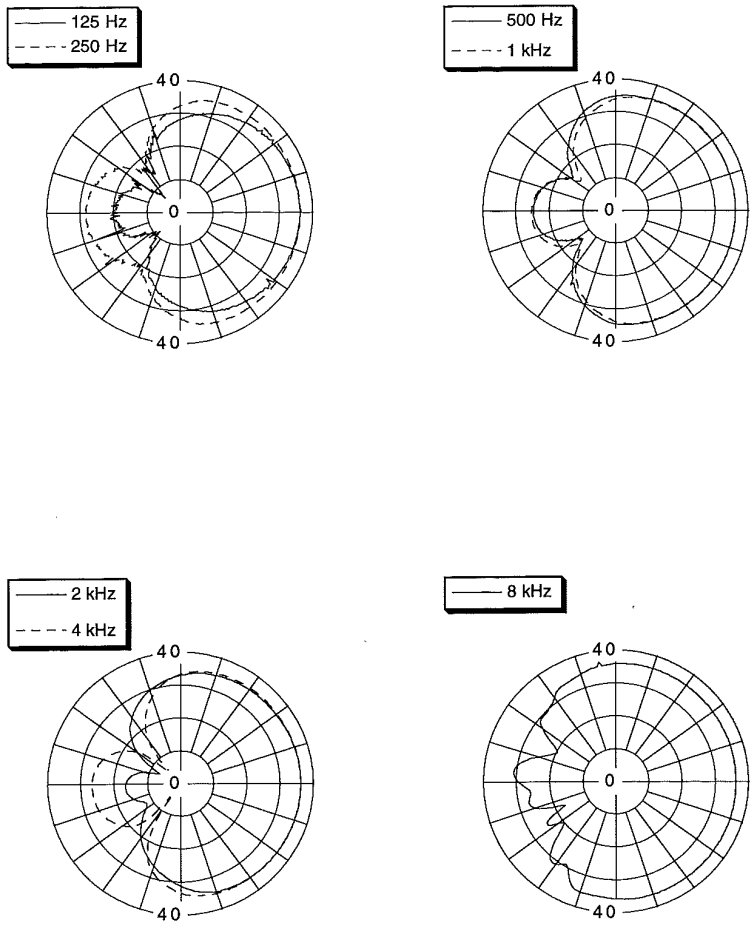

Figure C.2.3: *Directivity pattern of the Sennheiser ME40 microphone, at several frequency bands.*

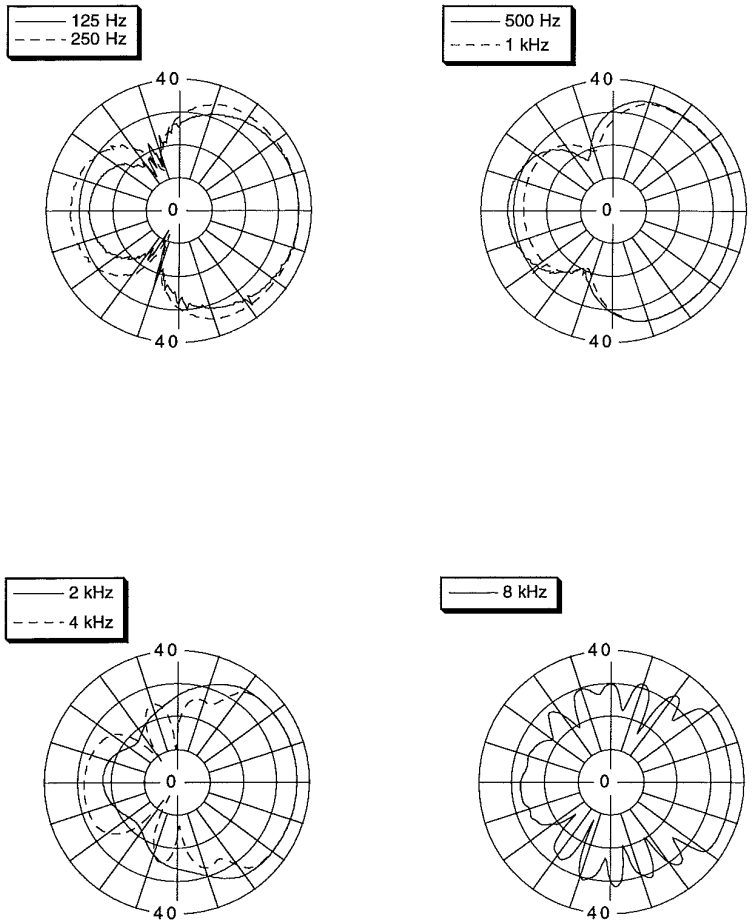

Figure C.2.4: *Directivity pattern of the Sennheiser ME80 microphone, at several frequency bands.*

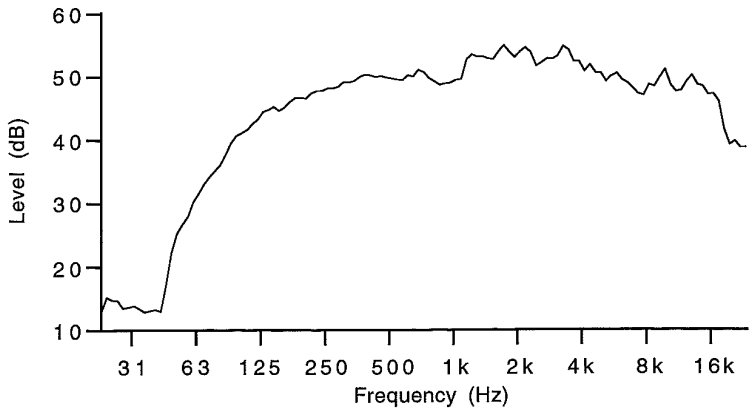

Figure C.2.5: *Frequency response of the wave field synthesis prototype system loudspeakers.*

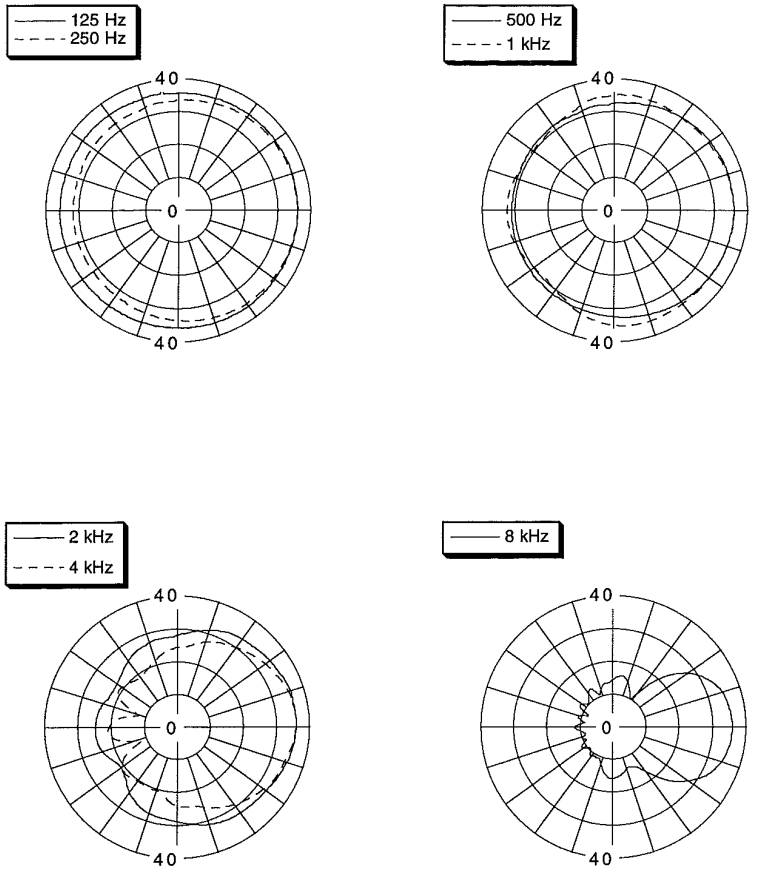

Figure C.2.6: *Directivity pattern of the wave field synthesis prototype system loudspeakers at several frequencies.*

Appendix D. SIGNAL PROPERTIES OF AN EXPONENTIAL DECAY CURVE

In this appendix the relation between the signal properties of an exponential reverberation curve (diffuse field) and the parameters commonly used in acoustics will be derived. The signal properties used are energy, first and second order moment and first and second order length. These measures will be expressed in terms of the reverberation time of the hall and the source power.

D.1 Energy of a decay curve

A noise source that emits a constant power W into a hall of volume V and total absorption A and switched off at time t=0 will yield a decaying reverberant field in the hall for times t>0. Assuming a diffuse reverberant field in the hall, the effective sound pressure $p_{rms}(t)$ in the hall is given by an exponential function:

$$p_{rms}(t) = p_{rms}(0)\, e^{-cAt/8V} = p_{rms}(0)\, 10^{-3t/T_{60}}, \qquad \text{(D.1.1)}$$

in which T_{60} is the reverberation time of the hall and $p_{rms}(0)$ denotes the effective sound pressure at the moment that the source was switched off.

Using definition (5.2.1), the energy of the decay curve can be written as

$$E(p_{rms}) = p_{rms}^2(0)\int_0^\infty 10^{-6t/T_{60}}dt = p_{rms}^2(0)\int_0^\infty \exp\left(\frac{-6\ln 10}{T_{60}}t\right)dt\,. \qquad (D.1.2)$$

By evaluating the integral in equation (D.1.2) it is found that

$$E(p_{rms}) = p_{rms}^2(0)\frac{T_{60}}{6\ln 10}\,. \qquad (D.1.3)$$

The effective sound pressure at times $t\leq 0$ can be expressed in terms of the source power, the reverberation time, the hall volume and the medium parameters density and sound speed. In a diffuse field the incident intensity I_{inc} on one side of a surface is given by

$$I_{inc} = \frac{p_{rms}^2(t\leq 0)}{4\rho c}\,, \qquad (D.1.4)$$

with c denoting the sound speed in the medium and ρ denoting the medium density. The total energy absorption per unit time is given by this incident intensity multiplied by the total absorption A of the room. In the stationary situation ($t\leq 0$), the energy absorption per unit time should be equal to the source power W:

$$W = I_{inc}A\,. \qquad (D.1.5)$$

Combining equations (D.1.4) and (D.1.5) yields for the effective sound pressure

$$p_{rms}^2(t\leq 0) = \frac{4\rho cW}{A}\,. \qquad (D.1.6)$$

Sabine's equation can be used to express the room absorption in its volume and its reverberation time:

$$A = \frac{24\ln 10V}{cT_{60}}\,, \qquad (D.1.7)$$

so that the stationary sound pressure is found to be

$$p_{rms}^2(0) = \frac{W\rho c^2T_{60}}{6\ln 10V}\,. \qquad (D.1.8)$$

Using equation (D.1.8), the energy of the decay curve can be written as

$$E(p_{rms}) = \frac{W\rho c^2}{V}\left(\frac{T_{60}}{6\ln 10}\right)^2\,. \qquad (D.1.9)$$

D.2 First order moment and first order length of a decay curve

Using definition (5.2.2), the first order moment of a decay curve $M_1(p_{rms})$ is given by

$$M_1(p_{rms}) = p_{rms}^2(0)\int_0^\infty t10^{-6t/T_{60}}dt = p_{rms}^2(0)\int_0^\infty t\exp\left(\frac{-6\ln 10}{T_{60}}t\right)dt\,. \qquad (D.2.1)$$

The integral in equation (D.2.1) can be evaluated using partial integration:

$$M_1(p_{rms}) = p_{rms}^2(0)\frac{T_{60}}{6\ln 10}$$

$$\left(\left[-t\exp\left(\frac{-6\ln 10}{T_{60}}t\right)\right]\Bigg|_0^\infty + \int_0^\infty \exp\left(\frac{-6\ln 10}{T_{60}}t\right)dt\right)\,. \qquad (D.2.2)$$

The first term in equation (D.2.2) evaluates to zero, so the first order moment of a decay curve is found to be

$$M_1(p_{rms}) = p_{rms}^2(0)\left(\frac{T_{60}}{6\ln 10}\right)^2\,. \qquad (D.2.3)$$

From definition (5.2.4) it is found that the first order length of a time signal is the ratio of the first order moment and its energy. Thus, by combining equation (D.1.3) and equation (D.2.3) it is found that the first order length of a decay curve $L_1(p_{rms})$ is given

by

$$L_1(p_{rms}) = \frac{T_{60}}{6\ln 10}. \qquad (D.2.4)$$

D.3 Second order moment and second order length of a decay curve

Using definition (5.2.3), the second order moment of a decay curve $M_2(p_{rms})$ is given by

$$M_2(p_{rms}) = p_{rms}^2(0)\int_0^\infty t^2 10^{-6t/T_{60}}dt = p_{rms}^2(0)\int_0^\infty t^2\exp(\frac{-6\ln 10}{T_{60}}t)\,dt. \qquad (D.3.1)$$

The integral in equation (D.2.1) can be evaluated using partial integration:

$$M_2(p_{rms}) = p_{rms}^2(0)\frac{T_{60}}{6\ln 10}$$

$$\left(\left[-t^2\exp(\frac{-6\ln 10}{T_{60}}t)\right]\Big|_0^\infty + 2\int_0^\infty t\exp(\frac{-6\ln 10}{T_{60}}t)\,dt\right). \qquad (D.3.2)$$

The first term in equation (D.2.2) evaluates to zero, the integral in the second term can be evaluated by partial integration. Thus, the second order moment of a decay curve is found to be

$$M_2(p_{rms}) = 2p_{rms}^2(0)(\frac{T_{60}}{6\ln 10})^2$$

$$\left(\left[-t\exp(\frac{-6\ln 10}{T_{60}}t)\right]\Big|_0^\infty + \int_0^\infty \exp(\frac{-6\ln 10}{T_{60}}t)\,dt\right). \qquad (D.3.3)$$

The first term in equation (D.2.2) evaluates to zero, so the second order moment of a decay curve is found to be

$$M_2(p_{rms}) = 2p_{rms}^2(0)(\frac{T_{60}}{6\ln 10})^3. \qquad (D.3.4)$$

From definition (5.2.5) it is found that the second order length of a time signal is the ratio of the second order moment and its energy. Thus, by combining equation (D.1.3) and equation (D.2.3) it is found that the second order length of a decay curve $L_2(p_{rms})$ is given by

$$L_2(p_{rms}) = 2(\frac{T_{60}}{6\ln 10})^2. \qquad (D.3.5)$$

Appendix E. SIGNAL PROPERTIES OF AN IMPULSE SEQUENCE

In this appendix the signal properties of an equidistant sequence of impulses as generated by a simple feedback loop will be calculated. The signal properties that will be discussed are energy, first and second order moment and first and second order length.

E.1 Energy of an impulse sequence

The impulse response h(t) of a simple feedback loop, as discussed in section 5.3, is given by

$$h(t) = \sum_{m=0}^{\infty} g^m \delta(t - m\tau) \ , \qquad \text{(E.1.1)}$$

in which g<1 denotes the loop gain and τ the loop delay.
The properties of the feedback loop system will be derived from the response on a spe-

cial input signal $s_n(t)$, shown in figure E.1.1 and defined by

$$\begin{cases} s_n(t) = 0, |t| > \dfrac{1}{2n} \\ s_n(t) = n, |t| \le \dfrac{1}{2n} \end{cases} . \qquad \text{(E.1.2)}$$

The constant n in equation (E.1.2) should be chosen such that the width of the impulse is less than the delay time τ of the feedback loop. The response of the feedback loop $q_n(t)$ on the input signal $s_n(t)$ is given by

$$q_n(t) = \sum_{m=0}^{\infty} g^m s_n(t - m\tau) . \qquad \text{(E.1.3)}$$

Using definition (5.2.1), the energy $E(q_n)$ of the signal $q_n(t)$ is found to be

$$E(q_n) = \int_0^{\infty} \left(\sum_{m=0}^{\infty} g^m s_n(t - m\tau) \right)^2 dt , \qquad \text{(E.1.4)}$$

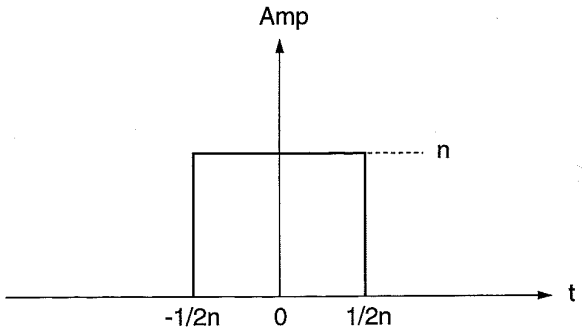

Figure E.1.1: *Rectangular box function $s_n(t)$, as used in the derivation of the properties of a feedback loop.*

which can be rewritten as

$$E(q_n) = \int_0^{\infty} \left(\sum_{m=0}^{\infty} g^{2m} s_n^2(t - m\tau) \right) dt , \qquad \text{(E.1.5)}$$

as there is no overlap between consecutive pulses in the response. Interchanging integration and summation in equation (E.1.5) yields

$$E(q_n) = \sum_{m=0}^{\infty} \left(g^{2m} \int_0^{\infty} s_n^2(t - m\tau)\, dt \right) . \qquad \text{(E.1.6)}$$

The integral in equation (E.1.6) evaluates to n, so the energy of the signal $q_n(t)$ becomes

$$E(q_n) = n \sum_{m=0}^{\infty} g^{2m} = \frac{n}{1 - g^2} . \qquad \text{(E.1.7)}$$

Defining the characteristic energy $\hat{E}(h)$ of the system response as the ratio of the output signal energy $E(q_n)$ and the input signal energy $E(s_n)$ yields

$$\hat{E}(h) \equiv \frac{E(q_n)}{E(s_n)} = \frac{1}{1 - g^2} . \qquad \text{(E.1.8)}$$

E.2 First order moment and first order length of an impulse sequence

As in the previous section, the signal $q_n(t)$ will be used here as a starting point to calculate the signal properties. Using definition (5.2.2), the first order moment $M_1(q_n)$ of the signal $q_n(t)$ is given by

$$M_1(q_n) = \int_0^{\infty} t \left(\sum_{m=0}^{\infty} g^m s_n(t - m\tau) \right)^2 dt . \qquad \text{(E.2.1)}$$

Equation (E.2.1) can be rewritten as

$$M_1(q_n) = \int_0^\infty t\left(\sum_{m=0}^{\infty} g^{2m} s_n^2(t-m\tau)\right)dt . \qquad (E.2.2)$$

Interchanging the summation and integration in equation (E.2.2) yields

$$M_1(q_n) = \sum_{m=0}^{\infty} g^{2m}\left(\int_0^\infty t s_n^2(t-m\tau)\,dt\right). \qquad (E.2.3)$$

The integral in equation (E.2.3) evaluates to $nm\tau$, so the first order moment of the signal $q_n(t)$ is found to be

$$M_1(q_n) = n\tau \sum_{m=0}^{\infty} m g^{2m} . \qquad (E.2.4)$$

Defining the characteristic first order moment $\hat{M}_1(h)$ of the system response as the ratio of the first order moment $M_1(q_n)$ of the output signal and the energy $E(s_n)$ of the input signal yields

$$\hat{M}_1(h) \equiv \frac{M_1(q_n)}{E(s_n)} = \tau \sum_{m=0}^{\infty} m g^{2m} . \qquad (E.2.5)$$

The first order length $L_1(q_n)$ of the signal $q_n(t)$ is defined by equation (5.2.4) as the ratio of its first order moment and its energy. Thus, $L_1(q_n)$ is given by

$$L_1(q_n) = \tau(1-g^2)\sum_{m=0}^{\infty} m g^{2m} = \tau\left(\sum_{m=0}^{\infty} m g^{2m} - \sum_{m=0}^{\infty} m g^{2(m+1)}\right). \qquad (E.2.6)$$

Rewriting the summations on the right hand side of equation (E.2.6) yields

$$L_1(q_n) = \tau\left(\sum_{m=1}^{\infty} m g^{2m} - \sum_{m=1}^{\infty} (m-1) g^{2m}\right) = \tau \sum_{m=1}^{\infty} g^{2m} = \frac{\tau g^2}{1-g^2} . \qquad (E.2.7)$$

Note that the first order length of the signal $q_n(t)$ is independent of the parameter n. Defining the characteristic first order length $\hat{L}_1(h)$ of the system response as the ratio of its characteristic first order moment $\hat{M}_1(h)$ and its characteristic energy $\hat{E}(h)$

yields the same result as equation (E.2.7):

$$\hat{L}_1(h) = \frac{\tau g^2}{1-g^2} . \qquad (E.2.8)$$

E.3 Second order moment and second order length of an impulse sequence

As in section E.1, the signal $q_n(t)$ will be used here as a starting point to calculate the signal properties. Using definition (5.2.3), the second order moment $M_2(q_n)$ of the signal $q_n(t)$ is given by

$$M_2(q_n) = \int_0^\infty t^2\left(\sum_{m=0}^{\infty} g^m s_n(t-m\tau)\right)^2 dt . \qquad (E.3.1)$$

Equation (E.2.1) can be rewritten as

$$M_2(q_n) = \int_0^\infty t^2\left(\sum_{m=0}^{\infty} g^{2m} s_n^2(t-m\tau)\right)dt . \qquad (E.3.2)$$

Interchanging the summation and integration in equation (E.2.2) yields

$$M_2(q_n) = \sum_{m=0}^{\infty} g^{2m}\left(\int_0^\infty t^2 s_n^2(t-m\tau)\,dt\right). \qquad (E.3.3)$$

The integral in equation (E.2.3) is approximately equal to $nm^2\tau^2$, so the second order moment of the signal $q_n(t)$ is found to be

$$M_2(q_n) = n\tau^2 \sum_{m=0}^{\infty} m^2 g^{2m} . \qquad (E.3.4)$$

Defining the characteristic second order moment $\hat{M}_2(h)$ of the system response as the ratio of the second order moment $M_2(q_n)$ of the output signal and the energy $E(s_n)$

of the input signal yields

$$\hat{M}_2(h) = \frac{M_2(q_n)}{E(s_n)} = \tau^2 \sum_{m=0}^{\infty} m^2 g^{2m} . \qquad (E.3.5)$$

The second order length $L_2(q_n)$ of the signal $q_n(t)$ is defined by equation (5.2.5) as the ratio of its second order moment and its energy. Thus, $L_2(q_n)$ is given by

$$L_2(q_n) = \tau^2 (1-g^2) \sum_{m=0}^{\infty} m^2 g^{2m} = \tau^2 \left(\sum_{m=0}^{\infty} m^2 g^{2m} - \sum_{m=0}^{\infty} m^2 g^{2(m+1)} \right) \qquad (E.3.6)$$

Rewriting the summations on the right hand side of equation (E.2.6) yields

$$L_2(q_n) = \tau^2 \left(\sum_{m=1}^{\infty} m^2 g^{2m} - \sum_{m=1}^{\infty} (m-1)^2 g^{2m} \right) = \tau^2 \sum_{m=1}^{\infty} (2m-1) g^{2m} . \qquad (E.3.7)$$

Note that the second order length of the signal $q_n(t)$ is independent of the parameter n. Defining the characteristic second order length $\hat{L}_2(h)$ of the system response as the ratio of its characteristic second order moment $\hat{M}_2(h)$ and its characteristic energy $\hat{E}(h)$ yields the same result as equation (E.2.7):

$$\hat{L}_2(h) = \tau^2 \sum_{m=1}^{\infty} (2m-1) g^{2m} . \qquad (E.3.8)$$

Appendix F. CONVOLUTION OF IMPULSE SEQUENCES

When a hall is equipped with an electro-acoustic system, the total hall response is built up by the normal source receiver transfer function and a contribution of the system. In chapter 5 it was shown that the system contribution is given by the convolution of the source-microphone response, the system processor response and the loudspeaker-receiver response. Each of these responses can be approximated by an impulse sequence. In this appendix the effect of the convolution process on these impulse sequences will be discussed.

F.1 Reflection density

The impulse sequences used in this appendix will all have the form p(t) given by

$$p(t) = \sum_{i=0}^{\infty} p_i \delta(t-\tau_i) , \qquad (F.1.1)$$

in which p_i denotes the amplitude of impulse i and τ_i its time delay. In this appendix impulse sequences with infinite bandwidth can be used, as the impulse bandwidth is not important in reflection density considerations. When the impulse sequence p(t) is

convolved with another impulse sequence q(t) given by

$$q(t) = \sum_{j=0}^{\infty} q_j \delta(t-\tau_j) \ , \qquad \text{(F.1.2)}$$

the result y(t) is given by

$$y(t) \equiv p(t) * q(t) = \sum_{i=0}^{\infty}\sum_{j=0}^{\infty} p_i q_j \delta(t-\tau_i-\tau_j) \ . \qquad \text{(F.1.3)}$$

It can be seen from equation (F.1.3) that any combination of an impulse of sequence p(t) and an impulse of sequence q(t) yields an impulse in the sequence y(t) with a delay given by the sum of the delays of the two original impulses and an amplitude given by the product of the amplitudes of the two impulses. As an example, figure F.1.1 shows two arbitrary impulse sequences p(t) and q(t), and the result y(t) of their convolution. Note that the number of impulses in the convolution result is much larger than in the original signals.

A mathematical analysis of the signal y(t) is most clear when both impulse sequences p(t) and q(t) are equidistant. Assuming that the impulse interval of p(t) is given by τ_1 and the impulse interval of q(t) by τ_2, the signal y(t) is given by

$$y(t) = \sum_{i=0}^{\infty}\sum_{j=0}^{\infty} p_i q_j \delta(t-i\tau_1-j\tau_2) \ . \qquad \text{(F.1.4)}$$

For both equidistant impulse sequences the impulse density or, in acoustical terms, the reflection density is constant. However, for the convolution of these two sequences the reflection density increases with time. To derive an expression for the reflection density the schematic diagram shown in figure F.1.2 can be helpful. In this diagram the impulses of p(t) are positioned on the horizontal axis, the impulses of q(t) on the vertical axis. The impulses of y(t) are shown by dots distributed over the whole plane.

The line $t=t_0$ shown in the diagram separates the impulses with delay time $t<t_0$ from those with delay time $t>t_0$. The number of reflections with delay time $t<t_0$ equals the area of the triangle that is cut off by the line $t=t_0$, divided by the "elementary area" $\tau_1\tau_2$ assigned to each reflection point. This area $A(t_0)$ is given by

$$A(t_0) = \frac{1}{2}\frac{t_0^2}{\tau_1\tau_2} \ , \qquad \text{(F.1.5)}$$

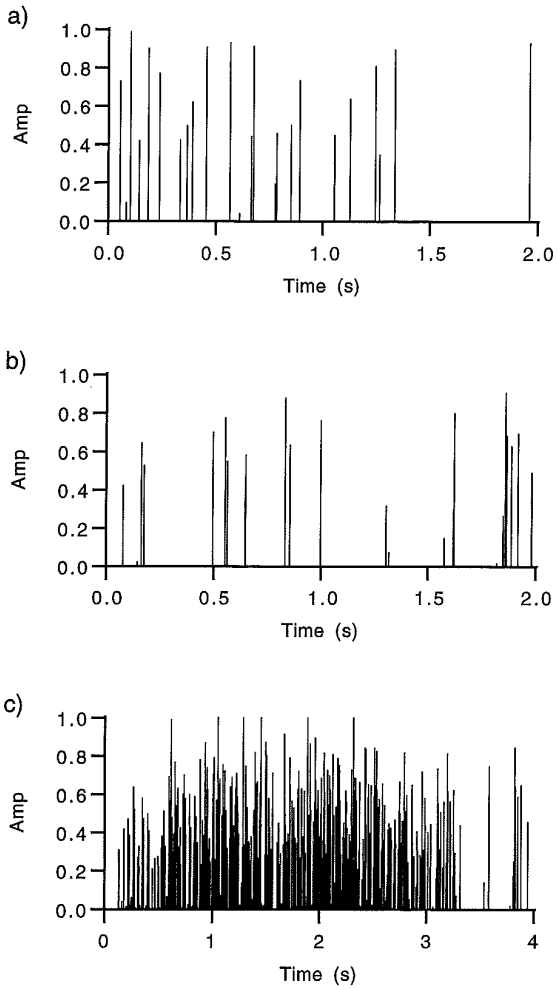

Figure F.1.1: *Convolution of two impulse sequences*
a) Pulse sequence p(t)
b) Pulse sequence q(t)
*c) Pulse sequence y(t) = p(t) * q(t)*

showing that the total number of reflections is quadratic in time. The reflection density $\rho_r(t)$ is the time derivative of the total number of reflections A(t), so it is given by

$$\rho_r(t) = \frac{t}{\tau_1 \tau_2}, \qquad \text{(F.1.6)}$$

and is thus seen to be linear in time. Note that increasing the reflection density of both p(t) and q(t) by a factor N will increase the reflection density of y(t) by a factor N^2. Following the same lines it can be shown that by convolving three equidistant impulse sequences an output signal with a reflection density quadratic in time is created. In general, it can be stated that when an impulse response with a reflection density increasing with t^m is convolved with an impulse response with a reflection density increasing with t^n, an output response is obtained with a reflection density increasing

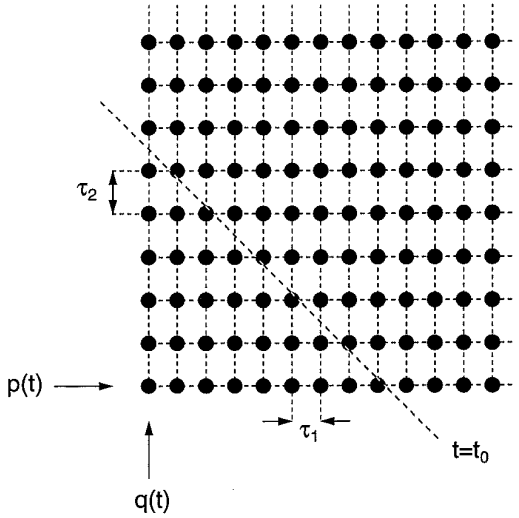

Figure F.1.2: *Schematic diagram showing the impulses of p(t) at the horizontal axis, the impulses of q(t) at the vertical axis and the impulses of y(t) as dots distributed over the whole plane.*

with t^{m+n}. Due to the very high reflection densities that can occur for large times, e.g., by convolving several hall impulse responses and electro-acoustic processor transfer functions as discussed in chapter 5, a large amount of late energy is obtained. The influence of this late energy on the decay curve will be discussed in the next section.

F.2 Decay curves

In addition to the impulse response, the decay curve is also used often in room acoustics. Thus, the effect of convolving impulse sequences on the decay curve will also be considered here. As the decay curve in a hall can usually be approximated by an exponential function, only the convolution of exponential functions and of exponentially decaying impulse sequences will be considered here.
First, the convolution of two decaying exponential functions P(t) and Q(t) will be discussed. Figure F.2.1a shows the functions P(t) and Q(t), and figure F.2.1b the function Y(t), defined as the convolution of P(t) and Q(t). Note that the maximum of the function Y(t) is at a time $t_0>0$. As a consequence, the decay curve calculated from the function Y(t) shown in figure F.2.1c has a flat part at the start and starts decaying with a constant slope for times $t>t_0$.
As a second example, two exponentially decaying impulse sequences will be convolved. Figure F.2.2a shows the two impulse sequences $P_d(t)$ and $Q_d(t)$, figure F.2.2b their convolution $Y_d(t)$ and figure F.2.2c the decay curve for $Y_d(t)$. Again the convex part of the decay curve is found.
Table F.2.1 gives the slopes of the decay curve for P(t), Q(t), Y(t), $P_d(t)$, $Q_d(t)$ and $Y_d(t)$. It can be seen that the slope of the decay for Y(t) is less steep than the slope of the decay for P(t) and Q(t). The same holds for $Y_d(t)$ in relation to $P_d(t)$ and $Q_d(t)$. Thus, the convolution of two decaying exponentials yields an output signal that has a convex start and a decay less steep than the original responses. As a consequence, applying an electro-acoustic system with an exponentially decaying output signal in a reverberant environment will always lead to an increase of the reverberation time. When the system decay time is much longer than the hall decay time, the reverberation in the hall will be dominated by the system and vice versa.

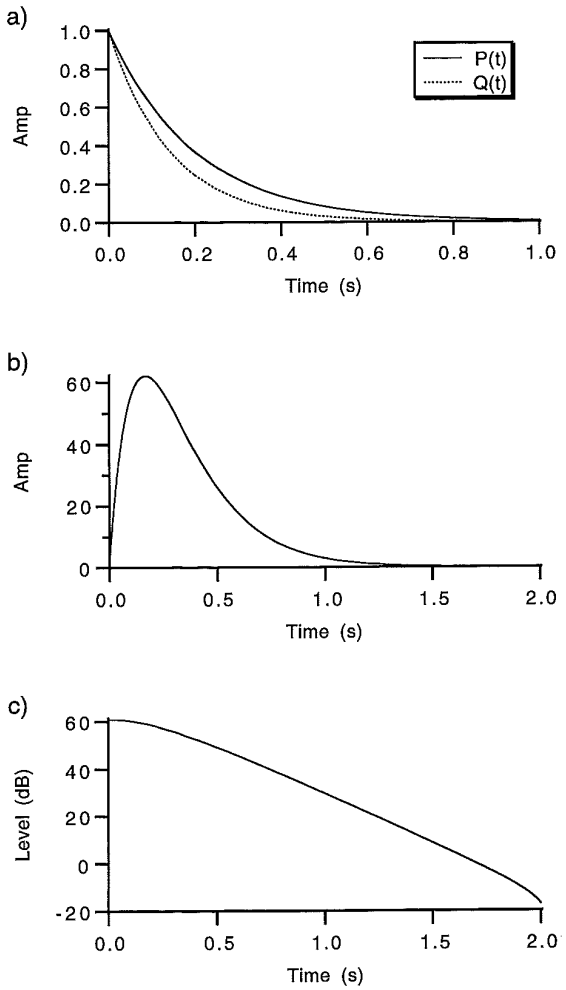

Figure F.2.1: *Convolution of two exponentially decaying functions P(t) and Q(t).*
a) P(t) and Q(t)
*b) Y(t) = P(t) * Q(t)*
c) Decay curve for Y(t)

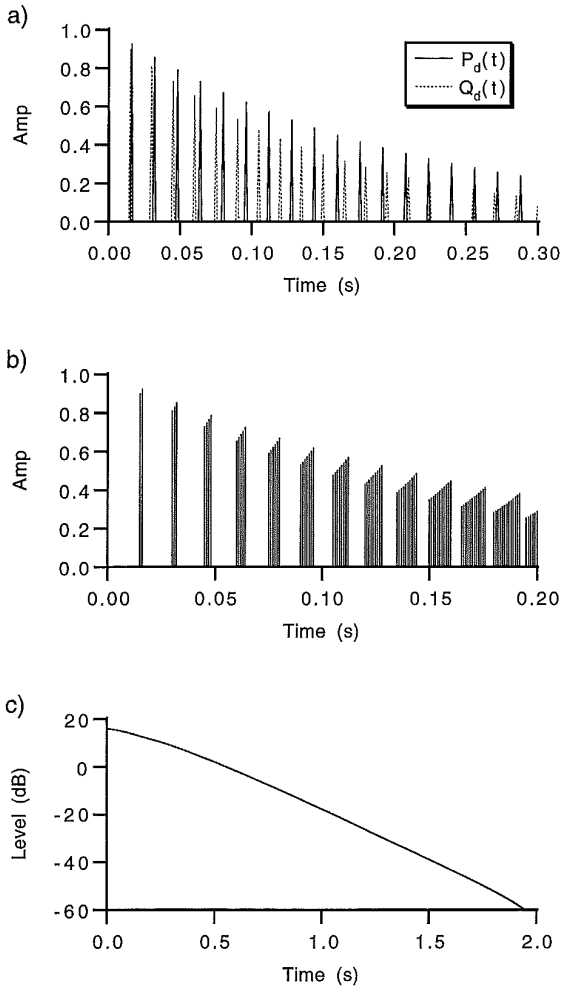

Figure F.2.2: *Convolution of two exponentially decaying impulse sequences $P_d(t)$ and $Q_d(t)$.*
a) $P_d(t)$ and $Q_d(t)$
b) $Y_d(t) = P_d(t) * Q_d(t)$
c) Decay curve for $Y_d(t)$

Function	Decay slope (dB/s)
P(t)	-45
Q(t)	-60
Y(t)	-40
$P_d(t)$	-45
$Q_d(t)$	-60
$Y_d(t)$	-40

Table F.2.1: *Decay slopes for P(t), Q(t), Y(t), $P_d(t)$, $Q_d(t)$ and $Y_d(t)$.*

REFERENCES

Abramowitz, M. and Stegun, I.A. (1965), Handbook of mathematical functions, Dover Publications Inc., New York

Ahnert, W. (1986), The complex simulation of acoustical sound fields by the delta stereophony system (DSS), presented at the 81st Convention of the Audio Engineering Society, J. Audio Eng. Soc. (Abstracts) **34**, p. 1035, preprint 2418

Ando, Y. (1985), Concert hall acoustics, Springer Verlag, Berlin

Barron, M. and Marshall, H.A. (1981), Spatial impression due to early reflections in concert halls, J. Sound and Vib. **77** (2), 211-232

Barron, M. and Lee, L.J. (1988), Energy relations in concert auditoriums I, J. Acoust. Soc. Am. **84** (2), pp. 618-628

Beranek, L.L. (1963), Music, acoustics and architecture, John Wiley & Sons Inc., New York

Beranek, L.L. (1992), Concert hall acoustics-1992, J. Acoust. Soc. Am. **92** (1), pp. 1-39

Berkhout, A.J., de Vries, D. and Boone, M.M. (1980), A new method to acquire impulse responses in concert halls, J. Acoust. Soc. Am. **68** (1), pp. 179-183

Berkhout, A.J. (1987), Applied seismic wave theory, Elsevier, Amsterdam

Berkhout, A.J. (1988), A holographic approach to acoustic control, J. Audio Eng. Soc. **36** (12), pp. 977-995

Berkhout, A.J., de Vries, D. and Vogel, P. (1993), Acoustic control by wave field synthesis, J. Acoust. Soc. Am. **93** (5), pp. 2764-2778

Biering, H. and Pedersen, O.Z. (1983), System analysis and time delay spectrometry (part I), Brüel & Kjær Technical Review 1983-**1**, pp. 3-51

Biering, H. and Pedersen, O.Z. (1983), System analysis and time delay spectrometry (part II), Brüel & Kjær Technical Review 1983-**2**, pp. 3-50

Bilsen, F.A. and Ritsma, R.J. (1970), Some parameters influencing the perceptibility of pitch, J. Acoust. Soc. Am. **47** (2), pp. 469-475

Bleistein, N. (1984), Mathematical methods for wave phenomena, Academic Press Inc., Orlando

Erdélyi, A. (1956), Asymptotic expansions, Dover Publications Inc.

Eyring, C.F. (1930), Reverberation time in "dead" rooms, J. Acoust. Soc. Am. **1**, pp. 217-241

Gade, A.C. (1989), Acoustical survey of eleven european concert halls, Technical University of Denmark, the acoustics laboratory, Report No. **44**

Haas, H. (1951), Einfluss eines Einfachechos auf die Hörsamkeit von Sprache, Acustica **1**, pp. 49-58

Hald, J. (1989), STSF-a unique technique for scan-based near-field acoustic holography without restrictions on coherence, Brüel & Kjær Technical Review 1989-**1**

Heringa, P.H. and Peutz, V.M.A. (1989), Variable acoustics, the design of different halls, Proc. 13th International Congress on Acoustics, pp. 239-242

Jacobsen, F. (1987), A note on decay measurements, J. Sound and Vib. **115** (1), pp. 163-170

Jacobsen, F. and Rindel, J.H. (1987), Time reversed decay measurements, J. Sound and Vib. **117** (1), pp. 187-190

Jordan, V.L. (1968), Appl. Acoustics **1**, pp. 29-36

Jordan, V.L. (1981), A group of objective acoustical criteria for concert halls, Appl. Acoustics **14**, pp. 253-266

Kollmeier, B. and Gilkey, R.H. (1990), Binaural forward and backward masking: Evidence for sluggishness in binaural detection, J. Acoust. Soc. Am. **87** (4), pp. 1709-1719

Kosten, C.W. (1960), The mean free path in room acoustics, Acustica **10**, pp. 245-250

Kosten, C.W. (1966), New method for the calculation of the reverberation time of halls for public assembly, Acustica **16**, pp. 325-330

Kürer, R. (1969), Zur Gewinnung von Einzahlkriterien bei Impulsmessungen in der Raumakustik, Acustica **21**, pp.370-372

Kuttruff, H. (1979), Room Acoustics (2nd ed.), Applied Science Publishers Ltd., London

Lochner, J.P.A. and Burger, J.F. (1959), The intelligibility of re-inforced speech, Acustica **9**, pp.31-38

Marshall, A.H., Gottlob, D. and Alrutz, H. (1978), Acoustical conditions preferred for ensemble, J. Acoust. Soc. Am. **64** (5), pp. 1437-1442

Maynard, J.D., Williams, E.G. and Lee, Y. (1985), Nearfield acoustic holography. I: Theory of generalized holography and the development of NAH, J. Acoust. Soc. Am. **78** (4), pp.1395-1405

Moore, B.C.J., Glasberg, B.R., Plack, C.J. and Biswas, A.K. (1988), The shape of the ear's temporal window, J. Acoust. Soc. Am. **83** (3), pp.1102-1116

Oppenheim, A.V., Willsky, A.S. and Young, I.T. (1983), Signals and systems, Prentice Hall Inc., Englewood Cliffs

Potter, J.M. (1993), On the binaural modelling of spaciousness in room acoustics, Dissertation, Delft University of Technology (NL)

Raatgever J. and Bilsen, F.A. (1986), A central spectrum theory of binaural processing. Evidence from dichotic pitch, J. Acoust. Soc. Am. **80** (2), pp. 429-441

Reichard, W. and Lehmann, U. (1978), Definition eines Raumeindrucksmasses R zur bestimmung des Raumeindrucks bei Musikdarbietungen auf der Grundlage subjectiver Untersuchungen, Applied Acoustics **11**, pp. 99-127

Reichard, W. and Lehmann, U. (1981), Optimierung von Raumeindruck und Durchsichtigkeit von Musikdarbietungen durch Auswertung von Impulsschalltests, Acustica **48**, pp. 174-185

Sabine, W.C. (1900), Reverberation, republished in Collected papers on acoustics by W.C. Sabine, Dover Publications Inc., New York, pp. 3-68

Schroeder, M.R. (1962), Natural sounding artificial reverberation, J. Audio Eng. Soc. **10**, pp. 219-223

Schroeder, M.R. (1965), A new method of measuring reverberation time, J. Acoust. Soc. Am. **37**, pp. 409-412

Thiele, R. (1953), Richtungsverteilung und Zeitfolge der Schallrückwürfe in Räumen, Acustica **3**, pp. 291-302

Vogel, P., Berkhout, A.J. and de Vries, D. (1989), A holographic approach to speech reinforcement, Proc. 13th international congress on acoustics, pp. 265-270

Vogel, P. and de Vries, D. (1992), A convolutional model for simulating the response of an electro-acoustic system inside a hall, presented at 124th meeting of the Acoustical Society of America

SUMMARY

The first part of this thesis discusses the design, implementation and evaluation of a prototype electro-acoustical system for wave field synthesis. The use of wave field synthesis in electro-acoustics was introduced by Berkhout (1988); the underlying theory is based on the Kirchhoff-Helmholtz representation theorem. The aim of the wave field synthesis system is to serve as an amplification system for direct sound that can be used in theatres to enhance the actors' voices, without disturbing the localisation cues in the sound field. This way the audience will hear the sound coming from the correct direction, irrespective of the position of sound source and listener.

Using wave theory and signal analysis it can be derived that an arbitrary wave field can be synthesised by a planar loudspeaker array, with an intermediate distance between the loudspeaker centres less than half the minimum apparent wave length in each direction. A system capable of synthesising arbitrary wave fields in the full audio frequency range from 20 Hz to 20 kHz would theoretically require a planar configuration of thousands of individually driven loudspeakers. However, by making use of the properties of the human ears, simplifications can be introduced.

As in the direct sound amplification system the horizontal source localisation is very important, whereas the vertical source position hardly changes, a linear loudspeaker array can be used that radiates wave fronts with the desired shape in the horizontal direction and spherical wave fronts centred around the loudspeakers in the vertical direction. This requires an adaptation of the standard equations of the extrapolation theory.

A further simplification could be obtained by limiting the frequency range in which the system has to operate. The very first experiments were performed with a simple 12

loudspeaker system that radiates the correct wave front in the frequency range up to 380 Hz only. Due to spatial aliasing the wave fronts for frequencies above 380 Hz will be distorted in such a very simple system.
The driving signal for each loudspeaker is given by a weighted and filtered version of the direct source wave field at the loudspeaker position. Thus, a (single track) tape recorder signal can be used to create a monopole source wave field by extrapolating this signal from the simulated source position to the loudspeakers and using the extrapolated signals to drive the loudspeakers. This extrapolation can be performed by applying the appropriate source-loudspeaker travel time delay and attenuation for each loudspeaker channel. A digital signal processor (DSP) is used to generate the required weighted delay lines.
Listening tests in an anechoic chamber pointed out that even with the very simple 12 loudspeaker system a monopole source wave field with the correct source localisation could be generated. The spatial aliasing caused some colouration of the sound field, especially when listening to noise sources.
When the loudspeaker array is to be used for direct sound enhancement, the sources that should be amplified are recorded by microphones. As above, the output signals of these microphones can be used to generate a monopole wave field. When the position of the source is known, it is possible to let the simulated source coincide with the true source, such that the loudspeaker array generates the same wave field as the direct source in horizontal direction.
By applying a set of directive microphones to address the stage, each microphone being directed to its own area on stage, the output signal of a particular microphone can be thought of as being generated by a source at the central spot of the microphone beam. Berkhout (1993) refers to this source as the "notional source". Using this technique, the synthesised wave field is built up from several point sources distributed over the stage. The spatial resolution will depend on the number of microphones used.
Because of the promising results obtained with the simple 12 loudspeaker system, a new system was built using 48 small loudspeakers spanning the same width as the original array. As a consequence, the spatial aliasing frequency is raised by a factor of four, which yields a considerable reduction in colouration.
The 48 loudspeaker system has been tested as an amplification system in the Auditorium of the Delft University using six microphones to address the stage area. This system proved to meet the prescribed requirements. Due to this successful experiment, the first wave field synthesis system has been installed in a theatre in Sweden (Malmö Stadsteater) by a Dutch firm, consisting of 12 input microphones and 96 loudspeakers. The author of this thesis was actively involved with the design and engineering aspects.

The second part of this thesis discusses a modelling scheme to simulate the acoustical behaviour of a hall equipped with an electro-acoustic system. This model takes into account all relevant hall transfer functions in the calculation of the system contribution to the hall response. Thus, the system contribution is described by a convolutional model.
A new modelling feature is discussed that takes into account diffuse reflections in the hall transfer functions. Implementation of this feature in a modelling scheme combines the advantages of the image source method and ray-tracing, and proves to be more accurate for halls with non-uniform absorption.
The modelling scheme is used to simulate the acoustical behaviour of a rectangular hall, with dimensions chosen such that it is representative for the Auditorium of the Delft University of Technology, a hall equipped with an electro-acoustic system for reflection generation and reverberation enhancement. The influence of the two system processors (early reflection processor, reverberation processor) is consecutively taken into account. The acoustic feedback between system loudspeakers and system microphones is also part of the calculation. The simulations are compared with measurements in the Auditorium of Delft University of Technology. The total modelling scheme appears to be capable of describing all effects specific for halls equipped with an electro-acoustic system.

SAMENVATTING

In het eerste deel van dit proefschrift worden het ontwerp en de implementatie van een elektro-akoestisch golfveldsynthesesysteem besproken. De met dit systeem verkregen resultaten worden geëvalueerd.
Het gebruik van golfveldsynthese in de elektro-akoestiek is geïntroduceerd door Berkhout (1988); de theoretische basis wordt gevormd door het Kirchhoff-Helmholtz representatietheorema. Het ontworpen systeem heeft tot doel het versterken van het directe geluid van acteurs op het podium van een theater, zonder daarbij de in het geluidssignaal aanwezige richtingsinformatie aan te tasten. Door op deze wijze geluidversterking toe te passen zullen de luisteraars, onafhankelijk van de positie van de geluidbron en onafhankelijk van hun eigen positie, de geluidbronnen op de juiste positie waarnemen.
Uit de golftheorie en de signaalanalyse kan worden afgeleid dat een willekeurig golfveld opgewekt kan worden door gebruik te maken van een planaire luidsprekerverdeling, waarbij de hart-op-hart afstand van de luidsprekers in alle richtingen kleiner is dan de helft van de minimale schijnbare golflengte in deze richting. Voor een systeem dat golfvelden in het gehele audiofrequentiegebied (20 Hz - 20 kHz) genereert betekent dit dat theoretisch een vlakverdeling van duizenden luidsprekers met ieder een eigen stuursignaal nodig is. Door gebruik te maken van de eigenschappen van het menselijk gehoororgaan kunnen echter aanzienlijke vereenvoudigingen worden doorgevoerd.
Aangezien bij geluidversterking van bronnen op een podium de horizontale positionering veel belangrijker is dan de verticale positionering kan worden volstaan met een lineaire luidsprekerverdeling, die in horizontale richting golffronten met de gewenste

vorm genereert, terwijl in verticale richting bolvormige golven rond de luidspreker worden opgewekt. De uitdrukkingen van de golfveldextrapolatietheorie moeten bij het gebruik van zo'n vereenvoudigd systeem aangepast worden.
Een verdere vereenvoudiging kan worden gemaakt door de bandbreedte van het systeem te beperken. Bij het allereerste proefsysteem werd gekozen voor een systeem met 12 luidsprekers, waarmee voor frequenties tot 380 Hz de juiste golffronten opgewekt konden worden. Als gevolg van de ruimtelijke onderbemonstering zullen bij het gebruik van een simpel systeem als dit de golffronten voor frequenties boven 380 Hz vervormd zijn.
De stuursignalen voor de luidsprekers worden gegeven door een gewogen en gefilterde versie van het directe golfveld ter plaatse. Dit betekent dat een (enkelspoors) geluidopname gebruikt kan worden om een monopoolbronveld te genereren, door het bandsignaal volgens de monopoolafstraling vanaf de gesimuleerde bronpositie naar de luidsprekers te extrapoleren. Dit betekent dat het signaal voor iedere luidspreker over de looptijd van de gesimuleerde bron naar de betreffende luidspreker vertraagd moet worden en met de bijbehorende amplitudeafname moet worden gewogen.
Luistertests in een reflectie-arme ruimte ("dode kamer") hebben aangetoond dat zelfs het simpele systeem met 12 luidsprekers in staat is een monopoolbronveld te genereren met een duidelijk bepaalde bronpositie. Door de spatiële onderbemonstering ontstaat kleuring in het geluidssignaal, die vooral bij ruissignalen duidelijk waarneembaar is.
Wanneer het systeem wordt gebruikt voor versterking van direct geluid in een theater zullen de bronnen op het podium met een microfoon opgenomen moeten worden. De signalen van de microfoons kunnen op de bovengenoemde wijze verwerkt worden tot een monopoolbronveld. Door het podiumgeluid op te nemen met een serie richtmicrofoons en voor iedere microfoon een monopoolbron te simuleren op de plaats van het centrum van de microfoonbundel, ontstaat een verdeling van gesimuleerde puntbronnen die een goede afspiegeling is van de bronverdeling op het podium. Berkhout (1993) noemt deze gesimuleerde bronnen "notional sources". De resolutie in plaats wordt bepaald door het aantal gebruikte microfoons.
Door de veelbelovende resultaten van het simpele 12 luidsprekersysteem is een nieuw systeem gerealiseerd waarbij de array van 12 luidsprekers vervangen werd door een array van 48 luidsprekers met dezelfde lengte, zodat de spatiële onderbemonstering met een factor vier kon worden gereduceerd. Dit resulteerde in een aanzienlijke afname van de kleuring.
Dit 48 luidsprekersysteem is in het Auditorium van de Technische Universiteit Delft

getest als spraakversterkingssysteem. Voor de opname van de geluidbronnen werden daarbij zes microfoons gebruikt. Het systeem bleek aan de gestelde eisen te voldoen. Als gevolg van dit succesvolle experiment is het eerste golfveldsynthesesysteem geïnstalleerd in een operatheater in Zweden (Malmö Stadsteater) door een Nederlandse maatschappij. Dit systeem bestaat uit 12 microfoons en 96 luidsprekers. De auteur van dit proefschrift was nauw bij het ontwerp en de technische realisatie van dit systeem betrokken.
Het tweede deel van dit proefschrift beschrijft een modelleringsschema dat in staat is het akoestisch gedrag van een ruimte met een elektro-akoestisch systeem voor het genereren van vroege reflecties en nagalm te simuleren. Bij dit model worden alle transmissiewegen van het geluid door de ruimte meegenomen. Ook de akoestische terugkoppeling van de systeemluidsprekers naar de systeemmicrofoons is in het model opgenomen. De werking van het elektro-akoestische systeem blijkt te worden beschreven door een reeks convoluties.
Voor het modelleren van de geluidstransmissie van de ruimte is diffuse reflectie als nieuw aspect aan de bestaande modelleringsschema's toegevoegd. Het nieuw ontwikkelde model combineert de voordelen van het spiegelbronnenmodel met de voordelen van stralenmodellen. De resultaten verkregen met dit model zijn nauwkeuriger dan de resultaten van het spiegelbronnenmodel, vooral in ruimten waarbij de absorptie niet uniform over de wanden verdeeld is.
Het modelleringsschema is gebruikt om het gedrag van een rechthoekige zaal te simuleren. De maten van deze zaal zijn zo gekozen dat deze representatief is voor het Auditorium van de Technische Universiteit Delft, een gehoorzaal uitgerust met een elektro-akoestisch systeem voor het genereren van geluidsreflecties en het verlengen van de nagalmtijd. De invloed van de twee systeemprocessoren (vroege reflectieprocessor, galmprocessor) wordt beschouwd door ze achtereenvolgens in het model toe te introduceren. De simulaties worden vergeleken met metingen uitgevoerd in het Auditorium van de Technische Universiteit Delft. Het totale simulatiemodel is in staat alle verschijnselen typerend voor een ruimte uitgerust met een elektro-akoestisch systeem te beschrijven.

CURRICULUM VITAE

Naam	Peter Vogel
Geboortedatum	18 juli 1963
Geboorteplaats	Den Haag

OPLEIDING

1969 - 1975	Basisonderwijs te Den Haag
1975 - 1980	HAVO aan de C.S.G. Overvoorde te Den Haag
1980 - 1982	VWO-B aan de C.S.G. Overvoorde te Den Haag
1982 - 1988	Studie Technische Natuurkunde aan de Technische Universiteit Delft. Afstudeeronderzoek: "The estimation of room-acoustical parameters from inaccurate data".

WERKERVARING

1988 - 1993	Wetenschappelijk onderzoeker aan de Technische Universiteit Delft, vakgroep Akoestische en Seismische Technieken, resp. als Assistent in Opleiding (STW project DTN70.1276) en als toegevoegd onderzoeker.